Electro-Mechanical Modelling of Cardiac Cells

by D. P. Nickerson.

Supervised by Professor P. J. Hunter.

A thesis submitted in partial fulfilment of the requirements for the degree of Master of Engineering at the University of Auckland.

Department of Engineering Science,
School of Engineering,
University of Auckland,
March 2, 1999.

Abstract

A coupled electro-mechanical model of a single cardiac cell is presented, which can be considered a first-step towards a full coupled model of a cardiac cell. The coupled model developed is based on three models of the electrical activity of a cardiac cell and the Hunter–McCulloch–ter Keurs (HMT) model of cardiac mechanics.

The three electrical models used in this research are the DiFrancesco–Noble (DFN), Luo–Rudy II (LR-II), and Jafri–Rice–Winslow (JRW) models. Each of these models has its own advantages over the others: the DFN model is applicable to a variety of different cardiac cell species; the LR-II model is a detailed model of the electrical activity of the ventricular myocyte; and the JRW model, based on the LR-II model, concentrates on accurate modelling of intracellular calcium handling.

In this thesis, the HMT mechanics model, developed with little consideration of the physiological details of cellular electrical activity, is coupled to the physiologically accurate JRW electrical model. The coupling implemented includes appropriate feedback mechanisms. This coupling provides the model with the abiltity to more accurately represent the actual behaviour of a single cardiac cell than either model would independently predict.

Three cases of behaviour were used to validate the model developed: isometric twitches, step releases, and the frequency response of a cardiac cell. The coupled JRW–HMT model was found to generally behave in accordance with physiological data for each of these cases. It was found that cell length has great effect on the isometric twitch characteristics, with the peak observed tension increasing as the cell is stretched. When step release experiments were investigated, the coupled model predicted that the time of the length step and the step's duration (or rate) were major factors in determining the effect of the step on the behaviour of the cell. The force-frequency relationship given by the model gave a peak for a stimulation frequency of 0.1 Hz, in agreement with experimental data.

As part of this research, a comprehensive graphical user interface for the mathematical models was developed. This interface enables a user to set-up the experiment they wish to perform (alter the models they want to solve and set the appropriate model parameters and variables) and then view/analyse the results of the simulation. The interface also has the ability to set parame-

ter values for use with the distributed finite element model of the whole heart developed in the Department of Engineering Science at the University of Auckland. This feature is particularly useful given that a coupled electro-mechanical model of a cardiac cell can involve upwards of 200 parameters and variables.

Preface

First and foremost, a huge thanks to my supervisor, Professor Peter Hunter. Without his help, assistance, and advice this project would never have got off the ground or had much chance of success. Thanks also to Dr. Andrew Pullan for his help and encouragement in the years leading to this Masters degree.

I would also like to acknowledge the assistance of Dr. David Bullivant with the development of the user interface, particularly the use of UNEMAP and CMGUI tools. Chris Bradley also deserves thanks for his general programming and LaTeX help.

Thanks also go to Leo “Space Monkey” Cheng, Richard “Munce” Boyes, Nick “Pan-Nic” Davey, and Warren “Wazza” Hedley for all their supportive and helpful suggestions and criticisms. Warren’s Motif advice was invaluable and Leo was full of extremely useful suggestions for the user interface, some of which were actually implemented. Thanks also to Michael Somervell and Toby Allsopp for their computer expertise and lunch-time entertainments.

Lastly, I would like to thank my family for all their support throughout the duration of this project, even if they never really understood the mathematics involved.

Contents

List of Figures

List of Tables

Chapter 1

Introduction

1.1 Cardiac Modelling

Due to the importance of the heart, extensive research has been performed in order to gain a greater understanding of this vital organ. Over the last century, one of the main components of this work has been the development of continuously improving experimental techniques (*e.g.,* patch clamp techniques) and equipment (*e.g.,* measurement and instrumentation devices). These developments have enabled researchers to perform detailed and accurate investigations into the form and function of the various sections that comprise the cardiac organ. While there is still plenty of work to perform before a complete understanding of cardiac physiology is obtained, these experimental investigations have resulted in a good understanding of the basic structures and processes involved in cardiac function.

This understanding has led to the development of a number of mathematical models based on these experimental investigations, which can successfully simulate the form and function of the heart, as we currently understand it. These models can be grouped into two broad categories: single cell models, which model the structure and function of single cardiac cells; and whole heart models, which model the entire cardiac system. Whole heart mathematical models usually model the heart as a continuum of material with spatially varying material properties and are usually based on underlying cell models, making physiologically accurate cardiac cell models critical to the advancement of all mathematical modelling of the cardiac system.

1.1.1 Cardiac cell modelling

Cardiac cell models can be split into three main groups, determined by the processes they are modelling. These three groups are electrical, mechanical, and metabolic or biochemical models. Electrical models model the electrical activity of the cell, involving processes such as the flow of ions through the cell membrane, the effect of the cardiac action potential on the cell, and the restoration of resting activity after the wave of depolarisation has propagated past the cell. Mechanical models deal with the mechanical behaviour of the cell, primarily modelling the cells contraction during stimulation. Metabolic or biochemical models model the cell's metabolic activity, modelling such processes as the generation of ATP in the mitochondria, the diffusion of oxygen into the cell, and the transport of lactate out of the cell. However, in the real world, all these processes occur together with each having an effect on the others (*i.e.*, the electrical activation of the cell leads to mechanical contraction, which requires energy from the metabolism and affects the electrical activity of the cell). This close interaction has led to a super-group of cardiac cell models which involves *coupled models*. These model two or more of the other model groups together, for example electro-mechanical models, or coupled metabolic and mechanics models.

Most research into cardiac cell models, to date, has involved mainly looking at only one of the three types of models mentioned above. This has led to the development of numerous electrical, mechanical, and metabolic models of cardiac cells, which model their particular processes with great detail and accuracy. It is the main objective of this research to implement some of the more widely used of these models, and couple them together to produce a fully coupled electrical and mechanical model of a cardiac cell. This model needs to include the effects of the electrical activation on the mechanical behaviour (electro-mechanical coupling) and the effect the mechanical behaviour has on the electrical activity of the cell (mechano-electric feedback), and be extendable to include a metabolic model.

1.2 Mathematical Models and Computers

With recent developments in computer technology (particularly over the last decade), mathematical models in general have become much more widely used, both as teaching aids and research tools. Computer programs which implement mathematical models give their users the ability to perform a variety of simultations which may not be possible to perform physically due to a number of factors such as cost, time, and availability of equipment. For example, the use of a computer program which implements a model of the electrical activity of a muscle cell, allows a number of students to investigate the effect of a number of factors (*e.g.*, composition of the bathing solution, caffine levels, and the size of the electrical stimulus) on the behaviour of the muscle cell. For a large number of factors, this type of investigation would be very time consuming and expensive to perform physically in a laboratory, while requiring much less time and only access to appropriate computing facilities to use the computer simulation.

This implies that for any mathematical model to be useful as both a teaching aid and a research tool, it must be implemented in such a way that it is easy to use, so that the user of the model can spend more time thinking about the underlying physiology than the interface to the mathematical model. This becomes especially important when you are dealing with coupled cardiac cell models, which can easily involve more than 200 model parameters. Another aim of this research is, therefore, to create a user interface for the developed mathematical model which fulfils this criterion.

1.3 Research Plan and Objectives

As stated earlier, the main objective of this research is to develop a fully coupled model of a cardiac cell. This will primarily involve developing a coupled electro-mechanical model, with mechano-electric feedback implemented. The code implementing both the electrical and mechanical models has been written and requires coupling together to obtain the desired coupled electro-mechanical model. This is simply done by using the intracellular calcium fluxes from the electrical model to drive the mechanical model, and applying appropriate feedback mechanisms.

A secondary objective of this research project is to develop a suitable user interface for the model. As stated in Section 1.2, the mathematical model must have an easy to use interface to increase its value as a teaching aid and research tool.

1.4 Achievements

All the thesis objectives given above have been achieved in the course of this research. This has involved the following:

- Implementation of the non-coupled DiFrancesco–Noble, Luo–Rudy, and Jafri–Rice–Winslow electrical models and the Hunter–McCulloch–ter Keurs mechanics model;
- Development and testing of a coupled electro-mechanical model of a single cardiac cell, with mechano-electric feedback;
- Development of a software package, with a graphical user interface, which has both research and teaching applications.

1.5 Thesis Outline

Before the mathematical models used can be understood, it is necessary to gain a basic understanding of the system being modelled. The purpose of Chapter 2 is to give this understanding.

In this chapter, an overview of all the necessary physiological detail is presented, including the structure and function of cardiac cells.

Once the underlying physiology is understood, it is possible to present the mathematical models used. Chapters 3 and 4 present the models used in this research project, and Chapter 5 presents the coupled model developed.

The software developed for the coupled model of a cardiac cell is presented in Chapter 6, describing the interface and the numerical techniques used to solve the models presented in Chapters (3)–(5).

Results obtained from this model are given in Chapter 7, along with discussion of the models and comparisons to experimental data. Chapter 8 gives the conclusions drawn from this research as well as possible extensions to this project.

Chapter 2

Cardiac Cell Physiology

2.1 Cardiac Physiology

The purpose of the heart is to pump blood. To do so continuously for 70 years or more at a rate varying from $5–35\ \mathrm{L/min}$ requires a very sophisticated organ (Glass, Hunter & McCulloch 1991).

The contractile activity of the muscular walls of the heart delivers nutrients to and removes wastes from each organ. This activity is also responsible for the transport of hormones, neurotransmitters, and other messengers between regions. Thus, the heart can be thought of as a hollow muscular pump provided with valves, moving blood in a circle continuously.

The structure and function of cardiac muscle is more complex than that of skeletal muscle. Cardiac muscle cells are provided with a complex control system which modulates the pumping of the heart to meet constantly changing demands of the body. Neither the initiation nor the conduction of the signal which activates the heart involves the central nervous system. Specialised heart cells initiate an electrical signal, the *action potential*, which is then propagated throughout the heart by other myocardial cells that are specialised for conduction. The nervous system plays a regulatory role in the function of the heart, increasing and decreasing various aspects of cardiac function.

2.1.1 Anatomy

The heart consists of four pumping chambers, the left and right atria and the left and right ventricles (Figure 2.1). Between the cavities of the atria and the ventricles lie the atrioventricular valves: on the right the *tricuspid valve* and on the left the *mitral (bicuspid) valve*. The semilunar valves lie between the outflow tracts of each ventricle and the great arteries into which each ventricle ejects blood: forward flow out of the right ventricle into the pulmonary artery is through the pulmonic valve, and between the left ventricle and the aorta lies the aortic valve.

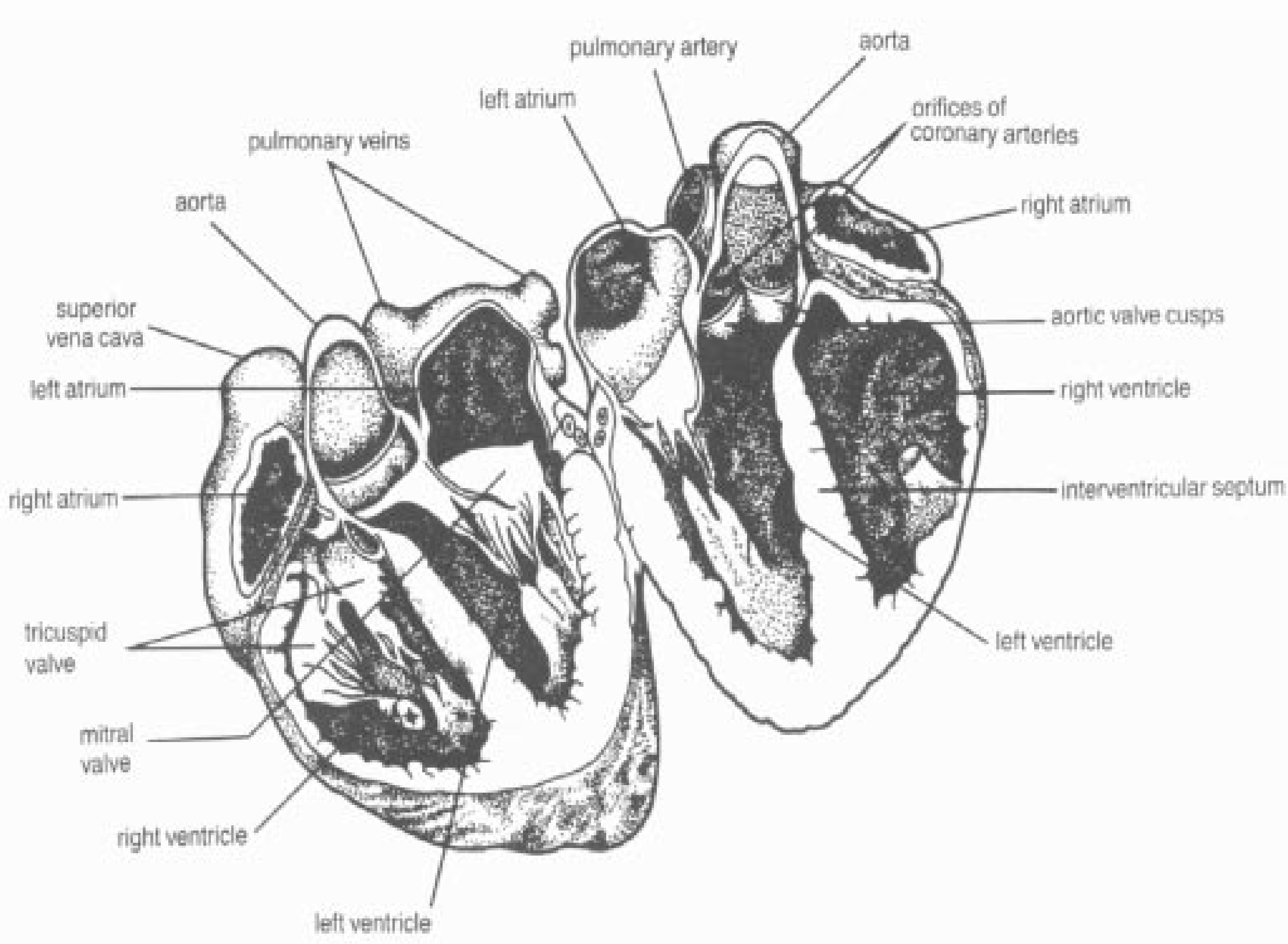

FIGURE 2.1: The heart transected slightly anterior to its midline. *From Katz (1992).*

It is essential to recognise that atrial myocardium is electrically isolated from that of the ventricles by a fibrous framework (the *"cardiac skeleton"*) formed by the rings (annuli) of the four valves and surrounding connective tissue (Figure 2.2). The *atrioventricular (AV) bundle*, normally the only electrically conducting pathway from the atria to the ventricles, penetrates the connective tissue in a somewhat precarious location - between the annuli of the mitral, aortic, and tricuspid valves. Damage to this critical conducting structure by abnormalities in these valves explains the common appearance of atrioventricular (conduction) block when these valve structures are abnormal in both congenital and acquired heart disease (Katz 1992).

The atria are thin walled chambers, as is appropriate for the low pressures found in the atria. The walls of the atria are irregular in thickness, with ridges of myocardium (*pectinate muscles*, (Figure 2.3)). These structures probably account for the rapidly conducting pathways

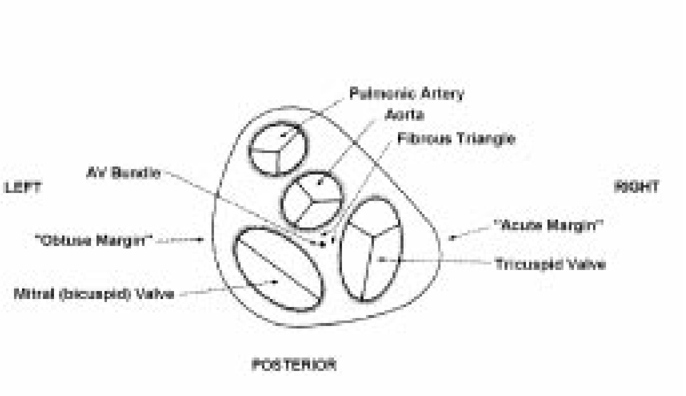

FIGURE 2.2: Schematic diagram of the fibrous skeleton of the heart, viewed from above with the atria removed. The sketch shows the more rounded shape of the left cardiac border (obtuse margin) than the right (acute margin). *From Katz (1992).*

(*internodal tracts*) found in the wall of the atria (Katz 1992). The ventricles, on the other hand, produce much greater pressures which necessitates thicker walls. This is especially true of the left ventricle which reaches a maximum pressure of approximately $15.3\ \mathrm{kPa}$ compared to the $2.3\ \mathrm{kPa}$ of the left atria (Berne & Levy 1993), giving the left ventricle three times the mass and two times the thickness of the right ventricle.

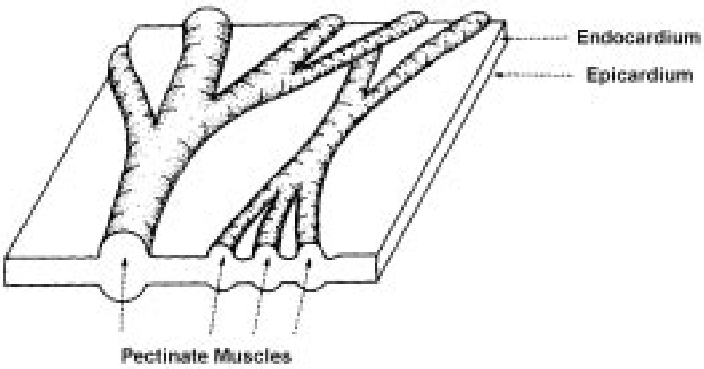

FIGURE 2.3: Schematic drawing of a cross-section of the atrial wall showing the pectinate muscles, which lie on the endocardial side of the atrial wall. *From Katz (1992).*

The cavity of the left ventricle resembles an elongated cone with both the inflow and outflow tracts adjacent to each other at the wider end of the left ventricular cavity (Figure 2.4). The right ventricle on the other hand, has a cresentic cross-section with inflow and outflow tracts separated so the right ventricular cavity forms a shallow $\bigcup$ (Figure 2.4). This adaptation of form to function can be understood in terms of the different pressures developed by the two ventricles.

The depiction of the left and right ventricles as distinct structures (Figure 2.4) should not be

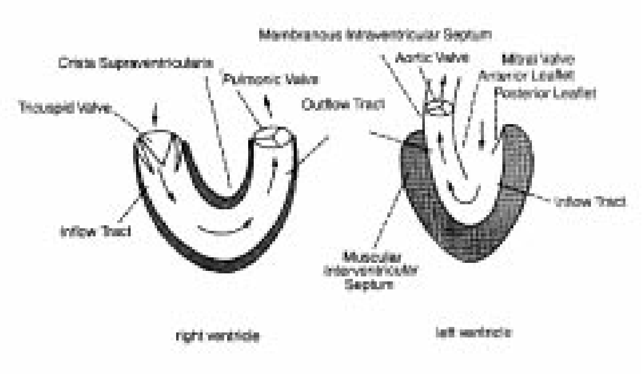

FIGURE 2.4: Right and left ventricular chambers, showing the elongated right ventricular cavity, and the narrower, more conical, pumping chamber of the left ventricle. *From Katz (1992).*

interpreted to mean that these two pumping chambers function independently. Important interactions between the ventricles occur in normal and diseased hearts. Usually the interventricular septum is functionally a part of the left ventricle, and it moves toward the left ventricular free wall during systole. However, with chronic right ventricular overload, as occurs in pulmonary hypertension, the septum can move paradoxically as part of the right ventricle, away from the left ventricular cavity during systole.

Inner surfaces of the atria and ventricles are covered with connective tissue, the *endocardium*, which also extends over the valves. The cell layer which lines the endocardium regulates transendocardial transport; these cells have also been suggested to produce chemical messengers, and possibly also to serve as a sensor for change in atrial and ventricular volume.

The outer surface of the heart is covered by the *epicardium*, or *visceral pericardium*, which is continuous with the *parietal pericardium* at the base of the heart, where the great vessels enter and leave. The pericardial cavity is therefore lined by a continuous layer of connective tissue that covers both the epicardial surface of the heart and the inner surface of the pericardial sac.

Ventricular *myocardium*, which lies between the epicardium and endocardium, consists of a series of overlapping sheets of muscle bundles (Figure 2.5) that arise from the fibrous skeleton at the base of the heart. These sheets of myocardium follow spiral paths as they sweep from the base to the apex of the heart. Ventricular muscle fibres tend to be oriented at an angle of 90° at the endocardial surface, circumferential at midwall, and at 60° at the epicardial surface (Figure 2.6). Analysis of the contraction patterns at different levels within the left ventricular wall support the view that the contracting ventricle resembles a series of concentric shells that, while thickening as they shorten, undergo only minor angular distortion.

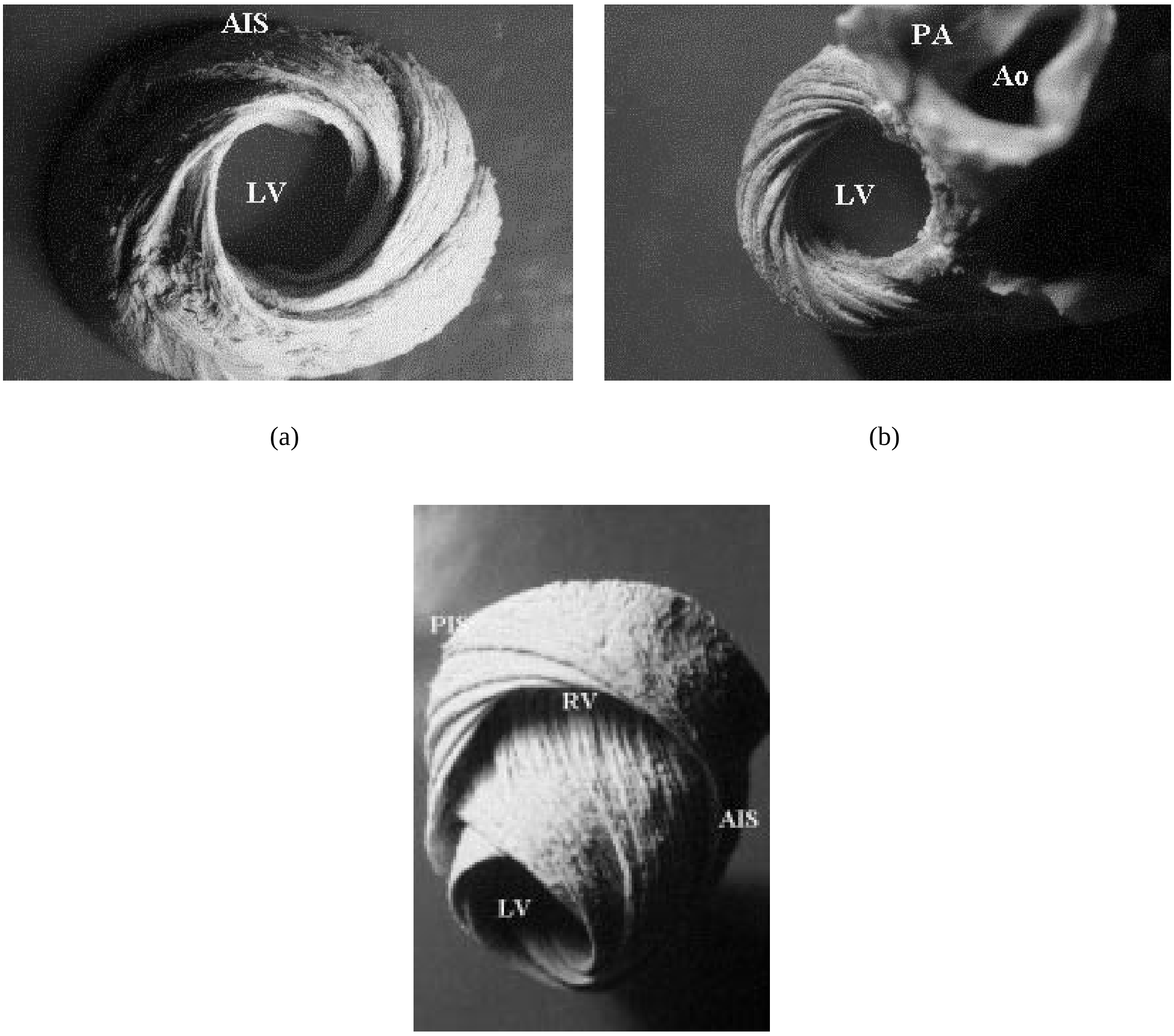

(a) (b)

(c)

FIGURE 2.5: Spiral musculature of the myocardium, illustrating the varying fibre angles throughout the heart. AIS, anterior interventricular sulcus; AO, aorta; LV, left ventricular cavity; PA, pulmonary artery; PIS, posterior interventricular sulcus; RV, right ventricular cavity. *From Torrent-Guasp (1996).*

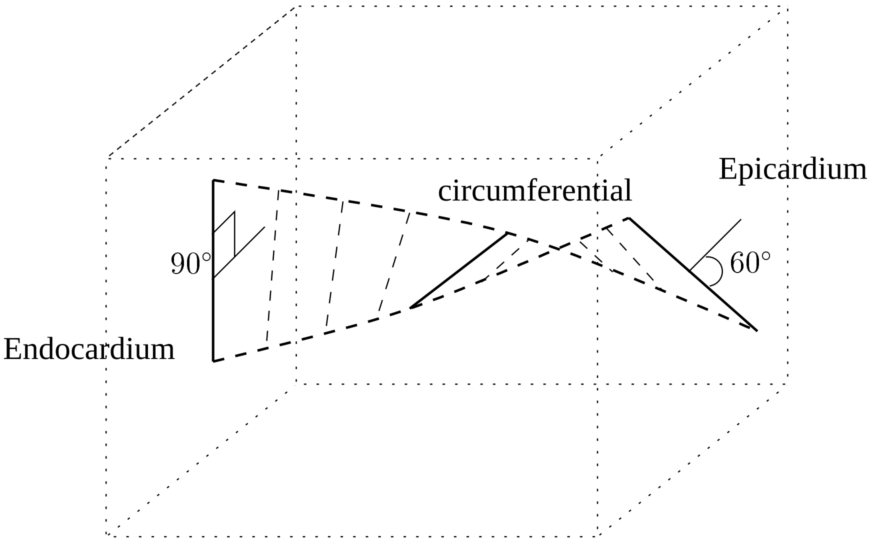

FIGURE 2.6: Schematic of a section removed from the ventricular wall. Illustrates the changing fibre angles when moving from the endocardium through the midwall to the epicardium.

2.1.2 Natural excitation of the heart

As mentioned previously, the nervous system has a regulatory role in the behavior of the heart, controlling such aspects as the frequency and vigor of each contraction. However, cardiac function does not require intact nervous pathways. Indeed a patient with a completely denervated heart (*e.g.*, a cardiac transplant patient) can function well and adapt to stressful situations (Berne & Levy 1993).

The properties of *automaticity*, the ability to initiate its own beat, and *rhythmicity*, the regularity of such pacemaking activity, are intrinsic to cardiac tissue. The region of the mammalian heart that ordinarily generates impulses at the greatest frequency is the *sinoatrial (SA)* node; it is called the natural pacemaker of the heart.

Detailed mapping of the electrical potentials on the surface of the right atrium has revealed that two or three sites of automaticity, located 1 or $2\ \mathrm{cm}$ from the SA node itself, serve along with the SA node as an atrial pacemaking complex. At times all of these loci initiate impulses simultaneously. At other times the site of earliest excitation shifts from locus to locus, depending on such conditions as the level of autonomic neural activity.

Other regions of the heart that initiate beats under special circumstances are called *ectopic foci*, or *ectopic pacemakers*. Ectopic foci may become pacemakers when (1) their own rhythmicity becomes enhanced, (2) the rhythmicity of higher order pacemakers becomes depressed, or (3) all conduction pathways between the ectopic focus and those regions with greater rhythmicity become blocked.

When the SA node and the other components of the atrial pacemaking complex are excised or destroyed, pacemaker cells in the AV junction usually are the next most rhythmic, and they become the pacemakers for the entire heart. After some time, which may vary from minutes to days, automatic cells in the atria usually become dominant. Purkinje fibres (see 13), in the specialised conduction system of the ventricles, also possess automaticity. Characteristically they fire at a very slow rate. When the AV junction becomes unable to conduct cardiac impulses from the atria to the ventricles, such idioventricular pacemakers in the Purkinje fibre network initiate the ventricular contractions. Such ventriclar contractions occur at a frequency of only $30\text{–}40\ \mathrm{beats/min}$.

Atrial conduction

From the SA node, the cardiac impulse spreads radially throughout the right atrium (Figure 2.7) along ordinary myocardial fibres, at a conduction velocity of approximately $1\ \mathrm{m} \cdot \mathrm{s}^{-1}$. A special pathway, the anterior interatrial myocardial band (or *Bachmann's bundle*), conducts the impulse from the SA node directly to the left atrium. Three tracts, the anterior, middle, and posterior internodal pathways, have been described. The tracts consist of a mixture of ordinary myocardial cells and specialised conducting fibres. Some authorities assert that these pathways constitute the principal routes for conduction of the cardiac impulse from the SA node to the AV node.

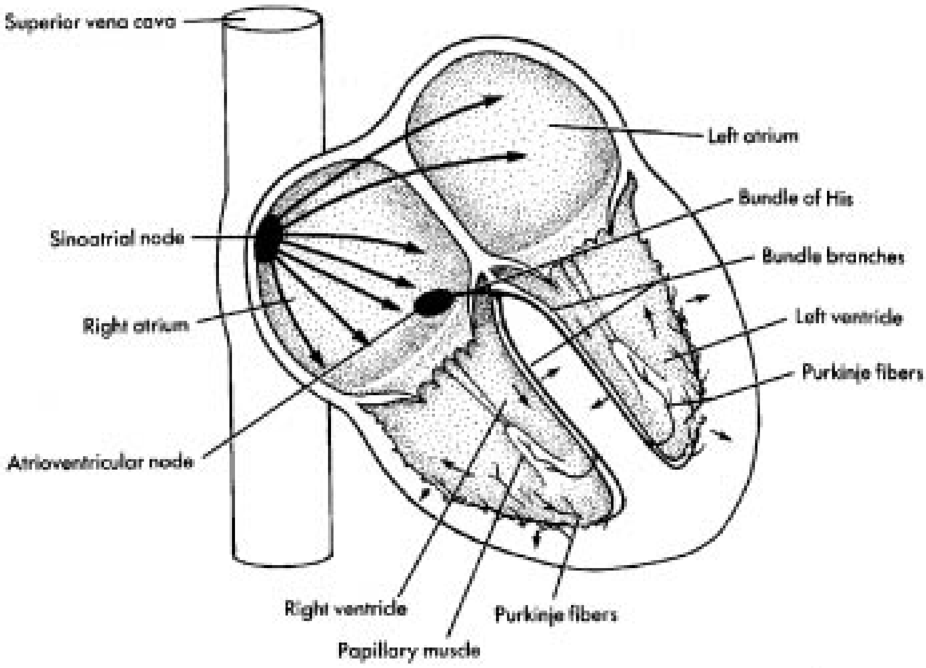

FIGURE 2.7: Schematic representation of the conduction system of the heart. *From Berne & Levy (1993).*

The configuration of the atrial transmembrane potential is depicted in (Figure 2.8, (c)). Compared with the potential recorded from a typical ventricular fibre (see Figure 2.8, (a)), the plateau (phase 2) is less well developed and repolarisation (phase 3) occurs at a slower rate.

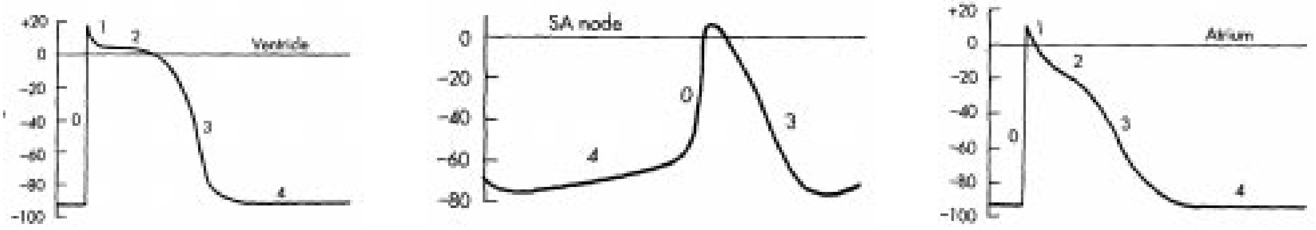

(a) (b) (c)

FIGURE 2.8: Typical action potentials (in millivolts) recorded from cells in the ventricle, (a), SA node, (b), and atrium, (c). Sweep velocity in (b) is one half that in (a) or (c). *From Berne & Levy (1993).*

Atrioventricular conduction

The cardiac action potential proceeds along the internodal pathways in the atrium and ultimately reaches the AV node. This node is approximately $22\ \mathrm{mm}$ long, $10\ \mathrm{mm}$ wide, and $3\ \mathrm{mm}$ thick in adult humans (Berne & Levy 1993). It is situated posteriorly on the right side of the interatrial septum near the ostium of the coronary sinus. The AV node contains the same two cell types as the SA node, but the round cells are more sparse and the elongated cells preponderate.

The AV node is separated into three functional regions: (1) the AN region, the transitional zone between the atrium and the remainder of the node; (2) the N region, the midportion of the AV node; and (3) the NH region, the zone in which the nodal fibres gradually merge with the *bundle of His*, which is the upper portion of the specialised conduction system for the ventricles. Normally the AV node and the bundle of His constitute the only conduction pathway from the atria to the ventricles. Accessory AV pathways are present in some people, however. Such pathways often serve as part of a reentry loop, which could lead to serious cardiac rhythm disturbances in these patients.

Several features of AV conduction are of physiological and clinical significance. The principal delay in passage of the impulse from the atria to the ventricles occurs in the AN and N regions of the AV node. Conduction velocity is less in the N region than the AN region, while the path length is substantially greater in the AN than the N region. The conduction time through the AN and N zones account for the delay between the onset of the P wave (the electrical manifestation of the spread of atrial excitation) and the QRS complex (spread of ventricular excitation) in the electrocardiogram (Figure 2.9). Functionally this delay between atrial and ventricular excitation permits optimal ventricular filling during atrial contraction.

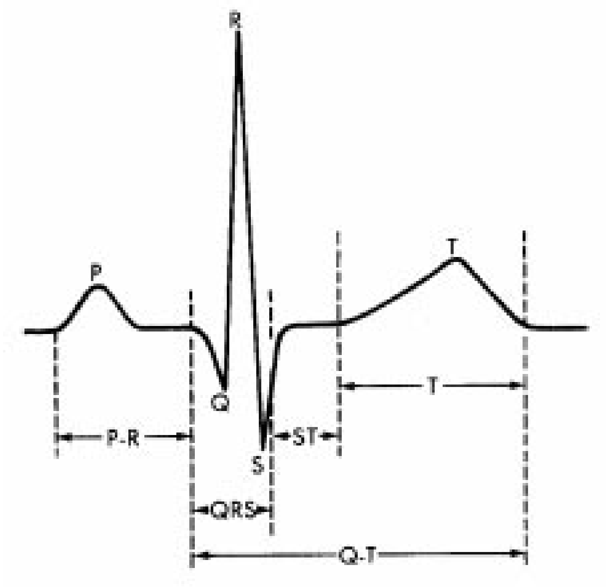

FIGURE 2.9: Configuration of a typical scalar electrocardiogram, illustrating the important deflections and intervals. *From Berne & Levy (1993).*

Ventricular conduction

The bundle of His passes subendocardially down the right side of the interventricular septum for about $1\ \mathrm{cm}$ and then divides into the left and right bundle branches (Figure 2.7). The right bundle branch is a direct continuation of the bundle of His and it proceeds down the right side of the interventricular septum. The left bundle branch, which is considerably thicker than the right, arises almost perpendicularly from the bundle of His and perforates the interventricular septum. On the subendocardial surface of the left side of the interventricular septum the main left bundle branch splits into a thin anterior division and a thick posterior division.

The right bundle branch and the two divisions of the left bundle branch ultimately subdivide into a complex network of conduction fibres called Purkinje fibres, which ramify over the subendocardial surfaces of both ventricles.

Purkinje fibres are the broadest cells in the heart, 35–$40\ \mu\mathrm{m}$ in diameter, compared with 10–$15\ \mu\mathrm{m}$ for ventricular myocardial cells (Opie 1984). The larger diameter accounts in part for the greater conduction velocity in Purkinje then myocardial fibres. Purkinje cells have abundant, linearly arranged sarcomeres, just as do myocardial cells. However the T-tubule system is absent in the Purkinje cells of many species, but is well developed in myocardial cells.

The conduction of the action potential over the Purkinje fibre system is the fastest of any tissue within the heart; estimates vary from 2 to $4\ \mathrm{m} \cdot \mathrm{s}^{-1}$. This permits a rapid activation of the entire endocardial surface of the ventricles.

Action potentials recorded from Purkinje fibres resemble that of ordinary ventricular myocardial fibres (see Figure 2.8, (a)). In general phase 1 is more prominent in Purkinje fibre action potentials than in those recorded from ventricular fibres (especially endocardial fibres) and the duration of the plateau (phase 2) is longer.

Due to the long refractory period of Purkinje fibres, many premature activations of the atria are conducted through the AV junction but are blocked by the Purkinje fibres. Therefore they fail to evoke a premature contraction of the ventricles.

The first portions of the ventricles to be excited are the interventricular septum (except the basal portion) and the papillary muscles. The wave of activation spreads into the substance of the septum from both its left and right endocardial surfaces. Early contraction of the septum tends to make it more rigid and allows it to serve as an anchor point for the contaction of the remaining ventricular myocardium. Also early contraction of the papillary muscles prevents eversion of the AV valves during ventricular systole.

The endocardial surfaces of both ventricles are activated rapidly, but the wave of excitation spreads from endocardium to epicardium at a slower velocity (about 0.3–$0.4\ \mathrm{m}\cdot\mathrm{s}^{-1}$). Because the right ventricular wall is appreciably thinner than the left, the epicardial surface of the right ventricle is activated earlier than that of the left ventricle. Also apical and central epicardial regions of both ventricles are activated somewhat earlier than their respective basal regions. The last portion of the ventricles to be excited are the posterior basal epicardial regions and a small zone in the basal portion of the interventricular septum.

2.2 Introduction to Cell Physiology

2.2.1 Cellular membranes and transmembrane transport of solutes and water

Membranes, consisting of phospholipids and proteins, separate the *cytosol*, or intracellular space, from the extracellular fluid and enclose the various organelles of the cell. The selective permeabilities of membranes maintain the compartmentation of the cell and the organelles. While lipid-soluble solutes and very small water-soluble substances can cross membranes by simple diffusion and water can move across by osmosis, larger water-soluble molecules require the mediation of particular membrane transport proteins. For example, the transport of Na^{+} out of the cell by the Na^{+},K^{+}-ATPase plays an important role in maintaining the osmotic balance over the cell.

Protein-mediated transport may occur by *facilitated transport* or by *active transport*. Facilitated transport can only transport a substance down its concentration gradient, while active transport is linked to metabolic energy and can transport a solute against its concentration gradient. *Primary active proteins* are directly linked to metabolic energy, most commonly by the phosphorylation by ATP, and *secondary active transport* is driven by the concentration gradient of another actively transported solute, most frequently Na^+ ions (Berne & Levy 1993).

Ion-transporting ATPases play a central role in the economy of the cell, with the $\mathrm{F}_1\mathrm{F}_2$ ATPase of mitochondria being the major source of ATP. The exchange of ions across the plasma membrane is mediated by the members of a family of ion exchange proteins, among which are the Na^+,Ca^{2+} exchanger, the Na^+,H^+ exchanger, and the anion exchanger. A family of glucose transporters promotes rapid cellular uptake of glucose from the extracellular fluid. In muscle and fat cells insulin markedly stimulates the uptake of glucose by fusing cytosolic vesicles, which contain preformed glucose transporters, with the plasma membrane (Berne & Levy 1993).

Plasma membranes contain three or more different transporters that mediate the uptake of neutral amino acids and separate transport proteins for basic and acidic amino acids. Some are facilitated transporters, whereas others can actively accumulate amino acids powered by the energy of the Na^+ gradient.

2.2.2 Ionic equilibria and resting membrane potentials

When an ion is distributed in equilibrium across a membrane, any tendency of the ion to diffuse across the membrane caused by concentration difference is exactly balanced by the effect of the electrical potential difference across the membrane. The *Nernst equation* (Equation (2.1)) describes the relationship between the concentration ratio of an ion across a membrane and the electrical potential difference across the membrane when the ion is distributed in equilibrium.

$$\begin{aligned} E &= \frac{RT}{z_X F} \ln \frac{[\mathrm{X}]_o}{[\mathrm{X}]_i} \\ &= 2.303 \frac{RT}{z_X F} \log \frac{[\mathrm{X}]_o}{[\mathrm{X}]_i} \end{aligned} \tag{2.1}$$

Cells contain impermeant molecules with net negative charge. The *Gibbs-Donnan Equilibrium* defines the consequences of the fixed charge on the distribution of cations and anions that can permeate the plasma membrane. The activity of the Na^+,K^+-ATPase causes animal cells to have a higher intracellular concentration of K^+ and a lower intracellular concentration of Na^+ than the extracellular concentrations of these ions. Because the Na^+,K^+-ATPase is *electrogenic* (*i.e.*, 3 Na^+ out and 2 K^+, unbalanced charge transfer), it makes a direct contribution to the resting membrane potential of the cell.

Each ion that can permeate a membrane tends to bring the resting membrane potential toward its equilibrium potential, given by the Nernst equation (Equation (2.1)). The ability of an ion to do this increases as the permeability of the membrane to the ion increases. The *chord conductance equation* states that the resting membrane potential is a weighted average of the equilibrium potentials of all permeant ions; the weighting factor for each ion is the fraction of the total ionic conductance of the membrane contributed by that ion.

2.2.3 Generation and conductance of action potentials

A hyperpolarisation or a subthreshold depolarisation of an axon or skeletal muscle fibre is conducted with decrement along the length of the cell. The distance, typically $1–2\ \mathrm{mm}$, over which the conducted signal decreases to $1/\mathrm{e}$ (about 38%) of its maximum strength, is called the *length constant* of the cell.

Depolarisation of an electrically excitable cell to threshold elicits an action potential, and the action potential is propagated over the entire plasma membrane of the cell without a significant decrease in its strength (Berne & Levy 1993). Action potentials are caused by the opening and closing of particular populations of voltage gated ion channels in the plasma membrane of an excitable cell. Cell types that have different types of ion channels have action potentials that differ in shape and time course (for examples, see Figure 2.8). In nerve and skeletal muscle cells action potentials are initiated by a rapid opening of fast Na^+ channels, which causes the depolarising phase of the action potential (see phase 0 in Figure 2.8). The depolarisation brings about voltage-inactivation of the Na^+ channels followed by delayed opening of K^+ channels, which cause repolarisation of the cell (see phase 0 in Figure 2.8).

An ion channel typically oscillates irregularly between a low conductance state and a high conductance state. For a voltage gated ion channel the probability that the channel is in the high conductance state is a function of the membrane potential. The voltage gated ion channels for Na^+, K^+, and Ca^{2+} are members of a family of structurally related proteins. The Na^+ and Ca^{2+} channel proteins have four repeated motifs, each with six transmembrane helices. The ion channel is apparently lined by the relatively hydrophilic faces of one helix from each motif (Berne & Levy 1993). The K^+ channel protein has only one of the motifs that is repeated in the Na^+ and Ca^{2+} channels; four of the K^+ channel proteins are required to form on K^+ channel.

Three types of voltage gated Ca^{2+} channels have been identified L-type (long lasting), T-type (transient), and N-type (neuronal). These channels differ in their voltage dependence, single channel conductance, and time course. The L-type Ca^{2+} channels are blocked by three different classes of Ca^{2+} channel blocking drugs. Action potentials in cardiac muscle cells have a plateau phase caused by the movement of Ca^{2+} through the L-type Ca^{2+} channels. In cardiac and smooth muscle cells the Ca^{2+} that enters the cytosol via these channels during the action potential plays an important role in excitation-contraction coupling.

During most of the action potential spike, the cell is absolutely refractory to further stimulation. This is caused by voltage-inactivation of such a large fraction of Na^+ channels that a sufficient number cannot be recruited to fire another action potential.

An action potential or subthreshold perturbation of the membrane potential is conducted by the local circuit currents, a mechanism called *electrotonic conduction*. The rate of electrotonic conduction is determined by the electrical properties of the plasma membrane and the cytosol, namely by the capacitance and resistance of the membrane and by the longitudinal resistance of the cytosol. For example, large diameter axons conduct more rapidly than do thin axons, and a myelinated axon conducts more rapidly than an unmyelinated axon that is 100 times larger in diameter.

The propagation of an action potential along a myelinated axon occurs by sultatory conduction. The action potential jumps (is conducted rapidly and with little decrement) from one node of Ranvier to the next and the action potential is regenerated at each node of Ranvier.

2.2.4 Contractile mechanism of muscle cells

The basic contratile unit is the *sarcomere*, which consists of a centrally located array of *thick filaments* that interdigitate with *thin filaments* attached to *Z disks* at each end of the sarcomere (Figure 2.10). *Myofibrils* contain many sarcomeres in series, and cells contain large numbers of myofibrils in parallel (Figure 2.10).

In vertebrate striated muscle, thin filaments consist of polymers of *actin* and *tropomyosin*, plus the Ca^{2+}-binding regulatory protein, *troponin* (Figure 2.16). Thick filaments are composed of *myosin* (Figure 2.17). The “head” regions of individual myosin molecules project laterally from the filament. These projections contain the actin- and ATP-binding sites and form *cross-bridges*.

A high free energy state of the cross-bridges occurs after ATP binding and hydrolysis to form the $\mathrm{myosin} - \mathrm{ADP} - \mathrm{P_i}$ complex, which has a high affinity for actin. This cross-bridge state rapidly binds to the thin filament in a preferred 90 degree conformation. However, release of bound $\mathrm{P_i}$ and ADP leads to a complex whose minimum free energy occurs after a conformational change to 45 degrees. This conformational change produces a force on the thin filament and movement toward the centre of the sarcomere. ATP binding reduces the affinity of myosin for actin, the cross-bridge detaches, and ATP is split to regenerate the high free energy, 90 degree $\mathrm{myosin} - \mathrm{ADP} - \mathrm{P_i}$ complex and completes the *cross-bridge cycle* (see Section 2.3.4 for a more complete description of the cross-bridge cycle). In relaxed muscles the cross-bridge cycle is interrupted in the detached, high energy state by regulatory mechanisms that are controlled by Ca^{2+}. The fall in cell content of ATP after death leads to accumulation of low energy actin-myosin complexes and stiffness or muscular rigidity, termed *rigor mortis*.

Contracting muscles often lengthen when opposing forces are very high, This situation is termed *negative work*, because work is done on, rather than by, the muscle. Stresses on muscle, tendons, or skeleton can be very high under such conditions, because cross-bridges can transiently bear loads that are about 1.6 times higher than they develop isometrically (Berne & Levy 1993). Velocity depends on the number of sarcomeres in a cell. Sarcomere shortening velocities are a function of cross-bridge cycling rates and load. Maximum cycling rates at zero load are determined by the isoform of myosin expressed in a cell.

2.3 Cardiac Cell Physiology

This section is intended to give the reader a detailed description of the physiological processes and structures involved in the activation and contraction of a general cardiac myocyte. It is intended to follow the process illustrated in Figure 2.10, giving enough detail at each step to enable the reader to fully comprehend the physiological problem this research is modelling.

Figure 2.10 illustrates the current view of the cardiac myocyte activation-contraction cycle. This view is that the changing concentration of calcium ions (Ca^{2+}) in the myocardial cell plays a predominant role in the physiological regulation of cardiac contraction. Calcium ions are shown entering via the plateau phase of an action potential (*i.e.,* the L-type Ca^{2+} current mentioned in Section 2.2.3) which travels along the *sarcolemma* (complex membrane which forms the boundary of a myocyte) to "trigger" the release of more calcium from the sarcoplasmic reticulum (SR) and thereby to initiate a contraction-relaxation cycle (see Figure 2.11 for the relative timing of these events). The small amount of Ca^{2+} that enters the cell will eventually leave predominantly by a sodium-calcium mechanism and, to a lesser extent, the sarcolemmal calcium pump.

2.3.1 General organisation

To understand the concept of Ca^{2+} fluxes into and within the myocyte explaining most aspects of the contractile behaviour of the heart, prior knowledge of the organisation, structure, and function of the myocyte (Table 2.1) is required.

Myocytes, which account for more than half of the heart's weight, are roughly cylindrical in shape (Figure 2.10). The cells in the atrium are relatively small, less than $10\ \mu\mathrm{m}$ in diameter and approximately $20\ \mu\mathrm{m}$ in length, compared to those in the ventricles which are 10–$25\ \mu\mathrm{m}$ in diameter and 50–$100\ \mu\mathrm{m}$ in length (Table 2.2).

Each myocyte is bounded by a complex membrane (the sarcolemma) and is filled with bundles of myofibrils, which are the contractile elements of the cell. The sarcolemma invaginates to form an extensive tubular network (T-tubules) which extends the extracellular space into the interior of the cell. The nucleus, which contains almost all of the cell's genetic information,

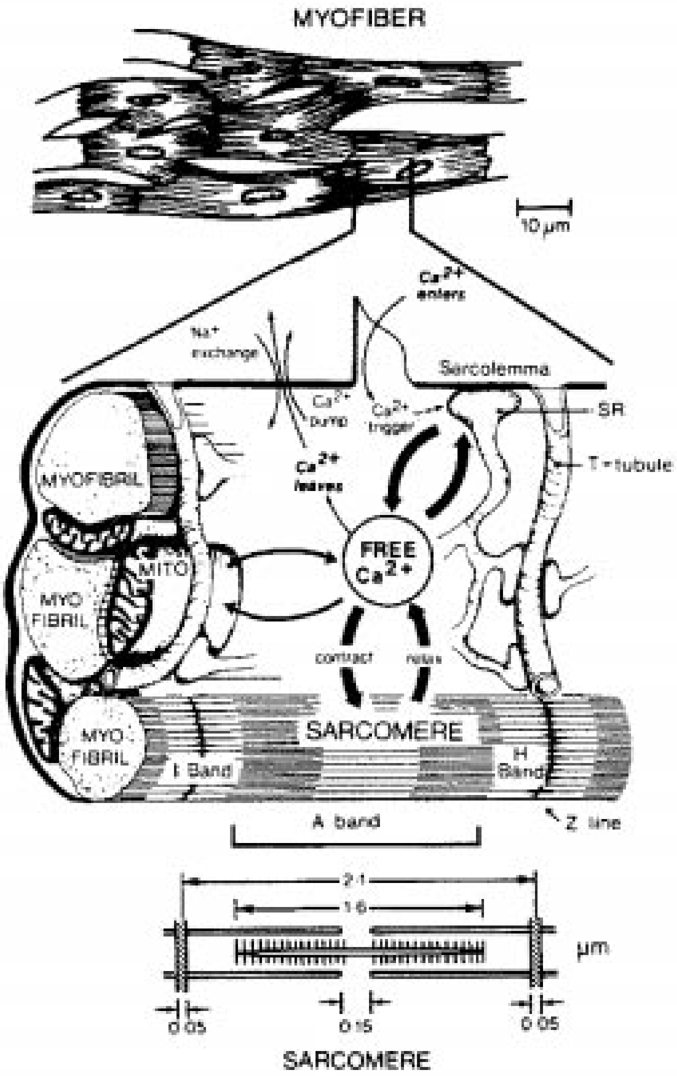

FIGURE 2.10: Overview of a cardiac myocyte illustrating the process and structures involved in activation and contraction of the myocyte. *From Opie (1984).*

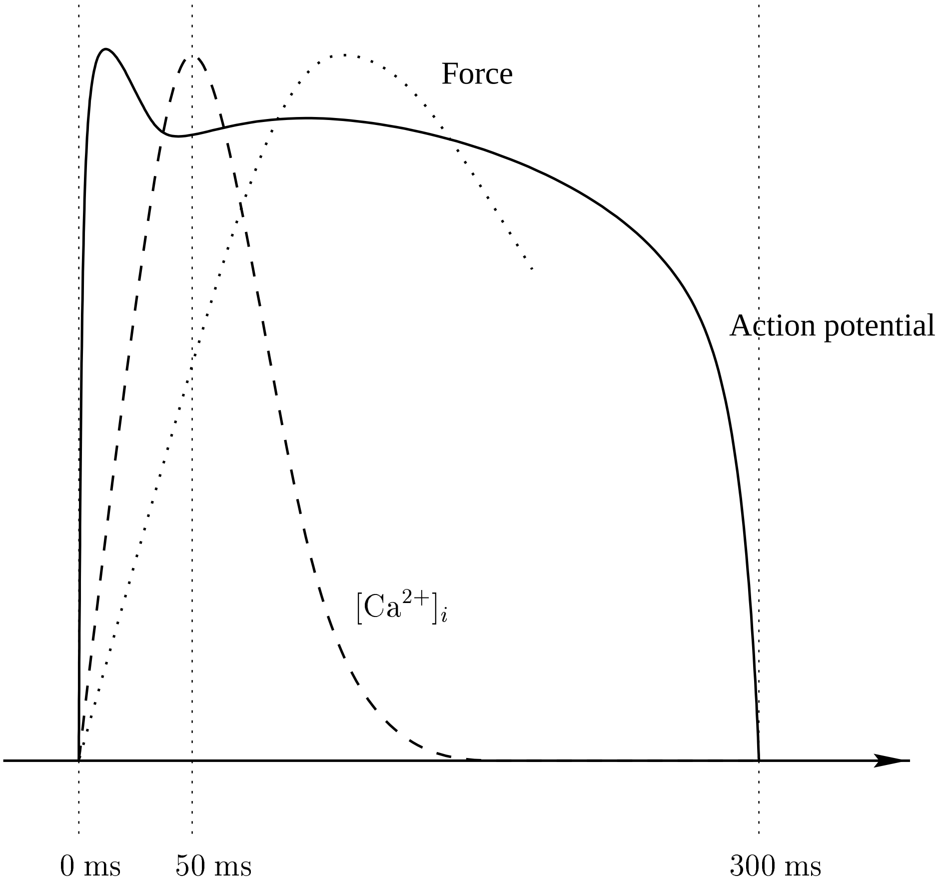

FIGURE 2.11: The relative timing of the action potential, the intracellular calcium ion concentration ($[\mathrm{Ca}^{2+}]_i$), and the force developed.

Organelle	Percent of cell volume	Function
Myofibril	About 50%	Interaction of thick and thin filaments during contraction cycle
Mitochondria	16% in neonate, 33% in adult	Provide ATP, chiefly for contraction
T-system	1%	Transmission of electrical signal from sarcolemma to cell interior
Sarcoplasmic reticulum	33% in neonate, 2% in adult	Takes up and releases Ca^{2+} during contraction cycle
Junctional SR	0.33% in adult	site of calcium storage and release
Network SR	Rest of volume	site of calcium uptake *en route* to cisternae
Sarcolemma	Very low	Control of ionic gradients, channels for ions (action potential), maintenace of cell integrity, receptors for drugs and hormones
Nucleus	5%	Protein synthesis
Lyosomes	Very low	Intracellular digestion and proteolysis
Sarcoplasm (cytoplasm)	12%	Provides cytosol in which rise and fall of ionised calcium occurs; contains other ions and small molecules

TABLE 2.1: Composition and function of a rat ventricular myocyte. *Modified from Opie (1984).*

	Ventricular myocyte	Atrial myocyte	Purkinje cells
Shape	Long and narrow	Elliptical	Long and broad
Length	50–100 μm	About 20 μm	150–200 μm
Diameter	10–25 μm	5–6 μm	35–40 μm
T-tubules	Plentiful	Rare or none	Absent
Intercalated disc	Prominent end-to-end transmission	Side-to-side as well as end-to-end transmission	Very prominent; abundant gap junctions. Fast end-to-end transmission
General appearence	Mitochondria and sarcomeres very abundant. Rectangular, branching bundles with little interstial collagen	Bundles of atrial tissue separated by wide areas of collagen	Fewer sarcomeres, more glycogen

TABLE 2.2: Micro-anatomy of heart cells. *Modified from Opie (1984).*

is centrally located; some myocytes have several nuclei. Interspersed between the myofibrils are the mitochondria, whose main function is the generation of the energy, in the form of ATP, required to maintain the heart's function and viability.

Purkinje cells are unusually large, being $35–40\ \mu\mathrm{m}$ in diameter and about $150–200\ \mu\mathrm{m}$ long (Table 2.2), making them about three times wider than ventricular myocytes and about eight times wider than atrial myocytes. The individual Purkinje cells are packed tightly together, with each cell abutting closely against its neighbour. This tight packing, combined with the relatively few connections between cells and the absence of T-tubules, results in minimal longitudinal resistance. The rate of longitudinal conduction is also enhanced by the frequency of the junctions spanning the interrelated discs (gap junctions). This explains the role of Purkinje fibres in ventricular activation (Section 2.1.2).

About 40% of the heart is not occupied by myocytes or pacemaker and conducting tissue. This extracellular space contains blood vessels, interstitial fluid, fibroblasts, some collagen and ground substances which consist mainly of proteoglycans. These last are very large, aggregated molecules in which long carbohydrate chains (bearing negative sulphate and carbohydrate charges) are attached to a protein "core"; this molecular structure helps to hold the heart together. The ionic composition of the interstitial fluid differs markedly from the intracellular fluid. The intracellular fluid (cytosol) is rich in K^+ and low in Na^+, while the opposite is true for interstitial fluid that bathes the cell. The maintenance of the ionic gradients that result from this distribution of ions between the inside and outside of the cells depends on a number of factors. ATP, a high energy phosphate, is required for the various pumps that drive ions against their respective concentration gradients (*e.g.,* the Na^+,K^+-ATPase , which moves K^+ into and Na^+ out of the cell). Also contributing to the ability of cell membranes to maintain ionic gradients is the correct orientation of their phospholipids and proteins. This orientation is lost when cells are exposed to detergents or to certain naturally occurring toxins. The membranes then become much more permeable and ions move along their concentration gradients; the cells become overloaded with sodium and calcium and lose potassium, just as when an *ischaemic* (lack of blood flow to the tissue) episode precipitates a decline in the tissue levels of ATP.

2.3.2 Pumps, channels, and currents

As with most cells, the sarcolemma consists of a lipid bilayer which provides both the structural framework of the myocyte and maintains a permeability barrier. As the wave of electrical excitation speeds throughout the ventricular myocardium, the sarcolemma becomes highly permeable to a number of ions by the opening of "channels" which allow ions to flow across the sarcolemma. Such ionic movements occur in a characteristic sequence – first Na^+, then Ca^{2+}, and then K^+– determining the typical shape of the ventricular action potential. The distribution of ions across the sarcolemma, when there is excitation during diastole, must be examined to understand the normal electrical properties of the ventricular cells.

Resting membrane potential

In the normal resting myocardial cell, there is a difference in the electrical charges within and without the sarcolemma, which can readily be measured by insertion of a fine tipped microelectode. The charges inside and outside the cell are different so that the *resting membrane potential* is about $-85\ \mathrm{mV}$ less inside the cell (*i.e.,* the potential difference across the sarcolemma is $-85\ \mathrm{mV}$). During electrical activation, this "polarity" of charges existing across the sarcolemma is lost. The cell now becomes depolarised; the juxtaposition of depolarised and polarised sarcolemma allows current to flow inwards to the polarised negative part of the cell, opening the sodium and other channels by the process of voltage-activation. The voltage is the electrical force moving the current.

Hypothetically, a "resting" cell could have equal concentrations of the principal charge-bearing ions (Na^+, K^+, Cl^-) on either side of the sarcolemma, and a low concentration of anions associated with the intracellular proteins on the inside. The activity of the Na^+,K^+-ATPase transfers K^+ into and Na^+ out of the cell. Now there are potassium ions accumulating on the inner surface of the sarcolemma trying to diffuse out along their concentration gradient, while sodium ions are accumulating on the outer surface of the sarcolemma trying to diffuse into the cell along their concentration gradient. Since the resting sarcolemma is approximately 50 times less permeable to sodium than to potassium, there are many more potassium ions flowing out the cell than there are sodium ions flowing into the cell. This results in a net negative charge inside the cell relative to the extracellular space, due to the diffusion of potassium ions out of the cell. The equilibrium potential for K^+ can be calulated using the Nernst equation (Equation (2.1)), and is found to be close to the measured resting potential of $-85\ \mathrm{mV}$. Thus, the resting membrane potential is largely set by the equlibrium potential of potassium ions.

Sodium-potassium pump

The sodium-potassium pump (Na^+,K^+-ATPase ; also called the sodium pump) shunts sodium out of the cell and potassium into the cell against the electrochemical gradients. The enzyme is activated by intracellular sodium and/or extracellular potassium and uses energy in the form of ATP complexed to magnesium.

$$\begin{aligned}
3(\mathrm{Na}^+)in &\rightarrow 3(\mathrm{Na}^+)out\\
2(\mathrm{K}^+)out &\rightarrow 2(\mathrm{K}^+)in\\
\mathrm{MgATP}^{2-} + \mathrm{H_2O} &\rightarrow \mathrm{MgADP}^{-} + \mathrm{P_i}^{2-} + \mathrm{H}^+
\end{aligned}$$

One ATP molecule is used per transport cyle, which adequately covers the energy requirements of the pump. One positive charge leaves the cell for each three sodium ions exported so that the pump is electrogenic, tending to make the inside of the cell negatively charged. The pump probably contributes about $-10\ \mathrm{mV}$ to the resting membrane potential (Opie 1984). The sodium pump indirectly extrudes calcium ions from the cell by removing those intracellular sodium ions which entered as calcium ions leave via the Na^+,Ca^{2+} exchanger.

Calcium pumps

Cardiac cells contain a number of calcium pumps, with one being located in the membrane of the SR and another located in the sarcolemma. These pumps require energy to transport calcium ions against the large concentration gradients that exist between the relatively low intracellular concentration of calcium ions and the much higher values in the SR or the extracellular space. The SR requires so much pumping activity to take up the calcium ions from the cytosol that the membrane of the SR has been described as a "batery of pumps". Calcium pumps are activated by a membrane protein called *phospholamban* which requires a phosphate group for its maximal activity. Such phosphorylation is achieved either by (i) the effect of catecholamine stimulation or (ii) an increased cytosolic calcium ion concentration, acting by combination with the calcium modulator compund, *calmodulin*. Therefore the systolic rise of calcium ions will stimulate the uptake of calcium into the SR to help initiate diastole. Catecholamine stimulation will accelerate the uptake of calcium ions into the SR to shorten diastole and to accelerate relaxation so the heart can fill more rapidly.

Sodium channel

The normal negative resting membrane potential of atrial and ventricular myocytes is abruptly lost when the sodium channels open to increase the permeability of sodium ions and to allow the rapid influx of sodium ions. Due to the speed at which the sodium channel acts, it is considered the fast action potential channel (Table 2.3). A working model of the sodium channel considers that there are several "gates" which open to "activate" the channel (activation gates). Sodium ions rapidly enter the cell when the activation gates are opened by a voltage stimulus (voltage-activation); these gates close with full depolarisation. There are other gates, the inactivation

Property	Fast action potential	Slow action potential
Ion specificity	Sodium	Calcium
Inhibitors	TTX, lidocaine, quinidine	Ca^{2+}-antagonists, l- more than d-verapamil
Physiological occurrence	Atrial, Purkinje, and ventricular tissue	Nodal and vascular tissue; as component of normal atrial, Purkinje, or ventricular action potential
Effect of beta-adrenergic receptor stimulation	No effect	Enhances Ca^{2+} entry by "opening" channels
Threshold of activation	-60 to $-70\,\mathrm{mV}$	-30 to $-40\,\mathrm{mV}$
Resting membrane potential	-80 to $-90\,\mathrm{mV}$	-40 to $-70\,\mathrm{mV}$
Overshoot	$+20$ to $+35\,\mathrm{mV}$	0 to $+15\,\mathrm{mV}$
Maximal rate of depolarisation (phase 0)	100–1000 $\mathrm{V} \cdot \mathrm{s}^{-1}$	1–10 $\mathrm{V} \cdot \mathrm{s}^{-1}$
Type of conduction	Fast	Slow
Role in arrhythmias	Tachyarrythmias; ectopic activity; possibly in ischemia as "slow" fast responses	Slow conduction predisposes to re-entry ; possible additional role in "slow response", and in ventricular fibrillation

TABLE 2.3: Contrasting properties of fast and slow channels. *Modified from Opie (1984).*

gates, which are open at resting potential and begin closing when the membrane is depolarised.

Calcium channel

Although the extracellular calcium ion concentration is very much higher than the intracellular concentration, the concentration gradient is effectively maintained because the sarcolemma is virtually impermeable to calcuim. Calcium chiefly enters a myocyte through a very strictly controlled calcium channel, by the process of voltage activated "opening" of the channel. It is the opening of the sodium channel that changes the voltage to bring it into the range which opens tha calcium channel. The entry of calcium through the L-type Ca^{2+} channel is the critical event in triggering the release of calcium from the SR ("calcium induced calcium release") and hence contraction (Opie 1984, Berne & Levy 1993).

Potassium channels

As stated above, potassium ions are brought into the cytosol via the activity of the sodium pump. They then may leave the cell spontaneously by virtue of the high permeability of the sarcolemma to potassium. There is a background outward potassium current and other potassium currents which are involved in shaping the action potential (Table 2.4). The voltage induced decrease in potassium conductance is called *inward going rectification* (Figure 2.12). As the membrane voltage becomes more negative at the start of repolarisation, the potassium current again starts to flow to help terminate the action potential plateau by *delayed rectification* (Figure 2.12). To achieve such rectification, there is another predominantly potassium current, which is both time and voltage dependent, so that it is induced a certain time after the onset of depolarisation and at a certain voltage (Opie 1984). Noble originally called this the I_X current to emphasise the possible contributions of components other than potassium.

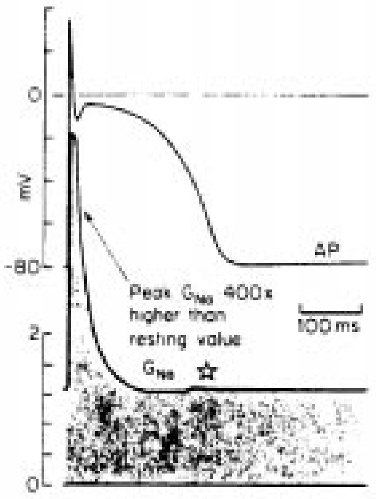

FIGURE 2.12: Computed Purkinje fibre action potential (in mV) and ionic conductances per uint area of membrane surface (in $10^{-4}\ \mathrm{S}\cdot\mathrm{cm}^{-2}$). G_{Na}: sum of rapid sodium conductance and background sodium conductance. The initial peak reaches $11\mathrm{x}10^{-2}\ \mathrm{S}\cdot\mathrm{cm}^{-2}$, *i.e.,* about 400 times the value shown here. This large magnification is used to higlight the G_{Na} “window” which occurs as a small hump ($\star$) on the background sodium conductance. *Modified from Opie (1984).*

It was thought that the outward-going potassium currents which help to terminate the action potential plateau might be triggered by the inward calcium current. However, the fact that the highly specific calcium channel blocker nisoldipine blocks the slow inward calcium current but does not reduce the potassium curent is a strong argument against this. Rather, the potassium rectifying current is voltage activated and therefore indirectly the result of the sodium and calcium ion movements occurring early in the action potential.

Ventricular action potential

The characteristic appearance of the ventricular action potential can now be interpreted in terms of opening and closing of sodium, calcium, and potassium channels with the resultant flow of

Current	Common abbreviation(s)	Qualities
Fast inward sodium current	I_{Na}	Abolished by tetrodotoxin (TTX); inhibited by Class I antiarrhythmic agents
Slow inward calcium current	$I_{Ca(L)}$	Important for plateau phase of cardiac action potential; involved in excitation-contraction coupling; inhibited by calcium-antagonist agents
Outward voltage and time dependent potassium current	I_K (I_{K_r} + I_{K_s})	Slow outward predominantly potassium current helps to terminate action potential plateau by delayed rectification; voltage dependent so that it increases as the membrane potential returns towards normal; time dependent so that it increases with time after the start of I_{Na}; Sometimes divided into fast (I_{K_r}) and slow (I_{K_s}) components; early fast component major component of delayed rectification in Purkinje fibres
Background potassium current	I_{K1}	Background outward current occurring throughout the cardiac cycle that lessens during depolarisation so that outward currents do not inhibit inward currents. Also called inward rectification current
Diastolic pacemaker current in Purkinje fibres	I_f	Inward "funny" sodium and potassium current may be responsible for initial phase of spontaneous depolarisation in Purkinje tissue. Replaces I_{K2}
Transient outward current	I_{to}	Transient outward early potassium current, previously called the chloride current (carries both K^+ and Na^+)

TABLE 2.4: Currents associated with the cardiac action potential. *Modified from Opie (1984).*

currents (Figure 2.13). The resting membrane potential of -70 to $-90\ \mathrm{mV}$ is largely due to the unequal distribution of potassium ions across the sarcolemma. The rapid phase of depolarisation of the action potential (phase 0) is the result of the opening of the sodium channels to allow the rapid influx of sodium which depolarises the cell. The wave of depolarisation changes the resting membrane potential to less negative values which open the sodium channel activation gates at -60 to $-70\ \mathrm{mV}$ and then almost immediately start to close the inactivation gates. Sodium conductance increases, as does the flow of the inward current I_{Na}, to peak rapidly within $1\ \mathrm{ms}$ and then rapidly falls off. The flash of inward sodium movement, carrying positive charges, continues to depolarise the cell to reach $0\ \mathrm{mV}$ with a small overshoot.

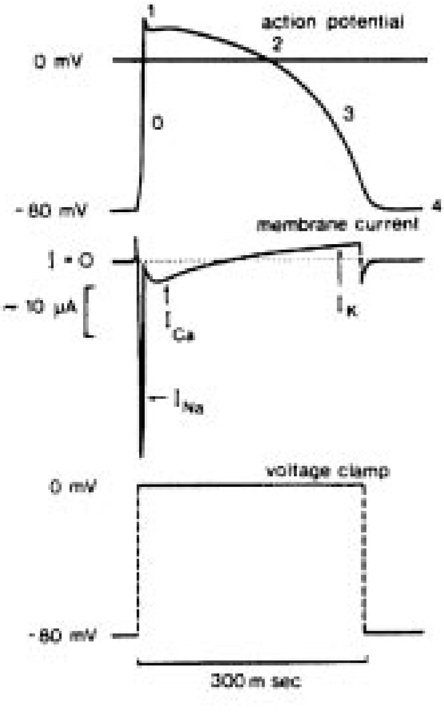

FIGURE 2.13: Schematic drawing of a ventricular cardiac action potential (top), of total membrane current flowing (middle), and of a voltage-clamp step from a holding potential of $-80\ \mathrm{mV}$ to $0\ \mathrm{mV}$ (bottom).*From Opie (1984).*

Meanwhile, the much slower calcium channel has already been opened at the time when the depolarisation process reached -30 to $-40\ \mathrm{mV}$ (Opie 1984). As the sodium current fades away, it is replaced by the slow inward calcium current, $I_{Ca(L)}$, which forms the plateau. Thus, from the peak depolarisation, the overshoot is lost (phase 1) (I_{to}) to form the relatively flat plateau (phase 2), which merges into the rapid repolarisation (phase 3).

Once the action potential is over, the resting membrane is restored and maintained. In contrast to this is the situation in nodal tissue (see Figure 2.8, (b)) where the resting membrane potential is much less negative and where spontaneous diastolic depolarisation takes place to initiate the whole cardiac cycle.

Calcium exit from the cell

Although only relatively small amounts of sodium and calcium ions enter by the fast and slow channels respectively, over a period the cytosol would potentially gain substantial amounts of these ions. The exit mechanism for sodium is the sodium pump while the chief exit for calcium is the sodium-calcium exchange mechanism (Na^+,Ca^{2+} exchanger). The exchanger responds to low concentrations of calcium ions, similar to those found within the cell, and transports these ions very effectively exchanging three sodium ions with one calcium ion (Berne & Levy 1993). Calcium ions can also leave the heart cell via the ATP-requiring calcium pump, although the maximal rate of the sodium-calcium exchanger is about 30 time higher than that of the pump. It has been proposed that it is the exchanger which operates during sytole and the calcium pump functions during diastole to help keep the cytosolic calcium ion concentration low (Opie 1984).

An interesting prediction was made by Reuter (1974) concerning the effects of increasing the intracellular sodium concentration. His sodium-calcium exchange scheme, combined with the recent knowledge that 3 sodium ions are exchange per calcium ion, can be simplified to the following equation (Opie 1984):

$$\frac{[\mathrm{Ca}^{2+}]_i}{[\mathrm{Ca}^{2+}]_o} = \frac{([\mathrm{Na}^+]_i)^3}{([\mathrm{Na}^+]_o)^3}$$

If internal sodium ions are increased in concentration by inhibition of the sodium pump by digitalis, then only a very small increase will dramatically increase the internal free calcium ion concentration to enhance contractility.

2.3.3 Calcium fluxes

After the propagation of the action potential from the pacemaker cells of the SA node to the ventricular myocytes, the next event of critical importance is the voltage-induced increased opening of the calcium channels of contractile cells, followed by a series of intracellular movements of calcium ions leading to myocardial contraction and relaxation. The intent of this section is to concentrate on the calcium ion fluxes which link the wave of excitation to contraction by the process of excitation-contraction coupling, followed by the uptake of calcium ions into the SR which is associated with the relaxation phase.

During the cardiac cycle, only small amounts of calcium actually enter and leave the myocyte, so that the majority of calcium ion movements are from the calcium stores to the cytosol and back again (Figure 2.14). The sarcolemma maintains a great concentration gradient of calcium ions from the extracellular value of about $1\ \mathrm{mM}$ to intracellular values of $10^{-4}\ \mathrm{mM}$ in diastole and $10^{-2}\ \mathrm{mM}$ in systole (Opie 1984). It is thought that the SR is the major intracellular calcium store (Berne & Levy 1993, Katz 1992). It is from the SR that calcium ions are released by the small, but varying, amounts of calcium entering the cell during depolarisation according to the theory of *calcium induced calcium release* (Fabiato 1983). As calcium is released into the cytosol from the SR it interacts with troponin-C so the interaction of actin and myosin is facilitated and contraction takes place. The rise of cytosolic calcium ends as the wave of excitation passes, so that no more calcium is released and the cyctosolic calcium is rapidly taken up by the calcium pump of the SR; a lesser amount of calcium is pumped out of the cell.

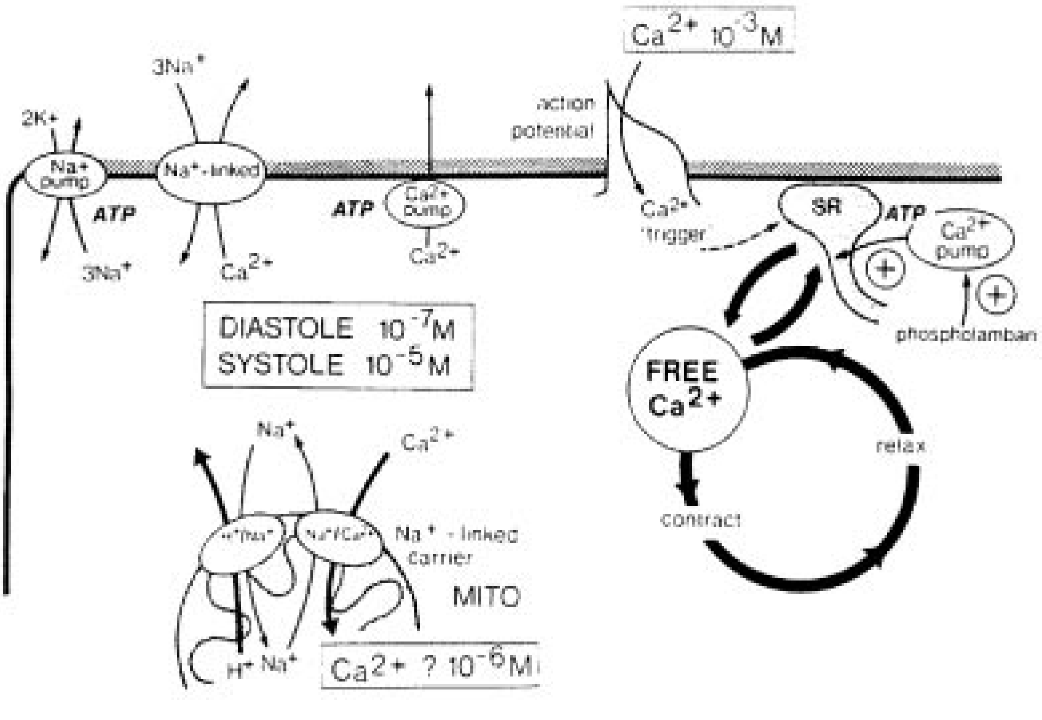

FIGURE 2.14: Calcium fluxes in the myocardium. SR = sarcoplasmic reticulum; MITO = mitochondria. *From Opie (1984).*

In order to balance the small amount of calcium that enters the cell with each depolarisation, calcium ions can leave the cell by one of two processes (Table 2.5). First, calcium ions leaving may be exchanged for sodium ions entering, and secondly an ATP-consuming calcium pump can transfer calcium back out into the extracellular space against the concentration gradient. In addition, cytosolic calcium can be taken up into the mitochondria, which is thought to be a site of storage for these ions. The mitochondrial calcium stores are probably only indirectly related to the contraction-relaxation cycle, by being one of the slower sites of calcium exchange.

	% of total uptake
Sarcoplasmic reticulum	88
Sarcolemma	
Na^+,Ca^{2+} exchanger	5
Ca^{2+}-pump	1
Mitochondria	6

TABLE 2.5: Mechanisms for lowering cytosolic Ca^{2+} concentration in myocardial cells. *Modified from Opie (1984).*

In addition to the highly controlled entry of calcium ions by the calcium channel described above (Section 2.3.2), there are two other possible routes. First, calcium can flow into the cells by a non-specific process. This is possible, despite the relative impermeability of the resting sarcolemma to calcium ions, due to the vast concentration gradient from extracellular to intracellular. Secondly, calcium ions can enter the cytosol by a reversal of the Na^+,Ca^{2+} exchanger.

2.3.4 The mechanism of myocardial contraction

There are two essential components of the heart's contractile machinery, the proteins concerned primarily with contraction (myosin and actin) and those whose function is regulatory (troponin and tropomyosin). The greatest proportion of myofibrillar protein is concerned with contraction (about 80%), with about 10% concerned with the regulation of this contraction and another 10% concerned with maintenance of the myofibrillar structure (Table 2.6). In living muscle, no matter how correctly these proteins are orientated, contraction will not occur unless ATP and calcium are also present.

Micro-anatomy of contraction

The thick filament of myosin (about $1.5\ \mu\mathrm{m}$ long and 10–$15\ \mathrm{nm}$ wide) is composed of about 300 individual myosin molecules, each very large and ending in a myosin head which is bilobed (Figure 2.15). Half of these heads are orientated towards one end of the sarcomere and half to the other, leaving a bare area in the middle of the thick filament, the M-line, where the centrally placed disc of the M-line proteins holds the entire array of thick filaments in register within the sarcomere (Opie 1984).

Thin filaments (about $1\ \mu\mathrm{m}$ long and 5–$7\ \mathrm{nm}$ wide) contain two helical chains of actin units, each carried on a backbone of tropomyosin, with troponin complexes placed at intervals of about $38\ \mathrm{nm}$ (Figure 2.16). *Troponin-C* (for calcium) is that component to which calcium can

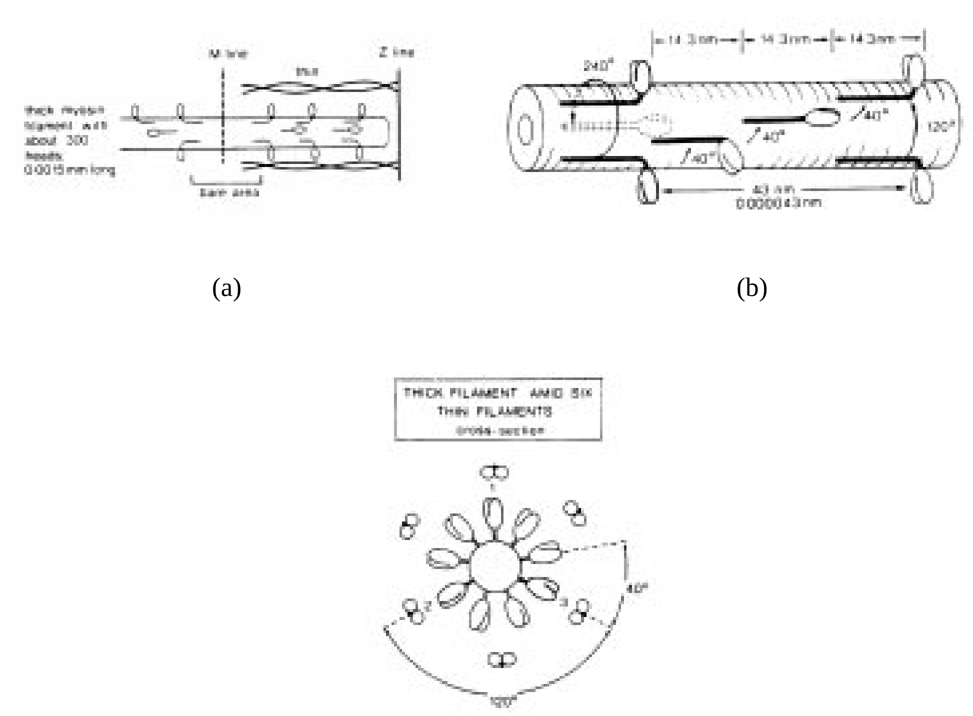

(a)

(b)

(c)

FIGURE 2.15: Scheme of thick and thin filaments (a), with the myosin "heads" coming off at right angles to the "body". The heads emerge in groups of three and shift their positions by 40 ° in succession (b). Thus nine rows of about 16 heads each are placed in a line on the surface of each arm of the bipolar filament. Note the position of the thick filament between six thin filaments (c). In the cross-sectional view, the shaded heads of myosin correspond to a group of three heads coming off at the same level (two of these heads are shaded in (b)). *From Opie (1984).*

Function	Location	% of myofibrillar protein	Molecular weight
Contractile			
Myosin	Thick filaments	55–60	500000
Actin	Thin filaments	20	43000
Regulatory			
Tropomyosin	Thin filaments	5	70000
Troponin-I	Thin filaments		
Troponin-C	Thin filaments	7	86000
Troponin-T	Thin filaments		
Structural			
C-protein	Thick filaments		
alpha-actinin	Thick filaments and Z-lines		
beta-actinin	Thin filaments	8–13	40000–750000
M-line proteins	M-lines		
Other proteins	Various		

TABLE 2.6: The proteins of myofibrils. There are about 7 actins : 2 myosins : 1 tropomyosin : 1 troponin in the myofibrils, but their different molecular weights account for the different picture given by the percentage contribution each makes to the total myofibrillar mass. *From Opie (1984).*

bind to remove the inhibitory effect of *troponin-I* (I for inhibitor) on the interaction between the actin and myosin heads. *Troponin-T* links the whole troponin complex to tropomyosin.

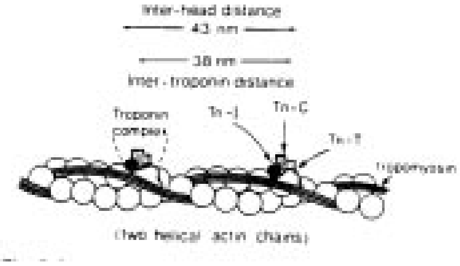

FIGURE 2.16: Thin filament structure. The rope-like filament is essentially a double helix of two half-filaments each consisting of seven actins lying along a dimeric coiled tropomyosin molecule with one troponin complex attached to it. The filament depicted would look identical from the back. The structure of the members of the troponin is purely diagramatic. *From Opie (1984).*

The bilobed head of each myosin molecule is connected to the thick filament by a rod-like “stalk” or “neck”, which then merges into the remaining rod-like body of the molecule which is permanently built into the filament by side-to-side aggregation with its fellows (Figure 2.17). These three domains of the molecule are thus joined by two flexible hinges which enable the head to reach out to the thin filaments even when the muscle shortens. This is necessary due to the isovolumetric nature of the myofibril contraction (*i.e.*, the thick and thin filaments become separated from each other more and more during contraction and the myosin hinges enable the system to operate unchanged during these processes).

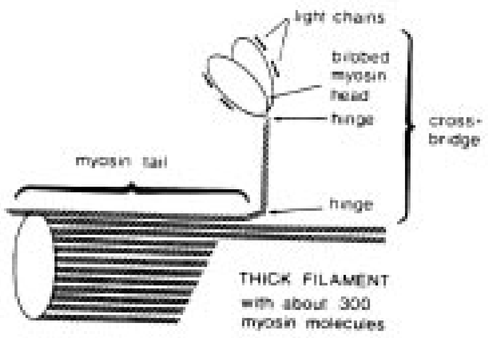

FIGURE 2.17: The bilobed myosin head is at the end of the cross-bridge and projects from the thick filament. Each lobe of the head lies at the end of a long strand; two such strands are twisted together to form a long rigid helical structure, the tail of which is buried in the thick filament and held in tight apposition by the tails of other myosin molecules. The two hinges at either end of the "neck" of the cross-bridge allow (i) flexion-extension movements of the head on the neck (Figure 2.18); and (ii) the cross-bridge to stretch across an increased gap between thick and thin filaments during contraction. *From Opie (1984).*

Cross-bridge cycle

A good starting point for a description of the individual contraction cycles is to start in diastole when the sarcomeres are at rest. At this time there is no interaction between any of the myosin heads and the actin units of the thin filaments (Step 1, Figure 2.18). In diasole, when the cytosolic calcium ion concentration falls, the loss of calcium from its binding sites on troponin-C is associated with a series of complex interactions among the proteins of the rope-like thin filament, which result in a shift in the relative positions of the filamentous molecules: tropomyosin moves to a position that essentially blocks any interaction of actin units with myosin. The inhibition is only imposed on actin subunits in the immediate vicinity of the particular "unoccupied" troponin-C molecule; about 7 actins are thus controlled "at a distance" by the master-switch sited in the troponin complex (Opie 1984).

At the start of systole, the cytosolic concentration of calcium ions increase and these ions bind to two (or more) specific sites on troponin-C so that the thin filaments revert to the conformation that permits interaction between the myosin heads and adjacent actin units, and the myosin heads now attach to the actin or induce local conformation changes. At this stage, the product of (prior) hydrolysis of ATP, in the form of ADP and inorganic phosphate (P_i), are

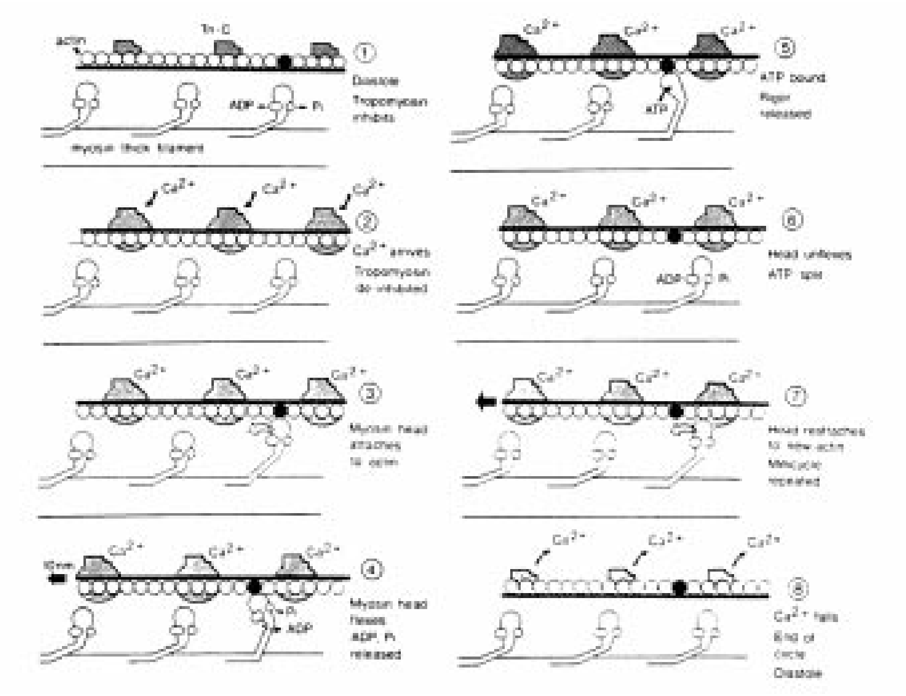

FIGURE 2.18: The cross-bridge cycle starts with relaxation in diastole, when tropomyosin (Tm) “blocks” the myosin head from binding to actin. At the start of systole, calcium ions combine with troponin-C (Tn-C) to unblock the actin so that myosin heads can bind (Step 2) and then “flex” whereupon ADP and inorganic phosphate ($\mathrm{P_i}$) are released (Step 3). The “rigor state” develops transiently (Step 4). ATP moves into the same binding site on the myosin head, vacated by ADP, to release the myosin head (Step 5). After ATP has been split to ADP and $\mathrm{P_i}$ by the myosin ATPase, the head extends (Step 6) to rebind to another actin 2–4 units “downstream” (Step 7). Steps 1 – 7 are repeated until calcium ions leave at the start of diastole (Step 8). *From Opie (1984).*

bound to the myosin head. The attachment of actin to myosin occurs at a preferred angle of about $90\,^\circ$ (Step 2, Figure 2.18).

Following the attachment of the myosin head to the actin unit there is a concerted movement of the myosin head towards an angle of $45\,^\circ$, with a discharge first of the bound inorganic phosphate and then of bound ADP (Step 3, Figure 2.18). This, together with the action of the other cross-bridges in the half sarcomere, performs the mechanical work of contraction by sliding the entire thin filaments over a distance of about $10\ \mathrm{nm}$ (Huxley 1969). During this shortening the distance between the thick and thin filaments increases slightly (Figure 2.17).

The state in which the flexed myosin head is bound to an actin at a preferred angle of $45\,^\circ$ without any bound ADP or inorganic phosphate is the “rigor state” (Step 4, Figure 2.18). When ATP occupies this site there is a shape change in the myosin head which causes it to “loosen its grip” on the actin unit (Step 5, Figure 2.18). Hydrolysis of the bound ATP immediately follows, so that the myosin head is returned to its unattached, $90\,^\circ$ position, with bound ADP and inorganic phosphate (Step 6, Figure 2.18). The myosin head is now in a position to bind a second time to an actin 2–4 units further along the thin filament than the one which just participated in the cycle described (Step 7, Figure 2.18), provided that the nearest troponin-C still binds calcium ions. When the calcium concentration falls the thin filament is again “switched off” and relaxation occurrs in that region of the sarcomere (Step 8, Figure 2.18).

During a single beat, tension develops by recruitment of more and more rapidly cycling cross-bridges as the cytosolic calcium concentration rises to a peak; relaxation begins when cross-bridge cycling activity diminishes in response to the removal of calcium from the thin filament sites where it acts. Since the cross-bridges cycle asynchronously, tension is maintained by those members of the population of cross-bridges which are attached at any given moment, while the rest are moving through the various detached phases of their individual cycles (Figure 2.19).

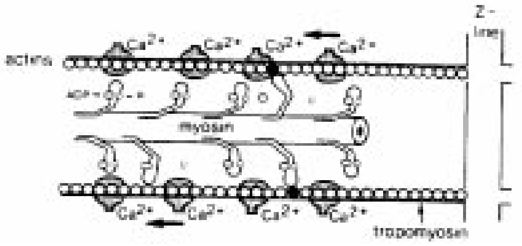

FIGURE 2.19: Asynchronous nature of cross-bridge cycling during sarcomeric contraction. Many myosin heads are unattached, with bound ADP and P_i, because attachment is probably the rate-limiting step in each individual cross-bridge cycle at low afterloads. Those which are attached to actin units (●) either exert tension towards the centre of the sarcomere or they are about to do so. For simplification only two thin filaments are shown and only one strand (actin-tropomyosin) of each; in addition, only two “lines” of heads emerging from a thick filament are shown (there are seven others). All actins are switched on because the Ca^{2+} occupancy of troponin-C is complete. *From Opie (1984).*

Chapter 3

Electrical Models

As stated in Section 1.1.1, cardiac electrical models are primarily concerned with the flow of ions through the cellular membrane and within the cell itself. As described in Section 2.3, the resting membrane potential is determined primarily by potassium ions, the action potential is initiated by a fast flux of sodium ions through the sarcolemma, and the cellular contraction is driven by the intracellular calcium ion concentration, with all three ions affecting the action potential characteristics. Thus, the ions of primary interest in any electrical model of a cardiac cell are potassium (K^+), sodium (Na^+), and calcium (Ca^{2+}). As will be shown in the following sections (Sections (3.1)–(3.3)), the three models used in this research (DiFrancesco–Noble, Luo–Rudy, and Jafri–Rice–Winslow) model the flow of these ions within the cell and through the sarcolemma (*i.e.*, cellular electrical models simply model the ionic currents of a single cardiac cell).

Ionic current models can be constructed by one of two main methods. One method is to attempt to accurately describe all of the behaviour of the cell, called a *biophysical* model (also known as *exact* or *complete* models). This type of model is either confirmed by experiments or have been developed to explain observed behavior. A problem with biophysical models is that they tend to be large and complex, which implies that the computational time required to solve these models becomes prohibitive for large problems. This problem is avoided in this research since we are only interested in a single cell, which is not a large system. However, this is a point to remember if considering modelling a larger system (*e.g.*, more than one cell, or the whole heart). Another problem with biophysical models is that the underlying physiology is constantly being investigated, leading to revisions and updates of the physiological models. Not much can be done about this, and as more is learnt about the cardiac cell we must accept that some models will become more favoured, while others my be proven invalid. This suggests that any computer based model of a cardiac cell must be flexible enough to make updating the models used, or including new models, possible.

Another method of constructing ionic current models is to create more simple models, which behave in a similar manner as the biophysical models, but are not derived directly from physiological observation. These *simplified* models attempt to replicate certain key features of electrical activation, such as propagation and recovery. The main advantage of these types of models is that they are typically very small and fast to solve, making them ideal for large problems. The main disadvantage of using a simplified model is that they are unable to determine the effect of any abnormallities in the cell, or deviation from the normal conditions of the cell, with any degree of certainty as the physiological influences on the electrical processes are not being adequately modelled. Examples of simplified models can be found in Sands (1998).

This research is concerned with developing a coupled, electro-mechanical model of a single cardiac cell (Section 1.3). Therefore, emphasis is placed more on accurately modelling the underlying cardiac physiology, with less emphasis on the computational speed or efficiency of the model. Thus, biophysical ionic current models were deemed more appropriate for this research. The following sections describe each of the three biophysical electrical models used in this research.

3.1 The DiFrancesco–Noble Model

Following earlier work (McAllister, Noble & Tsien 1975, Beeler & Reuter 1977), DiFrancesco & Noble (1985) constructed a new model of cardiac electrical activity which sought to incorporate much of the new data gathered since the McAllister et al. (1975) and Beeler & Reuter (1977) models were published. While in their paper DiFrancesco & Noble acknowledge that some of the currents are unlikely to remain the best available for very long, the DFN model has remained the most complete of all Purkinje fibre ionic current models to date.

As previously stated, the electrical activity of the cell is governed by the action potential, given by the membrane potential (V_m), which in the DFN model satifies the first-order differential equation:

$$\frac{dV_m}{dt} = \frac{-I_{DFN}}{C_m} \tag{3.1}$$

where C_m is the membrane capacitance and I_{DFN} is the total ionic current

$$I_{DFN} = I_f + I_K + I_{K1} + I_{to} + I_{Na,b} + I_{Ca,b} + I_{NaK} + I_{NaCa} + I_{Na} + I_{Ca(L)} + I_{stim} \tag{3.2}$$

Equation (3.2) describes the full DFN ionic current. This current can be modified depending on the tissue being modelled, and some of the component currents can also be modified to more accurately model different cellular species. The membrane potential obtained from this model for Purkinje cells is given in Figure 3.1.

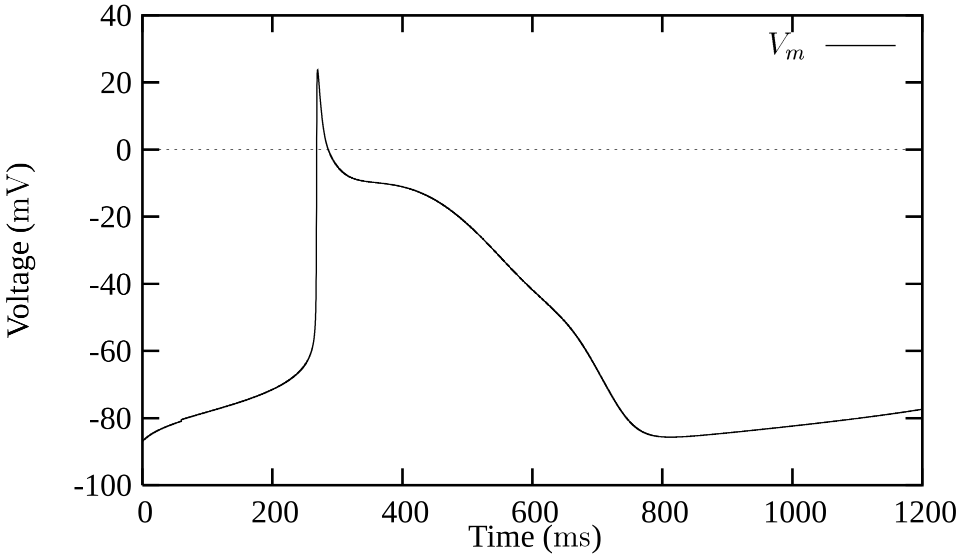

FIGURE 3.1: DFN model of the action potential in Purkinje cells.

3.1.1 Ionic currents

Hyperpolarising-activated current (I_f) As stated in Section 2.3.2, this current carries both Na^+ and K^+ ions. Contributions from each ion are approximately equal, so that the normal net reversal potential is around $20\ \mathrm{mV}$. The current is given by

$$I_f = y\overline{I_f} \tag{3.3}$$

where y is a gating variable representing the degree of activation of I_f and $\overline{I_f}$ is the fully activated current, and is given by

$$\overline{I_f} = \left(\frac{[\mathrm{K}^+]_c}{[\mathrm{K}^+]_c + K_{m,f}}\right)\{g_{f,K}(V_m - E_K) + g_{f,Na}(V_m - E_{Na})\} \tag{3.4}$$

where $[\mathrm{K}^+]_c$ is the cleft potassium concentration, $K_{m,f}$ is the concentration of the bulk potassium required for half activation of the current, and $g_{f,K}$ and $g_{f,Na}$ are the sodium and potassium conductances for the I_f channel respectively. E_K and E_{Na} are the reversal potentials of sodium and potassium, respectively, given by the Nernst equation (Equation (2.1)).

The gating variable y satisfies the Hodgkin-Huxley type gating differential equation

$$\frac{dy}{dt} = \alpha_y(1 - y) - \beta_y y \tag{3.5}$$

with the coefficients

$$\begin{aligned}\alpha_y &= 0.05\exp(-0.067(V_m+52))\\ \beta_y &= \frac{V_m+52}{1-\exp(0.2(V_m+52))}\end{aligned} \tag{3.6}$$

Time-dependent (delayed)* K^+ *current (I_K) This is an outward current which is controlled by a single gate given the symbol x, and a simple model of kinetics

$$I_K = x\overline{I_K} \tag{3.7}$$

where $\overline{I_K}$ is the fully-activated value of I_K and is derived from rate theory (Jack, Noble & Tsien 1983) to give

$$\overline{I_K} = I_{K,max}\cdot\frac{[\mathrm{K}^+]_i-[\mathrm{K}^+]_c\exp(-V_mF/RT)}{140} \tag{3.8}$$

The time-dependent gating variable x is controlled by the Hodgkin-Huxley type gating differential equation (Equation (3.5)) with the coefficients

$$\begin{aligned}\alpha_x &= \frac{0.5\exp(0.0826(V_m+50))}{1+\exp(0.057(V_m+50))}\\ \beta_x &= \frac{1.3\exp(-0.06(V_m+20))}{1+\exp(-0.04(V_m+20))}\end{aligned} \tag{3.9}$$

Time-independent (background)* K^+ *current (I_{K1}) The equation for this current is an empirical formulation that is formulated from a variety of experimental work during the late 1970's and early 1980's:

$$I_{K1} = \overline{g}_{K1}\cdot\frac{[\mathrm{K}^+]_c}{[\mathrm{K}^+]_c+K_{m,K1}}\cdot\frac{V_m-E_K}{1+\exp((V_m-E_K+10)2F/RT)} \tag{3.10}$$

Transient outward current (I_{to}) This current is an outward rectifier which is $[\mathrm{Ca}^{2+}]_i$-activated, and which depends on $[\mathrm{K}^+]_o$. The inactivation process of this channel was still not well understood at this stage, and was modelled with a first order equation for a rate variable r, so that

$$I_{to} = r\overline{I_{to}} \tag{3.11}$$

where $\overline{I_{to}}$ is the maximal current given by

$$\overline{I_{to}} = 0.28\frac{0.2 + [\mathrm{K}^+]_c}{K_{m,to} + [\mathrm{K}^+]_c} \cdot \frac{[\mathrm{Ca}^{2+}]_i}{K_{m,to} + [\mathrm{Ca}^{2+}]_i} \cdot \frac{V_m + 10}{1 - \exp(-0.2(V_m + 10))} \cdot \\ ([\mathrm{K}^+]_i \exp(0.02V_m) - [\mathrm{K}^+]_o \exp(-0.02V_m)) \tag{3.12}$$

where r is governed by the Hodgkin-Huxley type gating differential equation (Equation (3.5)) with the coefficients

$$\begin{aligned} \alpha_r &= 0.033\exp(-V_m/17) \\ \beta_r &= \frac{33}{1 + \exp(-(V_m + 10)/8)} \end{aligned} \tag{3.13}$$

Background sodium current ($I_{Na,b}$) This is a simple background current described by

$$I_{Na,b} = \frac{[\mathrm{Na}^+]_o}{[\mathrm{Na}^+]_{o,c}} \cdot \overline{g}_{Na,b} \cdot (V_m - E_{Na}) + I_{Ch,b} \tag{3.14}$$

where $[\mathrm{Na}^+]_{o,c}$ is a control level of external sodium (usually 140 mM) and $I_{Ch,b}$ is a background current due to choline, or some other sodium substitute, and the conductance $\overline{g}_{Na,b}$ is usually set to $0.18\ \mu$S.

Background calcium current ($I_{Ca,b}$) Another simple background current of the same form as $I_{Na,b}$:

$$I_{Ca,b} = \overline{g}_{Ca,b}(V_m - E_{Ca}) \tag{3.15}$$

Na^+,K^+-ATPase current (I_{NaK}) In its normal mode of operation, this pump exchanges 3 Na^+ ions out for 2 K^+ ions into the cell producing a net outward current. The assumption is made that the pump is activated by external K^+ and internal Na^+ by first-order binding processes, such that

$$I_{NaK} = \overline{I_{NaK}} \cdot \frac{[\mathrm{K}^+]_c}{K_{m,K} + [\mathrm{K}^+]_c} \cdot \frac{[\mathrm{Na}^+]_i}{K_{m,Na} + [\mathrm{Na}^+]_i} \tag{3.16}$$

where $K_{m,K}$ and $K_{m,Na}$ are the respective concentrations required for half-activation.

Na^+,Ca^{2+} ***exchanger current (*** I_{NaCa}***)*** The formulation of this current assumes that the only energy available to the process is that of the Na^+ and Ca^{2+} gradients and the transmembrane potential. DiFrancesco & Noble (1985) propose two alternative expressions for this current. The simplest assumes that the current is a hyperbolic sine function of the energy gradient expressed in millivolts

$$I_{NaCa} = k_{NaCa} \sinh((V_m - E_{NaCa})F/RT) \tag{3.17}$$

where the reversal potential of the exchange is given by

$$E_{NaCa} = \frac{n_{NaCa}E_{Na} - 2E_{Ca}}{n_{NaCa} - 2} \tag{3.18}$$

where n_{NaCa} is the stoichiometry of the exchange, now known to be 3.

Equation (3.17) is given as a simplification for a more general model (Mullins 1977, Mullins 1981), and may apply moderately well for sudden small voltage changes at fixed ion concentrations (DiFrancesco & Noble 1985). To account for the varying calcium ionic concentrations, DiFrancesco & Noble (1985) use a more complex equation for I_{NaCa} derived from Mullins full model, based on the fact that, over a few action potentials, sodium concentration changes are very small:

$$\begin{aligned} I_{NaCa} = k_{NaCa}(&\exp(\gamma(n_{NaCa} - 2)V_m F/RT)[\mathrm{Na}^+]_i^n[\mathrm{Ca}^{2+}]_o \\ &- \exp(-(1-\gamma)(n_{NaCa} - 2)V_m F/RT)[\mathrm{Na}^+]_o^n[\mathrm{Ca}^{2+}]_i / \\ &(1 + d_{NaCa}([\mathrm{Ca}^{2+}]_i[\mathrm{Na}^+]_o^n + [\mathrm{Ca}^{2+}]_o[\mathrm{Na}^+]_i^n)) \end{aligned} \tag{3.19}$$

where γ represents the shape or the position of the energy barrier in the electrical field. In Equation (3.17), k_{NaCa} has the value 20 when $[\mathrm{Na}^+]_i$ is in the range 5–10 mM and $[\mathrm{Ca}^{2+}]_i$ is in the range 0.05–0.1 $\mu\mathrm{M}$. For Equation (3.19) appropriate values are $k_{NaCa} = 0.02$ and $d_{NaCa} = 0.001$.

Fast sodium current (I_{Na}***)*** The DFN model uses a two-variable model of the sodium kinetics, the m and h gates. It is acknowledged, however, that the model does not represent the slower components of Na^+ inactivation and recovery. It is also assumed that the sodium channel shows a 12% permeability to K^+:

$$I_{Na} = m^3 h \overline{g}_{Na}(V_m - E_{mh}) \tag{3.20}$$

where the channel reversal potential is given by

$$E_{mh} = \frac{RT}{F} \ln\left(\frac{[\mathrm{Na}^+]_o + 0.12[\mathrm{K}^+]_c}{[\mathrm{Na}^+]_i + 0.12[\mathrm{K}^+]_i}\right) \tag{3.21}$$

and the gating variables m and h are governed by the Hodgkin-Huxley type gating differential equation (Equation (3.5)), with the rate constants

$$\begin{aligned} \alpha_m &= \frac{200(V_m + 41)}{1 - \exp[-0.1(V_m + 41)]} \\ \beta_m &= 8000 \exp[-0.056(V_m + 66)] \\ \alpha_h &= 20 \exp[-0.125(V_m + 75)] \\ \beta_h &= \frac{2000}{1 + 320 \exp[-0.1(V_m + 75)]} \end{aligned} \tag{3.22}$$

L-type calcium current ($I_{Ca(L)}$) In the original DiFrancesco & Noble (1985) paper, this current is called the second inward current, consisting of calcium and potassium (and sodium if required) components, and split into fast and slow components. The fast component is now called the L-type calcium current ($I_{Ca(L)}$) and the slower component is known as the T-type calcium current ($I_{Ca(T)}$).

The kinetics of the L-type calcium channel are still described in terms of two gate variables d and f, but the time constants for both the activation and inactivation processes are much shorter than those used for the McAllister et al. (1975) and Beeler & Reuter (1977) models.

$$I_{Ca(L)} = df(I_{Ca(L),Ca} + I_{Ca(L),K} + I_{Ca(L),Na}) \tag{3.23}$$

where

$$\begin{aligned} I_{Ca(L),Ca} = 4P_{si}(V_m - 50)(F/RT)/(1 - \exp(-(V_m - 50)2F/RT)) \cdot \\ ([\mathrm{Ca}^{2+}]_i \exp(100F/RT) - [\mathrm{Ca}^{2+}]_o \exp(-2(V_m - 50)F/RT)) \end{aligned} \tag{3.24}$$

$$I_{Ca(L),K} = 0.001 P_{si}(V_m - 50)(F/RT)/(1 - \exp(-(V_m - 50)F/RT)) \cdot \\ ([\mathrm{K}^+]_i \exp(50F/RT) - [\mathrm{K}^+]_c \exp(-(V_m - 50)F/RT)) \quad (3.25)$$

If required, an equation similar to Equation (3.25) can be used to describe a sodium component.

Again, the gating variables are controlled by the Hodgkin-Huxley type gating differential equation (Equation (3.5)), with the rate constants

$$\begin{aligned} \alpha_d &= 30\frac{V_m + 24}{1 - \exp(-(V_m + 24)/4)} \\ \beta_d &= 12\frac{V_m + 24}{\exp((V_m + 24)/10) - 1} \\ \alpha_f &= 6.25\frac{V_m + 34}{\exp((V_m + 34)/4) - 1} \\ \beta_f &= \frac{50}{1 + \exp(-(V_m + 34)/4)} \end{aligned} \quad (3.26)$$

3.1.2 Ionic concentrations

In addition to the ionic currents, the DFN model attempted to quantify the changes in several ion concentrations, including the $[\mathrm{Ca}^{2+}]_i$ of earlier models.

Intracellular sodium concentration The change in $[\mathrm{Na}^+]_i$ is defined as the sum of the various sodium currents divided by the intracellular fluid volume:

$$\frac{d[\mathrm{Na}^+]_i}{dt} = -(I_{Na} + I_{Na,b} + I_{f,Na} + I_{Ca(L),Na} + 3I_{NaK} + \frac{n_{NaCa}}{n_{NaCa} - 2} I_{NaCa})/V_{myo}F \quad (3.27)$$

where V_{myo} is the intracellular fluid volume, and the negative is due to outward currents being defined as positive.

Intracellular calcium concentration Changes in $[\mathrm{Ca}^{2+}]_i$ were first modelled in the Beeler & Reuter (1977) model. This process has been taken a step further in the DFN model, although this model still provides only a simple model of intracellular calcium (for a more detailed model of intracellular calcium movement, see Section 3.3). The Ca^{2+} is assumed to be sequestered by the network sarcoplasmic reticulum (NSR), and the amount stored here is $[\mathrm{Ca}^{2+}]_{NSR}$. Some fraction is transferred to a release store in the junctional sarcoplasmic reticulum (JSR) ($[\mathrm{Ca}^{2+}]_{JSR}$) before being released into the intracellular space, this release being induced by calcium (calcium induced calcium release (CICR) (Section 2.3.3)) . The concentration of calcium in each of these stores is modelled, together with the transfer between the calcium sites and the Ca^{2+} transfer across the sarcolemma via the other ionic currents. These seem to be the minimum assumptions required to model the calcium transient (Sands 1998).

The associated currents are described as

$$\begin{aligned} I_{up} &= \alpha_{up}[\mathrm{Ca}^{2+}]_i(\overline{[\mathrm{Ca}^{2+}]_{NSR}} - [\mathrm{Ca}^{2+}]_{NSR}) - \beta_{up}[\mathrm{Ca}^{2+}]_{NSR} \\ I_{tr} &= \alpha_{tr}p([\mathrm{Ca}^{2+}]_{NSR} - [\mathrm{Ca}^{2+}]_{JSR}) \\ I_{rel} &= \alpha_{rel}[\mathrm{Ca}^{2+}]_{JSR}\frac{[\mathrm{Ca}^{2+}]_i^r}{[\mathrm{Ca}^{2+}]_i^r + K_{m,Ca}} \end{aligned} \tag{3.28}$$

where $\overline{[\mathrm{Ca}^{2+}]_{NSR}}$ is the maximum value of $[\mathrm{Ca}^{2+}]_{NSR}$ and is set to $5\ \mathrm{mM}$, r is the number of Ca^{2+} ions assumed to bind to the release site (usually 2), and p is governed by a first order Hodgkin-Huxley type equation (Equation (3.5)) with rate constants identical to those for f (Equation (3.26)) but slowed by a factor of 10. $K_{m,Ca}$ is usually set to $0.001\ \mathrm{mM}$. The α parameters are determined from time constants measured for the movement of calcium from one space to another.

This results in the change in concentrations being given by

$$\begin{aligned} \frac{d[\mathrm{Ca}^{2+}]_{NSR}}{dt} &= (I_{up} - I_{tr})/2V_{NSR}F \\ \frac{d[\mathrm{Ca}^{2+}]_{JSR}}{dt} &= (I_{tr} - I_{rel})/2V_{JSR}F \\ \frac{d[\mathrm{Ca}^{2+}]_i}{dt} &= -(I_{Ca(L),Ca} + I_{Ca,b} - \frac{2I_{NaCa}}{n_{NaCa} - 2} + I_{up} - I_{rel})/2V_{myo}F \end{aligned} \tag{3.29}$$

where $V_{NSR} = 0.05V_{myo}$ is the volume of the uptake stores (approximately 5% of the total intracellular volume) and $V_{JSR} = 0.02V_{myo}$ is the volume of the release stores.

Extracellular potassium concentration Assuming a homogeneous K^+ concentration in a three-compartment model, the change in extracellular potassium is given by

$$\frac{d[\mathrm{K}^+]_c}{dt} = -P([\mathrm{K}^+]_c - [\mathrm{K}^+]_b) + I_{m,K}/V_eF \tag{3.30}$$

where $[\mathrm{K}^+]_b$ is the bulk extracellular K^+ concentration, P is the rate constant for exchange (between 0.2 to $1.0\ \mathrm{s}^{-1}$), V_e is the extracellular space volume, and the total potassium membrane flux $I_{m,K}$ is given by

$$I_{m,K} = I_{K1} + I_K + I_{f,K} + I_{Ca(L),K} + I_{K,b} - 2I_{NaK} \tag{3.31}$$

Intracellular potassium concentration This is related to the total K^+ membrane flux.

$$\frac{d[\mathrm{K}^+]_i}{dt} = -I_{m,K}/V_{myo}F \tag{3.32}$$

where V_{myo} is the volume of the intracellular space.

3.1.3 Extensions to the model

The DFN model was initially developed for a Purkinje fibre cell, and was subsequently altered and extended, firstly to describe the behaviour of the SA node (Noble & Noble 1984) and later the ionic processes observed within rabbit atrial cells (Hilgemann & Noble 1987). The Hilgemann model significantly extended the DFN model in terms of the movement of Ca^{2+} within the cell, and particulary in relation to the uptake and release through the SR.

The DFN model implemented in this research is based on the OxSoft HEART program, developed at Oxford university, which includes numerous modifications that enable the model to represent a number of cardiac cell species simply by setting appropriate parameters (see Chapter 6).

3.2 The Luo–Rudy Models

3.2.1 Luo–Rudy I

The Luo & Rudy (1991) model is the next significant update to the Beeler & Reuter (1977) mammalian ventricular model. It is known as the Luo–Rudy I (LR-I) model because it is the first of the two Luo-Rudy models. The second model, Luo–Rudy II (LR-II), published three years later, incorporates aspects which were not investigated in the original model.

As with the DFN model, the membrane potential is governed by the differential equation

$$\frac{dV_m}{dt} = \frac{-I_{LR-I}}{C_m} \tag{3.33}$$

where C_m is the membrane capacitance and I_{LR-I} is the total ionic current

$$I_{LR-I} = I_{Na} + I_{si} + I_K + I_{K1} + I_{Kp} + I_b + I_{stim} \tag{3.34}$$

Inward currents

Fast sodium current (I_{Na}) The LR-I model adopts the same activation (m) and inactivation (h) gate variables as the DFN model, and also incorporates a slow inactivation gate (j) as suggested by the Beeler & Reuter (1977) model. The sodium current has the form

$$I_{Na} = \overline{g}_{Na} \cdot m^3 \cdot h \cdot j \cdot (V_m - E_{Na}) \tag{3.35}$$

where $\overline{g}_{Na}$ is the maximum conductance of the sodium channel and E_{Na} is the reversal potential of the channel (given by Equation (2.1)). All three gates are controlled by the Hodgkin-Huxley type gating differential equation (Equation (3.5)) with rate constant coefficients given by

$$\begin{aligned}
\alpha_m &= \frac{0.32(V_m + 47.13)}{1 - \exp(-0.1(V_m + 47.13))} \\
\beta_m &= 0.08 \exp(-V_m/11) \\
\alpha_h &= \begin{cases} 0 & \text{if } V_m \geq -40 \text{ mV} \\ 0.135 \exp[(-80.0 - V_m)/6.8] & \text{if } V_m < -40 \text{ mV} \end{cases} \\
\beta_h &= \begin{cases} \frac{1}{0.13(1+\exp[-(V_m+10.66)/11.1])} & \text{if } V_m \geq -40 \text{ mV} \\ 3.56 \exp(0.079 V_m) + 3.1 \times 10^5 \exp(0.35 V_m) & \text{if } V_m < -40 \text{ mV} \end{cases} \\
\alpha_j &= \begin{cases} 0 & \text{if } V_m \geq -40 \text{ mV} \\ \frac{-1.2714\times10^5 \exp(0.2444 V_m) - 3.474\times10^{-5} \exp(-0.04391 V_m)}{1+\exp(0.311(V_m+79.23))}(V_m + 37.78) & \text{if } V_m < -40 \text{ mV} \end{cases} \\
\beta_j &= \begin{cases} \frac{0.3 \exp(-2.535\times10^{-7} V_m)}{(1+\exp(-0.1(V_m+32)))} & \text{if } V_m \geq -40 \text{ mV} \\ \frac{0.1212 \exp(-0.01052 V_m)}{(1+\exp(-0.1378(V_m+40.14)))} & \text{if } V_m < -40 \text{ mV} \end{cases}
\end{aligned} \tag{3.36}$$

Slow inward current (I_{si}) This current is the same as in the Beeler & Reuter (1977) model, which has the form

$$I_{si} = \overline{g}_{si} \cdot d \cdot f \cdot (V_m - E_{si}) \tag{3.37}$$

where E_{si} is given by

$$E_{si} = 7.7 - 13.0287 \ln \left([\mathrm{Ca}^{2+}]_i\right) \tag{3.38}$$

Again, the d and f gates are governed by the first-order Hodgkin-Huxley gating differential equation (Equation (3.5)), with the rate constant coefficients given by

$$\begin{aligned}
\alpha_d &= \frac{0.095\exp(-\frac{V_m-5}{100})}{1+\exp(-\frac{V_m-5}{13.89})}\\
\beta_d &= \frac{0.07\exp(-\frac{V_m+44}{59})}{1+\exp(\frac{V_m+44}{20})}\\
\alpha_f &= \frac{0.012\exp(-\frac{V_m+28}{125})}{1+\exp(\frac{V_m+28}{6.67})}\\
\beta_f &= \frac{0.0065\exp(-\frac{V_m+30}{50})}{1+\exp(-\frac{V_m+30}{5})}
\end{aligned} \tag{3.39}$$

The concentration of intracellular calcium is governed by

$$\frac{d\left([\mathrm{Ca}^{2+}]_i\right)}{dt} = -10^{-4}I_{si} + 0.07(10^{-4} - [\mathrm{Ca}^{2+}]_i) \tag{3.40}$$

and the concentration is measured in units of mM (milli-moles per litre).

Outward currents

Time-dependent potassium current (I_K) This channel is controlled by a time dependent activation gate (X) and a time independent inactivation gate (X_i), neither of which are dependent on $[\mathrm{K}^+]_o$.

$$I_K = \overline{g}_K \cdot X \cdot X_i \cdot (V_m - E_K) \tag{3.41}$$

where the maximum conductance of the potassium channel $\overline{g}_K$ is dependent on $[\mathrm{K}^+]_o$ and is given by

$$\overline{g}_K = 0.282\sqrt{[\mathrm{K}^+]_o/5.4} \tag{3.42}$$

and the reversal potential E_K is given by

$$E_K = \frac{RT}{F} \cdot \ln\left(\frac{[\mathrm{K}^+]_o + P_{NaK}\cdot[\mathrm{Na}^+]_o}{[\mathrm{K}^+]_i + P_{NaK}\cdot[\mathrm{Na}^+]_i}\right) \tag{3.43}$$

where P_{NaK} is the Na/K permeability ratio (given as 0.01833).

X_i is the inward rectification parameter, and is given by

$$X_i = \begin{cases} \frac{2.837(\exp(0.04(V_m+77))-1)}{(V_m+77)\exp(0.04(V_m+35))} & \text{if } V_m > -100\,\text{mV} \\ 1 & \text{if } V_m \leq -100\,\text{mV} \end{cases} \tag{3.44}$$

The gating variable, X, is governed by the Hodgkin-Huxley gating differential equation (Equation (3.5)) with the rate constants given by

$$\begin{aligned} \alpha_X &= 5 \times 10^{-4} \cdot \frac{\exp\left(\frac{V_m+50}{12.1}\right)}{1+\exp\left(\frac{V_m+50}{17.5}\right)} \\ \beta_X &= 0.0013 \cdot \frac{\exp\left(-\frac{V_m+20}{16.67}\right)}{1+\exp\left(-\frac{V_m+20}{25}\right)} \end{aligned} \tag{3.45}$$

Time-independent potassium current (I_{K1}) This channel contains a single inactivation gate ($K1$) whose time constant is small enough that it can be approximated by its steady-state value $K1_\infty$.

$$I_{K1} = \overline{g}_{K1} \cdot K1_\infty \cdot (V_m - E_{K1}) \tag{3.46}$$

where the maximum conductance of the potassium channel $\overline{g}_{K1}$ is given by

$$\overline{g}_{K1} = 0.6047\sqrt{[\text{K}^+]_o/5.4} \tag{3.47}$$

and the reversal potential E_{K1} is equal to E_K, given by Equation (2.1).

The rate constants for $K1$ are given by

$$\begin{aligned} \alpha_{K1} &= \frac{1.02}{1+\exp(0.2385(V_m - E_{K1} - 59.215))} \\ \beta_{K1} &= \frac{0.49124\exp(\frac{V_m-E_{K1}+5.476}{12.45}) + \exp(\frac{V_m-E_{K1}-594.31}{16.2})}{1+\exp(-0.5143(V_m - E_{K1} + 4.753))} \end{aligned} \tag{3.48}$$

and the steady-state value $K1_\infty$ is given by

$$K1_\infty = \frac{\alpha_{K1}}{\alpha_{K1} + \beta_{K1}} \tag{3.49}$$

Plateau potassium current (I_{Kp}) This current has been created in order to describe the contribution of a time independent $[\mathrm{K}^{+}]_o$-insensitive channel at plateau potentials.

$$I_{Kp} = \overline{g}_{Kp} \cdot \mathrm{Kp} \cdot (V_m - E_{Kp}) \tag{3.50}$$

where $\overline{g}_{Kp} = 0.0183$, $E_{Kp} = E_{K1}$, and

$$\mathrm{Kp} = \frac{1}{1 + \exp(\frac{7.488 - V_m}{5.98})} \tag{3.51}$$

Background current (I_b) This is an additional current which contributes at plateau potentials.

$$I_b = \overline{g}_b \cdot (V_m - E_b) \tag{3.52}$$

where $\overline{g}_b = 0.03921$ and $E_b = -59.87\ \mathrm{mV}$

3.2.2 Luo–Rudy II

In a subsequent pair of papers, Luo & Rudy (1994*a*, 1994*b*) further developed the LR-I model by addressing some of the issues which were not investigated in the original model. In particular, the LR-II model incorporates a more thorough description of the processes which regulate $[\mathrm{Ca}^{2+}]_i$ and the movement of Ca^{2+} throughout the cell and within the SR. It is the LR-II model which is implied in this research when referring to the Luo–Rudy (LR) model. The various currents which comprise the LR-II model are summarised in Table 3.1, and show the gate variables associated with each current and the ions which are involved. A schematic describing the ionic currents defined by the LR-II model is given in Figure 3.2. Figure 3.3 shows the membrane potential generated by this model.

Ionic currents in the sarcolemma

The following is a brief discussion of each current, highlighting how it differs from the previous LR-I model. The full equations are given when they differ from those presented in Section 3.2.1, and the parameter values are given in Section A.2.

Fast sodium current (I_{Na}) The formulation of this current is identical to that in the earlier model (Equations (3.35) and (3.36)) in that it describes three gate variables (m, h, and j) with identical rate constants, except that the maximum conductance has decreased to compensate for

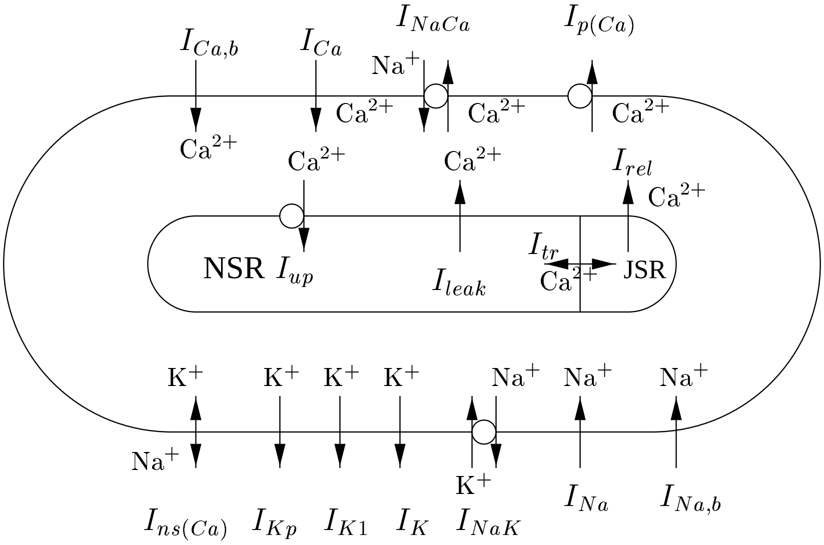

FIGURE 3.2: Schematic diagram of the LR-II model of ionic currents, pumps, and exchangers. *From Sands (1998).*

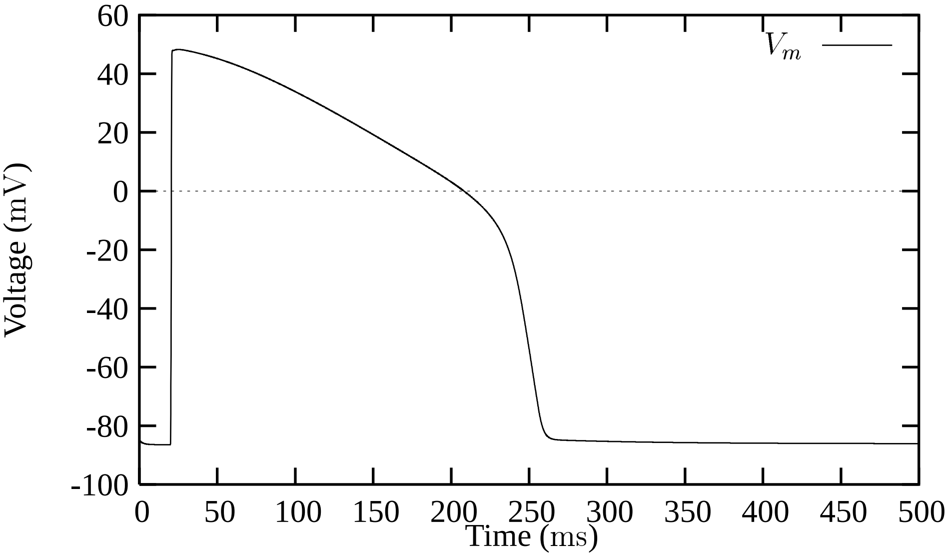

FIGURE 3.3: Membrane potential obtained from the LR-II model of the guinea-pig ventricular myocyte, with the myocyte stimulated at 20 ms with a current of $-100\ \mu\mathrm{A}\cdot\mathrm{cm}^{-2}$ for 5 ms.

	Currents	Gates		Ions	Comments
		Activ.n	Inact.n		
1)	I_{Na}	$\{m^3\}$	$\{h, j\}$	Na$^+$	Fast Na$^+$ channel
2)	$I_{Ca(L)} = I_{Ca(L),Ca} + I_{Ca(L),Na} + I_{Ca(L),K}$	$\{d\}$	$\{f, f_{Ca}\}$	Ca^{2+},Na$^+$,K$^+$	L-type Ca^{2+} channel $f_{Ca} \sim 1/(1 + ([\mathrm{Ca}^{2+}]_i)^2)$
3)	I_K	$\{X^2\}$	$\{X_i\}$	K$^+$	delayed rectifier; $g_{max} \sim \sqrt{[\mathrm{K}^+]_o}$ X_i is V_m-dependent only
4)	I_{NaCa}			Na$^+$,Ca^{2+}	3Na$^+$:Ca^{2+} exchanger
5)	$I_V = I_{K1} + I_{Kp} + I_{p(Ca)} + I_{Na,b} + I_{Ca,b} + I_{NaK}$				total time-independent current
	I_{K1}	$\{K_1\}$		K$^+$	inward rectifier; $g_{max} \sim \sqrt{[\mathrm{K}^+]_o}$
	I_{Kp}			K$^+$	plateau K$^+$ channel
	$I_{p(Ca)}$			Ca^{2+}	Ca^{2+} pump in sarcolemma
	$I_{Na,b}$			Na$^+$	background Na$^+$ leakage
	$I_{Ca,b}$			Ca^{2+}	background Ca^{2+} leakage
	I_{NaK}			Na$^+$,K$^+$	ATP-dep. 3Na$^+$:2K$^+$ pump
6)	$I_{ns(Ca)} = I_{ns,Na} + I_{ns,K}$			Na$^+$,K$^+$	non-specific Ca^{2+} activated
7)	Ca^{2+} cycling				
	I_{rel}			Ca^{2+}	CICR from JSR to myoplasm
	I_{up}			Ca^{2+}	Ca^{2+} uptake from myoplasm to NSR
	I_{leak}			Ca^{2+}	Ca^{2+} leak from NSR to myoplasm
	I_{tr}			Ca^{2+}	Ca^{2+} transfer from NSR to JSR

TABLE 3.1: Description of the ionic currents defined by the LR-II (LR) model.

the increased reversal potentail due to a lower $[\mathrm{Na}^{+}]_i$ which matches observed values in more recent experiments.

Ionic currents through the L-type calcium channel ($I_{Ca(L)}$) This current is the sum of three individual currents (Equation (3.53)) relating to the passage of Ca^{2+}, Na^{+}, and K^{+} ions through this channel in a manner similar to the $I_{Ca(L)}$ current of the DFN model. The channel is permeable to these three ions in the ratio of 2800:3.5:1 (Ca^{2+}:Na^{+}:K^{+}), and therefore the largest individual current is $I_{Ca(L),Ca}$. The model also adds a second inactivation gate f_{Ca} in addition to the standard activation gate d and inactivation gate f. The kinetics of these gates also differ from any previous model to match with recent experimental data.

$$I_{Ca(L)} = I_{Ca(L),Ca} + I_{Ca(L),Na} + I_{Ca(L),K} \tag{3.53}$$

where

$$\begin{aligned} I_{Ca(L),Ca} &= d \cdot f \cdot f_{Ca} \cdot \overline{I_{Ca(L),Ca}} \\ I_{Ca(L),Na} &= d \cdot f \cdot f_{Ca} \cdot \overline{I_{Ca(L),Na}} \\ I_{Ca(L),K} &= d \cdot f \cdot f_{Ca} \cdot \overline{I_{Ca(L),K}} \end{aligned} \tag{3.54}$$

and for ion S, including Ca^{2+}, Na^{+}, and K^{+}, the fully activated current is given by:

$$\overline{I_S} = P_S \cdot z_S^2 \cdot \frac{V_m F^2}{RT} \cdot \frac{\gamma_{Si} \cdot [\mathrm{S}]_i \cdot \exp\left(z_S V_m F/RT\right) - \gamma_{So} \cdot [\mathrm{S}]_o}{\exp\left(z_S V_m F/RT\right) - 1} \tag{3.55}$$

where P_S is the permeability of the membrane to ion S; z_S is the valence of ion S; γ_{Si} and γ_{So} are the intracellular and extracellular activity coefficients of ion S.

The gating variables d and f are governed by the Hodgkin-Huxley type gating differential equation (Equation (3.5)), with the rate constant coefficients

$$\begin{aligned} \alpha_d &= d_\infty/\tau_d \\ \beta_d &= (1 - d_\infty)/\tau_d \\ \alpha_f &= f_\infty/\tau_f \\ \beta_f &= (1 - f_\infty)/\tau_f \end{aligned} \tag{3.56}$$

where

$$\begin{aligned} d_\infty &= \frac{1}{1+\exp\left(-\frac{V_m+10}{6.24}\right)} \\ \tau_d &= d_\infty \cdot \frac{1-\exp\left(-\frac{V_m+10}{6.24}\right)}{0.035\cdot(V_m+10)} \end{aligned} \tag{3.57}$$

and

$$\begin{aligned} f_\infty &= \frac{1}{1+\exp\left(\frac{V_m+35.06}{8.6}\right)} + \frac{0.6}{1+\exp\left(\frac{50-V_m}{20}\right)} \\ \tau_f &= \frac{1}{0.0197\cdot\exp\left(-\left[0.0337\cdot(V_m+10)\right]^2\right)+0.02} \end{aligned} \tag{3.58}$$

The new inactivation gate, f_{Ca}, is given by

$$f_{Ca} = \frac{1}{1+\left(\frac{[\mathrm{Ca}^{2+}]_i}{K_{m,Ca}}\right)^2} \tag{3.59}$$

where $K_{m,Ca}$ is the half activation concentration for Ca^{2+}.

Time-dependent potassium current (I_K) This current now includes an X^2 dependence on the activation gate which was suggested as necessary in the earlier model, but was unable to be successfully incorporated until the $I_{Ca(L)}$ current was properly formulated. The X_i inactivation gate is still present, but both gates have new kinetics. I_K is now given by

$$I_K = \overline{g}_K \cdot X_i \cdot X^2 \cdot (V_m - E_K) \tag{3.60}$$

where $\overline{g}_K$ and E_K are the same as in the LR-I model (Equations (3.42) and (3.43)). X_i is now controlled by

$$X_i = \frac{1}{1+\exp\left(\frac{V_m-56.26}{32.1}\right)} \tag{3.61}$$

and the rate constant coefficients for the X gate are now

$$\begin{aligned} \alpha_X &= \frac{7.19\times10^{-5}\cdot(V_m+30)}{1-\exp(-0.148\cdot(V_m+30))} \\ \beta_X &= \frac{1.31\times10^{-4}\cdot(V_m+30)}{-1+\exp(0.0687\cdot(V_m+30))} \end{aligned} \tag{3.62}$$

Na^+,Ca^{2+} *exchanger* (*I_{NaCa}*) This current has a new formulation from the original in the DFN model which corrects several deficiencies in its dependence on the various ions, and is given as

$$I_{NaCa} = k_{NaCa} \cdot \frac{1}{K_{m,Na}^3 + [\mathrm{Na}^+]_o^3} \cdot \frac{1}{K_{m,Ca} + [\mathrm{Ca}^{2+}]_o} \cdot \frac{1}{1 + k_{sat} \cdot \exp\left((\eta - 1) \cdot V_m \cdot \frac{F}{RT}\right)} \cdot \left\{ \exp\left(\eta \cdot V_m \cdot \frac{F}{RT}\right) \cdot [\mathrm{Na}^+]_i^3 \cdot [\mathrm{Ca}^{2+}]_o - \exp\left((\eta - 1) \cdot V_m \cdot \frac{F}{RT}\right) \cdot [\mathrm{Na}^+]_o^3 \cdot [\mathrm{Ca}^{2+}]_i \right\} \tag{3.63}$$

where η is the position of the energy barrier controlling voltage dependence (given as 0.35), and k_{sat} is the saturation factor of I_{NaCa} at very negative potentials.

***Time-independent potassium current* (*I_{K1}*)** This current is identical to the LR-I formulation (Equations (3.46)–(3.49)) except that, because of the more accurately formulated $I_{Ca(L)}$, the maximum conductance can be increased slightly to a more realistic level

$$\overline{g}_{K1} = 0.75\sqrt{[\mathrm{K}^+]_o/5.4} \tag{3.64}$$

***Plateau potassium current* (*I_{Kp}*)** Identical to the LR-I model (Equations (3.50) and (3.51)).

***Sarcolemmal calcium pump* (*$I_{p(Ca)}$*)** An additional mechanism for removing Ca^{2+} from the myoplasm to help maintain a low $[\mathrm{Ca}^{2+}]_i$ at rest, given as

$$I_{p(Ca)} = \overline{I_{p(Ca)}} \cdot \frac{[\mathrm{Ca}^{2+}]_i}{K_{m,p(Ca)} + [\mathrm{Ca}^{2+}]_i} \tag{3.65}$$

where $\overline{I_{p(Ca)}} = 1.15\ \mu\mathrm{A} \cdot \mathrm{cm}^{-2}$ and $K_{m,p(Ca)} = 0.5\ \mu\mathrm{M}$.

***Sodium background current* (*$I_{Na,b}$*)** Similar to the background sodium current in the DFN model.

$$I_{Na,b} = \overline{g}_{Na,b} \cdot (V_m - E_{Na,N}) \tag{3.66}$$

where $E_{Na,N} = E_{Na}$.

***Calcium background current* (*$I_{Ca,b}$*)** The same as for the DFN model (Equation (3.15)), except for a difference in the maximal conductance.

Na^+**,**K^+***-ATPase*** ***(***I_{NaK}***)*** This is reformulated from the equations in the DFN model to correctly simulate the voltage dependence of this current on the level of $[\mathrm{Na}^+]_o$.

$$I_{NaK} = \overline{I_{NaK}} \cdot f_{NaK} \cdot \frac{1}{1 + \sqrt{\left(K_{m,Nai}/[\mathrm{Na}^+]_i\right)^3}} \cdot \frac{[\mathrm{K}^+]_o}{[\mathrm{K}^+]_o + K_{m,Ko}} \tag{3.67}$$

where

$$f_{NaK} = \frac{1}{1 + 0.1245 \cdot \exp\left(-0.1 \cdot \frac{V_m F}{RT}\right) + 0.0365 \cdot \sigma \cdot \exp\left(-\frac{V_m F}{RT}\right)} \tag{3.68}$$

with

$$\sigma = \frac{1}{7} \cdot \left[\exp\left(\frac{[\mathrm{Na}^+]_o}{67.3}\right) - 1\right] \tag{3.69}$$

Total time-independent current (I_V***)*** The previous six currents are combined into a single time-independent, purely voltage-dependent current, which is the equivalent of $I_{K1(T)}$ from Luo & Rudy (1991).

$$I_V = I_{K1} + I_{Kp} + I_{p(Ca)} + I_{Na,b} + I_{Ca,b} + I_{NaK} \tag{3.70}$$

Non-specific calcium-activated current ($I_{ns(Ca)}$***)*** This current describes a channel which is activated by Ca^{2+}, but is permeable to only Na^+ and K^+,

$$I_{ns(Ca)} = I_{ns,Na} + I_{ns,K} \tag{3.71}$$

where the component currents are

$$I_{ns,Na} = \overline{I_{ns,Na}} \cdot \frac{1}{1 + \left(K_{m,ns(Ca)}/[\mathrm{Ca}^{2+}]_i\right)^3} \tag{3.72}$$

and

$$I_{ns,K} = \overline{I_{ns,K}} \cdot \frac{1}{1 + \left(K_{m,ns(Ca)}/[\mathrm{Ca}^{2+}]_i\right)^3} \tag{3.73}$$

The fully activated currents, $\overline{I_{ns,Na}}$ and $\overline{I_{ns,K}}$, are calculated from Equation (3.55), using $P_{ns(Ca)} = 1.75 \times 10^{-7}\ \mathrm{cm} \cdot \mathrm{s}^{-1}$ with the same γ values.

Ionic concentrations

The LR-II model keeps track of the three main ions (Ca^{2+}, Na^{+}, and K^{+}), as well as Ca^{2+} concentrations in the JSR and NSR. The total calcium ion entry up to $2\ \mathrm{ms}$ after the onset of a stimulus ($[\mathrm{Ca}^{2+}]_{foot}$) is also tracked, to be used for the triggering of CICR. These concentrations are given by

$$\frac{d[\mathrm{Na}^+]_i}{dt} = -\left(I_{Na} + I_{Ca(L),Na} + I_{Na,b} + I_{ns,Na} + 3I_{NaCa} + 3I_{NaK}\right) \cdot \frac{A_{cap}}{V_{myo}F} \tag{3.74}$$

$$\begin{aligned} \frac{d[\mathrm{Ca}^{2+}]_i}{dt} &= -\left(I_{Ca(L),Ca} - I_{NaCa} + I_{p(Ca)} + I_{Ca,b}\right) \cdot \frac{A_{cap}}{2V_{myo}F} + I_{rel} \cdot \frac{V_{JSR}}{V_{myo}} \\ &\quad + \left(I_{leak} - I_{up}\right) \cdot \frac{V_{NSR}}{V_{myo}} \end{aligned} \tag{3.75}$$

$$\frac{d[\mathrm{K}^+]_i}{dt} = -\left(I_{Ca(L),K} + I_K + I_{K1} + I_{Kp} - 2I_{NaK} + I_{ns,K}\right) \cdot \frac{A_{cap}}{V_{myo}F} \tag{3.76}$$

$$\frac{d[\mathrm{K}^+]_o}{dt} = \left(I_{Ca(L),K} + I_K + I_{K1} + I_{Kp} - 2I_{NaK} + I_{ns,K}\right) \cdot \frac{A_{cap}}{V_{cleft}F} \tag{3.77}$$

$$\frac{d[\mathrm{Ca}^{2+}]_{JSR}}{dt} = -\left(I_{rel} - I_{tr} \cdot \frac{V_{NSR}}{V_{JSR}}\right) \tag{3.78}$$

$$\frac{d[\mathrm{Ca}^{2+}]_{NSR}}{dt} = -\left(I_{leak} + I_{tr} - I_{up}\right) \tag{3.79}$$

$$\frac{d[\mathrm{Ca}^{2+}]_{foot}}{dt} = -I_{Ca(L),Ca} \cdot \frac{A_{cap}}{2V_{myo}F} \cdot R_{A,V} \tag{3.80}$$

where A_{cap} is the capacitive membrane area and $R_{A,V}$ is an arbitrary adjustment factor for reduction in volume and area, since we are only interested in the region closest to the L-type Ca^{2+} channels and the release channels of the JSR. I_{up}, I_{rel}, I_{leak}, and I_{tr} are Ca^{2+}-fluxes into and out of the SR, and are defined below.

Calcium buffers in the myoplasm

The LR-II model begins to define the Ca^{2+} buffers in the myoplasm: troponin (Tn) and calmodulin (CMDN), with

$$[\mathrm{Tn}]_{buffered} = \overline{[\mathrm{Tn}]} \cdot \frac{[\mathrm{Ca}^{2+}]_i}{[\mathrm{Ca}^{2+}]_i + K_{m,Tn}} \tag{3.81}$$

and

$$[\mathrm{CMDN}]_{buffered} = \overline{[\mathrm{CMDN}]} \cdot \frac{[\mathrm{Ca}^{2+}]_i}{[\mathrm{Ca}^{2+}]_i + K_{m,CMDN}} \tag{3.82}$$

Calcium fluxes in the SR

A much more sophisticated model of calcium movement to and from (and within) the SR has been developed for this model which is substantially different from the calcium transport model formulated in the DFN model. It includes an additional current I_{leak} which describes the leakage of Ca^{2+} from the NSR to the myoplasm as well as a detailed model of the processes of CICR.

Calcium release from the JSR is given by

$$I_{rel} = G_{rel} \cdot \left([\mathrm{Ca}^{2+}]_{JSR} - [\mathrm{Ca}^{2+}]_i\right) \tag{3.83}$$

where G_{rel} is the rate constant of Ca^{2+} release from the JSR and is given by

$$G_{rel} = \overline{G_{rel}} \cdot \frac{\Delta[\mathrm{Ca}^{2+}]_{i,2} - \Delta[\mathrm{Ca}^{2+}]_{i,th}}{K_{m,rel} + \Delta[\mathrm{Ca}^{2+}]_{i,2} - \Delta[\mathrm{Ca}^{2+}]_{i,th}} \cdot \left(1 - \exp\left[-\frac{t}{\tau_{on}}\right]\right) \cdot \exp\left[-\frac{t}{\tau_{off}}\right] \tag{3.84}$$

where $\Delta[\mathrm{Ca}^{2+}]_{i,2}$ is the cumulative Ca^{2+} entry into the cell $2\ \mathrm{ms}$ after the onset of stimulus or $\dot{V}_{max}$ (where $\dot{V}_{max}$ is the maximum rate of change of potential), $\Delta[\mathrm{Ca}^{2+}]_{i,th}$ is the threshold for external triggering of Ca^{2+} release from the JSR, τ_{on} and τ_{off} are the time constants of activating (on) and deactivating (off) Ca^{2+} release from the JSR, time (t) is set to zero at the time of CICR, and $\overline{G_{rel}}$ is given by

$$\overline{G_{rel}} = \begin{cases} 60\ \mathrm{ms}^{-1} & \text{if } \Delta[\mathrm{Ca}^{2+}]_{i,2} > \Delta[\mathrm{Ca}^{2+}]_{i,th} \text{ at 2 ms after } \dot{V}_{max} \\ 0\ \mathrm{ms}^{-1} & \text{if } \Delta[\mathrm{Ca}^{2+}]_{i,2} < \Delta[\mathrm{Ca}^{2+}]_{i,th} \text{ at 2 ms after } \dot{V}_{max} \end{cases} \tag{3.85}$$

When the cell is under Ca^{2+}-overload conditions, the second term is dropped from Equation (3.84) to give

$$G_{rel} = \overline{G_{rel}} \cdot \left(1 - \exp\left[-\frac{t}{\tau_{on}}\right]\right) \cdot \exp\left[-\frac{t}{\tau_{off}}\right] \tag{3.86}$$

and Equation (3.85) becomes

$$\overline{G_{rel}} = \begin{cases} 4\ \mathrm{ms}^{-1} & \text{if } [\mathrm{CSQN}]_{buffered} \geq [\mathrm{CSQN}]_{th} \\ 0\ \mathrm{ms}^{-1} & \text{if } [\mathrm{CSQN}]_{buffered} < [\mathrm{CSQN}]_{th} \end{cases} \tag{3.87}$$

where $[\mathrm{CSQN}]_{th}$ is the threshold of Ca^{2+}-bound $[\mathrm{CSQN}]$ for internal triggering of Ca^{2+} release from the JSR under Ca^{2+}-overload conditions, and

$$[\mathrm{CSQN}]_{buffered} = \overline{[\mathrm{CSQN}]} \cdot \frac{[\mathrm{Ca}^{2+}]_{JSR}}{[\mathrm{Ca}^{2+}]_{JSR} + K_{m,CSQN}} \tag{3.88}$$

The uptake of calcium into the NSR is given by

$$I_{up} = \overline{I_{up}} \cdot \frac{[\mathrm{Ca}^{2+}]_i}{[\mathrm{Ca}^{2+}]_i + K_{m,up}} \tag{3.89}$$

and the calcium leakage from the NSR is given by

$$I_{leak} = K_{leak} \cdot [\mathrm{Ca}^{2+}]_{NSR} \tag{3.90}$$

where K_{leak} is the rate constant of Ca^{2+} leakage from the NSR, given by

$$K_{leak} = \overline{I_{up}} / \overline{[\mathrm{Ca}^{2+}]_{NSR}} \tag{3.91}$$

The translocation of Ca^{2+} ions from the NSR (uptake store) to the JSR (release store) is given by the translocation current,

$$I_{tr} = \frac{[\mathrm{Ca}^{2+}]_{NSR} - [\mathrm{Ca}^{2+}]_{JSR}}{\tau_{tr}} \tag{3.92}$$

with $\tau_{tr} = 180\,\mathrm{ms}$

3.2.3 Species restriction

The authors note in the papers (Luo & Rudy (1991, 1994*a*, 1994*b*)) that the results generated are specific to the guinea-pig ventricular cells, and cannot be extrapolated to other animals, as the contribution of each of the various currents is markedly different.

3.2.4 The Luo–Rudy model

The governing equation for the LR model is

$$\frac{dV_m}{dt} = \frac{-I_{LR}}{C_m} \tag{3.93}$$

where I_{LR} is the sum of the ionic currents, given in Section 3.2.2,

$$I_{LR} = I_{Na} + I_{Ca(L)} + I_K + I_{NaCa} + I_V + I_{ns(Ca)} + I_{stim} \tag{3.94}$$

and Figure 3.3 shows a plot of the membrane potential.

3.3 The Jafri–Rice–Winslow Model

Both the DFN and LR models discussed above generate action potentials using biophysically detailed descriptions of membrane currents, but the calcium subsystem is represented by a phenomenological model that mimics CICR. Other models exist (Dupont, Pontes & Goldbeter 1996, Tang & Othmer 1994, Schouten, van Deen, de Tombe & Verveen 1987) which model the Ca^{2+} handling aspects of the cardiac myocyte, but do not model the membrane currents. The JRW model takes an accurate model of the membrane currents and adds a more sophisticated model of Ca^{2+} handling.

The JRW model is based on the LR-II model for ventricular action potentials with several modifications (Figure 3.4):

- the L-type Ca^{2+} current is replaced with a new formulation based on the mode-switching behaviour observed in rats by Imredy & Yue (1994);
- the LR-II Ca^{2+} SR release mechanism is replaced with the Keizer-Levine ryanodine receptor (RyR) model with adpatation (Keizer & Levine 1996) based on data from isolated canine RyRs;
- the RyRs and L-type Ca^{2+} channels are assumed to empty into a restricted subspace located between the JSR and T-tubules;
- both high- and low-affinity Ca^{2+} binding sites for troponin (Tn) are included;
- the magnitude of the LR-II membrane currents I_{Kp}, I_{Na}, I_{NaCa}, $I_{ns(Ca)}$, and $I_{Ca,b}$ are scaled to preserve myoplasmic ionic concentrations and action potential shape. See Section A.3 for parameter values.

The following sections give an overview of the JRW model and the differences with the LR-II model.

3.3.1 Background

L-type Ca^{2+} ***channel*** It has been shown recently (de Leon, Wang, Jones, Perez-Reyes, Wei, Soong, Snutch & Yue 1995) that inactivation of the L-type Ca^{2+} channel depends on local Ca^{2+} concentration instead of other hypothesised extrinsic mechanisms such as phosphorylation or second messengers. Inactivation occurs as Ca^{2+} binding induces the channel to switch (from

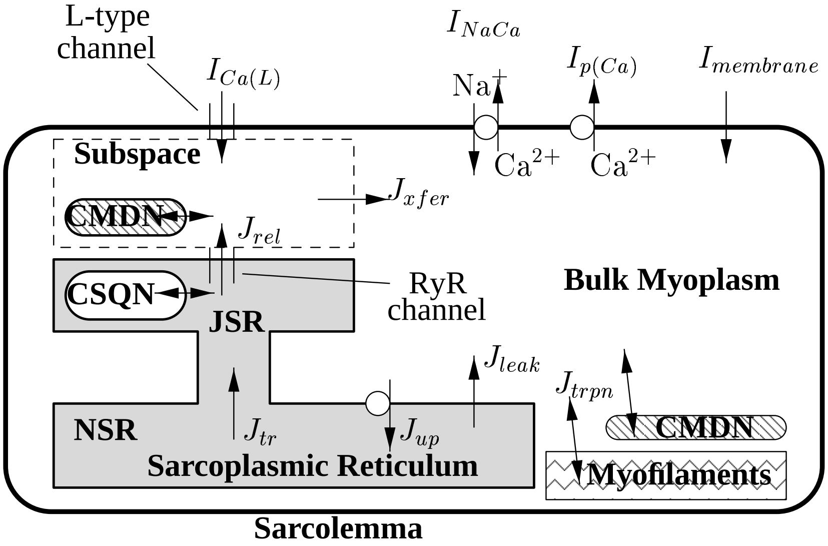

FIGURE 3.4: Schematic diagram of of mechanisms involved in cardiac Ca^{2+} dynamics. In response to membrane depolarisation during an action potential, L-type Ca^{2+} channels open, allowing the influx of Ca^{2+} ($I_{Ca(L),Ca}$) into a restricted subspace, where it triggers Ca^{2+} release from the JSR (J_{rel}) via RyR. Ca^{2+} diffuses from the subspace to the bulk myoplasm (J_{xfer}), where it is removed from the cell by Na$^+$,Ca^{2+} exchangers (I_{NaCa}) and the ATP-dependent Ca^{2+} pumps ($I_{p(Ca)}$) or resequestered into the NSR (J_{up}). The JSR is refilled by diffusion from the NSR (J_{tr}). Ca^{2+} is buffered by CMDN in the subspace and myoplasm, by Tn in the myplasm, and by CSQN in the JSR. There is a leak (J_{leak}) from the NSR and a background Ca^{2+} current across the sarcolemma (included in $I_{membrane}$), which help to maintain Ca^{2+} homeostasis. $I_{membrane}$ includes all the other transarcolemmal currents that are not defined above. *From Jafri et al. (1998).*

mode normal) to a mode in which transitions to open states are extremely slow (mode Ca), as described in a model by Imredy & Yue (1994). This model, in contrast to current models (*e.g.*, DFN and LR) which use a function of $[\mathrm{Ca}^{2+}]_i$ that can instantaneously prevent channel permeation, predicts that inactivation via mode switching occurs with some delay after channel activation. Similarly, the model predicts that recovery to mode normal is not instantaneous when Ca^{2+} concentration falls.

The data of Imredy & Yue (1994) shows that with an increase of local Ca^{2+}, the L-type channel shifts to a gating mode that shows very infrequent openings. A state diagram for the mode switching and voltage-dependent activation of the JRW model is shown in Figure 3.5. This description of the two-mode behaviour is based on the original Imredy-Yue model, with several modifications. The proportionality of the forward or reverse rates between the closed states is dictated by the four-way symmetry assumed for the channel subunits. Voltage-dependent activation is incorporated through α and β, which are increasing and decreasing functions of voltage.

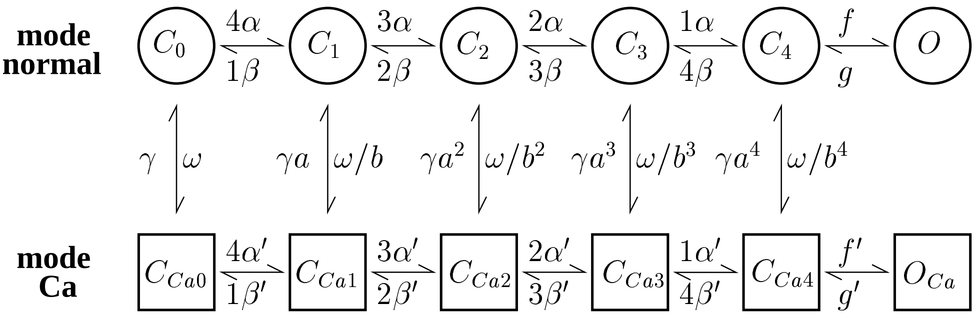

FIGURE 3.5: Schematic diagram for the transitions between the states of the L-type Ca^{2+} channel. The upper row of states comprises the mode normal, and the lower row comprises mode Ca. The channel is composed of four independent subunits, each of which can close the channel. The corresponding states are C_n, where n is the number of permissive subunits. With depolarisation, the channels undergo transitions from left to right. With four permissive subunits, there is a voltage-independent transition to the conducting state O. With elevation of $[\mathrm{Ca}^{2+}]_{SS}$ the channel transition occurs from the mode normal (top) to the mode Ca (bottom). $f' \ll f$, so that transitions into O_{Ca} are rare, which effectively inactivates the channel in mode Ca. *From Jafri et al. (1998).*

The transitions to mode Ca are controlled by γ, which is a function of Ca^{2+}. As one moves right in Figure 3.5, there are incremental increases in the multiplier of γ and the divisor on ω. The effect of this is to greatly increase the transition rate to mode Ca at high voltages when the channel is opening. The close symmetry between mode normal and mode Ca closed states and similarity of rates is dictated by the experimental finding that gating currents are very similar in the mode normal and mode Ca cases (Shirokov, Levis, Shirokov & Rios 1993, Hadley & Lederer 1991).

Voltage-dependent inactivation is modelled as a Hodgkin-Huxley type gate. This gate can inactivate the channel independently of the states discussed above. The time constant of inactivation is significantly longer than that of the DFN and LR models, due to the assumption of these models that Ca^{2+}-induced inactivation is an instantaneous function of $[\mathrm{Ca}^{2+}]_i$ with dynamics due solely to voltage-gated inactivation.

Ryanodine receptors Ca^{2+} release from the JSR is based on a model for RyR by Keizer & Levine (1996) (Figure 3.6). The RyR is modified from the original Keizer & Levine (1996) model to account for the environment of the subspace. The Keizer-Levine model assumes that the RyR can be exposed to peak $[\mathrm{Ca}^{2+}]_i$ values of $\sim 1.0\ \mu\mathrm{M}$. In the JRW model, the RyR is located in the subspace, where it is exposed to $[\mathrm{Ca}^{2+}]_{SS}$ in excess of $10.0\ \mu\mathrm{M}$. In addition, $[\mathrm{Ca}^{2+}]_{SS}$ levels change more rapidly than $[\mathrm{Ca}^{2+}]_i$. Thus, the rate constants are modified to adjust the channel sensitivity to Ca^{2+}, so that the channel functions properly in the appropriate Ca^{2+} range.

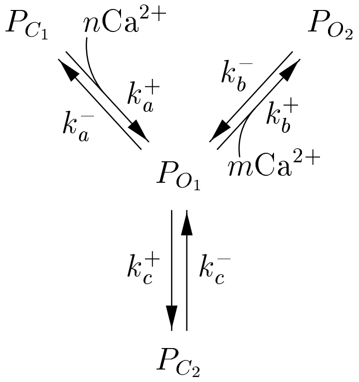

FIGURE 3.6: Schematic diagram of the transitions between the states of the RyR. P_{C_1} and P_{C_2} are closed states, and P_{O_1} and P_{O_2} are open states. The k's are the transition rates. The transition from P_{C_1} to P_{O_1} and from P_{O_1} to P_{O_2} are Ca^{2+} dependent. At resting Ca^{2+} levels, most of the channels are in state P_{C_1}. With an increase in Ca^{2+}, the channels undergo transitions to P_{O_1} before channel adaptation by transition to P_{C_2}. Additional increases in Ca^{2+} cause reopening by transitions into P_{O_2}. *From Jafri et al. (1998).*

Subspace Many existing cardiac action potential models have Ca^{2+} influx from an L-type channel and release from the SR via RyR emptying into the bulk myoplasm (*e.g.*, the DFN and LR models). In contrast, following recent experimental findings, the JRW model have these channels emptying into a more restricted subspace, where Ca^{2+} concentration may increase to much greater levels than in the bulk myoplasm. The volume of this restricted subspace is found to be approximately four orders of magnitude smaller than the total volume of the myoplasm (Jafri et al. 1998). The rate of Ca^{2+} flux out of this subspace (J_{xfer}) allows $[\mathrm{Ca}^{2+}]_{SS}$ and $[\mathrm{Ca}^{2+}]_i$

to equilibriate with a time constant τ_{xfer} (Equation (3.101)).

Buffering Ca^{2+} buffers sequester in excess of 98% of the total Ca^{2+} released during a contraction (Berlin, Bassani & Bers 1994). In cardiac cells, the buffers are calmodulin (CMDN) and troponin (Tn) in the myoplasm, and calsequestrin (CSQN) in the NSR. Buffer B binds Ca^{2+} by the equation

$$B + \mathrm{Ca}^{2+} \rightleftharpoons B\mathrm{Ca}^{2+} \tag{3.95}$$

If the kinetics of binding are fast compared to Ca^{2+} release, Equation (3.95) remains close to equilibrium during the Ca^{2+} transient. In this case, the rapid buffering approximation is used (Wagner & Keizer 1994). CSQN and CMDN are considered fast buffers, based on their rate constants. Otherwise, Ca^{2+} binding to buffers lags behind the equilibrium values, as is the case with Tn. In this case, differential equations based on reaction kinetics must be solved. Both the high- and low-affinity sites for Tn are used in the JRW model.

3.3.2 Ca^{2+} subsystem

The Ca^{2+} subsystem consists of ten differential equations specifying the time rate of change in

- the myoplasmic Ca^{2+} concentrations ($[\mathrm{Ca}^{2+}]_i$);
- the subapce Ca^{2+} concentration ($[\mathrm{Ca}^{2+}]_{SS}$);
- the JSR Ca^{2+} concentration ($[\mathrm{Ca}^{2+}]_{JSR}$);
- the NSR Ca^{2+} concentration ($[\mathrm{Ca}^{2+}]_{NSR}$);
- the probability that RyR is in the first closed state (P_{C_1});
- the probability that RyR is in the first open state (P_{O_1});
- the probability that RyR is in the second open state (P_{O_2});
- the probability that RyR is in the second closed state (P_{C_2});
- the concentration of Ca^{2+} bound to high-affinity Tn-binding sites ($[\mathrm{HTRPNCa}]$);
- the concentration of Ca^{2+} bound to low-affinity Tn-binding sites ($[\mathrm{LTRPNCa}]$).

There are six Ca^{2+} fluxes to consider (Figure 3.4) – J_{rel}, J_{leak}, J_{up}, J_{tr}, J_{xfer}, and J_{trpn}. In addition, three membrane current fluxes are also necessary for the formulation of Ca^{2+} regulation – $I_{p(Ca)}$, $I_{Ca(L),Ca}$, and I_{NaCa}.

The RyR channel flux is given by

$$J_{rel} = v_1 \cdot RyR_{open} \cdot \big([\mathrm{Ca}^{2+}]_{JSR} - [\mathrm{Ca}^{2+}]_{SS}\big) \tag{3.96}$$

where v_1 is the maximum RyR channel Ca^{2+} flux, and RyR_{open} is the sum of the fraction of channels in the RyR channel open states P_{O_1} and P_{O_2} ($RyR_{open} = P_{O_1} + P_{O_2}$). The equations describing RyR are

$$\begin{aligned}
\frac{dP_{C_1}}{dt} &= -k_a^+ \cdot [\mathrm{Ca}^{2+}]_{SS}^n \cdot P_{C_1} + k_a^- \cdot P_{O_1} \\
\frac{dP_{O_1}}{dt} &= k_a^+ \cdot [\mathrm{Ca}^{2+}]_{SS}^n \cdot P_{C_1} - k_a^- \cdot P_{O_1} \\
&\quad - k_b^+ \cdot [\mathrm{Ca}^{2+}]_{SS}^m \cdot P_{O_1} + k_b^- \cdot P_{O_2} \\
&\quad - k_c^+ \cdot P_{O_1} + k_c^- \cdot P_{C_2} \\
\frac{dP_{O_2}}{dt} &= k_b^+ \cdot [\mathrm{Ca}^{2+}]_{SS}^m \cdot P_{O_1} - k_b^- \cdot P_{O_2} \\
\frac{dP_{C_2}}{dt} &= k_c^+ \cdot P_{O_1} - k_c^- \cdot P_{C_2}
\end{aligned} \tag{3.97}$$

The leak from the NSR into the myoplasm is given by

$$J_{leak} = v_2 \cdot \big([\mathrm{Ca}^{2+}]_{NSR} - [\mathrm{Ca}^{2+}]_i\big) \tag{3.98}$$

where v_2 is the Ca^{2+} leak rate constant from the NSR. Ca^{2+} uptake into the NSR by the SR Ca^{2+}-pump is given by

$$J_{up} = v_3 \cdot \frac{[\mathrm{Ca}^{2+}]_i^2}{K_{m,up}^2 + [\mathrm{Ca}^{2+}]_i^2} \tag{3.99}$$

where v_3 is the SR Ca^{2+}-pump maximum pump rate, and $K_{m,up}$ is the half-saturation constant for the SR Ca^{2+}-pumps. The transfer flux of Ca^{2+} from the NSR to the JSR is described by

$$J_{tr} = \frac{[\mathrm{Ca}^{2+}]_{NSR} - [\mathrm{Ca}^{2+}]_{JSR}}{\tau_{tr}} \tag{3.100}$$

where τ_{tr} is the time constant for the transfer from NSR to JSR. The transfer flux from the subspace to the myoplasm is

$$J_{xfer} = \frac{[\mathrm{Ca}^{2+}]_{SS} - [\mathrm{Ca}^{2+}]_i}{\tau_{xfer}} \tag{3.101}$$

where τ_{xfer} is the time constant for transfer from subapce to myoplasm. Buffering by Tn is described by

$$\begin{aligned} J_{trpn} = k^{+}_{htrpn} \cdot [\mathrm{Ca}^{2+}]_i \cdot ([\mathrm{HTRPN}]_{tot} - [\mathrm{HTRPNCa}]) - k^{-}_{htrpn} \cdot [\mathrm{HTRPNCa}] \\ + k^{+}_{ltrpn} \cdot [\mathrm{Ca}^{2+}]_i \cdot ([\mathrm{LTRPN}]_{tot} - [\mathrm{LTRPNCa}]) - k^{-}_{ltrpn} \cdot [\mathrm{LTRPNCa}] \end{aligned} \tag{3.102}$$

where $[\mathrm{LTRPN}]_{tot}$ is the total myoplasmic Tn low-affinity site concentration, $[\mathrm{HTRPN}]_{tot}$ is the total myoplasmic Tn high-affinity site concentration, k^{+}_{htrpn} and k^{-}_{htrpn} are the Ca^{2+} on and off rate constants, respectively, for Tn high-affinity sites, k^{+}_{ltrpn} and k^{-}_{ltrpn} are the Ca^{2+} on and off rate constants, respectively, for Tn low-affinity sites.

The buffering effects of CMDN and CSQN can be approximated by the rapid buffering approximation (Wagner & Keizer 1994). This simplification assumes that the free and bound Ca^{2+} buffers with fast kinetics are at equilibrium. Using this assumption, a Ca^{2+}-dependent function can be found that will scale the fluxes that comprise the rate of change in total free Ca^{2+} by the factors B_i, B_{SS}, and B_{JSR} for the myoplasm, subspace and JSR, respectively:

$$B_i = \left\{ 1 + \frac{[\mathrm{CMDN}]_{tot} \cdot K_m^{CMDN}}{\left(K_m^{CMDN} + [\mathrm{Ca}^{2+}]_i\right)^2} \right\}^{-1} \tag{3.103}$$

$$B_{SS} = \left\{ 1 + \frac{[\mathrm{CMDN}]_{tot} \cdot K_m^{CMDN}}{\left(K_m^{CMDN} + [\mathrm{Ca}^{2+}]_{SS}\right)^2} \right\}^{-1} \tag{3.104}$$

$$B_{JSR} = \left\{ 1 + \frac{[\mathrm{CSQN}]_{tot} \cdot K_m^{CSQN}}{\left(K_m^{CSQN} + [\mathrm{Ca}^{2+}]_{JSR}\right)^2} \right\}^{-1} \tag{3.105}$$

The balance equation for $[\mathrm{Ca}^{2+}]_i$ is

$$\frac{d[\mathrm{Ca}^{2+}]_i}{dt} = B_i \left\{ J_{leak} + J_{xfer} - J_{up} - J_{trpn} - \left(I_{Ca,b} - 2I_{NaCa} + I_{p(Ca)}\right) \cdot \frac{A_{cap}}{2 \cdot V_{myo} \cdot F} \right\} \tag{3.106}$$

where A_{cap} is the capacitive membrane area, V_{myo} is the myoplasmic volume, 2 is the valence of Ca^{2+}, and F is Faraday's constant. Changes to $[\mathrm{Ca}^{2+}]_{SS}$ are determined by

$$\frac{d[\mathrm{Ca}^{2+}]_{SS}}{dt} = B_{SS} \left\{ J_{rel} \frac{V_{JSR}}{V_{SS}} - J_{xfer} \frac{V_{myo}}{V_{SS}} - I_{Ca(L),Ca} \cdot \frac{A_{cap}}{2 \cdot V_{SS} \cdot F} \right\} \tag{3.107}$$

Note the the fluxes J_{rel} and J_{xfer} are scaled for the volume of the compartment. See Section 3.3.3 for a detailed description of $I_{Ca(L),Ca}$, and Section 3.3.4 for descriptions of the $I_{Ca,b}$, I_{NaCa}, and $I_{p(Ca)}$ currents. The $[\mathrm{Ca}^{2+}]_{JSR}$ and $[\mathrm{Ca}^{2+}]_{NSR}$ balance equations are

$$\frac{d[\mathrm{Ca}^{2+}]_{JSR}}{dt} = B_{JSR}\left\{J_{tr} - J_{rel}\right\} \tag{3.108}$$

$$\frac{d[\mathrm{Ca}^{2+}]_{NSR}}{dt} = \left\{J_{up} - J_{leak}\right\} \cdot \frac{V_{myo}}{V_{NSR}} - J_{tr} \cdot \frac{V_{JSR}}{V_{NSR}} \tag{3.109}$$

3.3.3 L-type Ca^{2+} channel

The JRW model creates a new mathematical model to describe the L-type channel that is based on the experimentally observed mode-switching behaviour of the channel. The rate constants for the L-type Ca^{2+} channel depend on material parameters (Section A.3) and

$$\alpha = 0.4 \exp\left(\frac{V_m + 12}{10}\right) \tag{3.110}$$

$$\beta = 0.05 \exp\left(\frac{-(V_m + 12)}{13}\right) \tag{3.111}$$

$$\alpha' = \alpha \cdot a \tag{3.112}$$

$$\beta' = \frac{\beta}{b} \tag{3.113}$$

$$\gamma = 0.1875 \cdot [\mathrm{Ca}^{2+}]_{SS} \tag{3.114}$$

where α, β, γ, α', and β' are in units of ms^{-1}. This yields the following set of equations for channel states:

$$\frac{dC_0}{dt} = \beta C_1 + \omega C_{Ca0} - (4\alpha + \gamma)C_0 \tag{3.115}$$

$$\frac{dC_1}{dt} = 4\alpha C_0 + 2\beta C_2 + \frac{\omega}{b}C_{Ca1} - (\beta + 3\alpha + \gamma a)C_1 \tag{3.116}$$

$$\frac{dC_2}{dt} = 3\alpha C_1 + 3\beta C_3 + \frac{\omega}{b^2}C_{Ca2} - (2\beta + 2\alpha + \gamma a^2)C_2 \tag{3.117}$$

$$\frac{dC_3}{dt} = 2\alpha C_2 + 4\beta C_4 + \frac{\omega}{b^3}C_{Ca3} - (3\beta + \alpha + \gamma a^3)C_3 \tag{3.118}$$

$$\frac{dC_4}{dt} = \alpha C_3 + gO + \frac{\omega}{b^4}C_{Ca4} - (4\beta + f + \gamma a^4)C_4 \tag{3.119}$$

$$\frac{dO}{dt} = fC_4 - gO \tag{3.120}$$

$$\frac{dC_{Ca0}}{dt} = \beta' C_{Ca1} + \gamma C_0 - (4\alpha' + \omega)C_{Ca0} \tag{3.121}$$

$$\frac{dC_{Ca1}}{dt} = 4\alpha' C_{Ca0} + 2\beta' C_{Ca2} + \gamma a C_1 - \left(\beta' + 3\alpha' + \frac{\omega}{b}\right) C_{Ca1} \tag{3.122}$$

$$\frac{dC_{Ca2}}{dt} = 3\alpha' C_{Ca1} + 3\beta' C_{Ca3} + \gamma a^2 C_2 - \left(2\beta' + 2\alpha' + \frac{\omega}{b^2}\right) C_{Ca2} \tag{3.123}$$

$$\frac{dC_{Ca3}}{dt} = 2\alpha' C_{Ca2} + 4\beta' C_{Ca4} + \gamma a^3 C_3 - \left(3\beta' + \alpha' + \frac{\omega}{b^3}\right) C_{Ca3} \tag{3.124}$$

$$\frac{dC_{Ca4}}{dt} = \alpha' C_{Ca3} + g' O_{Ca} + \gamma a^4 C_4 - \left(4\beta' + f' + \frac{\omega}{b^4}\right) C_{Ca4} \tag{3.125}$$

$$\frac{dO_{Ca}}{dt} = f' C_{Ca4} - g' O_{Ca} \tag{3.126}$$

The state O in Equation (3.120) is the conducting state. Equations (3.115)–(3.120) describe the normal mode, and Equations (3.121)–(3.126) describe the mode Ca. The voltage inactivation gate y of the L-type Ca^{2+} channel is determined by

$$\frac{dy}{dt} = \frac{y_\infty - y}{\tau_y} \tag{3.127}$$

where

$$y_\infty = \frac{1}{1 + \exp\left(\frac{V_m + 55}{7.5}\right)} + \frac{0.1}{1 + \exp\left(\frac{-V_m + 21}{6}\right)} \tag{3.128}$$

and

$$\tau_y = 20 + \frac{600}{1 + \exp\left(\frac{V_m + 30}{9.5}\right)} \tag{3.129}$$

The L-type Ca^{2+} channel Ca^{2+} current can then be written as

$$I_{Ca(L),Ca} = \overline{P}_{Ca} \cdot y \cdot \{O + O_{Ca}\} \cdot 4 \cdot \frac{V_m F^2}{RT} \cdot \frac{0.001 \exp(2 \cdot V_m \cdot \frac{F}{RT}) - 0.341[\mathrm{Ca}^{2+}]_o}{\exp(2 \cdot V_m \cdot \frac{F}{RT}) - 1} \tag{3.130}$$

where $\overline{P}_{Ca}$ is the maximum L-type Ca^{2+} channel conductance, y is the voltage inactivation gate, $\{O + O_{Ca}\}$ is the open proability based on the mode switching model (Equations (3.120) and (3.126)), and 4 corresponds to the square of the valence of the charge of Ca^{2+}.

The final component of the L-type Ca^{2+} channel is the K^{+} current through the channel,

$$I_{Ca(L),K} = P'_K \cdot y \cdot \{O + O_{Ca}\} \cdot \frac{V_m F^2}{RT} \cdot \frac{[\mathrm{K}^{+}]_i \exp(V_m \cdot \frac{F}{RT}) - [\mathrm{K}^{+}]_o}{\exp(V_m \cdot \frac{F}{RT}) - 1} \tag{3.131}$$

where the variables y and $\{O + O_{Ca}\}$ are the same as described in Equation (3.130), and the permeability of K^{+} as modified by the Ca^{2+} current ($I_{Ca(L),Ca}$), P'_K, is given by

$$P'_K = \frac{\overline{P}_K}{1 + \frac{I_{Ca(L),Ca_{max}}}{I_{Ca(L),Ca_{half}}}} \tag{3.132}$$

where $\overline{P}_K$ is the permeability of K^{+} in the absence of Ca^{2+} current, $I_{Ca(L),Ca_{half}}$ is the level of Ca^{2+} current that reduces the permeability of K^{+} by 50%, and $I_{Ca(L),Ca_{max}}$ is the maximal L-type Ca^{2+} current

$$I_{Ca(L),Ca_{max}} = \overline{P}_{Ca} \cdot 4 \cdot \frac{V_m F^2}{RT} \cdot \frac{0.001 \exp(2 \cdot V_m \cdot \frac{F}{RT}) - 0.341[\mathrm{Ca}^{2+}]_o}{\exp(2 \cdot V_m \cdot \frac{F}{RT}) - 1} \tag{3.133}$$

3.3.4 Differences with LR-II

Apart from the L-type Ca^{2+} channel currents and Ca^{2+} fluxes described above, the remaining equations for membrane currents and gating variables are taken from the LR-II model described in Section 3.2.2, with some modifications. Most changes in the model are simply using parameters based on more recent experimental data (compare Sections A.2 and A.3). Changes in the actual equations are descibed below.

Differential equations The governing equations for the membrane potential and the gating variables (for the fast sodium and the time-dependent potassium channels) are identical to the LR-II model, with identical gating variable rate constant coefficients (given in Section 3.2.2).

The descriptions of the rate of change of $[\mathrm{Na}^+]_i$ and $[\mathrm{K}^+]_i$ are the same as the LR-II model (Equations (3.74) and (3.76), respectively) . The concentration of Ca^{2+} bound to high-affinity Tn is given by

$$\frac{d[\mathrm{HTRPNCa}]}{dt} = k^+_{htrpn} \cdot [\mathrm{Ca}^{2+}]_i \cdot ([\mathrm{HTRPN}]_{tot} - [\mathrm{HTRPNCa}]) - k^-_{htrpn} \cdot [\mathrm{HTRPNCa}] \tag{3.134}$$

and the concentration of Ca^{2+} bound to low-affinity Tn is described by

$$\frac{d[\mathrm{LTRPNCa}]}{dt} = k^+_{ltrpn} \cdot [\mathrm{Ca}^{2+}]_i \cdot ([\mathrm{LTRPN}]_{tot} - [\mathrm{LTRPNCa}]) - k^-_{ltrpn} \cdot [\mathrm{LTRPNCa}] \tag{3.135}$$

The action potential generated by the JRW model is given in Figure 3.7.

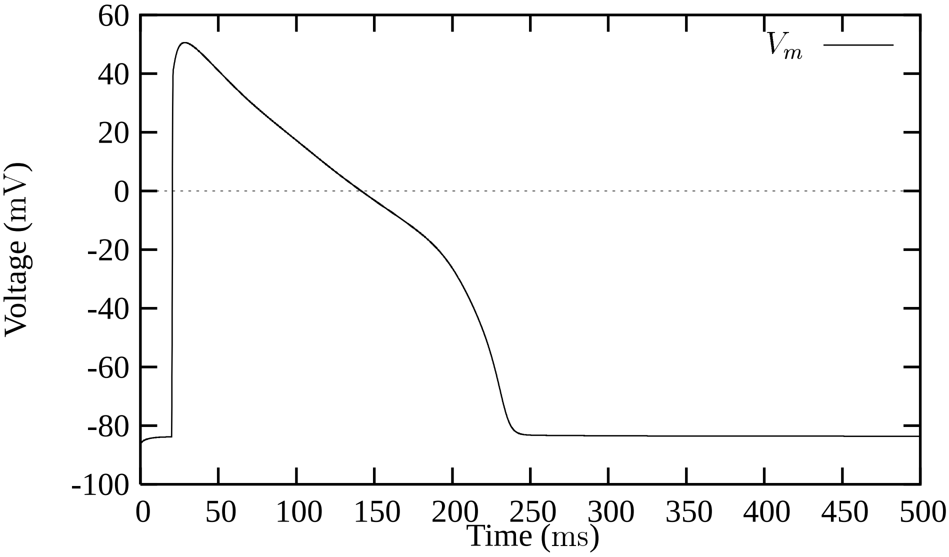

FIGURE 3.7: An action potential generated by the JRW model. The myocyte is stimulated at 20 ms with a current of $-100\ \mu\mathrm{A} \cdot \mathrm{cm}^{-2}$ for a period of 5 ms. *c.f.* Figure 3.3

***Fast* Na^+ *current* (I_{Na})** This current is identical to the LR-II model formulation (Equations (3.35) and (3.36)).

***Time-dependent* K^+ *current* (I_K)** The JRW model uses the same equations for I_K (Equations (3.60)–(3.62)), but $\overline{g}_K$ is now given as

$$\overline{g}_K = 0.1128\sqrt{\frac{[\mathrm{K}^+]_o}{5.4}} \tag{3.136}$$

Remaining ionic curents The remaining ionic currents (time-independent K^+ current (I_{K1}), Plateau K^+ current (I_{Kp}), Na^+,Ca^{2+} exchanger current (I_{NaCa}), Na^+,K^+-ATPase current (I_{NaK}), nonspecific Ca^{2+}-activated current ($I_{ns(Ca)}$), sarcolemmal Ca^{2+} pump current ($I_{p(Ca)}$), Ca^{2+} background current ($I_{Ca,b}$), and Na^+ background current ($I_{Na,b}$)) are all identical to the LR-II model, see Section 3.2.2 for their formulation.

Chapter 4

The HMT Model of Cardiac Mechanics

The Hunter–McCulloch–ter Keurs (HMT) model of cardiac mechanics (Hunter, McCulloch & ter Keurs 1998) was developed to address the lack of a set of published equations enscapsulating the mechanical properties of actively contracting cardiac muscle. Since this model is intended for use in continuum mechanics models of the intact heart, where computational efficiency is a major consideration, it does not accurately model the biophysical events underlying muscle contraction. However, the rate constants can be interpreted in terms of certain biophysical processes.

The HMT model builds on the "fading memory" model of cross-bridge kinetics first proposed by Bergel & Hunter (1979) and further developed in Hunter (1995). The model is developed in the following stages: (i) the passive properties of cardiac muscle (since these influence the measurements of active force at low and high sarcomere length); (ii) the kinetics of Ca^{2+} binding to troponin-C (Tn-C); (iii) tropomyosin (Tm) kinetics (leading to availability of cross-bridge binding sites) and the length dependence of certain parameters in that model; and (iv) the cross-bridge kinetics associated with myofilament length perturbations.

This model is based on an extensive review of experimental data from a variety of preparations (intact trebeculae, skinned fibres, and myofibrals) and species (mainly rat and ferret) at temperatures from 20 to $27\ ^\circ\mathrm{C}$. Experimental tests used in the development of this model include isometric tension development, isotonic loading, quick-release/restretch, length step, and sinusoidal perturbations.

4.1 Passive Elasticity

Active tension in intact cardiac muscle is generated within a three-dimensional visco-elastic matrix. For a small range of sarcomere length above slack length (the length of the unloaded, unstimulated muscle) the contribution of the passive elasticity may be neglected, but for sarcomere lengths below $1.85\ \mu\mathrm{m}$ or above $2.2\ \mu\mathrm{m}$ it makes a significant contribution to the total tension. Numerous authors have suggested that extracellular conective tissue, by limiting the lateral expansion of the cells, provides an internal load which opposes the actively generated tension in cardiac muscle (*e.g.,* Winegrad (1980) and Huntsman, Rondinone & Martyn (1983)). Externally developed tension in maximally stimulated intact muscle typically falls to zero at a sarcomere length of 1.6–$1.7\ \mu\mathrm{m}$, yet skinned fibres still develop 30% of slack length tension at this length. The fact that there is a clearly defined "slack length" in intact muscle at 1.85–$2.1\ \mu\mathrm{m}$ (depending on species and age) is itself evidence for significant restoring forces.

Recent studies of the microstructure of myocardial tissue (LeGrice, Smaill, Chai, Edgar, Gavin & Hunter 1995) have shown that the myocardium consists of layers of interconnected sheets of tissue separated by cleavage planes. Each sheet is 3 to 4 cells thick (about $100\ \mu\mathrm{m}$) and loosely coupled together by the perimysial collagen network. The muscle fibres, which lie in the plane of the sheet, are bound together by the endomysial collagen network. Thus adjacent fibres are coupled more strongly in the plane of the sheet than transverse to it. Three micro-structural axes are therefore evident: one along the fibre direction, the *fibre axis*, one orthogonal to the fibre axis but also in the plane of the sheet, the *sheet axis*, and a third, orthogonal to these two, directed across the cleavage planes, the *sheet normal*. The uniaxial stress-strain properties are quite different in the three orthogonal directions, reflecting in part the organisation of collagen relative to these three axes (Figure 4.1).

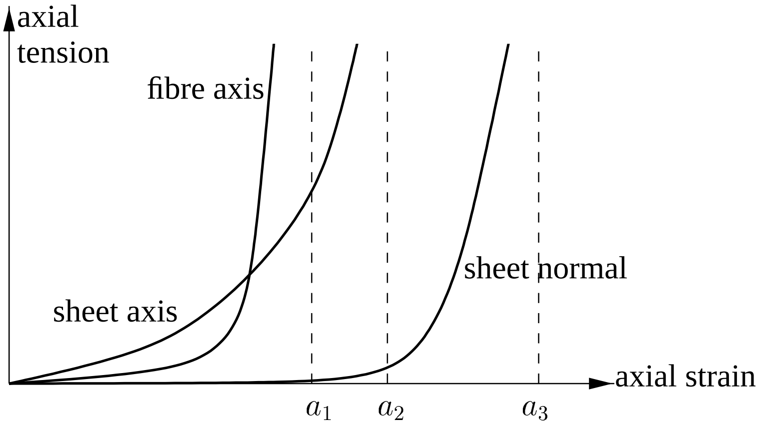

FIGURE 4.1: Uniaxial stress-strain relations along the fibre, sheet, and sheet-normal directions. The solid lines show the "pole-zero" stress-strain relations (see Section 4.1.1) approaching the elastic strain limits a_1, a_2, and a_3, respectively.

A fundamental feature of the stress-strain behaviour as the muscle is stretched along an axis is the very steep rise in stress as the limiting elastic strain along each axis is approached (see Figure 4.1). For the fibre direction the limiting stretch ratio is about 1.2 (a sarcomere length of about $2.4\ \mu\mathrm{m}$). Note that the muscle length is measured by the fibre extension ratio λ and the actively developed tension in the muscle fibre is denoted by T . The extension ratio is the current sarcomere length divided by the slack length. It is assumed that $\lambda = 1$ at a sarcomere length of $2.0\ \mu\mathrm{m}$.

Intracellular structures provide another source of passive elasticity in muscle (Brady 1991). *Titan* filaments are thought to be responsible for a significant fraction of passive tension for sarcomere lengths below $2.1\ \mu\mathrm{m}$ (Linke, Popov & Pollack 1994, Granzier & Irving 1995, Granzier, Helmes & Trombitas 1996, Granzier, Kellermayer, Helmes & Trombitas 1997, Helmes, Trombitas & Granzier 1996). At sarcomere lengths below resting length there is also likely to be an internal elastic load arising from interference between the ends of the thick filament and the Z-lines (Hunter et al. 1998).

4.1.1 Contribution of passive tension during active contraction

For incompressible materials the components of the 2^nd^ Piola-Kirchoff stress tensor referred to material coordinates and measured per unit area of the undeformed material, are given by

$$T^{MN} = -p \cdot \delta^{MN} + \frac{1}{2} \cdot \left(\frac{\partial W}{\partial e_{MN}} + \frac{\partial W}{\partial e_{NM}} \right) \tag{4.1}$$

where W is an elastic strain energy function and p is the hydrostatic pressure (Hunter & Smaill 1989). To accomodate the microstructural observations and biaxial test results (Smaill & Hunter 1991) the HMT model proposed a strain energy function, called the *pole-zero law* (Hunter, Neilsen, LeGrice & Smaill 1992), of the form

$$\begin{aligned} W = {} & k_1 \cdot \frac{e_{11}^2}{(a_1 - |e_{11}|)^{b_1}} + k_2 \cdot \frac{e_{22}^2}{(a_2 - |e_{22}|)^{b_2}} + k_3 \cdot \frac{e_{33}^2}{(a_3 - |e_{33}|)^{b_3}} + k_4 \cdot \frac{e_{12}^2}{(a_4 - |e_{12}|)^{b_4}} \\ & + k_5 \cdot \frac{e_{23}^2}{(a_5 - |e_{23}|)^{b_5}} + k_6 \cdot \frac{e_{31}^2}{(a_6 - |e_{31}|)^{b_6}} \end{aligned} \tag{4.2}$$

where: e_{MN} are the components of the Green strain tensor referred to the material coordinates aligned with the structually defined axes of the tissue; $a_1 \ldots a_6$ are parameters expressing the limiting strain for a particular type of deformation (*i.e.*, the strain energy becomes very large as e_{11} approaches a_1, *etc.*) and $a_1 > e_{11}, a_2 > e_{22}, a_3 > e_{33}, a_4 > e_{12}, a_5 > e23, a_6 > e_{31}$; $b_1 \ldots b_6$ are parameters expressing the curvature of the uniaxial stress-strain curves; and $k_1 \ldots k_6$ are parameters giving the relative contribution of each strain energy term and k_1, k_2, and k_3 are defined to be zero if e_{11}, e_{22}, or e_{33}, respectively, are negative.

Using a separate pole for each microstructurally defined axis accomodates the different strain limiting behaviour seen along each axis. This strain energy function can be considered as the first part of a polynomial expansion in the pole-zero terms (*i.e.,* terms of the form $W(e) = k \cdot e^2/(a-e)^b$). There are 18 free parameters in Equation (4.2) but some of these must be strongly correlated because some tensile and shearing deformations are likely to involve the same underlying collagen microstructure (Hunter et al. 1998).

The HMT model derives the uniaxial tension-length relation first for tension ($\lambda > 1$) and then for compression ($\lambda < 1$). The HMT model considers a cylindrical segment of muscle under the assumption that the material properties in the plane orthogonal to the axis are isotropic (*i.e.*, the muscle is assumed to be transversely isotropic). Then, maintaining the incompressibility constraint $\lambda_1 \cdot \lambda_2 \cdot \lambda_3 = 1$ results in $\lambda_2 = \lambda_3 = 1/\sqrt{\lambda_1}$ which gives

$$e_{11} = \frac{1}{2} \cdot \left(\lambda_1^2 - 1\right) \quad \text{and} \quad e_{22} = e_{33} = \frac{1}{2} \cdot \left(\lambda_2^2 - 1\right) = \frac{1}{2} \cdot \left(\frac{1}{\lambda_1} - 1\right)$$

For axial tension ($\lambda_1 > 1$) the strain energy function, Equation (4.2), reduces to

$$W = k_1 \cdot \frac{e_{11}^2}{\left(a_1 - e_{11}\right)^{b_1}}$$

since e_{22} and e_{33} are negative and therefore W contains no other contribution from fibre stretch.

From Equation (4.1), $T^{22} = \partial W / \partial e_{22} - p = 0$ gives $p = \partial W / \partial e_{22} = 0$ and the axial 2nd Piola-Kirchoff stress is

$$T^{11} = \frac{k_1 \cdot e_{11}}{\left(a_1 - e_{11}\right)^{b_1}} \cdot \left[2 + \frac{b_1 \cdot e_{11}}{\left(a_1 - e_{11}\right)}\right] \tag{4.3}$$

Equation (4.3) is shown in Figure 4.2 with the pole at $e_{11} = a_1$ when $\lambda_1 = \sqrt{1 + 2 \cdot a_1} = 1.2$.

For axial compression ($\lambda_1 < 1$) the strain energy function, Equation (4.2), reduces to

$$W = 2 \cdot k_2 \cdot \frac{e_{22}^2}{\left(a_2 - e_{22}\right)^{b_2}}$$

since e_{22} and e_{33} are assumed equal and now e_{11} is negative so there is no contribution from the axial term.

From Equation (4.1), $T^{22} = \partial W / \partial e_{22} - p = 0$ gives

$$p = \frac{\partial W}{\partial e_{22}} = \frac{2 \cdot k_2 \cdot e_{22}}{\left(a_2 - e_{22}\right)^{b_2}} \cdot \left[2 + \frac{b_2 \cdot e_{22}}{a_2 - e_{22}}\right]$$

and the axial 2nd Piola-Kirchoff stress is

$$T^{11} = -p = \frac{-2 \cdot k_2 \cdot e_{22}}{\left(a_2 - e_{22}\right)^{b_2}} \cdot \left[2 + \frac{b_2 \cdot e_{22}}{a_2 - e_{22}}\right] \tag{4.4}$$

where $e_{22} = \frac{1}{2} \cdot \left(\frac{1}{\lambda_1} - 1\right)$.

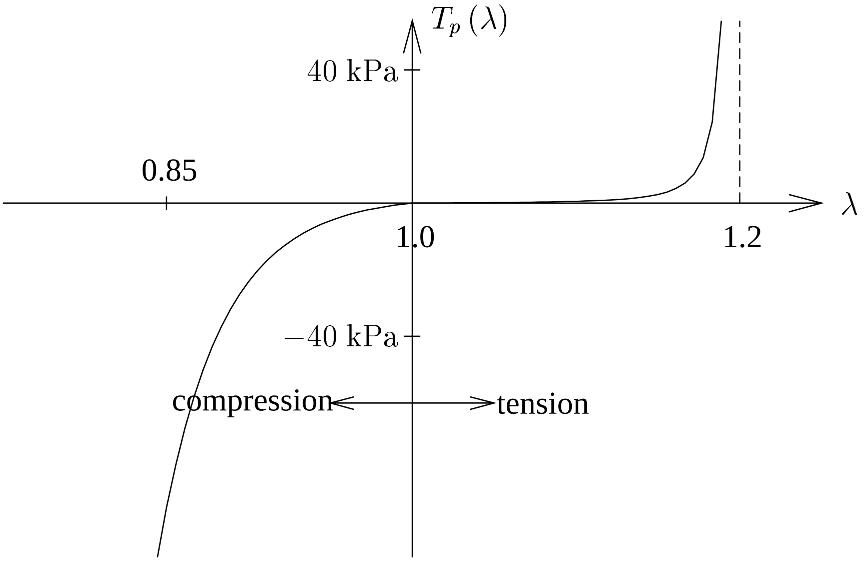

FIGURE 4.2: Passive stress-strain relation in uniaxial tension and compression. The dashed line on the right shows the pole position (*i.e.*, stretch limit) in tension at $\lambda_1 = \sqrt{1 + 2 \cdot a_1} = 1.2$ (a sarcomere length of aproximately $2.4\ \mu\mathrm{m}$). The point marked at $\lambda = 0.85$ corresponds to the minimum attainable sarcomere length of $1.7\ \mu\mathrm{m}$. The line for $\lambda > 1$ is Equation (4.3) with $k_1 = 0.2$ kPa, $a_1 = 0.22$, and $b_1 = 1.0$, and the line for $\lambda < 1$ (in compression) is from Equation (4.4) with $k_2 = 0.06$ kPa, $a_2 = 0.41$, and $b_2 = 6.8$ (Hunter et al. 1998).

This relation (for $\lambda = \lambda_1 < 1$), with parameter values determined from biaxial loading experiments (Smaill & Hunter 1991), is shown in Figure 4.2. Note that the pole at $e_{22} = a_2$ occurs when

$$e_{22} = \frac{1}{2} \cdot \left(\frac{1}{\lambda_1} - 1 \right) = a_2 \quad \text{or} \quad \lambda_1 = \frac{1}{1 + 2 \cdot a_2} = 0.55$$

The effect of adding the passive fibre axis stress to a linear (maximally activated) active tension relation is shown in Figure 4.3. At a sarcomere length of $1.7\ \mu\mathrm{m}$ the actively developed tension exactly balances the internal load and external tension is therefore zero.

4.2 Intracellular Calcium

Ca^{2+} binds to many sites within the cell, with the most important (from a mechanics point of view) being troponin-C (Tn-C), calmodulin, and SR. Tn-C has three binding sites but two of them (the high affinity Ca^{2+}–Mg^{2+} sites) are saturated at resting levels of $[\mathrm{Ca}^{2+}]_i$ ($0.01\ \mu\mathrm{M}$) and therefore do not regulate myofilament force development. The third (Ca^{2+}-specific) Tn-C binding site, present in cardiac myocytes at a concentration of $70\ \mu\mathrm{M}$ (Hunter et al. 1998), is the regulatory site (Shiner & Solaro 1984). Binding to Tn-C is essentially instantaneous and limited

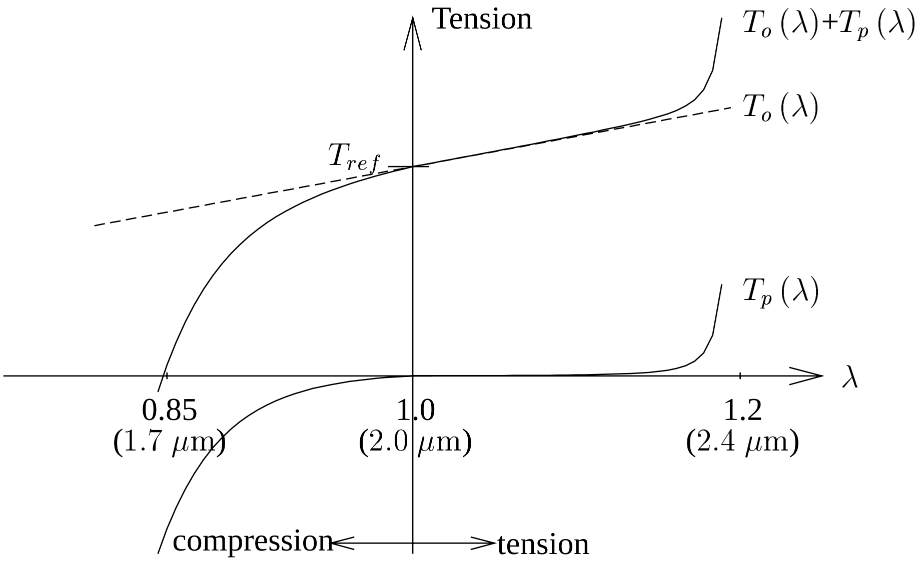

FIGURE 4.3: Tension-length relation for active muscle. The passive tension from Figure 4.2 is shown as $T_p\left(\lambda\right)$. The total tension (upper solid curve) is the sum of the passive tension and a linear active tension $T_o\left(\lambda\right)$ (shown by the dashed line) (Equation (4.11)). Sarcomere lengths are indicated at extension ratios of 1.0 (resting length), 1.2 (maximum extension), and 0.85 (minimum extension). The active tension at resting length, T_{ref}, is about 125 kPa

only by the speed of diffusion from the JSR Ca^{2+}-release sites (a delay of approximately 0.5 ms) (Hunter et al. 1998). Consequently the Ca^{2+} transient (a measure of $[\mathrm{Ca}^{2+}]_i$) typically rises to a peak of only $1\ \mu\mathrm{M}$. However, since substantial changes in the time course of the decline of the Ca^{2+} transient can occur without affecting force, the fall in $[\mathrm{Ca}^{2+}]_i$ is evidently not the rate limiting step in relaxation of force, which is more likely to be determined by the dissociation of Ca^{2+} from Tn-C (Hunter et al. 1998).

The HMT model was developed using a single exponential representation of the calcium transient, obtained by fitting experimental data and given by

$$[\mathrm{Ca}^{2+}]_i\left(t\right) = [\mathrm{Ca}^{2+}]_0 + \left([\mathrm{Ca}^{2+}]_{max} - [\mathrm{Ca}^{2+}]_0\right) \cdot \frac{t}{\tau_{Ca}} \cdot \exp\left(1 - \frac{t}{\tau_{Ca}}\right) \tag{4.5}$$

where $[\mathrm{Ca}^{2+}]_i\left(t\right)$ is the time-dependent intracellular concentration of Ca^{2+}, which has a resting level $[\mathrm{Ca}^{2+}]_0$ and achieve its maximum value $[\mathrm{Ca}^{2+}]_{max}$ at time $t = \tau_{Ca}$. The HMT calcium transient is shown in Figure 4.4 with $[\mathrm{Ca}^{2+}]_0 = 0.01\ \mu\mathrm{M}$, $[\mathrm{Ca}^{2+}]_{max} = 1\ \mu\mathrm{M}$, and $\tau_{Ca} = 60$ ms. Chapter 5 shows how this approximation to the true intracellular calcium transient can easily be replaced with that obtained from the physiologically based ionic current models given in Chapter 3.

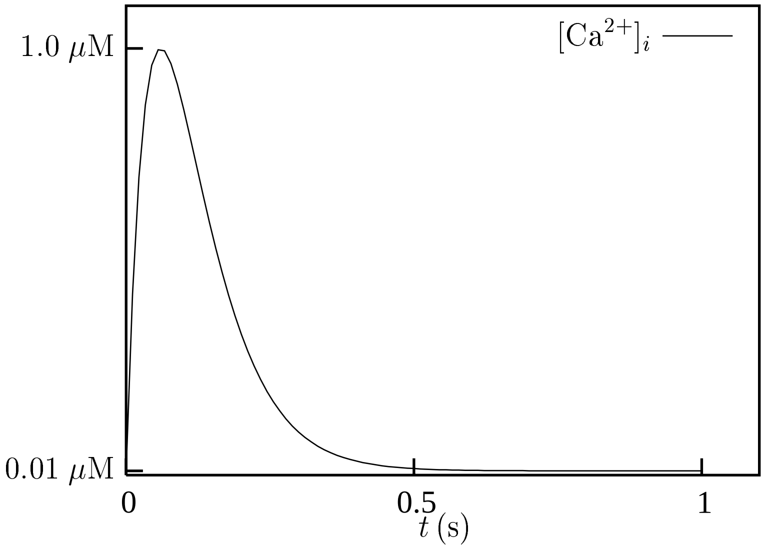

FIGURE 4.4: The HMT intracellular calcium transient, from Equation (4.5) with $[\mathrm{Ca}^{2+}]_0 = 0.01\ \mu\mathrm{M}$, $[\mathrm{Ca}^{2+}]_{max} = 1\ \mu\mathrm{M}$, and $\tau_{Ca} = 60$ ms.

4.3 Tn-C – Ca^{2+} Binding Kinetics

The binding of Ca^{2+} to Tn-C occurs very rapidly and appears to be limited by diffusion gradients from the JSR release site to the Tn-C binding site. The release of Ca^{2+} from the Tn-C binding site has long been known to be dependent on the mechanical state of the muscle. For example, an isotonic twitch terminates much more quickly than an isometric twitch, and if a muscle is subjected to a quick release during a twitch its ability to generate force decays rapidly (Edman 1975). These phenomena are explained by Ca^{2+} being released from the Tn-C binding site when the myofilament force declines (Hunter et al. 1998). The release of Ca^{2+} from Tn-C, seen by the rise in $[\mathrm{Ca}^{2+}]_i$, following a reduction on muscle length (isotonic twitches or quick release) was shown by Allen & Kurihara (1982) to correlate with a change in tension and not length. This has since been confirmed by other studies (*e.g.*, Janssen & Hunter (1995)).

Hunter et al. model the above phenomena with the following equation for Tn-C–Ca^{2+} binding kinetics:

$$\frac{d[\mathrm{Ca}^{2+}]_b}{dt} = \rho_0 \cdot [\mathrm{Ca}^{2+}]_i \cdot \left([\mathrm{Ca}^{2+}]_{bmax} - [\mathrm{Ca}^{2+}]_b\right) - \rho_1 \cdot \left(1 - \frac{T}{\gamma \cdot T_o}\right) \cdot [\mathrm{Ca}^{2+}]_b \qquad (4.6)$$

where $[\mathrm{Ca}^{2+}]_i$ is the concentration of free myoplasmic Ca^{2+} and $[\mathrm{Ca}^{2+}]_b$ is the concentration of Ca^{2+} bound to the Ca^{2+}-specific binding site on Tn-C. The maximum value $[\mathrm{Ca}^{2+}]_{bmax}$ is attained at equilibrium when $T = \gamma \cdot T_o$. Attachment is governed by a fixed rate constant ρ_0, estimated to be $100\ \mathrm{s}^{-1} \cdot \mu\mathrm{M}^{-1}$ of the available Ca^{2+} (Hilgemann & Noble 1987). Detachment at zero tension T is governed by the rate constant ρ_1 and as T increases towards a maximum value $\gamma \cdot T_o$, the release rate slows down proportionately.

The equilibrium relationship from Equation (4.6),

$$\frac{[\mathrm{Ca}^{2+}]_b}{[\mathrm{Ca}^{2+}]_{bmax}} = \frac{[\mathrm{Ca}^{2+}]_i}{[\mathrm{Ca}^{2+}]_i + (\rho_1/\rho_0) \cdot (1 - T/(\gamma \cdot T_o))} \tag{4.7}$$

is used in Equation (4.13).

The time course of bound calcium in response to the intracellular calcium transient given by Equation (4.5), is shown in Figure 4.5 for $T = 0$ and the isometric case $T = T_o$.

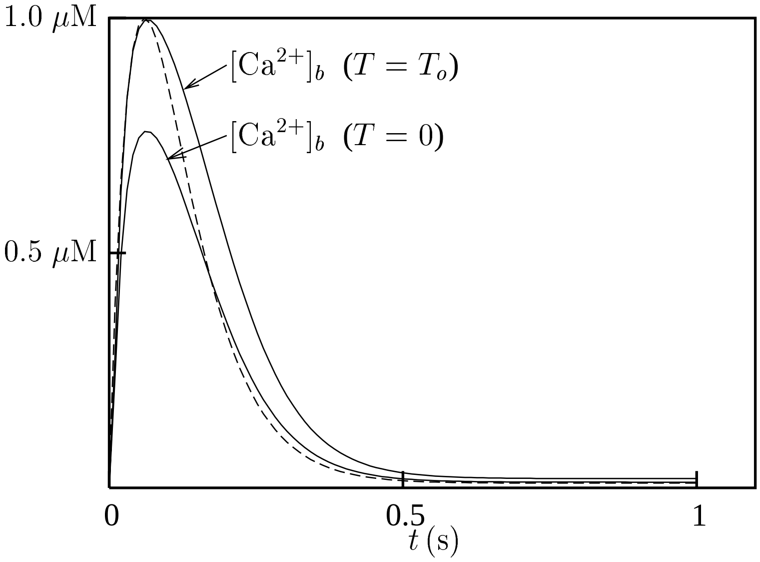

FIGURE 4.5: Time course of the bound calcium, $[\mathrm{Ca}^{2+}]_b$, using the calcium transient given by Equation (4.5) (shown by the dashed line). The dependence on cross-bridge binding is illustrated by showing the two extremes $T = 0$ and $T = T_o$ (isometric).

4.4 Thin Filament Kinetics

Ca^{2+} binding to Tn-C initiates a chain of events in the thin filament which results in myosin head binding to actin and the development of force (Holmes 1995) (Figure 2.18). Tight binding of Tn-C–Ca^{2+} to troponin-I (Tn-I) weakens Tn-I–actin interaction and alters the Tn-T–Tm complex in such a way that tropomyosin (Tm) moves into the groove of the thin filament, thereby removing a steric obstruction of the actin–cross-bridge reaction (Solaro 1993).

4.4.1 Tropomyosin kinetics

To model the tropomyosin kinetics, the HMT model introduces a non-dimensional parameter z ($0 \le z \le 1$), representing the proportion of actin sites available for cross-bridge binding, and given by

$$\frac{dz}{dt} = \alpha_0 \cdot \left[\left(\frac{[\mathrm{Ca}^{2+}]_b}{C_{50}} \right)^n \cdot (1 - z) - z \right] \tag{4.8}$$

where α_0 is the rate constant of tropomyosin (Tm) movement and C_{50} and n are the Hill parameters fitted to the equilibrium relationship between z and $[\mathrm{Ca}^{2+}]_b$ at a given sarcomere length, *i.e.,* under steady state conditions Equation (4.8) gives

$$z_{SS} = \frac{\left([\mathrm{Ca}^{2+}]_b\right)^n}{\left([\mathrm{Ca}^{2+}]_b\right)^n + (C_{50})^n} \tag{4.9}$$

where C_{50} is the value of $[\mathrm{Ca}^{2+}]_b$ required to achieve 50% availability ($z_{SS} = 0.5$) and n governs the steepness of the curve. Under the assumption that steady state force is proportional to the number of available actin cross-bridge binding sites, z_{SS} is the ratio of the isometric tension, T_o , to its maximum value, T_{omax}, obtained at saturating levels of $[\mathrm{Ca}^{2+}]_b$. Thus, $z_{SS} = T_o/T_{omax}$.

The exponential change in z following a step change to a new level as obtained from Equation (4.8) by substituting

$$z = z_{SS} + A \cdot \exp\left(-k_{tr} \cdot t\right)$$

to give

$$k_{tr} = \alpha_0 \cdot \left[1 + \left(\frac{[\mathrm{Ca}^{2+}]_b}{C_{50}} \right)^n \right] \tag{4.10}$$

Figure 4.6 (a) shows the S-shaped equilibrium relationship given by Equation (4.9) and the rate constant k_{tr} is plotted as a function of $[\mathrm{Ca}^{2+}]_b$ from Equation (4.10) in Figure 4.6 (b).

4.4.2 Steady state length dependence

The direct length dependence of steady state muscle tension at various constant levels of intracellular calcium was first measured by Fabiato & Fabiato (1976) and (1978) in skinned cardiac fibres and by ter Keurs, Rijnsburger, van Heuningen & Nagelsmit (1980) in intact rat trabeculae. Figure 4.7 shows plots of the actively developed tension/length for various levels of

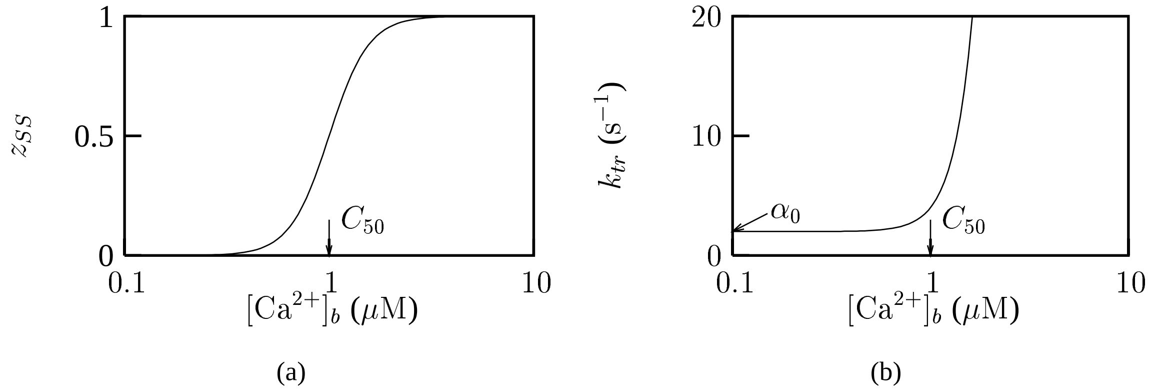

FIGURE 4.6: (a) Equilibrium relationship between actin site availability (z_{SS}) and bound Ca^{2+} ($[\mathrm{Ca}^{2+}]_b$) given by Equation (4.9). (b) Rate constant for tension redevelopment k_{tr} given as a function of $[\mathrm{Ca}^{2+}]_b$ by Equation (4.10). The Hill parameters for these plots are $C_{50} = 1\ \mu\mathrm{M}$ and $n = 4.5$ and the rate constant of tropomyosin movement is $\alpha_0 = 2\ \mathrm{s}^{-1}$ (shown as the limiting value of k_{tr} as $[\mathrm{Ca}^{2+}]_b \to 0$ in (b)).

$[\mathrm{Ca}^{2+}]_i$. At maximum activation the isometric tension–length relation $T_o(\lambda)$ is linear with a slope $dT_o/d\lambda = 145$ kPa, or (for maximal activation)

$$T_o = T_{ref} \cdot (1 + \beta_0 \cdot (\lambda - 1)) \tag{4.11}$$

where $T_{ref} = 125$ kPa is the reference tension at $\lambda = 1$ and $\beta_0 = 1/T_{ref} \cdot dT_o/d\lambda = 1.45$. If the increase in tension with length came about solely as a result of changing myofilament overlap, this parameter wold be $\beta_0 = 1$. Thus, $\beta_0 > 1$ reflects myofilament “cooperativity” (Hunter et al. 1998).

For less than full activation the dependence on Ca^{2+} under isometric conditions is given by

$$T_o = T_{ref} \cdot (1 + \beta_0 \cdot (\lambda - 1)) \cdot z \tag{4.12}$$

where $z = z_{SS}$ is given by Equation (4.9) under steady state conditions but otherwise is obtained from the solution of Equation (4.8). Figure 4.7 clearly shows that the linear relationship evident at maximum activation is not preserved at lower levels of bound calcium. The parameters n and C_{50} must therefore be length dependent. The HMT model uses a linear length dependence for n and pC_{50}, found to be sufficient to model the full range of $T_o\left(\lambda, \mathrm{Ca}^{2+}\right)$, with the length dependence given by

$$z_{SS} = \frac{(Ca)^n}{(Ca)^n + (C_{50})^n} \tag{4.13}$$

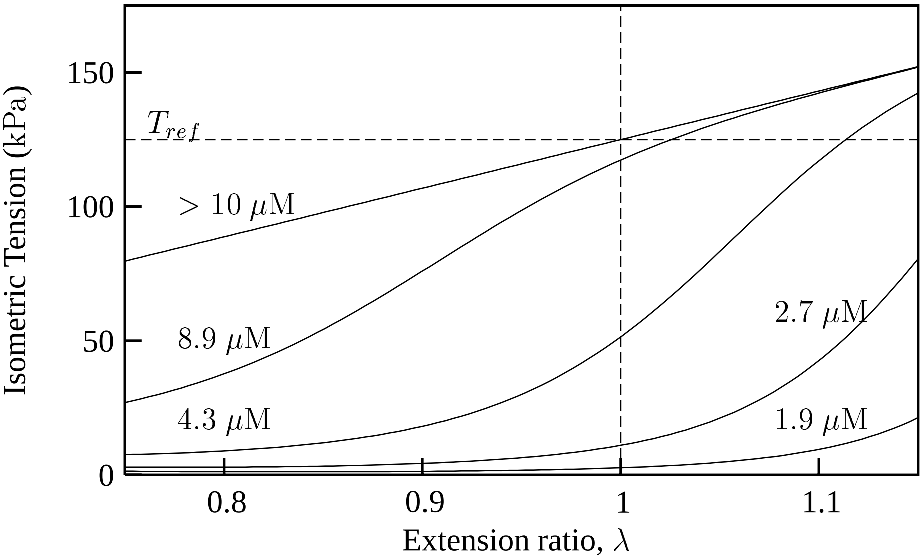

FIGURE 4.7: Isometric tension-length relations for various levels of $[\mathrm{Ca}^{2+}]_i$ ($> 10\ \mu$M represents the fully activated case). The plots are from Equations (4.12)–(4.16) with $T_{ref} = 125$ kPa, $\beta_0 = 1.45$, $\beta_1 = 1.95$, $\beta_2 = 0.31$, $n_{ref} = 4.25$, and $pC_{50ref} = 5.33$.

with

$$n = n_{ref} \cdot (1 + \beta_1 \cdot (\lambda - 1)) \tag{4.14}$$

and

$$pC_{50} = pC_{50ref} \cdot (1 + \beta_2 \cdot (\lambda - 1)) \tag{4.15}$$

given that

$$C_{50} = 10^{6 - pC_{50}} \quad (\mu\mathrm{M}) \tag{4.16}$$

Figure 4.7 is obtained from Equations (4.12)–(4.16) using $T_{ref} = 125$ kPa, $\beta_0 = 1.45$, $n_{ref} = 4.25$, $\beta_1 = 1.95$, $pC_{50ref} = 5.33$, and $\beta_2 = 0.31$ (Hunter et al. 1998).

Note that Equation (4.13) absorbs both the $[\mathrm{Ca}^{2+}]_b$ saturation curve, Equation (4.9), and the $[\mathrm{Ca}^{2+}]_i$–$[\mathrm{Ca}^{2+}]_b$ binding relation, Equation (4.7). Also note that in the HMT model the length dependent Ca^{2+} sensitivity of tension is expressed via Equations (4.12)–(4.16), where Ca in Equation (4.13) is bound calcium $[\mathrm{Ca}^{2+}]_b$. This is independent of Tn-C–Ca^{2+} binding and is justified by experiments (Hunter et al. 1998).

An alternative method of presenting $T_o\left(\lambda, [\mathrm{Ca}^{2+}]_i\right)$ is illustrated in Figure 4.8, where T_o is plotted against $[\mathrm{Ca}^{2+}]_i$ for various values of λ .

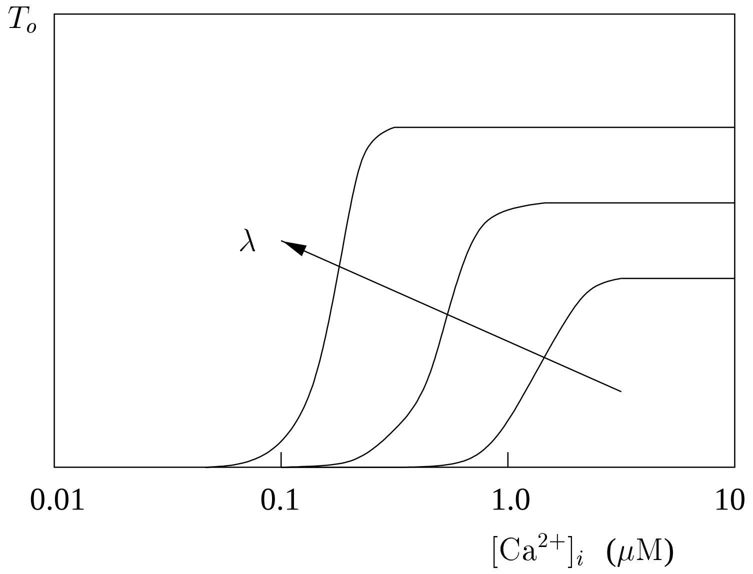

FIGURE 4.8: Schematic representation of the steady state isometric tension $T_o\left([\mathrm{Ca}^{2+}]_i\right)$. λ is increasing in the direction of the arrow (from $\lambda = 0.8$ to $\lambda = 1.3$). *Modified from Hunter et al. (1998).*

4.5 Crossbridge Kinetics

The most notable feature of the dynamic properties of cardiac muscle is the fact that very small dynamic length changes are associated with large changes in tension. For example, shortening the muscle by less than 1% of its length in 1 ms produces a 100% drop in tension (Hunter et al. 1998). Three types of experiment are often used to characterise cross-bridge kinetics under a constant level of activation:

- Length step experiments.
- Constant velocity experiments.
- Frequency response experiments.

Hunter et al. use the first two of these in the development of this model. The tension changes following a rapid length step are shown in Figure 4.9 (a). Notice (i) the drop in tension concomitant with the length change $\Delta\lambda$ (the lowest tension reached is labelled T_1), (ii) the rapid recovery of tension, often with a slight oscillation before (iii) a slower recovery to equilibrium. When the experiment is performed with a different initial value of T_o , the entire response is found to scale with T_o (Hunter et al. 1998). The magnitude of T_1/T_o shows a nonlinear dependence on $\Delta\lambda$, as shown in Figure 4.9 (b).

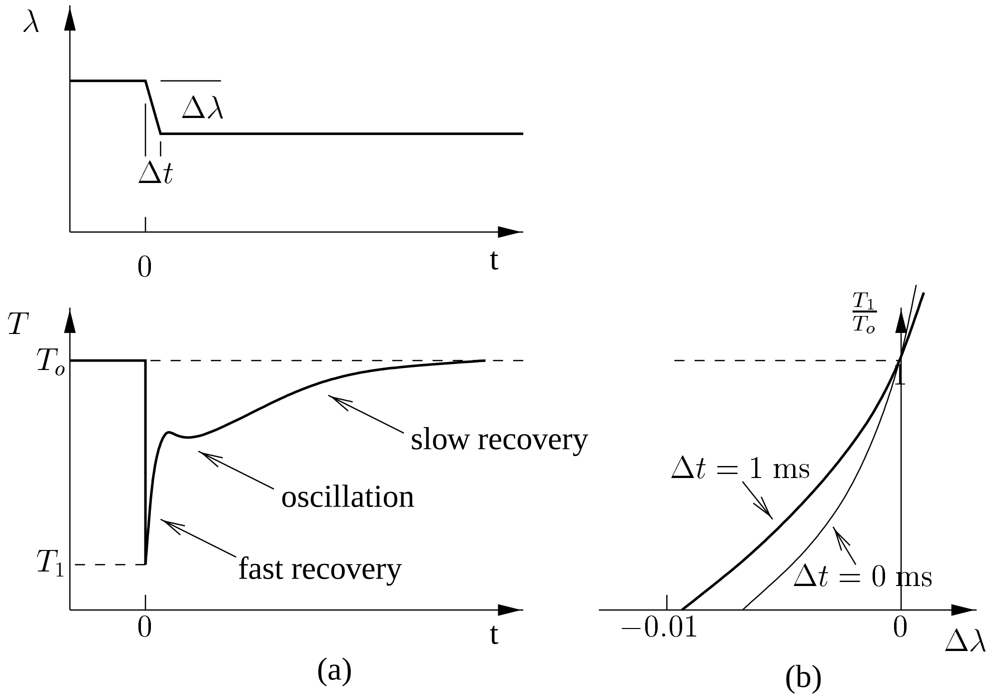

FIGURE 4.9: (a) Tension recovery (lower figure) following a length step of $\Delta\lambda$ of duration Δt (upper figure). Notice the different phases of the tension recovery. (b) Tension T_1 reached at the end of the length step, divided by isometric tension T_o , plotted against the magnitude of the length step $\Delta\lambda$. One curve is for a length step of 1 ms duration and the other for an idealised instantaneous step. *From Hunter et al. (1998).*

4.5.1 Fading memory model

To model these observations, Hunter et al. used the *fading memory model* (Bergel & Hunter 1979, Hunter 1995). In the fading memory model a nonlinear function of tension $Q\left(T, T_o\right)$ is written as a linear superposition of dynamic length changes:

$$Q\left(T, T_o\right) = \int_{-\infty}^{t} \phi\left(t-\tau\right) \cdot \overset{\bullet}{\lambda}\left(\tau\right) \cdot d\tau \tag{4.17}$$

where $\overset{\bullet}{\lambda} \equiv d\lambda/dt$, $\phi\left(t\right)$ is a material response function, and $T_o\left(\lambda, [\mathrm{Ca}^{2+}]_i\right)$ is the isometric tension-length-Ca^{2+} relation for cardiac muscle given by Equations (4.12)–(4.16). Under steady state conditions the right hand side of Equation (4.17) is zero and the function $Q\left(T, T_o\right)$ must be defined such that

$$Q\left(T_o, T_o\right) = 0$$

A system defined by Equation (4.17) is known as a *Wiener cascade model*, a linear dynamic system followed by a static nonlinearity.

Two further experimental observations are now used. The first is that all tension measurements on cardiac muscle scale with the isometric tension (the justification for using T/T_o in Figure 4.9 (b)) and therefore:

$$Q\left(T, T_o\right) = Q\left(T/T_o\right)$$

The second observation is that the current tension is influenced more by recent length changes than earlier length changes, the *fading memory assumption* (Hunter et al. 1998). This latter assumption allows the material response function to be written as the sum of exponentials:

$$\phi\left(t\right) = \sum_{i=1}^{N} A_i \cdot \exp\left(-\alpha_i \cdot t\right) \tag{4.18}$$

where α_i and A_i, $i = 1, \ldots, N$, are the exponential rate constants and associated weighting coefficients, respectively.

The tension recovery curve in Figure 4.9 (a) shows evidence of three distinct physical processes: the inital fast recovery with a slight oscillation is indicative of a second order process (*e.g.*, myosin head rotation, *i.e.*, Step 4 in Figure 2.18) and the subsequent slow recovery phase is evidence of a first order process (the cross-bridge detachment-attachment cycle, *i.e.*, Steps 1–7 in Figure 2.18, with the rate limiting step probably being detachment (Hunter et al. 1998)).

Therefore, Hunter et al. limit the number of rate constants N in Equation (4.18) to 3 and Equation (4.17) becomes

$$Q\left(T/T_o\right) = \sum_{i=1}^{3} A_i \cdot \int_{-\infty}^{t} \exp\left(-\alpha_i \cdot (t-\tau)\right) \cdot \overset{\bullet}{\lambda}\left(\tau\right) \cdot d\tau \tag{4.19}$$

where α_1 is the rate constant associated with the first order slow tension recovery, and α_2 and α_3 are the rate constants for the second order fast recovery process in Figure 4.9 (a).

4.5.2 Constant velocity experiments

A parametererised form of the nonlinear function $Q\left(T/T_o\right)$ can be determined from constant velocity experiments. In these experiments, the muscle shortens at a constant rate (following an initial transient) in response to a reduction in tension to a value less than T_o . The plot of tension versus velocity is called a *force–velocity curve*. These curves are typically hyperbolic and are accurately described for tetanised (maximally activated) muscle by the equation first proposed by Hill (1938):

$$\frac{-V}{a \cdot V_o} = \frac{\overset{\bullet}{\lambda}}{a \cdot V_o} = \frac{T/T_o - 1}{T/T_o + a} \tag{4.20}$$

where V_o is the maximum velocity (achieved when $T = 0$) and a is a parameter which controls the curvature of of the force–velocity relation. As with force recovery following a length step, the force–velocity curves scale with isometric tension, T_o (Hunter et al. 1998).

The unloaded shortening velocity V_o has had a special significance for muscle physiologists because it appered to be independent of length and level of activation, at least for lengths greater than resting length ($\lambda > 1$). For $\lambda < 1$ the passive muscle structures are in compression and the “unloaded” shortening is then shortening against an internal load (see Section 4.1).

Ignoring the two rate constants α_2 and α_3 associated with the initial transient following the tension step and putting $\overset{\bullet}{\lambda} = -V$ (the constant velocity of shortening), Equation (4.19) reduces to

$$Q\left(T/T_o\right) = \frac{-A_1}{\alpha_1 \cdot V}$$

An exact match to Hill’s classic force–velocity relation (Hill 1938) is then obtained by choosing

$$Q\left(T/T_o\right) = \frac{T/T_o - 1}{T/T_o + a}$$

and

$$V_o = \frac{\alpha_1}{a \cdot A_1}$$

giving

$$\overset{\bullet}{\lambda} = -V = \frac{\alpha_1}{A_1} \cdot \frac{T/T_o - 1}{T/T_o + a} \tag{4.21}$$

Experimental results from cardiac muscle give a relative velocity (V/V_o) of about 25% at a relative tension (T/T_o) of 50% (Hunter et al. 1998). Putting $T/T_o = \frac{1}{2}$ in Equation (4.21) gives

$$V/V_o = \frac{\frac{1}{2} \cdot a}{\frac{1}{2} + a}$$

and hence $V/V_o = 0.25$ gives $a = 0.5$. The maximum (unloaded) velocity of shortening is found to be $11.3\ \mu\mathrm{m} \cdot \mathrm{s}^{-1}$ per $1.9\ \mu\mathrm{m}$ sarcomere, or $V_o = 6\ \mathrm{s}^{-1}$, and hence $\alpha_1/A_1 = a \cdot V_o = 3\ \mathrm{s}^{-1}$ (Hunter et al. 1998).

The fading memory model of cross-bridge mechanics is now given by

$$\frac{T/T_o - 1}{T/T_o + a} = \sum_{i=1}^{3} A_i \cdot \int_{-\infty}^{t} \exp\left(-\alpha_i \cdot (t - \tau)\right) \cdot \overset{\bullet}{\lambda}(\tau) \cdot d\tau \tag{4.22}$$

It is convenient to express Equation (4.22) in the form

$$T = T_o \cdot \frac{1 + a \cdot Q}{1 - Q}, \quad \text{where} \quad Q = \sum_{i=1}^{3} A_i \cdot \int_{-\infty}^{t} \exp\left(-\alpha_i \cdot (t - \tau)\right) \cdot \overset{\bullet}{\lambda}(\tau) \cdot d\tau \tag{4.23}$$

i.e., the observed tension T is the isometric tension T_o scaled by a nonlinear function of the hereditary integral of length changes.

4.5.3 Length step experiments

The response to an instantaneous length step is found by putting $\lambda(t) = \Delta\lambda \cdot H(t)$ (the *Heaviside step function*) or $\overset{\bullet}{\lambda}(t) = \Delta\lambda \cdot \delta(t)$ (the *Dirac delta function*), in which case Equation (4.22) becomes

$$\frac{T/T_o - 1}{T/T_o + a} = \Delta\lambda \cdot \sum_{i=1}^{3} A_i \cdot \exp\left(-\alpha_i \cdot t\right) \tag{4.24}$$

The tension reached immediately after the step is found by putting $T = T_1$ and $t = 0$ in Equation (4.24) to give

$$\frac{T_1/T_o - 1}{T_1/T_o + a} = \Delta\lambda \cdot \sum_{i=1}^{3} A_i \tag{4.25}$$

The instantaneous length change $\Delta\lambda_o$ required to drop the tension to zero immediately after the step is found from Equation (4.25) by putting $T_1 = 0$:

$$-\Delta\lambda_o = \frac{1}{a \cdot \sum_{i=1}^{3} A_i} \tag{4.26}$$

In practice the inertia of the muscle testing equipment mean that an "instantaneous" length step on cardiac muscle actually requires $1\ \mathrm{ms}$ or more to complete (Hunter et al. 1998). The HMT model therefore examines the consequences of a finite duration length step.

Finite Duration Length Steps

The response to a rapid but finite duration length change is found by putting

$$\dot{\lambda}(t) = \begin{cases} 0 & t < 0 \\ \frac{\Delta\lambda}{\Delta t} & 0 < t < \Delta t \\ 0 & t > \Delta t \end{cases} \tag{4.27}$$

in Equation (4.21) (see Figure 4.9 (a), top) and integrating to give

$$\frac{T/T_o - 1}{T/T_o + a} = \frac{\Delta\lambda}{\Delta t} \cdot \sum_{i=1}^{3} \frac{A_i}{\alpha_i} \cdot \exp\left(-\alpha_i \cdot t\right) \cdot \left(\exp\left(\alpha_i \cdot \Delta t\right) - 1\right) \tag{4.28}$$

The tension T_1 immediately after the length step is found from Equation (4.28) by putting $t = \Delta t$ and $T = T_1$:

$$\frac{T_1/T_o - 1}{T_1/T_o + a} = \frac{\Delta\lambda}{\Delta t} \cdot \sum_{i=1}^{3} \frac{A_i}{\alpha_i} \cdot \left(1 - \exp\left(-\alpha_i \cdot \Delta t\right)\right) \tag{4.29}$$

Equation (4.29) gives the plot of T_1/T_o against $\Delta\lambda$ shown in Figure 4.9 (b). For a step of duration Δt the magnitude of step change required to drop the tension T_1 to zero, from

Equation (4.29), is

$$-\Delta\lambda = \frac{\Delta t}{a} \cdot \sum_{i=1}^{3} \frac{A_i}{\alpha_i} \cdot \left(1 - \exp\left(-\alpha_i \cdot \Delta t\right)\right) \tag{4.30}$$

Taking the limit of Equation (4.30) as $\Delta t \to 0$ recovers the instantaneous relationship, Equation (4.26), as expected.

An important feature of the HMT model of cross-bridge kinetics is that all constants (a, α_i, A_i) are independent of both length (λ) and calcium ($[\mathrm{Ca}^{2+}]_i$ or $[\mathrm{Ca}^{2+}]_b$). The influence of λ and $[\mathrm{Ca}^{2+}]_b$ occurs solely within the model of thin filament kinetics.

4.6 HMT Summary

If the free calcium concentration $[\mathrm{Ca}^{2+}]_i$ and the muscle fibre extension ratio λ are regarded as inputs to the system, this model consists of a set of four fundamental equations in the four state variables $[\mathrm{Ca}^{2+}]_b$, z , T_o , and T which may be expressed as

$$\begin{aligned} [\mathrm{Ca}^{2+}]_b &= f_1\left([\mathrm{Ca}^{2+}]_i, [\mathrm{Ca}^{2+}]_b, T, T_o\right) && \text{(Equation (4.6))} && (4.31)\\ z &= f_2\left(z, \lambda, [\mathrm{Ca}^{2+}]_b\right) && \text{(Equation (4.8))} && (4.32)\\ T_o &= f_3\left(\lambda, z\right) && \text{(Equations (4.12)–(4.16))} && (4.33)\\ T &= f_4\left(T_o, \lambda, t\right) && \text{(Equation (4.23))} && (4.34) \end{aligned}$$

The first two of these are first order differential equations, the third is an algebraic relation and the last is an hereditary integral. The model parameters are given in Section A.4.

Chapter 5

Coupled Models

5.1 Introduction

As stated in Section 1.1.1, cardiac cells do not have electrical and mechanical components working independently. There is a great deal of interaction between the electrical, mechanical, and metabolic components of the cell. This research, however, only includes the mechanical and electrical components of a cardiac cell, ensuring enough flexibility that metabolic components can be incorporated.

There are two main aspects involved with coupling the electrical components to the mechanical. The first is the electro-mechanical coupling, which involves the effect that the electrical components have on the mechanical (*i.e.,* the calcium transient driving the mechanical contraction). The second aspect of the coupling, is the mechano-electric feedback. Mechano-electric feedback looks at the effect the mechanics has on the electrical activity of the cell – for example, how does stretching a resting cell affect the electrical activity, or what happens to the intracellular Ca^{2+} concentration when an isometrically contracting cell undergoes a length step. The two processes of excitation-contraction coupling and mechano-electric feedback constitute a regulatory loop intrinsic to the heart (Kohl, Day & Noble 1998).

It is known that the main interaction between electrical and mechanical components of a cardiac cell is through the intracellular Ca^{2+} concentration. Therefore, most of this research concentrates on the coupling of the Jafri–Rice–Winslow electrical model (Section 3.3) and the Hunter–McCulloch–ter Keurs mechanical model (Chapter 4), due to the superior $[\mathrm{Ca}^{2+}]_i$ handling abilities of the JRW model over the DFN and LR models.

5.1.1 Electro-mechanical coupling

Obviously, the electro-mechanical coupling between an electrical model and the HMT mechanics model can be achieved by simply replacing the single exponential model for the calcium transient used in the HMT model (Equation (4.5)) with that generated by an electrical model (*e.g.,* Equation (3.29), Equation (3.75), and Equation (3.106)). Indeed, this is the only coupling implemented in CELL between the DFN and LR models and the mechanical model. However, a further step is used from the JRW model and instead of taking just the calcium transient from this membrane model, it is the calcium bound to low-affinity Tn (*i.e.,* the Ca^{2+}-specific Tn-C binding sites) that is used. This is done by replacing Equations (4.5) and (4.6) with a modified version of Equation (3.135) from the JRW model (see Sections 5.1.2 and 5.2).

5.1.2 Mechano-electric feedback

There are two main terms used to describe the effect of the mechanical components on the electrical in cardiac cells: contraction-excitation feedback, which is effector-oriented; and mechano-electric feedback, which is result-oriented (Kohl 1995) (see Figure 5.1). Contraction-excitation feedback looks only at the effect of the mechanical contraction of the heart on its electrical activity, while mechano-electric feedback encompasses the entire mechanical environment of the heart including such effects as those brought about through changes in posture and breathing-induced flucuations in thoracic pressure. The term mechano-electric feedback is the preferred term since it includes bio-electric phenomena induced by changes in the mechanical environment of the heart which are not caused by cardiac contraction (Kohl 1995).

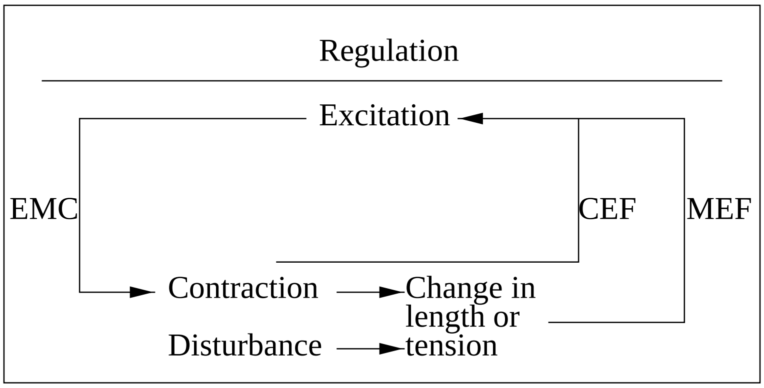

FIGURE 5.1: Scheme of interaction between cardiac excitation and contraction. Electro-mechanical coupling (EMC) provides the control by the excitation (regulator) over the contraction (effector). The feedback is either effector-oriented and called contraction excitation feedback (CEF), or result-oriented mechano-electric feedback (MEF). *From Kohl (1995).*

There are three basic mechanisms by which mechano-electric feedback might influence cardiac muscle cells (Kohl 1995):

1. mechano-electric feedback induced by operation of mechanosensitive ion channels;
2. stretch-induced changes in intracellular calcium handling;
3. mechano-electric feedback based on interaction of cardiac myocytes with non-muscle cells.

Only the second of these is investigated in this research.

There are several well documented effects that mechano-electric feedback can have on cardiac cells, and the model developed needs to be able to replicate these effects. Some examples are:

- resting force increases in cardiac muscle as resting or initial sacromere length is increased (Lakatta 1992), noting that the sacromere length is related to the extension ratio, λ , used by the HMT model via the slack length (Section 4.1);
- mechanical stimuli, such as osmotic cell swelling or cell inflation via the patch pipette, enhances the L-type Ca^{2+} current (Matsuda, Hagiwara, Shoda, Kasanuki & Hosoda 1996);
- Peak developed force and maximum rate of positive and negative force development decrease as diastolic muscle length is reduced from a maximum, L_{max} to 90% L_{max} (Gamble, Taylor & Kenno 1992);
- the speed with which stretch is applied influences the response of the cell - rapid stretch causes greater response in the electrical activity of the cell than slow stretch even though their force or displacement are identical (Arai, Kodama & Toyama 1996);
- more Ca^{2+} is released into the myoplasm subsequent to excitation in cardiac muscle contracting in the steady state at longer sarcomere lengths than in the steady state at shorter lengths (Lakatta 1992);
- the frequency of electrical stimulation affects the mechanical behaviour of cardiac cells (Banijamali, Gao, MacIntosh & ter Keurs 1991, Schouten & ter Keurs 1986);
- the force-frequency relationship of rat myocardium shows a peak at a frequency of $0.1\ \mathrm{Hz}$ (Schouten & ter Keurs 1986);
- imposing forced length oscillations on the cell results in corresponding observed tension oscillations and rapid increases in intracellular calcium followed by a transient decrease (Gordon & Ridgway 1990);

- following a step decrease in the length of a cell, Ca^{2+} is released from Tn-C and is then either re-bound to Tn-C or extracted from the myoplasm by intracellular or transmembrane processes (Hunter et al. 1998);

- the time of a step decrease in cell length and the duration of the step influence the effect of the step on the behaviour of the cell (Gordon & Ridgway 1990, Hunter et al. 1998).

These effects are used to assess the validity of the coupled JRW–HMT model developed (Section 7.2).

5.2 Coupled Model Implementation

As stated above, the only coupling implemented within CELL between the DFN or LR electrical models and the HMT mechanics model is the replacement of the single exponential representation of the intracellular calcium transient of the HMT model (Equation (4.5)) with that calculated in the chosen membrane model (*i.e.*, Equation (3.29) or Equation (3.75)). While this simple coupling can represent some aspects of a "real" cardiac cell, it is very limited as it involves no mechano-electric feedback, which has been shown to have some influence on the functioning of a cardiac myocyte (Kohl 1995). Due to the superior intracellular handling abilities of the JRW model, it was decided that for this research the main coupled model investigated should consist of the JRW membrane model and the HMT mechanics model.

When implementing the coupling of the JRW and HMT models, there are several points to note: (i) the HMT model concentrates on the accurate modelling of the mechanical activity; (ii) the JRW model was created to address the lack of accurate modelling of intracellular calcium within the LR-II model; and (iii) the mechano-electric feedback mechanism investigated in this research is the tension dependent release of Ca^{2+} from Tn-C. Therefore, the calcium modelling of the coupled model should be dominated by the JRW model, namely replacing Equation (4.6) with a modified version of Equation (3.135). The modification, also necessary in Equation (3.102), is required due to the tension dependent release of Ca^{2+} from Tn-C (the low-affinity troponin binding sites in the JRW model). This effect is modelled by the HMT model as:

$$-\rho_1 \cdot \left(1 - \frac{T}{\gamma \cdot T_o}\right) \cdot [\mathrm{Ca}^{2+}]_b$$

in Equation (4.6). Including this term in Equation (3.135) results in

$$\frac{d[\mathrm{LTRPNCa}]}{dt} = \rho_0 \cdot [\mathrm{Ca}^{2+}]_i \cdot ([\mathrm{LTRPN}]_{tot} - [\mathrm{LTRPNCa}]) - \rho_1 \cdot \left(1 - \frac{T}{\gamma \cdot T_o}\right) \cdot [\mathrm{LTRPNCa}] \tag{5.1}$$

where ρ_0 and ρ_1 from the HMT model replace k^+_{ltrpn} and k^-_{ltrpn}, respectively, from the JRW model. Also $[\mathrm{LTRPN}]_{tot} \equiv [\mathrm{Ca}^{2+}]_{bmax}$ and $[\mathrm{LTRPNCa}] \equiv [\mathrm{Ca}^{2+}]_b$. The parameter values are also modified to reflect the increased accuracy of the intracellular calcium modelling (see Appendix A.5). Modifing the equation for J_{trpn} (Equation (3.102)) results in

$$\begin{aligned} J_{trpn} = {} & k^+_{htrpn} \cdot [\mathrm{Ca}^{2+}]_i \cdot ([\mathrm{HTRPN}]_{tot} - [\mathrm{HTRPNCa}]) - k^-_{htrpn} \cdot [\mathrm{HTRPNCa}] \\ & + \rho_0 \cdot [\mathrm{Ca}^{2+}]_i \cdot ([\mathrm{LTRPN}]_{tot} - [\mathrm{LTRPNCa}]) - \rho_1 \cdot \left(1 - \frac{T}{\gamma \cdot T_o}\right) \cdot [\mathrm{LTRPNCa}] \end{aligned} \tag{5.2}$$

The coupling described above between the JRW and HMT models includes both the electromechanical coupling (*i.e.*, using the $[\mathrm{Ca}^{2+}]_i$ calculated by the membrane model) and mechanoelectric feedback described in Section 5.1.

Another major difference between the HMT and the JRW models is the value of $[\mathrm{Ca}^{2+}]_{bmax}$ – $2\ \mu\mathrm{M}$ for the HMT model and $70\ \mu\mathrm{M}$ for the JRW model (a more physiologically correct value). This difference results in the JRW model having a much higher peak $[\mathrm{Ca}^{2+}]_b$ than was used in the development of the HMT model (compare Figures 7.14 and 7.10)). Thus, the equation for the time rate of change of z requires scaling by the normalised concentration of calcium bound to low-affinity troponin, $[\mathrm{Ca}^{2+}]_b/[\mathrm{Ca}^{2+}]_{bmax}$, to give

$$\frac{dz}{dt} = \alpha_0 \cdot \left[\left(\frac{[\mathrm{Ca}^{2+}]_b}{C_{50}} \cdot \frac{[\mathrm{Ca}^{2+}]_b}{[\mathrm{Ca}^{2+}]_{bmax}} \right)^n \cdot (1 - z) - z \right] \tag{5.3}$$

The values of n_{ref} and pC_{50ref}, Equations (4.14) and (4.15), are decreased as a consequence of the modification given in Equation (5.3) (see Section A.5). These modifications keep all units consistent and simply scale z to be consistent with the increased level of $[\mathrm{Ca}^{2+}]_b$.

Chapter 6

CELL

6.1 User Interface

As stated in Sections 1.2 and 1.3, one of the aims of this research is to create and easy-to-use interface to the mathematical models. There are two main reasons for doing this. The first reason is that, as shown in Chapters (3)–(5), when dealing with cardiac cell models, there can easily be greater than 200 parameters in the model being used. Thus, some kind of user interface is required if the models are going to be used for any kind of parameter investigation, either at the single cell level or when used with continuum models, see Section 6.1.3, to investigate, for example, myocardial infarcts and re-entrant waves

The second reason for developing the user interface is that the models are useful teaching aids. When used for this purpose, it is most likely that the students are going to be more interested in the underlying physiology than the mathematical models themselves. In this case, the purpose of the interface is two fold: firstly, to “hide” the mathematics from the students so that they are free to concentrate on the physiological effects of changing physiologically significant parameter values; and secondly, to enable the students to easily find and change the appropriate parameters for the experiment they wish to perform.

6.1.1 The CELL interface

In order to obtain the goals stated above, the program CELL was designed and implemented as part of this research project. This interface was implemented as part of the general mathematical modelling package, developed within the Department of Engineering Science at Auckland University, known as CMISS. More specifically, CELL was designed as both a stand-alone program and a CMGUI tool, where CMGUI is the graphical front-end of the CMISS package.

As previously stated, the interface to the mathematical models implemented in this research needs to be intuitive and easy to use. One popular method of implementing a graphical user interface is known as an image map, where the user of the interface is presented with a representation of the system being modelled (*e.g.,* a cardiac cell, an air conditioning system, or an internet based virtual shopping mall) and the user can access the various components of the system by simply clicking on the representation of that component in the image map. Then, depending on the system being modelled, the user is presented with the appropriate information (*e.g.,* model parameters, ventilation duct dimensions, or a particular music shop).

This type of interface is ideally suited to a model of a cardiac cell, where the entire model is based on a single cardiac cell which can be easily represented as an image map, using standard representaions of the components of the system. The image map developed is given in Figure 6.1, showing the entire cardiac cell.

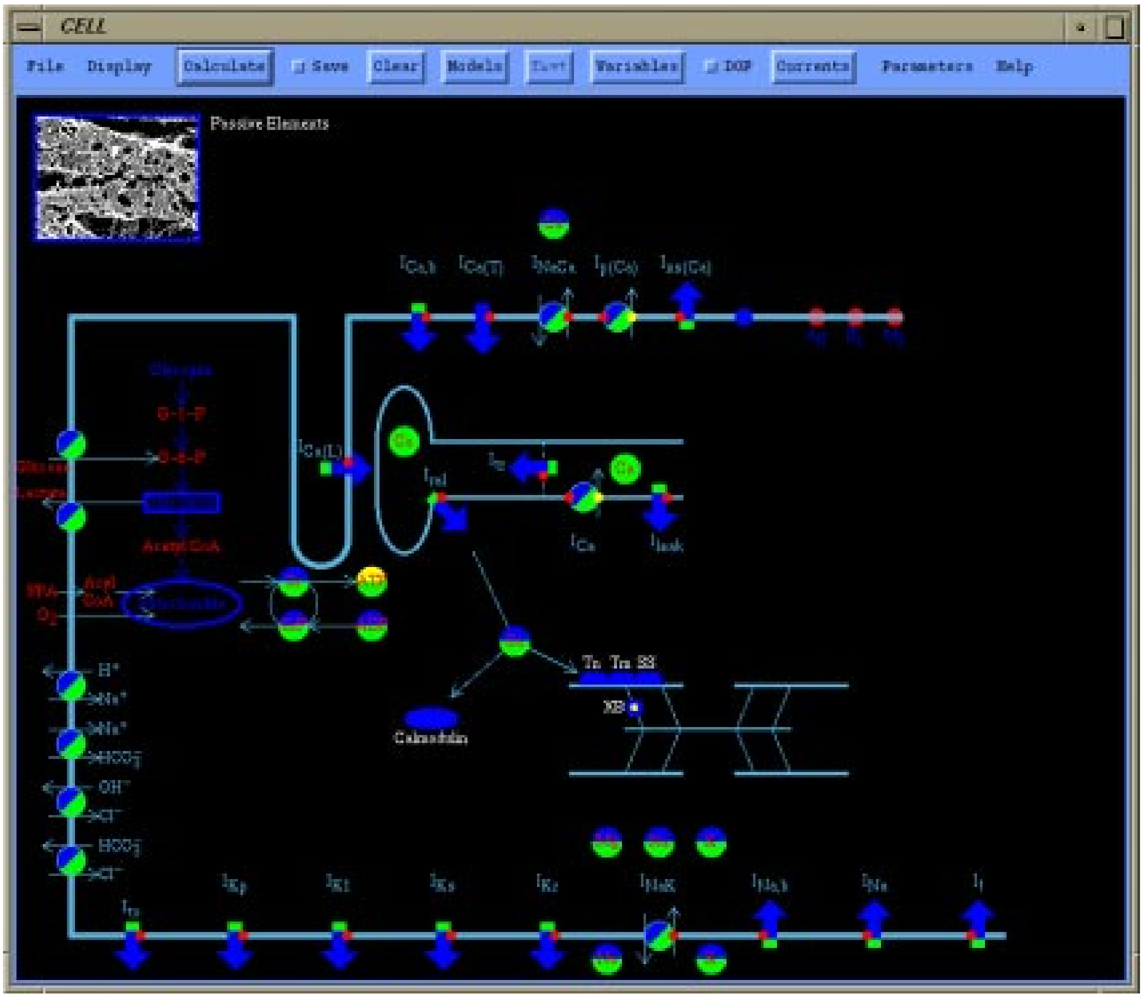

FIGURE 6.1: The full CELL image map interface.

Figure 6.1 shows the schematic diagram of a cardiac cell used to represent a cardiac cell. The ionic channels, pumps, and exchangers are all represented in this diagram, as are the mechanical components of the cell (with the passive elements outside the cell representing the passive extracellular matrix). The metabolic and proton regulation mechanisms of the cell are also represented, but were not used as part of this research. The user can set the overall model design (which model/models to use, mechanical test setup, read parameters from a file, initial conditions, *etc.*), using the items contained in the menu bar at the top of the image map.

Model parameters

The model parameters are accessed simply by clicking on the appropriate region in the image map – *i.e.*, clicking on the $I_{Ca(L)}$ channel will bring up the parameters associated with the L-type Ca^{2+} channel, given in Figure 6.2. The following is a brief overview of the three main areas of a parameter dialog.

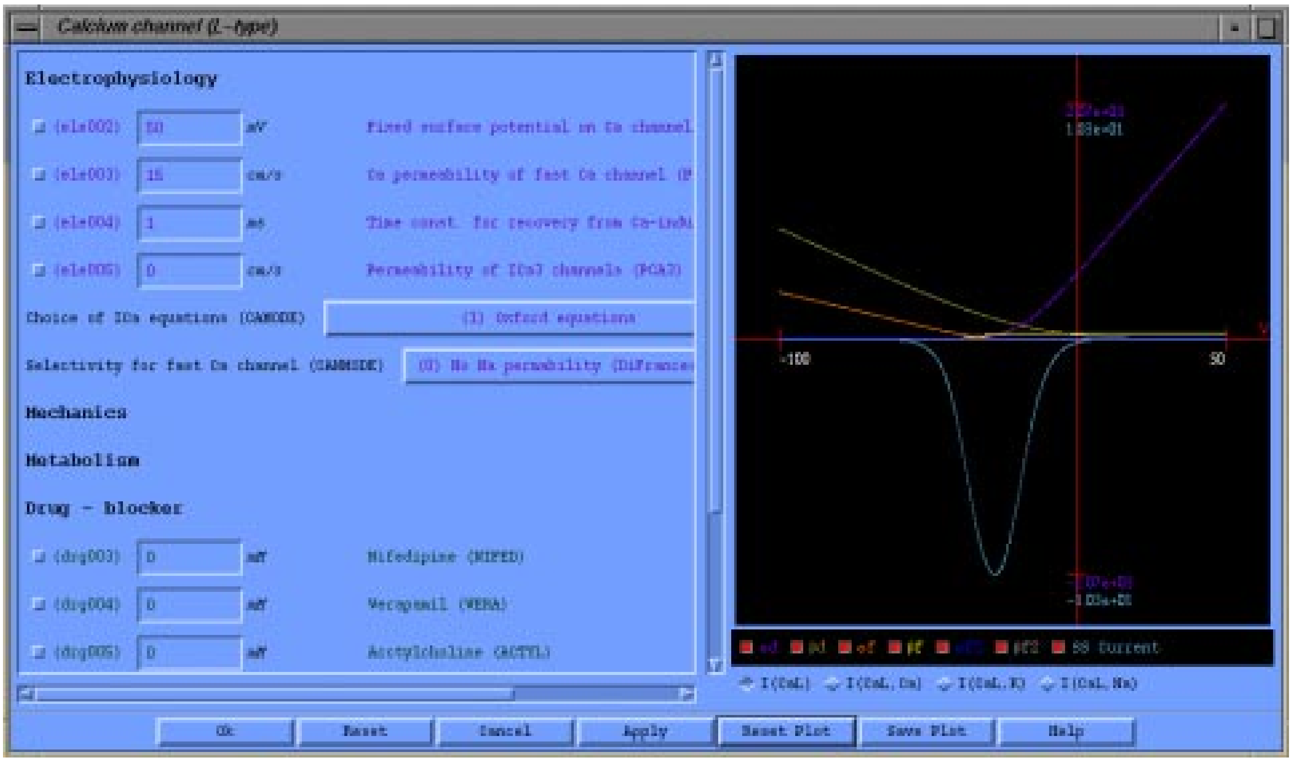

Electrophysiology

☐ (ele002) 50 mV Fixed surface potential on Ca channel
☐ (ele003) 15 cm/s Ca permeability of fast Ca channel (P
☐ (ele004) 1 ms Time const. for recovery from Ca-indu
☐ (ele005) 0 cm/s Permeability of ICaT channels (PCAT)
Choice of ICa equations (CAMODE) (1) Oxford equations
Selectivity for fast Ca channel (CAMNSDE) (0) No Na permeability (DiFrance

Mechanics

Metabolism

Drug – blocker

☐ (drg003) 0 mM Nifedipine (NIFED)
☐ (drg004) 0 mM Verapamil (VERA)
☐ (drg005) 0 mM Acetylcholine (ACTYL)

FIGURE 6.2: An example of a CELL parameter dialog box. The dialog is split into three main sections: (1) the model parameter area, where the actual model parameters can be modified; (2) the drawing area, which illustrates the voltage dependence of the channel (or pump or exchanger); and (3) the action buttons which let the user update the parameters and plots, cancel any changes or obtain help (extra information) for this particular channel.

Parameter area This is the area which gives the user of the interface control over the model parameters associated with a given channel. This area is split into four further sections: electrophysiology, mechanics, metabolism, and drug. As with the image map, only the electrophysiology and mechanics areas are used for this research, with the drug and metabolism areas included for future development.

Each model parameter in the parameter dialogs contain four pieces of information:

1. A spatial toggle – this allows the user to set the parameter to be spatially varying (toggle on) or spatially constant (toggle off). This is for use with the distributed finite element model of the whole heart, discussed in more detail below (Section 6.1.3).
2. The parameter value text field – this is where the user actually changes the parameter value. The changes to parameter values are not accepted until the user clicks the `Ok` or `Apply` button, until which time the user can revert to the previous parameter values by clicking the `Reset` or `Cancel` button.
3. Parameter units – these are the units expected by the interface, and any conversion of units required occurs in the back-end numerical code.
4. The parameter label – a brief description of the parameter.

The dialog given in Figure 6.2 also shows an option menu with the electrophysiology parameters. This option menu , and others associated with various channels and pumps, are only used when the electrical model is set to the DFN model. These options are included due to the implementation of the DFN model used being based on the OxSoft HEART program developed at Oxford University. HEART includes numerous new developments that were not included in the original DiFrancesco & Noble (1985) paper, and uses these options to determine which modifications to include in the model.

Drawing area Within this region of the parameter dialog, a plot of the voltage dependence of the channel is given. This plot includes the gating rate constants (α's and β's) if any exist for the particular channel, the steady state current and/or steady state conductance. These plots can be modified by changing the parameter values within the dialog, and clicking the `Apply` button. This will update the model parameters and re-calculate the voltage dependent values, adding the new lines to the existing plot. The plot can be cleared of all lines, except the most recent, by clicking on the `Reset plots` button. Each component of the plot can have its visibility toggled on or off by the individual toggle buttons. For channels with multiple components (*i.e.*, $I_{Ca(L)} = I_{Ca(L),Ca} + I_{Ca(L),Na} + I_{Ca(L),K}$ or $I_f = I_{f,Na} + I_{f,K}$), the visible component can be set by the appropriate toggle.

Plots similar to those described above, can be obtained by clicking in the green "plotting regions" attached to the different channels, pumps, and exchangers in the image map. However, these plots are not automatically updated when model parameter values change, but they will contain the calculated channel current if the model has been solved.

Action buttons The lower edge of the parameter dialog contains the action buttons:

- `Ok` – when clicked, this button updates the model parameter values and "pops down" the parameter dialog.
- `Reset` – this button resets the parameter values to their previous value (set by the `Ok` or `Apply` buttons).
- `Apply` – this button updates the model parameter values and updates the plot contained in the dialog.
- `Cancel` – when clicked, this button resets the dialog box and "pops it down".
- `Reset plots` – this button clears the plot of all but the most recently drawn lines (*i.e.*, those representing the current parameter values shown in the dialog).
- `Help` – this button, when clicked, will bring up additional information about the particular mechanism represented by the dialog. This information is displayed as a web page in a Netscape (web browser) window.

6.1.2 UnEMAP – solution display and analysis

Once the current model has been solved (by clicking the `Calculate` button), some method of displaying the solution is required. For this research, the solution obtained from the models is in the form of dependent variable values through time – *i.e.*, once the model is solved you have the membrane potential at discrete points in time from some start time till a given end time, usually including at least one stimulation of the cell. The number of points at which you want the solution is set by the tabulation time interval, which can be specified in the time step dialog from the parameters menu in the image map window.

Another CMGUI tool, UnEMAP (Universal Electrophysiological Mapping System), has been developed for aquisition and analysis of electrophysiological data. UnEMAP consists of both the hardware and software required to aquire and analyse electrophysiological data, using up to 256 electrodes (a system capable of utilising over 4000 electrodes is currently under development).

The section of UnEMAP relevent to CELL is the ability to display and analyse numerous signals. When using the UnEMAP package, these signals are the information recorded from the electrodes (which may placed on the body surface to obtain a body surface potential map, or used to record directly from the epicardial surface). The solution obtained from the models in this research are the same as these recorded signals, except that each signal corresponds to a different solution variable and instead of being recorded they are calculated. This makes it possible to use UnEMAP modules to display and analyse the solution obtained from the mathematical models.

The main UnEMAP module used by CELL is the “Analysis window”, shown in Figure 6.3, which displays all the signals (solution variables) for the model.

The analysis window shows all the calculated signals in one window. The user can then click on a particular signal and get an enlarged view of that signal (Figure 6.4). Within this new window, the user can zoom in on a particular area of the signal, or perform different kinds of filtering, beat averaging, and a number of other types of signal analysis that are not particulary relevent to calculated rather than recorded signals. Another useful feature of UnEMAP is the ability to keep track of multiple recordings of the same signal, and display them together in one plot. Thus, multiple runs of the model may be calculated (*e.g.,* changing the stimulus time for each experiment) and then displayed together, as shown in Figure 6.4.

A major advantage of using UnEMAP within CELL, is that it is possible to compare calculated values with those recorded experimentally via UnEMAP. This applies mainly to the transmembrane potential, V_m, and the computed action potential can be compared directly to a recorded action potential to test the accuracy of the model.

6.1.3 CMISS

CMISS is a set of numerical modelling tools for use in Continuum Mechanics, Image analysis, Signal processing and System identification based on finite element, boundary element and finite difference techniques. It has been developed primarily for biomedical research but can also be regarded as a general purpose modelling tool for solving partial differential equations. The equations can be non-linear, time-dependent and defined in one, two or three spatial dimensions in a number of alternative coordinate systems.

One of the main driving forces behind the development of the CMISS package has been the evolution of a distributed finite element model the the heart. This model started as a basic description of the ventricular geometry and has evolved (in conjunction with CMISS) into a detailed model of cardiac form and function, including such features as muscle fibres, mechanical contraction, and electrical activation. To date, however, most work on the development of this model has been concerned with the heart as a whole, rather than a combination of cells or blocks of similar cells.

Work is now being performed to develop suitable cellular models which can then be implemented as part of the distributed finite element model of the whole heart. However, as stated above, these cellular models involve large numbers of model parameters, some of which are go-

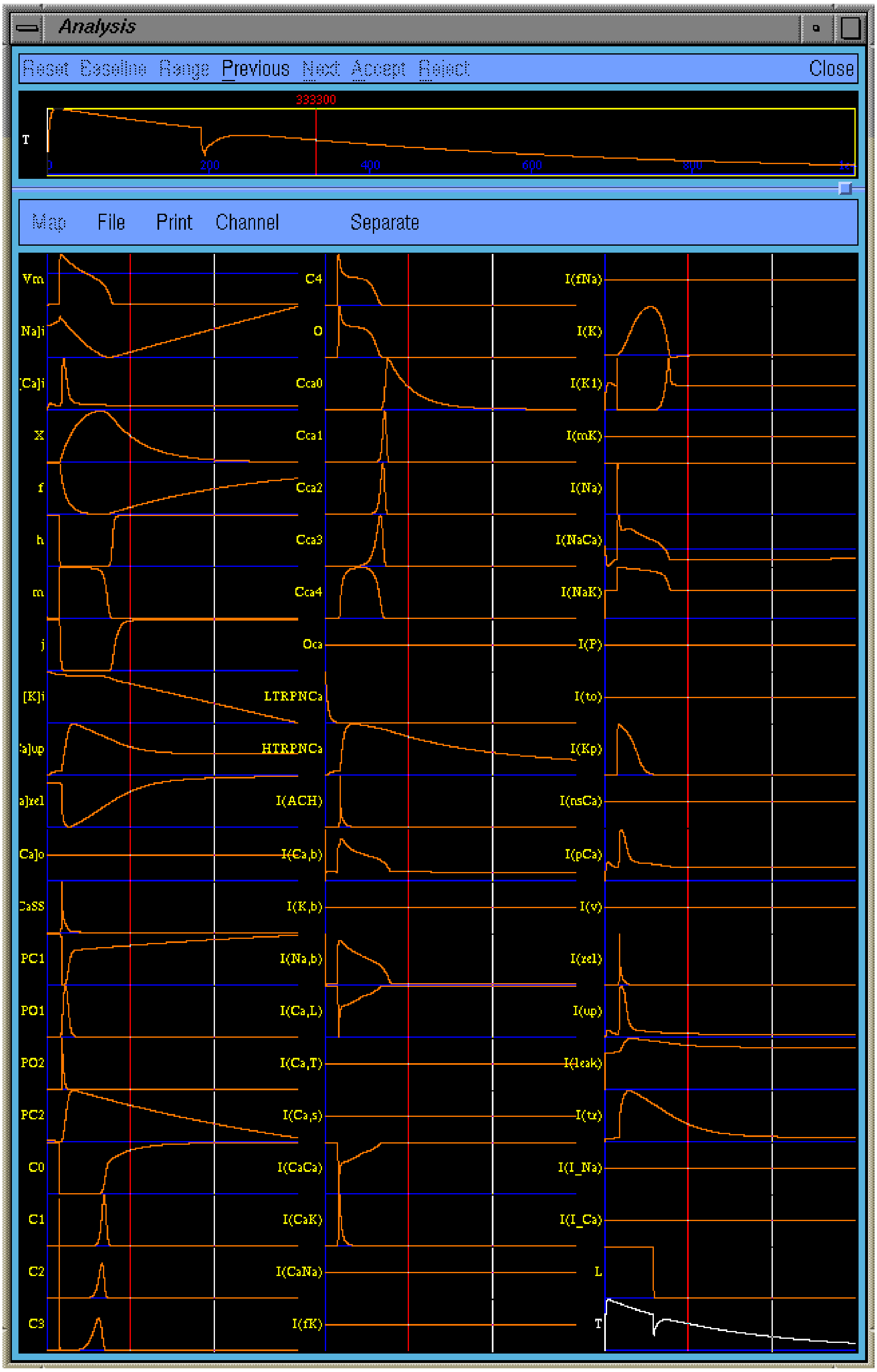

FIGURE 6.3: The UNEMAP analysis window, displaying the solution for the coupled JRW and HMT model.

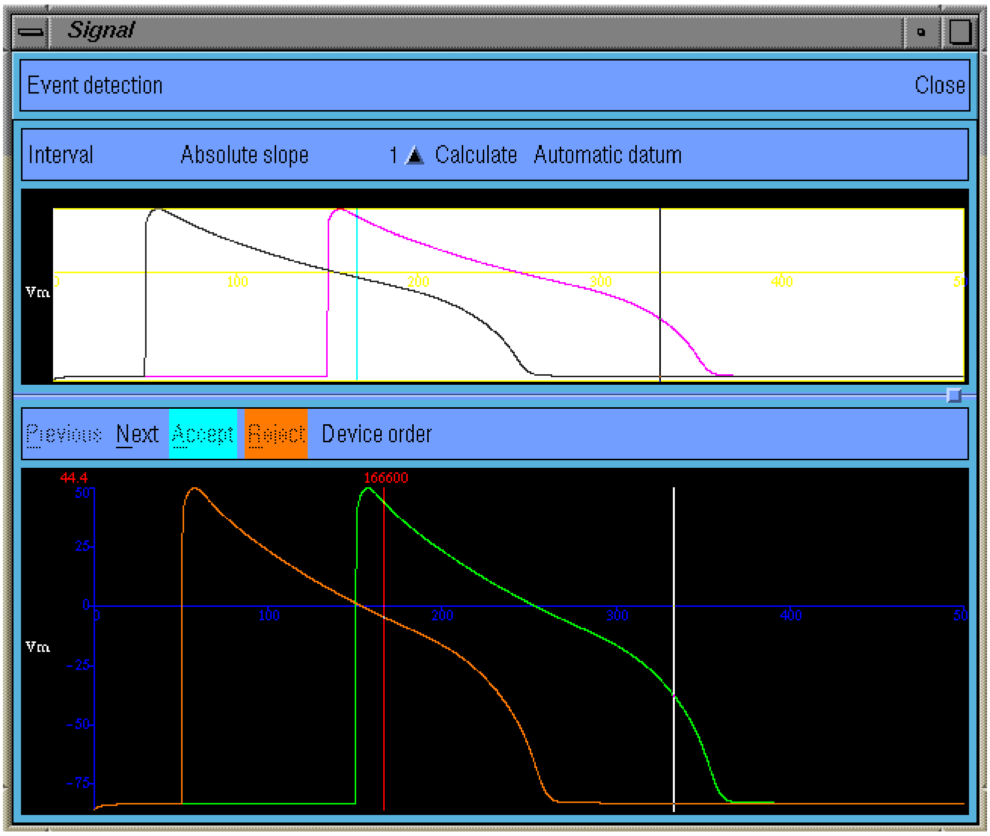

FIGURE 6.4: The UNEMAP trace window, displaying the action potential generated by the JRW model. The two traces represent two different experiments, each with a different stimulus time.

ing to vary depending on the location of the cell within the heart. Another purpose of the CELL interface is to be able to set the model parameters for use in this finite element model of the heart, and use the spatial toggles (described in Section 6.1.1) to tell CMISS which parameters are spatially varying. CMISS can then incorporate this information into the dexcription of the heart model.

6.2 Numerical Solution of the Models

Appendix B gives a listing of the code developed to solve the models implemented in this reseach. This listing simply presents the “coded” version of the model equations presented in Chapters (3)–(5).

6.2.1 Electrical models

As stated previously, the electrical processes of cardiac cells occurs very rapidly (for example see the I_{Na} current in Figure 7.3 or the subspace calcium transient in Figure 7.8). The speed at which these processes occur implies that a fine time resolution is required to correctly resolve the solution. This resolution can be acheived two ways – use a low order approximation to the actual system of equations (first order differential equations) and then use a very small time step to solve the model; or use a higher order (more accurate) approximation to the equations with a larger time step.

CELL uses a third order, variable stepsize Adams (Shampine & Gordon 1975) second order predictor–third order corrector formulation to approximate the system of equations. This allows a high degree of accuracy when solving the electrical models, while using a reasonable time step. With the implementation of this method used in CELL, the user specifies a tabulation time step (*e.g.,* $0.1\ \mathrm{ms}$ if the user wants a solution every $0.1\ \mathrm{ms}$) and the solver will step from tabulation point to tabulation point using variable time steps – *i.e.,* the solver is told to solve the model from $105.2\ \mathrm{ms}$ to $105.3\ \mathrm{ms}$ and is given the solution at $105.2\ \mathrm{ms}$, the solver will then return the solution at $105.3\ \mathrm{ms}$ using as many steps it deems necessary. In theory, this allows a relatively large tabulation time step to be specified. However, due to the rapid processes being modelled, a sufficiently small tabulation time step is required in order to ensure that all important information is captured (*i.e.,* the peak of the I_{Na} current and the peak $[\mathrm{Ca}^{2+}]_i$).

OxSoft HEART

The implementaion of the DFN membrane model (and the Adams solver) used in CELL is based on the OxSoft HEART program developed by a research group based at Oxford University. This software package was developed to simulate the experiments which they perform – *i.e.*, they fit mathematical models to the physiological data which they have gathered.

The first version of HEART was developed in conjunction with the original DiFrancesco & Noble (1985) model. Since this time, the program has developed as more experiments are performed, and hence, the underlying mathematical models also evolve to better fit the new experimental data (see Appendix B.1). This leads to subtle differences when the results given by CELL (and the newer versions of HEART) are compared those given in the original DiFrancesco & Noble (1985) paper (see Section 7.1.1).

6.2.2 The HMT mechanics model

Unlike the electrical activity of the cell, the mechanical components work at a much slower rate (for example, see Figure 7.10). This enables the use of simpler integration schemes for the differential equations (Equations (4.31)–(4.32)), while still keeping a reasonable time step.

The implementation of the HMT model within CELL uses a first-order Euler method (with a prediction step) to solve the two differential equations. For example, looking at the variable z :

$$\begin{aligned} z_{new} &= z_i + \Delta t \cdot \left.\frac{dz}{dt}\right|_{z_i,[\mathrm{Ca}^{2+}]_{bi},\lambda_i} \\ z_{i+1} &= z_i + \frac{1}{2} \cdot \Delta t \cdot \left(\left.\frac{dz}{dt}\right|_{z_i,[\mathrm{Ca}^{2+}]_{b(i)},\lambda_i} + \left.\frac{dz}{dt}\right|_{z_{new},[\mathrm{Ca}^{2+}]_{b(i+1)},\lambda_{i+1}} \right) \end{aligned}$$

Evaluating the isometric tension, T_o , is a simple matter of evaluating the algebraic relation given by Equation (4.12), now that z has been evaluated and the extension ratio, λ , is specified completely by the user for all time.

The final step in the solution of the HMT model is the calculation of the observed tension, T , which is given by the isometric tension scaled by a nonlinear function of hereditary integral of length changes (Equation (4.23)). The hereditary integral is evaluated by keeping a record of its value at the previous time step and then adding to this for the current value (*i.e.*, keeping a running total). For a more detailed version of how this is implemented see the `FN_Q` function in Appendix B.

Chapter 7

Results

7.1 Non-coupled Problems

In the following sections (Sections (7.1.1)–(7.1.3)), results obtained from the three membrane models and the HMT mechanics are presented. These results are are given with comparisons to the results shown in their respective original publications (see Chapters 3 and 4). This section is purely for the validation of the implementation of the individual models contained within CELL. Results of the coupled model developed are presented in Section 7.2.

7.1.1 DiFrancesco–Noble

Figures 7.1 and 7.2 show some of the results obtained from the DFN model. These results were calculated using the parameter values given in Appendix A.1, with an initial stimulus of $-250\ \mathrm{nA}$ (not shown in the plots). The plots show the first and second pacemaker action potentials triggered by the stimulus.

The results given in Figures 7.1 and 7.2 can be compared with those given in Figures 6 and 7 of DiFrancesco & Noble (1985) (the second, pacemaker, action potential and noting that $I_{NaK} \equiv I_p$) to show that the implementation of the DFN model within CELL gives the expected results. The slight differences between the plots given in DiFrancesco & Noble (1985) and those in Figures 7.1 and 7.2 can be explained by the fact that the DFN model within CELL is based on the OxSoft HEART implementation, which includes a number of additions and improvements over the original DiFrancesco & Noble (1985) model (see Chapter 6). This results in slight differences in the equations being solved. Thus, the results are not exactly the same but are very similar.

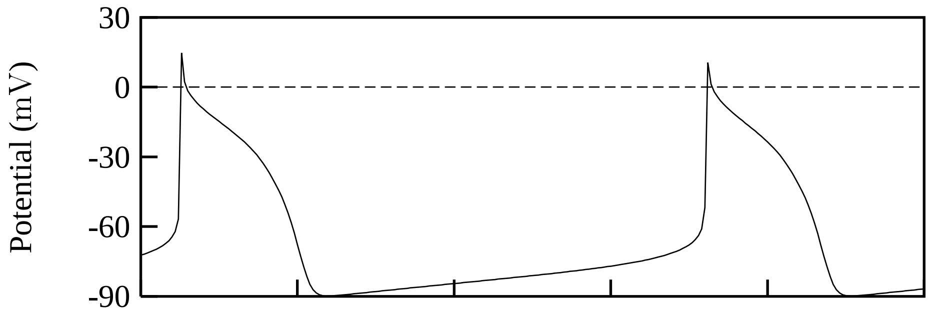

(a) Membrane potential

(b) $[\mathrm{Ca}^{2+}]_i$

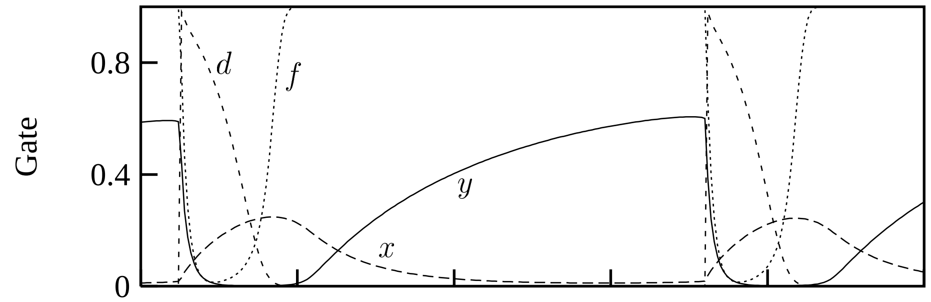

(c) Gating variables

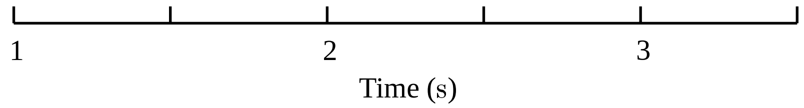

FIGURE 7.1: Plots of the membrane potential, $[\mathrm{Ca}^{2+}]_i$, and gating variables obtained from the DFN model. The plots show the induced pacemaker action potentials after an initial stimulation. Parameters used are given in Appendix A.1. Results are continued in Figure 7.2.

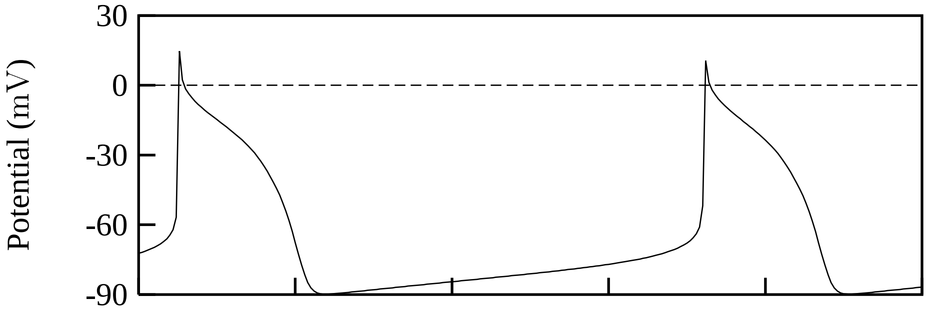

(a) Membrane potential

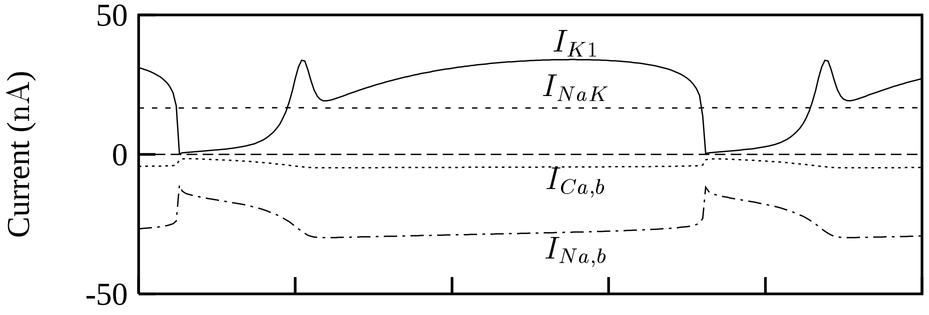

(b) Ionic currents

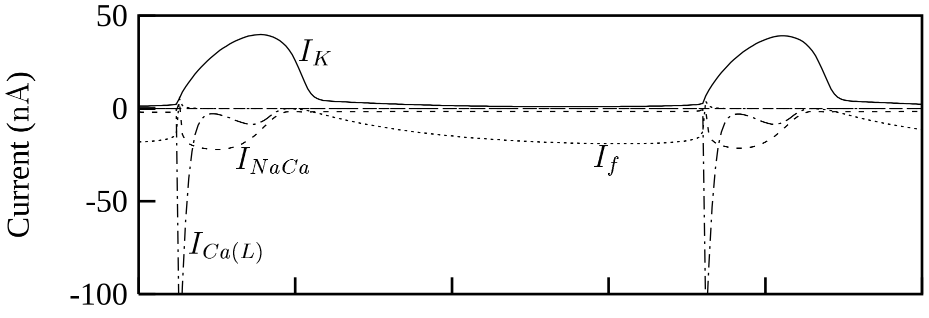

(c) Ionic currents

FIGURE 7.2: Continuation of results presented in Figure 7.1, showing the ionic currents obtained from the DFN model. Parameters used are given in Appendix A.1. Note: $I_{NaK} \equiv I_p$ from DiFrancesco & Noble (1985).

7.1.2 Luo–Rudy and Jafri–Rice–Winslow

Figures (7.3)–(7.6) show some of the main results generated by CELL when solving the LR model. These results were calculated using the parameter and initial values given in Appendix A.2 with a single stimulation of $-100\ \mu\mathrm{A}\cdot\mathrm{cm}^{-2}$ at time $0\ \mathrm{ms}$. Unlike the DFN model, LR models only ventricular myocytes which, under normal conditions, have no pacemaking ability. Thus only the one action potential shown (with recovery to a resting state) is expected.

Figure 7.3 shows plots of the major ionic currents which determine the characteristics of the action potential (also shown in Figure 7.3). This figure can be directly compared to Figure 13 of Luo & Rudy (1994*a*), where $1\ \mu\mathrm{A}\cdot\mathrm{cm}^{-2} = 1\ \mu\mathrm{A}\cdot\mu\mathrm{F}^{-1}$ due to the specific membrane capacity being set to $1\ \mu\mathrm{F}\cdot\mathrm{cm}^{-2}$ (Luo & Rudy 1994*a*).

As shown in Figure 7.3, the action potential and ionic currents are very similar to those given in Luo & Rudy (1994*a*) with the main differences being the duration of the plateau phase of the action potential, the peak of $I_{Ca(L),Ca}$, and the end of the I_{NaCa} trace. These differences can be explained by the Ca^{2+} buffering within the myoplasm and JSR. Luo & Rudy (1994*a*) do not give an explicit description of their method of implementation of Ca^{2+} buffering within the myoplasm (calmodulin and troponin) and JSR (calsequestrin). This makes it difficult to accurately recreate the experiments presented in Luo & Rudy (1994*a*). For the purpose of this research, a simple method of Ca^{2+} buffering within the JSR is implemented but no buffering within the myoplasm is implemented. Since the plateau phase of the action potential is determined by the L-type calcium current, the enhanced “plateau” of the clacium component of the L-type calcium current results in the extension to the plateau phase of the action potential.

In later papers, a more detailed description of intracellular calcium buffering for the LR model is described in many forms (*e.g.*, Zeng, Laurita, Rosenbaum & Rudy (1995) and Jafri et al. (1998)). However, due to time constraints, these implementations were not investigated for use with the implementation of the LR model used within CELL.

Figure 7.4 shows plots of the intracellular calcium transient with the two main intracellular calcium fluxes, I_{rel} and I_{up}. As with the currents shown in Figure 7.3, these plots are very similar to those presented by Luo & Rudy (Figure 15 (a), (b), (c) Luo & Rudy (1994*a*)), with slight differences in the peak values and duration time. These differences can be explained by the lack of myoplasmic buffering, as described above.

The L-type calcium current, $I_{Ca(L)}$, is shown in Figure 7.5 along with the three component currents. The comparison of these plots with those given by Luo & Rudy (Figure 17, Luo & Rudy (1994*a*)) emphasises the effect of the lack of myoplasmic Ca^{2+} buffering on the main trans-sarcolemmal Ca^{2+} transport mechanism.

Comparing Figure 7.6 to Figure 18 of Luo & Rudy (1994*a*), it is clear that the only significant difference in the time-independent currents is the peak and duration of the sarcolemmal

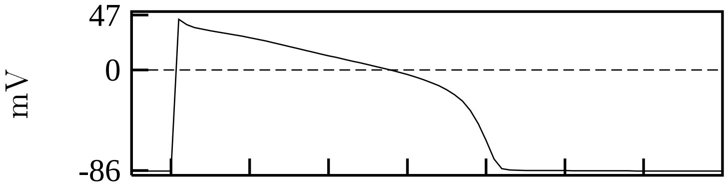

(a) Membrane potential

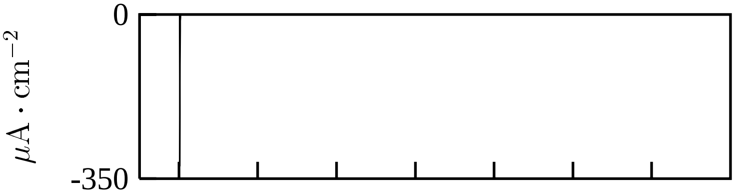

(b) I_{Na}

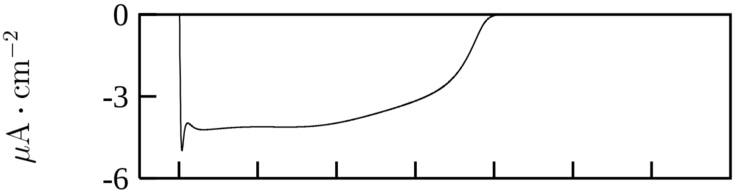

(c) $I_{Ca(L),Ca}$ (I_{Ca})

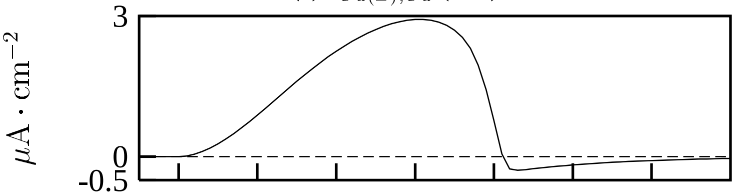

(d) I_K

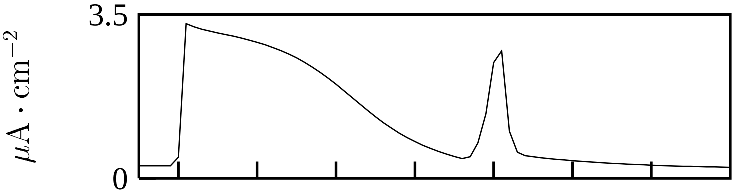

(e) I_V

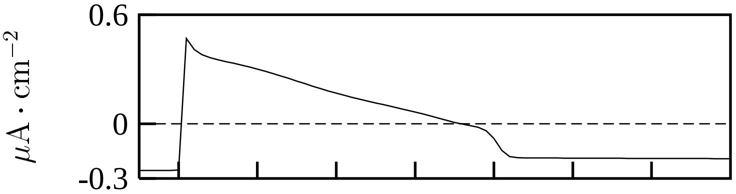

(f) I_{NaCa}

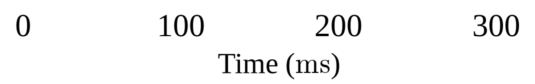

FIGURE 7.3: The action potential calculated by the LR model, shown with the major ionic currents which determine its shape. The parameters and initial conditions used for this simulation are given in Appendix A.2.

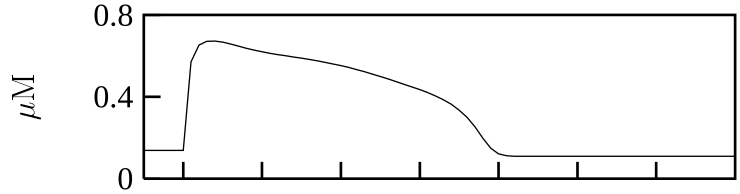

(a) $[\mathrm{Ca}^{2+}]_i$

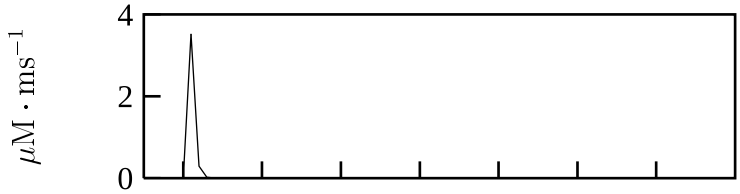

(b) I_{rel} (JSR $\rightarrow$ myoplasm)

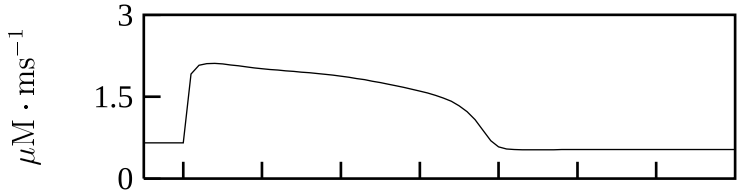

(c) I_{up} (NSR $\leftarrow$ myoplasm)

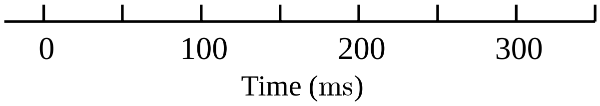

FIGURE 7.4: Plots showing the intracellular Ca^{2+} fluxes during an action potential calculated by the LR model. The parameters and initial conditions used for this simulation are given in Appendix A.2.

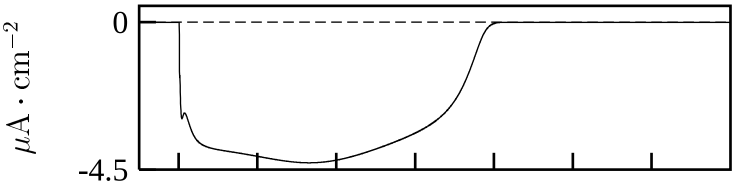

(a) $I_{Ca(L)}$ $(I_{Ca,t})$

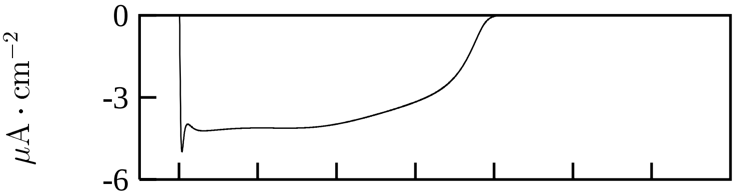

(b) $I_{Ca(L),Ca}$ (I_{Ca})

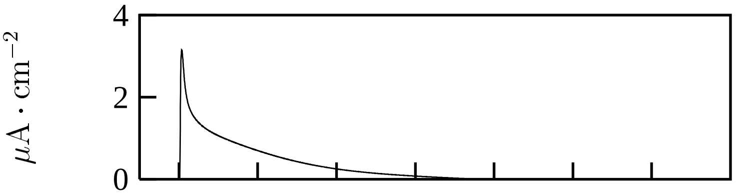

(c) $I_{Ca(L),K}$ $(I_{Ca,K})$

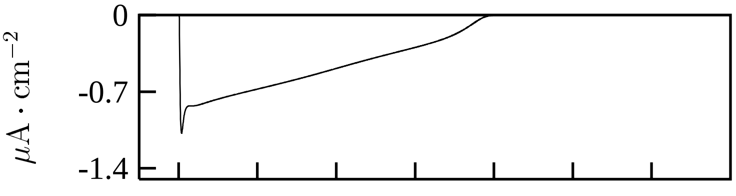

(d) $I_{Ca(L),Na}$ $(I_{Ca,Na})$

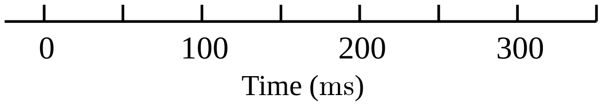

FIGURE 7.5: The ionic currents through the L-type Ca^{2+} channel calculated by the LR model. The parameters and initial conditions used for this simulation are given in Appendix A.2. The current names in brackets are those used by Luo & Rudy (1994*a*).

calcium pump, $I_{p(Ca)}$. As with all the differences above, this is due to the lack of myoplasmic Ca^{2+} buffering.

Figures (7.7)–(7.9) show some of the results obtained from CELL when solving the JRW model. The parameter and initial values used are given in Appendix A.3 with a stimulus of $-100\ \mu\mathrm{A}\cdot\mathrm{cm}^{-2}$ at time $50\ \mathrm{ms}$. As stated in Section 3.3, the JRW model is based on the LR model. Thus, Figure 7.7 can be compared to Figure 7.3 to show the marked difference in the $I_{Ca(L),Ca}$ current. This difference highlights the effect of myoplasmic (and, to a lesser extent, sarcoplasmic) Ca^{2+} buffering, since the JRW implementation of the LR model includes a complete description of Ca^{2+} buffering. There are also differences due to the increased accuracy of the intracellular Ca^{2+} handling in general.

Shown in Figure 7.8 are the action potential and calcium transients calculated by CELL when solving the JRW model. These plots can be compared to those of Jafri et al. (Figure 5 (e) – (h), solid line, Jafri et al. (1998)) to show that the expected results of the improved calcium handling of the JRW model are achieved.

Another aspect of the improved intracellular calium handling abilities of the JRW model is the modelling of multi-state ryanodine receptors. The role of the RyR channels is shown in Figure 7.9, which compares well with the results presented by Jafri et al. (Figure 7, solid line, Jafri et al. (1998)).

7.1.3 Hunter–McCulloch–ter Keurs

Figure 7.10 shows the tension development during an isometric twitch (*i.e.,* the muscle is held at a constant length, and then stimulated once). This isometric contraction is driven by the intracellular calcium transient, described by Equation (4.5), and plotted with the trace of Ca^{2+} bound to Tn-C in Figure 7.10 (a). Figure 7.10 (b) shows the non-dimensional variable, z , representing the proportion of actin binding sites available for cross-bridge binding. The tension development is given in Figure 7.10 (c). These results compare well with those given by Hunter et al. (1998) (Figure 18, solid line), with the difference in the tension due to the higher value of T_{ref}, $125\ \mathrm{kPa}$, compared to $100\ \mathrm{kPa}$ used by Hunter et al. (1998).

The results of performing a 2% length step on a maximally activated cell are presented in Figure 7.11. Figure 7.11 clearly shows the initial fast recovery phase, followed by slow recovery to the resting state, as depicted in Figure 4.3. The oscillation phase of the tension recovery is not present in Figure 7.11, due to the size and duration ($2\ \mathrm{ms}$) of the length step.

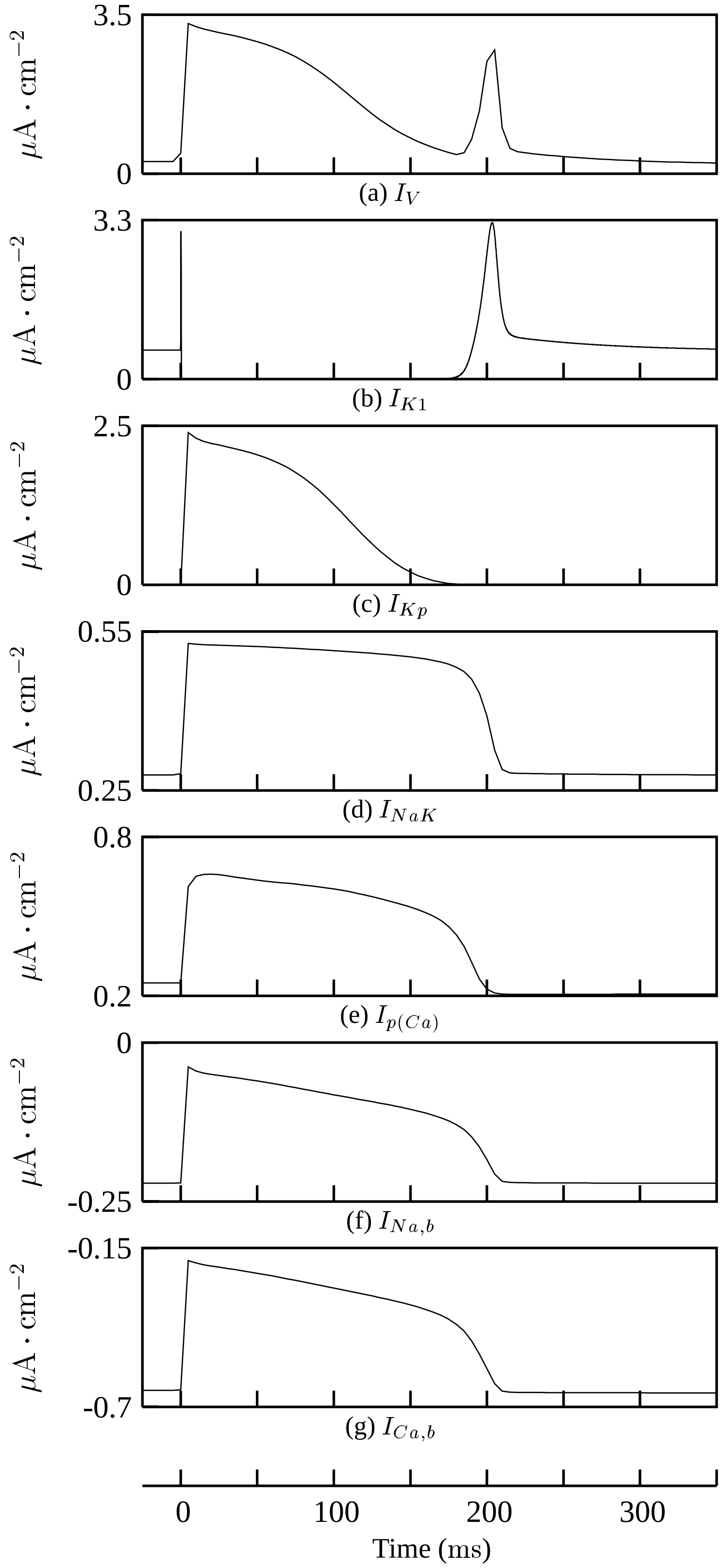

FIGURE 7.6: The total time-independent current, I_V, and its component currents, as calculated by the LR model. The parameters and initial conditions used for this simulation are given in Appendix A.2.

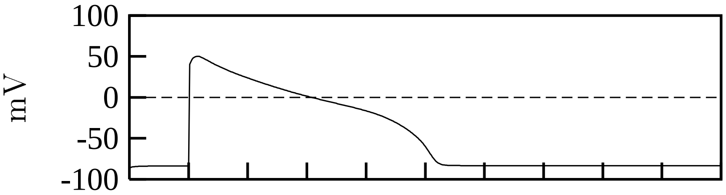

(a) Membrane potential, V_m

(b) I_{Na}

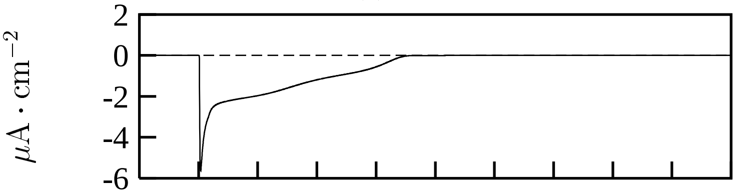

(c) $I_{Ca(L),Ca}$

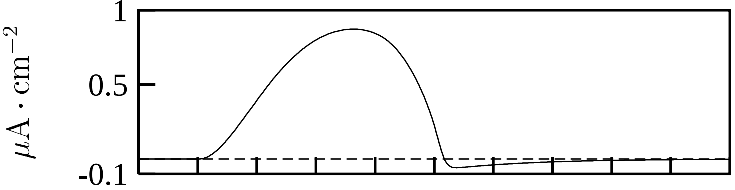

(d) I_K

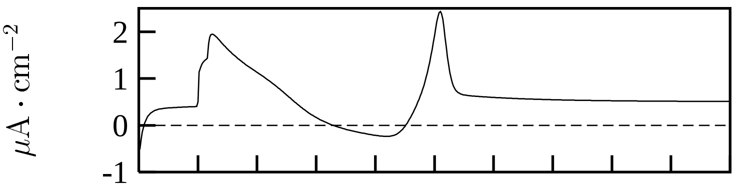

(e) I_V

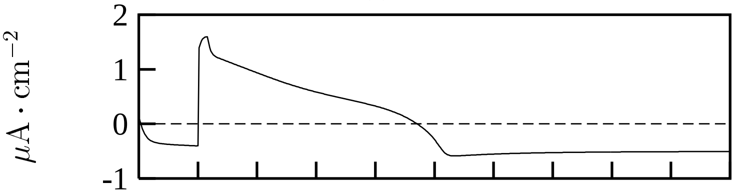

(f) I_{NaCa}

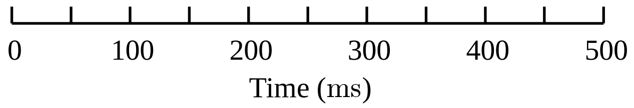

FIGURE 7.7: The action potential calculated by the JRW model, shown with the major ionic currents. Compare with Figure 7.3. The parameters and initial conditions used for this simulation are given in Appendix A.3.

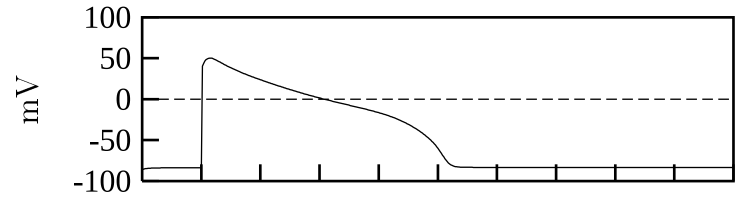

(a) Membrane potential, V_m

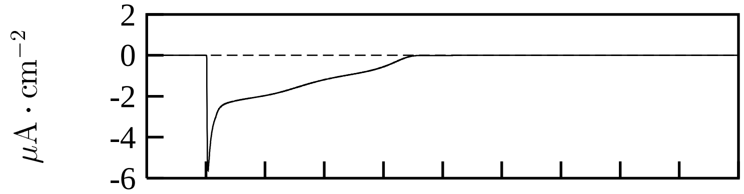

(b) $I_{Ca(L),Ca}$

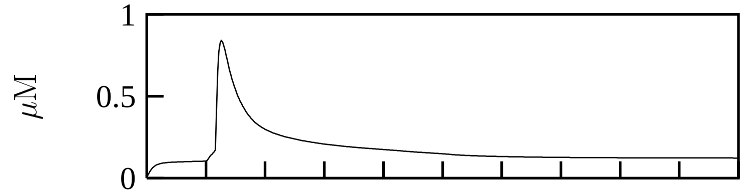

(c) $[Ca^{2+}]_i$

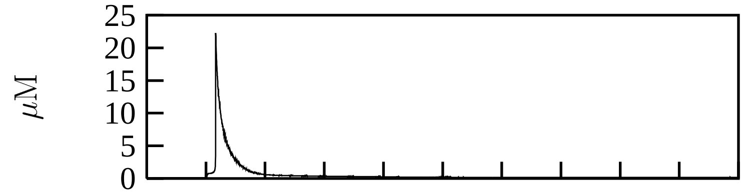

(d) $[Ca^{2+}]_{SS}$

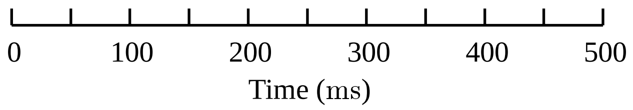

FIGURE 7.8: The action potential,V_m, calcium component of the L-tpye calcium channel current, $I_{Ca(L),Ca}$, intracelular Ca^{2+} concentration, and the JRW specific subspace Ca^{2+} contration, calculated by the JRW model. The parameters and initial conditions used for this simulation are given in Appendix A.3.

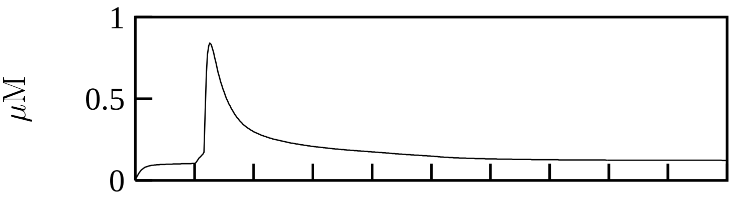

(a) $[\mathrm{Ca}^{2+}]_i$

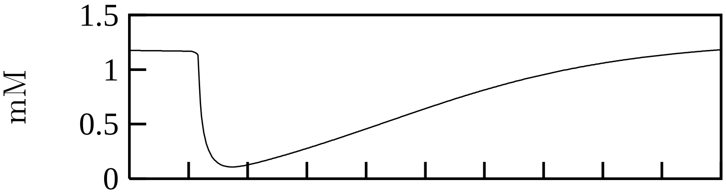

(b) $[\mathrm{Ca}^{2+}]_{JSR}$

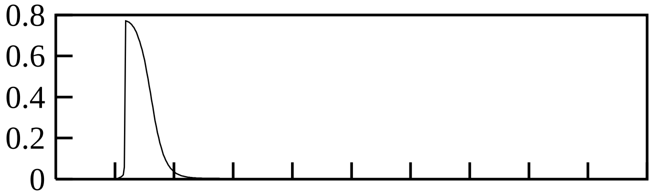

(c) RyR_{open}

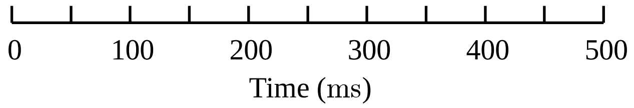

FIGURE 7.9: The role of RyR channels in the regulation of the release of Ca^{2+} from the JSR. The parameters and initial conditions used for this simulation are given in Appendix A.3.

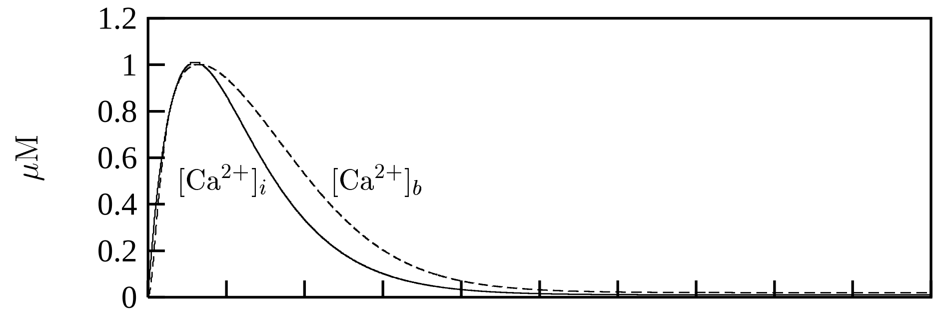

(a) Intracellular Ca^{2+} traces

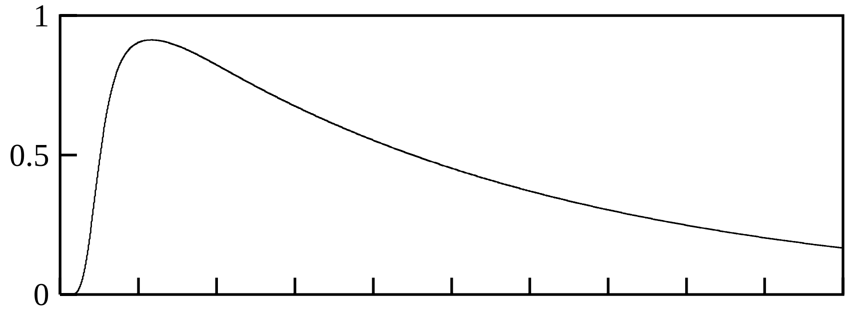

(b) Proportion of actin sites available for binding, z

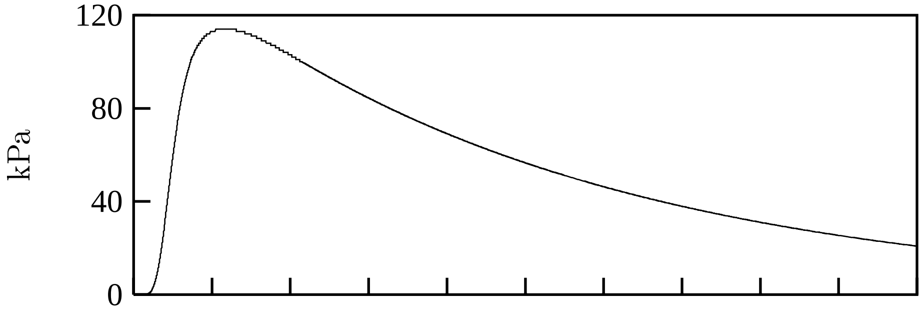

(c) Developed tension, T

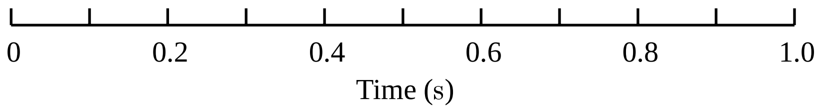

FIGURE 7.10: The results of a non-coupled isometric twitch calculated by the HMT model (*i.e.*, $[\mathrm{Ca}^{2+}]_i$ is given by Equation (4.5)). The parameters and initial values used in this simulation are given in Appendix A.4.

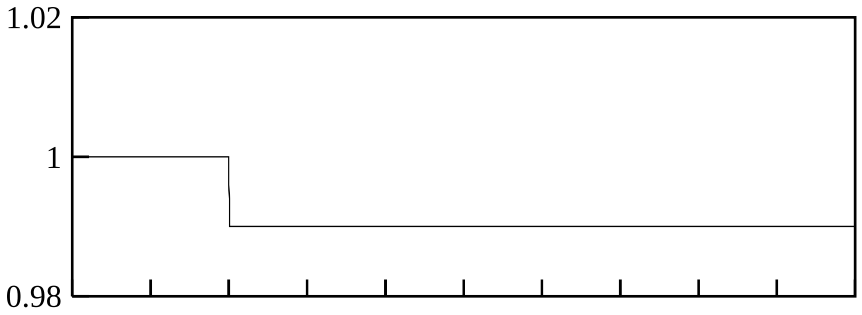

(a) Extension ratio, λ

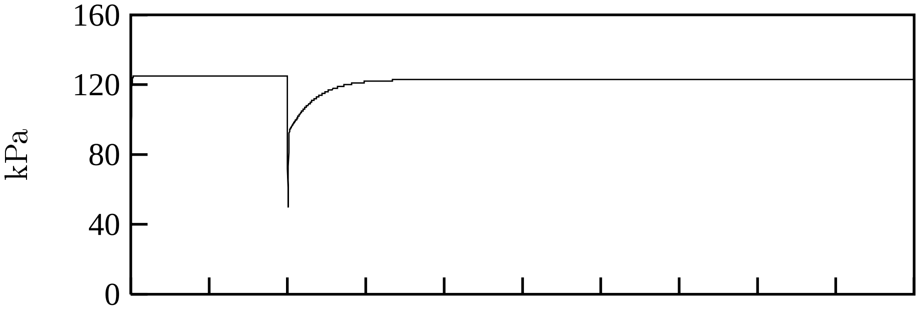

(b) Active tension, T

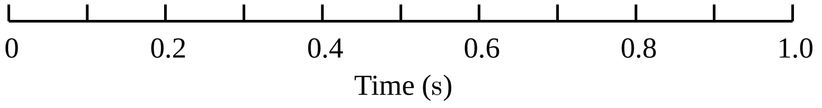

FIGURE 7.11: Extension ratio and active tension developed during a 2% length step of duration 2 ms. The cell is maximally activated. The parameters and initial values used in this simulation are given in Appendix A.4.

7.2 The coupled JRW–HMT model

In this section, the coupled JRW–HMT model developed in Section 5.2 (and implemented in CELL (Chapter 6)) is used to simulate the physiological effects mentioned in Section 5.1.2.

7.2.1 Isometric twitches

Gamble et al. concluded from their experiments (Gamble et al. 1992) that peak developed force and maximum rate of positive and negative force development decrease as diastolic muscle length is reduced from a maximum, L_{max}, to 90% L_{max}. They showed this by performing numerous experiments, in which resting muscle samples were stretched to the desired value (L_{max}, 95% L_{max}, and $\%90L_{max}$) and then stimulating the muscle while recording the developed force (which was normalised with respect to muscle cross-sectional area). Similar results are also presented by Allen & Kurihara (1982).

Assuming that one is examining only the central portion of the muscle sample (to avoid any possible end effects[1]), the stress (or tension) generated by the muscle can be evenly divided amongst all the cells. This implies that the observations Gamble et al. (1992) and Allen & Kurihara (1982) made will be the same, at least qualitatively, when examining single cells. Namely, that as the extension ratio (normalised sarcomere length) decreases it would be expected that the peak developed tension and maximum rate of positive and negative force development also decreases. As Figures 7.12 and 7.13 clearly show, this does indeed occur when using the coupled JRW–HMT model.

The action potential, intracellular Ca^{2+} concentration, and concentration of Ca^{2+} bound to Tn-C is shown in Figure 7.14 for the case where $\lambda = 1.0$. Since this is purely an isometric case, there is no difference in the electrical activity for each of the different lengths (*i.e.*, since $T = T_o$ at all times during the experiment, no mechano-electric feedback occurs (see Equation (5.1))).

7.2.2 Step release experiments

In this section, the effect of length changes during muscle twitches is investigated. The length changes of interest are step releases, where the muscle sample is held at a constant length, then at a specified time the length of the sample is decreased (over some specified duration) to a new fixed value (see upper plot of Figure 4.9 (a)).

When the length is decreased in such a manner, there are certain well documented events that should occur (Hunter et al. 1998). Following the step release tension should decrease, which displaces Ca^{2+} from Tn-C so that the post-step isometric tension is always lower than

---

[1] These consist mainly of damage caused to the muscle sample by clamping the ends to the apparatus used to stretch the muscle sample

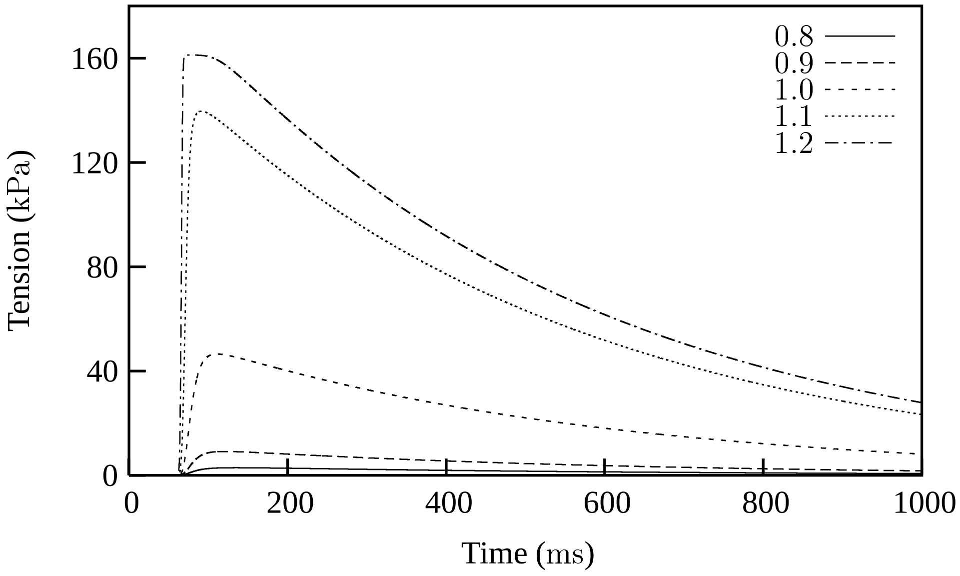

FIGURE 7.12: Isometric twitches calculated by the coupled JRW–HMT model, showing the tension transients for varying extension ratios, $0.8 \rightarrow 1.2$, corresponding to sarcomere lengths from 1.6 to 2.4 $\mu\mathrm{m}$ (assuming a slack length of 2.0 $\mu\mathrm{m}$ (Hunter et al. 1998)). The plot clearly shows the increasing peak tension for increasing extension ratio values, as well as increasing development and relaxation rates (*i.e.*, the slopes of the upstroke and recovery portions get steeper as the extension ratio values increase. See also Figure 7.13.

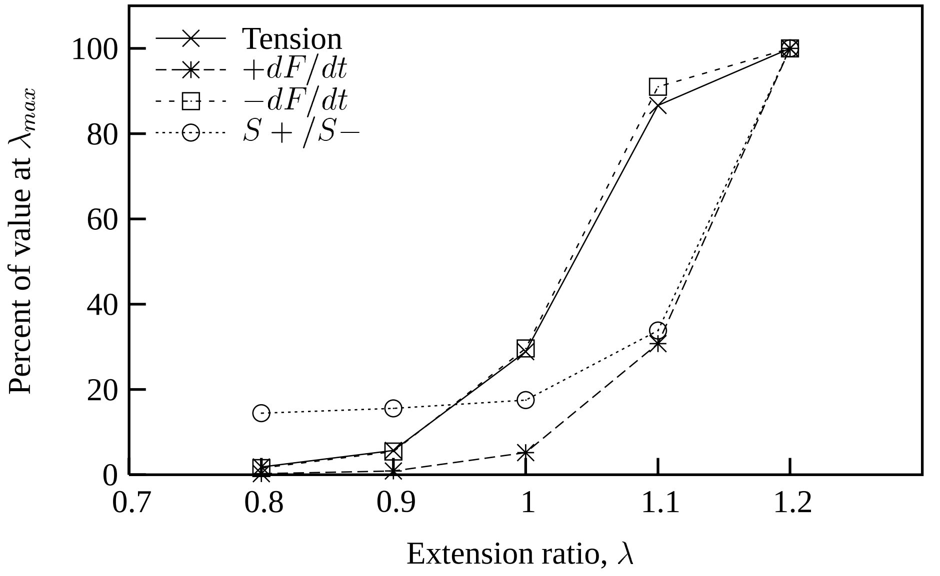

FIGURE 7.13: The isometric twitch characteristics, as defined by Gamble et al. (1992), for the tension transients given in Figure 7.12. Note: Tension denotes the peak developed tension; $+dF/dt$ and $-dF/dt$ are the maximum rates of positive and negative force development, respectively; and $S+/S-$ is the ratio of the two maximum rates.

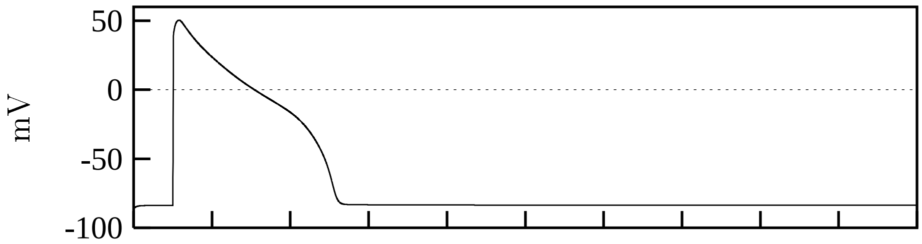

(a) Action potential, V_m

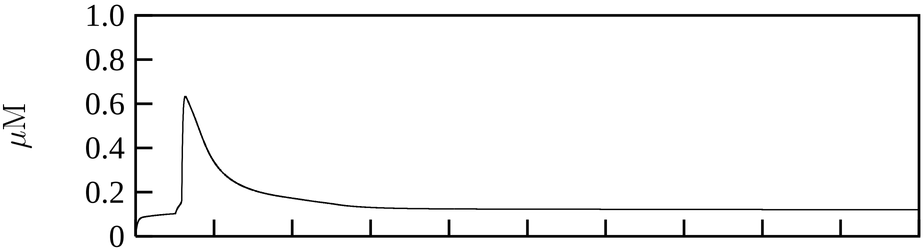

(b) Intracellular calcium, $[\mathrm{Ca}^{2+}]_i$

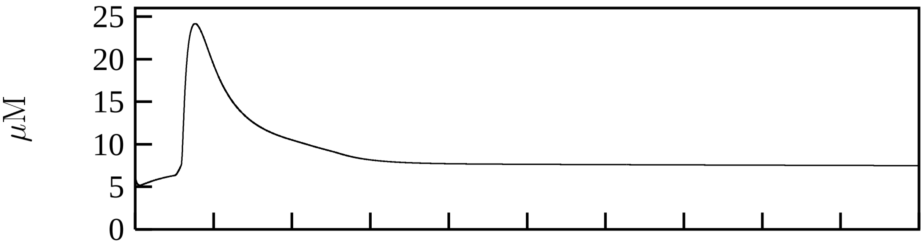

(c) Calcium bound to Tn-C, $[\mathrm{Ca}^{2+}]_b$

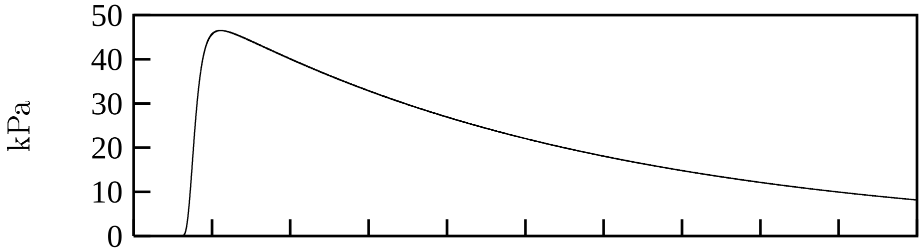

(d) Tension, T

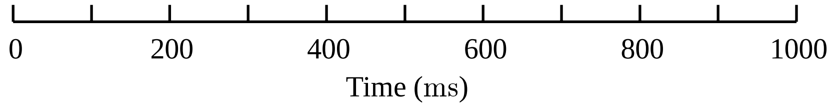

FIGURE 7.14: The results of a coupled isometric twitch calculated by the JRW–HMT model. The twitch shown is for $\lambda = 1.0$, but plots (a), (b), and (c) are the same for all values of λ . The parameters and initial values used in this simulation are given in Appendix A.5.

the unperturbed isometric twitch. Some of the displaced Ca^{2+} is available for rebinding to Tn-C (which allows the redevelopment of tension) and some is removed from the cytosol by the SR Ca^{2+}-pump. The increase in intracellular Ca^{2+} concentration can also have an affect on the $[\mathrm{Ca}^{2+}]_i$-dependent currents I_{NaCa} (Na^{+},Ca^{2+} exchanger) and $I_{p(Ca)}$ (sarcolemmal Ca^{2+} pump).

Step timing

One of the main factors influencing the effect that the length step has on the mechanical and electrical processes of the cell is when the step occurs during the isometric twitch. This section looks at the effect of a length step, with a magnitude of 0.5% and duration of $2.0\ \mathrm{ms}$, at different times during the isometric twitch.

The times chosen for the length step are $76.0\ \mathrm{ms}$, $111.0\ \mathrm{ms}$, and $400.0\ \mathrm{ms}$, corresponding to peak $[\mathrm{Ca}^{2+}]_b$, peak tension, and late in the isometric twitch. The results for these experiments are given in Figures 7.15 and 7.16.

Figure 7.15 (c) shows that the length steps have no significant affect on the action potential. This is not unexpected, as most of the changes which occur involve the intracellular movement of Ca^{2+} (illustrated by Figure 7.16 (c) and (e), which show very small changes in magnitude which nearly cancel the effect of each other on the action potential). It must also be remembered that the only form of mechano-electric feedback implemented in this research is the effect of tension on calcium binding to Tn-C. Were mechano-sensitive channels included in the model, a much greater response in the action potential would be expected due to the actual modification of the ionic currents (Kohl et al. 1998).

The tension traces presented in Figure 7.15 (k) show that the expected tension drop does occur, followed by the slow (first-order) and fast (second-order) recovery phases (Figure 4.9). These results (as well as those presented in Figures 7.17 and 7.18) support the supposition of Gordon & Ridgway (1990) that the increase in myoplasmic calcium caused by muscle shortening is due to the release of calcium from the troponin binding sites.

Figure 7.15 (k) and (l) show that the earliest length step (corresponding to peak $[\mathrm{Ca}^{2+}]_b$) causes the greatest change in the overall tension transient (compared to the isometric twitch). This is reflected by the fact that this step also causes the largest change in the $[\mathrm{Ca}^{2+}]_b$ transient. Since this step occurs at the peak of the $[\mathrm{Ca}^{2+}]_b$ transient the step release is able to “free” a relatively large proportion of the bound Ca^{2+}. This calcium is then available to be re-bound to Tn-C or to be extracted from the myoplasm by other mechanisms. As shown by Figure 7.15 (h), this early step also corresponds to the largest change in the time course of the concentration of Ca^{2+} within the NSR, with a similar increase in the SR Ca^{2+}-pump flux, I_{up} (not shown). These results show that when the length step occurs at peak $[\mathrm{Ca}^{2+}]_b$, not only is the most Ca^{2+}

(a) Extension ratio, λ (b) Extension ratio, λ

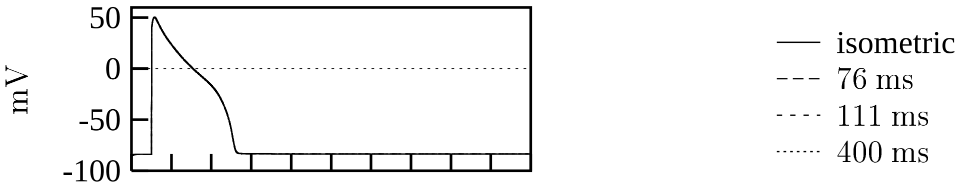

(c) Action potential, V_m

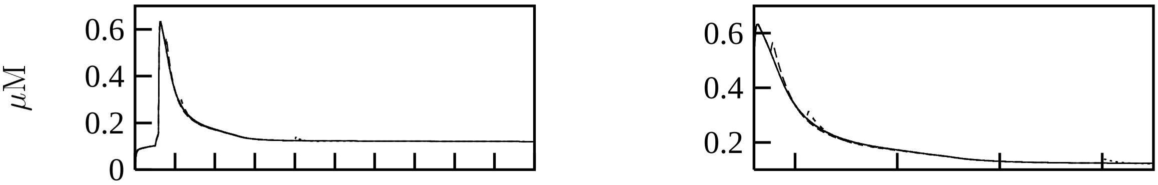

(e) Intracellular calcium, $[\mathrm{Ca}^{2+}]_i$ (f) Intracellular calcium, $[\mathrm{Ca}^{2+}]_i$

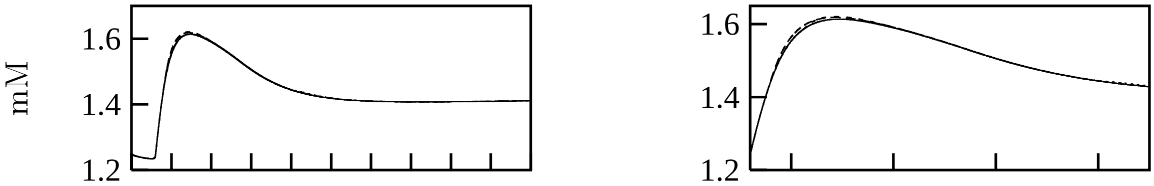

(g) $[\mathrm{Ca}^{2+}]_{NSR}$ (h) $[\mathrm{Ca}^{2+}]_{NSR}$

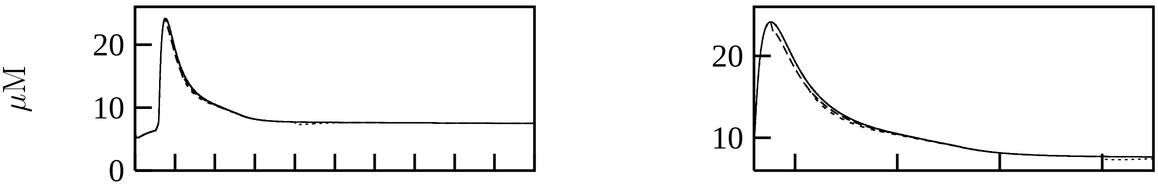

(i) Calcium bound to Tn-C, $[\mathrm{Ca}^{2+}]_b$ (j) Calcium bound to Tn-C, $[\mathrm{Ca}^{2+}]_b$

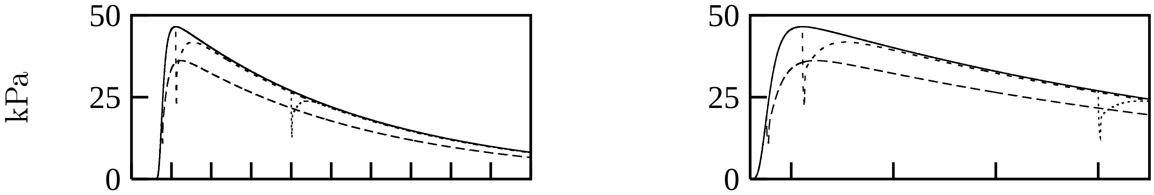

(k) Tension, T (l) Tension, T

FIGURE 7.15: Results from experiments looking at the effect of the time of the length step. The times correspond to peak $[\mathrm{Ca}^{2+}]_b$, peak tension, and late in the isometric twitch. The plots in the right column show an enlarged view of the plots in the left column (60 ms $\to$ 450 ms). Results from these experiments are continued in Figure 7.16. The parameters and initial values used in this simulation are given in Appendix A.5.

(a) Extension ratio, λ (b) Extension ratio, λ

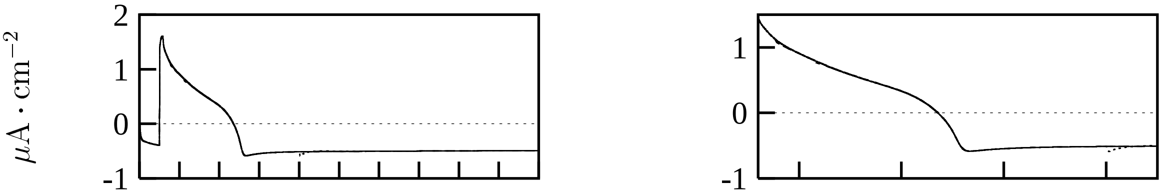

(c) I_{NaCa} (d) I_{NaCa}

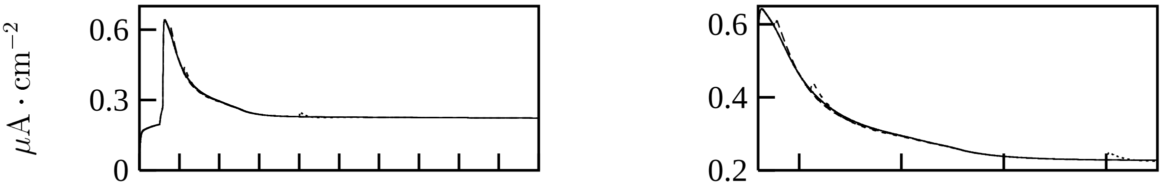

(e) $I_{p(Ca)}$ (f) $I_{p(Ca)}$

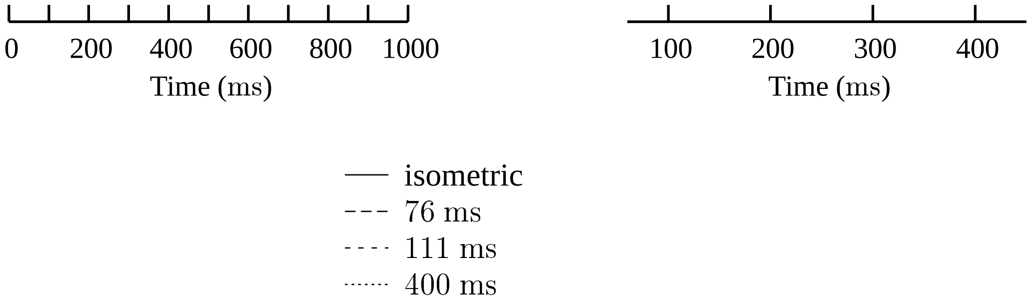

FIGURE 7.16: Results of step release experiments continued from Figure 7.15. Shows the two trans-sarcolemmal, $[\mathrm{Ca}^{2+}]_i$-dependent currents and the effect of the time that the length step occurs. The parameters and initial values used in this simulation are given in Appendix A.5.

released from Tn-C but the most Ca^{2+} is pumped into the SR, leaving a smaller fraction of free myoplasmic Ca^{2+} available to be re-bound to Tn-C. This results in the tension never being able to recover to the isometric twitch, which is also caused by the extension ratio of the cell being at the lower limit for most of the twitch.

Similar results are shown for length steps occuring at peak trension and late in the isometric twitch. These results (Figure 7.15) show that when the length step occurs at the peak of the tension transient there is the largest initial decrease in tension (*i.e.*, $T_0 - T_1$, Figure 4.9). At peak tension, there is the maximum number of cross-bridges formed, so when the length of the cell is suddenly decreased the maximum number of cross-bridges are unloaded. However, as shown in Figure 7.15, the time of peak tension corresponds to the declining phase of the $[\mathrm{Ca}^{2+}]_b$ transient. This results in the length step "freeing" much less Ca^{2+} from Tn-C (shown by the barely visible change in Figure 7.15 (j)), and most of the Ca^{2+} released is re-bound to Tn-C (see Figure 7.15 (h) and Figure 7.16). The rapid re-attachment of Ca^{2+} to Tn-C and the minor losses of Ca^{2+} results in the recovery of tension to almost the isometric level for both the peak tension and late length steps.

The only noticable difference in the peak tension and late length steps is the smaller initial drop in tension following the late step. This is due to there being fewer cross-bridges attached at the time of the step, so when the cell is rapidly unloaded there are fewer cross-bridges to detach and hence, the tension drop will decrease correspondingly. Both of these times for the length steps have a similar effect on the electrical activity of the cell, most likely due to both times being during the declining phase of the electrical activity (*i.e.*, during the electrical recovery phase when all electrical activity is returning to the resting state).

Figure 7.16 show the two transmembrane ionic currents affected by the length steps, I_{NaCa} and $I_{p(Ca)}$. As mentioned above, the SR Ca^{2+}-uptake flux was also affected by the length steps, as required to allow the increase in the Ca^{2+} concentration within the NSR. These results show that the length steps have little effect on the transmembrane ionic currents, due to the fact that the only mechano-electric feedback mechanism implemented in this research is the regulation of intracellular calcium transients.

Step duration

Another factor inluencing the effect of the length step on the behaviour of the cell is the duration of the step (*i.e.*, Δt in Figure 4.9 (a)). The duration of the length step can also be interpreted as the rate of the length step, which has been shown to be of importance (Hunter et al. 1998, Gordon & Ridgway 1990). Figures 7.17 and 7.18 show the results obtained for experiments with varying durations for the length step.

Figure 7.17 shows the effect of varying duration length steps on the tension and intracellular

Ca^{2+} handling. All length steps start at the same time, corresponding to peak tension, and vary in duration from $0.0\ \mathrm{ms}$ to $10.0\ \mathrm{ms}$. This figure shows that the rate of the length step does have a significant affect on the tension transient, Figure 7.17 (k) and (l), with a smaller effect on the intracelllular calcium transients, (e) – (j). As with the timing resutls presented above, the varying duration showed no significant effect on the action potential, (c).

Shown in Figure 7.17 (l), as the duration of the length step increases, or the rate of the step decreases, the initial drop in tension ($T_0 - T_1$, Figure 4.9) increases significantly. This figure shows that the tension transients for the case of an instantaneous length step and one of $0.2\ \mathrm{ms}$ duration are indistinguishable, suggesting that the fastest, physically achievable length step which has a duration of $0.2\ \mathrm{ms}$ (Hunter et al. 1998), is a suitable approximation to an instantaneous length step.

These results show that for all the transient characteristics shown in Figures 7.17 and 7.18, as the rate of the length step decreases a similar decrease in the rate of the initial response of the characteristic is also observed, while the following recovery to the isometric transients is almost identical.

For example, as the rate of the length step decreases (from a duration of $0.0\ \mathrm{ms}$ to $10.0\ \mathrm{ms}$) the rate of the initial tension relaxation and fast recovery also decrease, while the following slow recovery phase for all steps rapidly converge towards a single line in Figure 7.17 (l). This can be explained by the behaviour of the cross-bridges. When an instantaneous length step is performed, the cross-bridges are completely unloaded and the tension drops rapidly (to zero in this case), then cross-bridges re-form (Ca^{2+} re-binding to Tn-C) and cross-bridge cycling occurs to redevelop tension at the new length. When the length step is not instantaneous the cross-bridges are never completely unloaded, and hence the developed tension does not drop as rapidly or as far (*i.e.*, there are always some cross-bridges formed, and some degree of cross-bridge cycling occurs during the length step).

Figure 7.18 shows the effect of varying durations of the length steps on the two affected transmembrane ionic currents. As with the transients in Figure 7.17, as the rate of the step decreases the rate of the initial response in these ionic currents also decreases, but then converge before recovery to a level close to the isometric levels.

7.2.3 Frequency response

In this section, the frequency response of the coupled JRW–HMT model is invesitgated. Two different experiments were conducted: forced oscillations, where the extension ratio of the cell is is oscillated about the resting length with no electrical stimulus applied; and the force-frequency relationship, where the effect on the peak tension of different stimulation frequencies is investigated.

(a) Extension ratio, λ

(b) Extension ratio, λ

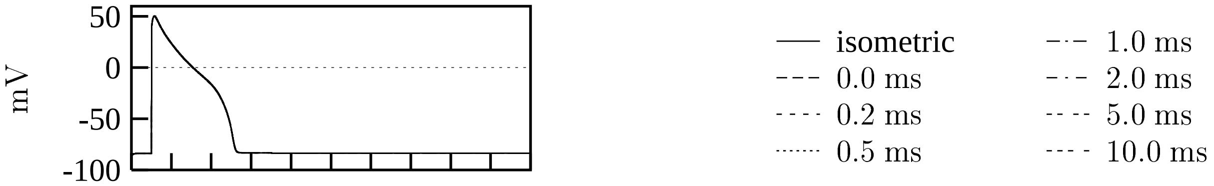

(c) Action potential, V_m

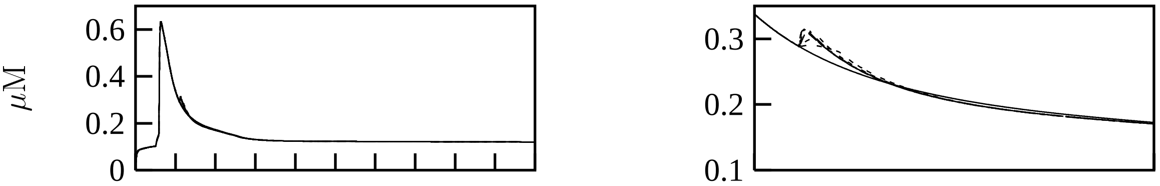

(e) Intracellular calcium, $[\mathrm{Ca}^{2+}]_i$

(f) Intracellular calcium, $[\mathrm{Ca}^{2+}]_i$

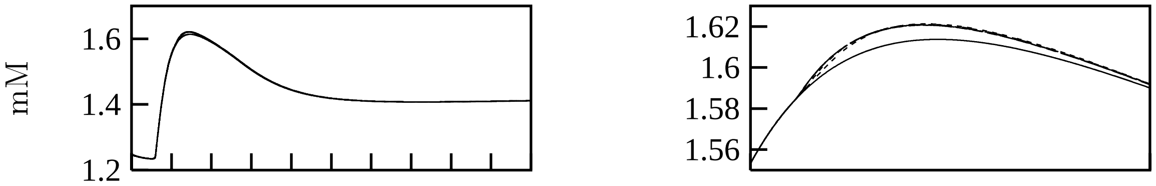

(g) $[\mathrm{Ca}^{2+}]_{NSR}$

(h) $[\mathrm{Ca}^{2+}]_{NSR}$

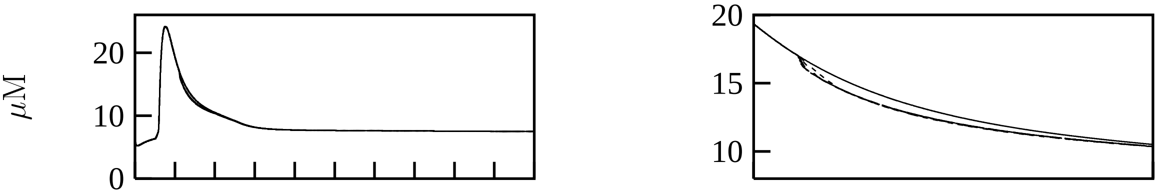

(i) Calcium bound to Tn-C, $[\mathrm{Ca}^{2+}]_b$

(j) Calcium bound to Tn-C, $[\mathrm{Ca}^{2+}]_b$

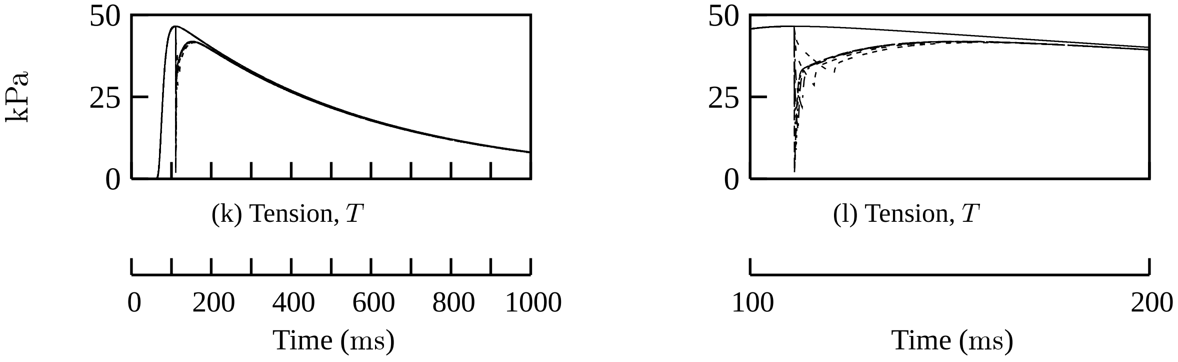

(k) Tension, T

(l) Tension, T

FIGURE 7.17: Results of varying duration length steps. The durations investigated range from 0.0 ms (instantaneous) to 10.0 ms. These results are continued in Figure 7.18. The plots in the right column are enlarged views of those in the left (100 ms→200 ms). The parameters and initial values used in this simulation are given in Appendix A.5.

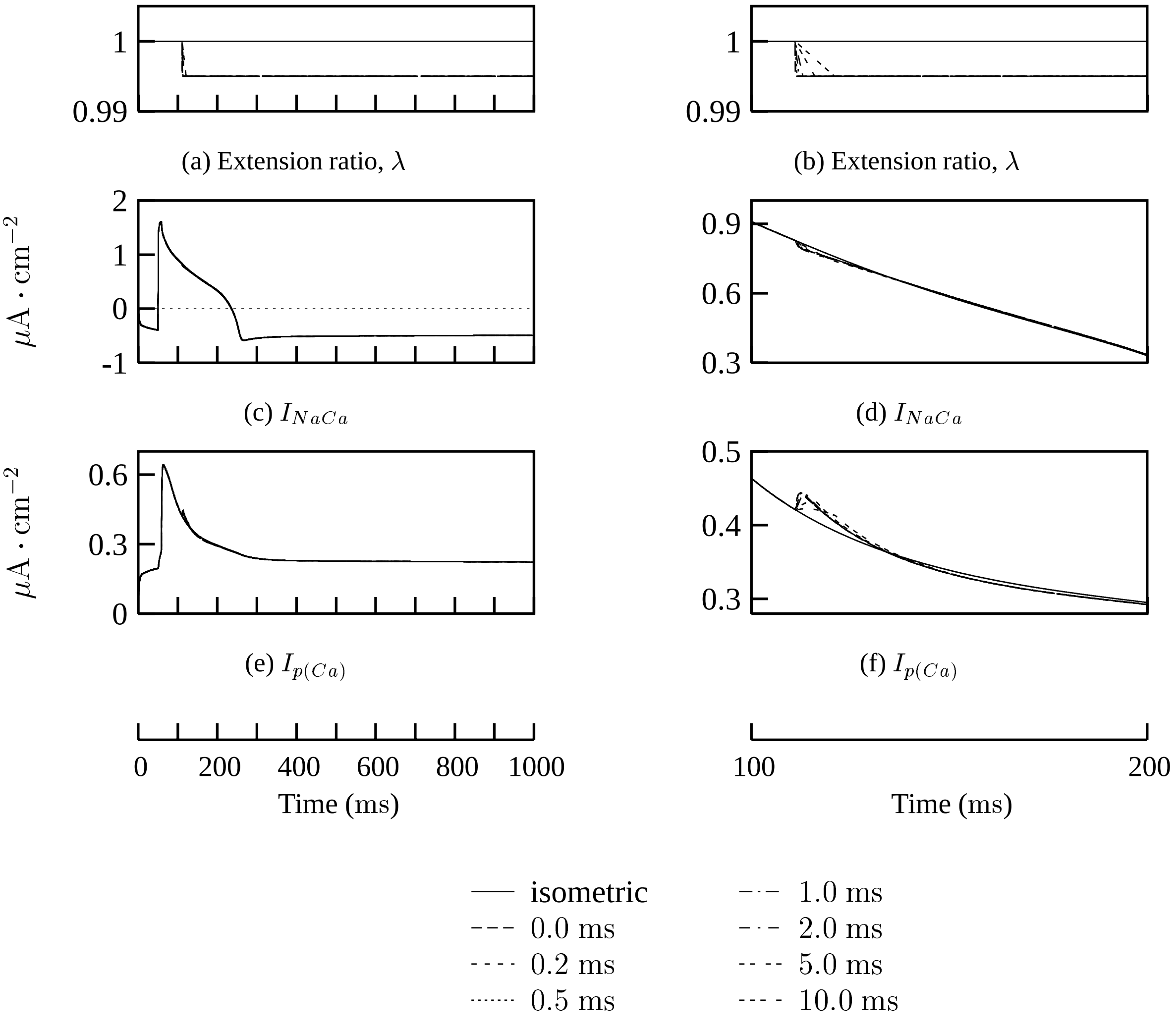

FIGURE 7.18: The ionic currents associated with the results presented in Figure 7.17. The parameters and initial values used in this simulation are given in Appendix A.5.

Forced oscillations

In this experiment, the effect of oscillatory length perturbations about the resting length of the cell ($\lambda = 1.0$) is investigated. Figures 7.19 and 7.20 show the results of this experiment for a oscillation frequency of $5\ \mathrm{Hz}$ and a peak-to-peak amplitude of 4%. The tension transient presented in Figure 7.19 (i) shows similar increasing peak-to-peak amplitude with time as do results presented by Brady & Farnsworth (1986).

The initial decrease in λ to the first trough appears to have no significant effect on the activity of the cell. Following this, the response of the cell is dominated by the fast binding – slow release of Ca^{2+} to Tn-C and the nonlinear length and $[\mathrm{Ca}^{2+}]_i$ dependence of the isometric tension (Figure 4.8).

The fast binding and slow release characteristics of the contraction – relaxation cycle are clearly illustrated in Figure 7.19 (f), where the proportion of actin sites available for cross-bridge binding increases rapidly following the upward stroke of the length oscillation and then slowly declines as the cell is relaxed. Due to the difference in the binding and release rates (and the frequency of the length perturbations), the value of z never returns to a steady value causing a gradual rise in the average value of z which leads to a similar rise in the isometric tension. The difference in the binding and release rates is also illustrated by the sharp peaks and shallow troughs of the $[\mathrm{Ca}^{2+}]_b$ transient given in Figure 7.19 (d).

The rapid increase and slow decline observed in the z transient is also influenced by the nonlinear length and $[\mathrm{Ca}^{2+}]_i$ dependence of isometric tension (which depends on λ and z). As the cell is stretched, there is a rapid increase in $[\mathrm{Ca}^{2+}]_i$ (consistent with results presented by Gordon & Ridgway (1990)) which results in an increase in the rate of isometric tension development (Hunter et al. 1998). At the same time, the length of the cell is increasing which also increases the developed isometric tension. Then as the cell is allowed to relax, $[\mathrm{Ca}^{2+}]_i$ decreases (at a slower rate, which is consistent with Gordon & Ridgway (1990)) with Ca^{2+} uptake into the SR and Ca^{2+} exit from the cell via the sarcolemmal Ca^{2+}-pump. This causes the rate of isometric tension relaxation to decrease (Hunter et al. 1998), resulting in much slower tension relaxation than development. This gives rise to the transient increase in the average value of T_o which implies that the average value of z must also display this transient increase due to the constant nature of the average value of λ .

Figure 7.19 shows that the developed tension is out of phase with the length, with the tension leading the length oscillations. The tension appears to be in phase with the oscillations in $[\mathrm{Ca}^{2+}]_b$, with the peaks of the tension oscillations not as sharp as the $[\mathrm{Ca}^{2+}]_b$ peaks. This is caused by the shallow, uneven oscillations of the isometric tension. As expected, the average value of the developed tension increases in a manner similar to the isometric tension.

Figure 7.20 shows that the forced oscillations have little effect on the action potential, caus-

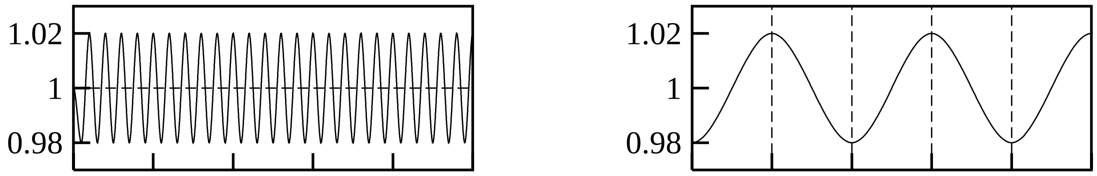

(a) Extension ratio, λ

(b) Extension ratio, λ

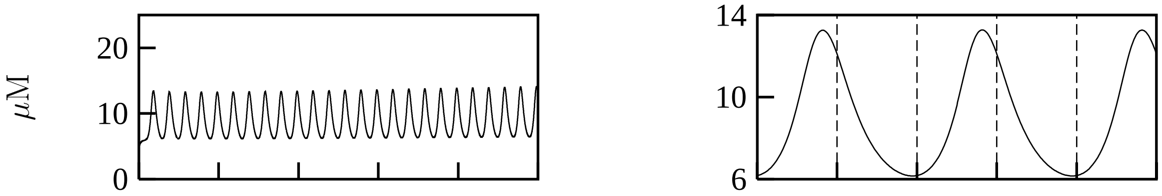

(c) Bound calcium concentration, $[\mathrm{Ca}^{2+}]_b$

(d) Bound calcium concentration, $[\mathrm{Ca}^{2+}]_b$

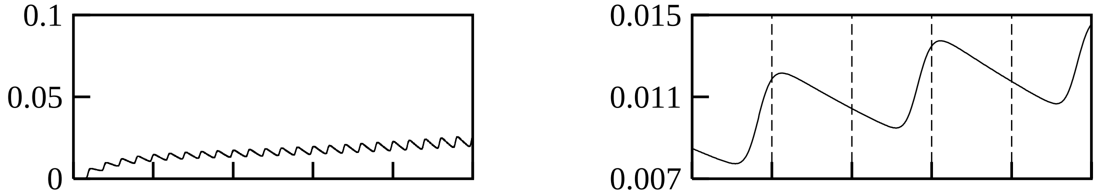

(e) Proportion of available binding sites, z

(f) Proportion of available binding sites, z

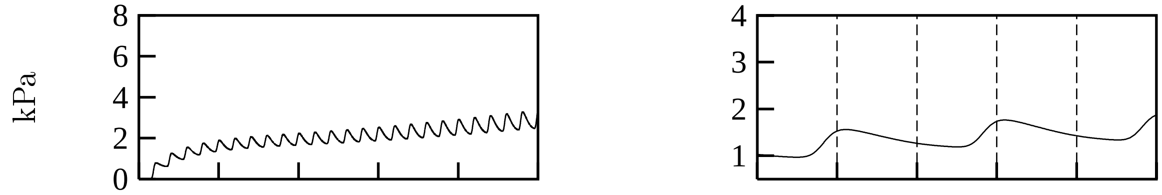

(g) Isometric tension, T_o

(h) Isometric tension, T_o

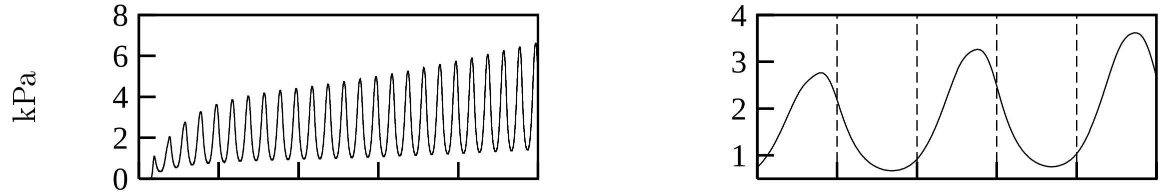

(i) Developed tension, T

(j) Developed tension, T

FIGURE 7.19: The response of the mechanical components of the cell to forced length oscillations with a frequency of $5\ \mathrm{Hz}$ and peak-to-peak amplitude of 4%. The plots in the right column show an enlargement of those in the left column for the time interval 0.5–$1.0\ \mathrm{s}$. The parameters and initial values used in this simulation are given in Appendix A.5.

ing small perturbations about the normal resting potential.

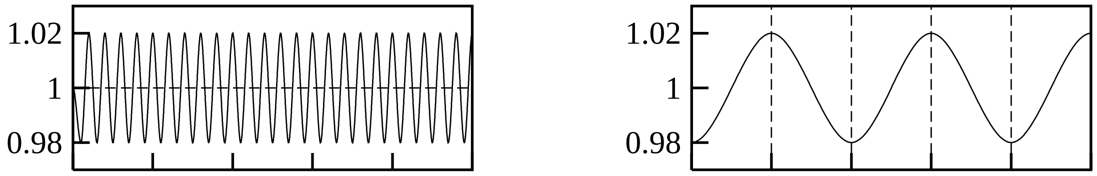

(a) Extension ratio, λ (b) Extension ratio, λ

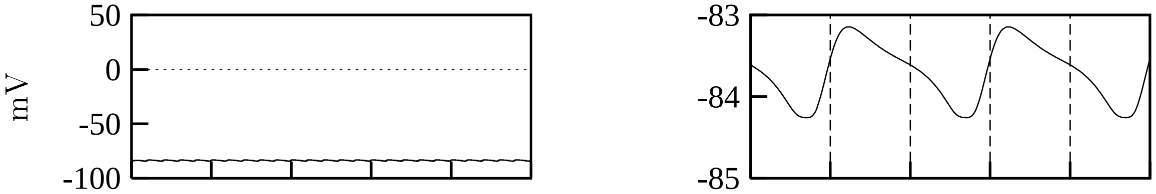

(c) Membrane potential, V_m (d) Membrane potential, V_m

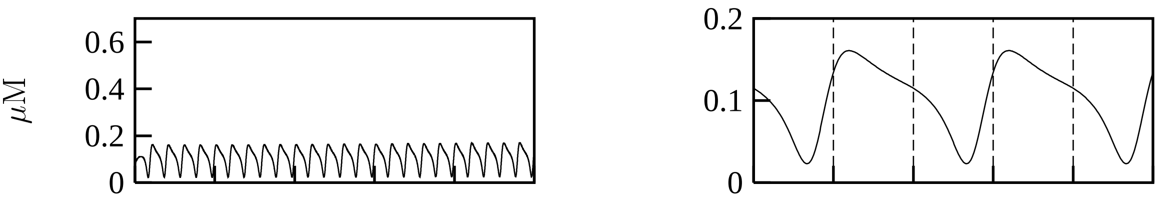

(e) Intracellular calcium concentration, $[\mathrm{Ca}^{2+}]_i$ (f) Intracellular calcium concentration, $[\mathrm{Ca}^{2+}]_i$

FIGURE 7.20: Response of the electrical components to forced length oscillations with a frequency of 5 Hz and amplitude 4%. The parameters and initial values used in this simulation are given in Appendix A.5.

Force-frequency relationship

In this set of experiments, the effect of stimulus frequency on the isometric tension is investigated. The pacing regime used for this set of experiments was based on that used by Schouten & ter Keurs (1986), who examined the not only the frequency response of a variety of cardiac cell species but also the effect of the diameter of the muscle sample.

The pacing regime of Schouten & ter Keurs (1986) varied the frequency from 0.03–3.3 Hz and maintained each frequency for approximately 2.5–3 min, resulting in tension traces of over 20 min duration. To simulate this experiment would be very computationally intensive, so the experiment of Schouten & ter Keurs (1986) was split into a number of smaller sub-experiments. Each of these sub-experiments just modelled the effect of one particular stimulus frequency and was run only for as long as it took for each frequency to reach steady-state.

Similar experiments as that presented in Figure 8 of Jafri et al. (1998) were simulated, but are not shown here. These experiments gave results similar to those published by both Jafri et al. (1998) and Schouten & ter Keurs (1986).

Figure 7.21 shows a summary of the results obtained by both the coupled JRW–HMT model and by Schouten & ter Keurs (1986). Banijamali et al. (1991) present similar results, but their specific experiments were not simulated for a direct comparison. This figure shows that as the stimulation frequency increases above 0.1 Hz the peak developed tension decreases, as it does for frequencies below 0.1 Hz.

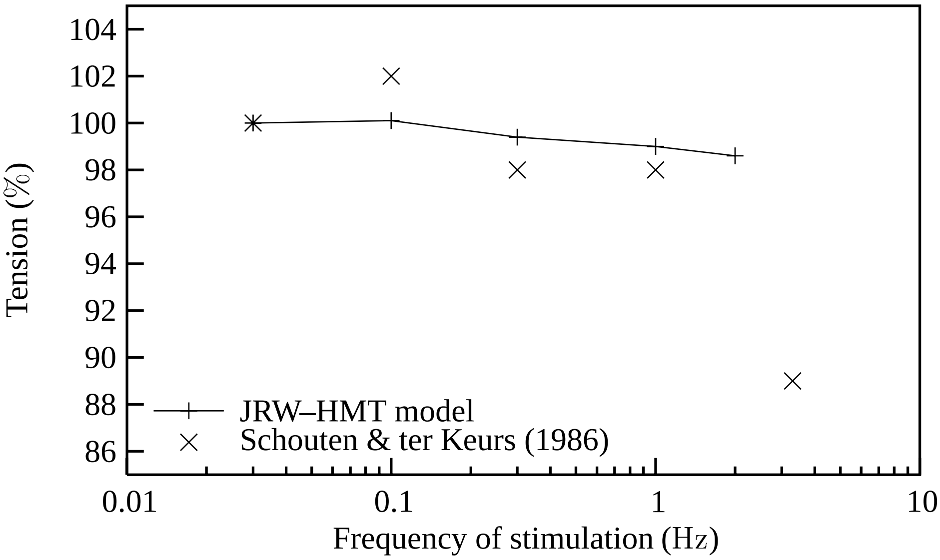

FIGURE 7.21: Force-frequency relationship, comparing model predictions with experimental data from Schouten & ter Keurs (1986) for rat myocardium. There is a small increase in the tension from 0.03 Hz to 0.1 Hz of 0.1% which is not clearly visible in this plot. The parameters and initial values used in this simulation are given in Appendix A.5.

Schouten & ter Keurs (1986) show that the peak at 0.1 Hz is very dependent on a number of factors, with the most dominant of these being the extracellular Ca^{2+} concentration, the temperature of the sample, and the sample's size (diameter). None of these factors were considered in this research, and more investigation of each of them is required.

Comparing the model results given in Figure 7.21 with the experimental data from Schouten & ter Keurs (1986) (and also that of Banijamali et al. (1991)) shows that the coupled JRW–HMT model behaves generally as expected. More work on the development of the coupled model is, however, required before some of the other observations of Schouten & ter Keurs (1986) and Banijamali et al. (1991) can be simulated. For example, the effect of the size of the muscle sample, which can cause problems with the exchange of metabolites and oxygen if the sample is sufficiently large, can not be modelled by the current coupled model and requires the inclusion of some form of metabolic modelling. See Section 8.3 for more details.

Chapter 8

Conclusions

8.1 Model Development

The aim of this thesis was to develop a coupled electro-mechanical model of a single cardiac cell, including some form of mechano-electric feedback. To achieve this, the non-coupled electrical and mechanical models first needed to be implemented and tested.

The electrical models implemented are the DiFrancesco–Noble, Luo–Rudy II, and Jafri–Rice–Winslow models (see Sections (3.1)–(3.3)). These models were all successfully implemented and tested, with some illustrative results given in Section 7.1.

The mechanical model implemented for this research is the Hunter–McCulloch–ter Keurs model of cardiac mechanics (Chapter 4). This model was also successfully implemented and tested, as shown in Section 7.1.3.

The coupled model developed in Chapter 5 is based on the JRW electrical model and the HMT mechanics model. Rudimentary coupling was implemented for the DFN and LR models, but for the purposes of this thesis only the coupled JRW–HMT model was investigated with any depth.

As part of this research, a graphical user interface was developed to aid in the use of the models developed. The interface developed is presented in Chapter 6 and was found to be very useful in the understanding and representation of the experiments simulated with the models.

8.2 Model Validation and Predictions

Three standard sets of experiments were used to validate the development of the coupled electromechanical JRW–HMT model: isometric twitches, step releases, and frequency response experiments.

Investigation of isometric twitches found that the coupled model predicted the strong dependence of the twitch characteristics on the length of the cell known to exist from physiological experiments.

Step release experiments peformed using the coupled model correctly simulated the expected phases of tension relaxation and redevelopment following a step decrease in cell length. The electrical components, particulary the intracellular calcium handling, also behaved in accordance with physiological data. It was found that the time of the length step within the isometric twitch and the duration of the step can vary the effect of the step on the behaviour of the cell, as predicted by physiological experiments.

The force-frequency relationship predicted by the coupled model agrees with that obtained from physiological experiments. The effect of applying mechanical stimuli to an resting cell was also investigated. It was found that application of oscillatory length changes about the resting length illicits an oscillatory response in the developed tension which leads the length changes, while the membrane potential has small oscillations about the normal resting potential.

8.3 Future Work

8.3.1 Single cell modelling

This project can be seen as a first step towards the development of a full model of a single cardiac cell. To be considered a full model of a cardiac cell, there are two main additions required to the coupled model developed in this thesis:

1. mechano-electric feedback – as mentioned in Section 5.1.2, there are three basic mechanisms by which mechano-electric feedback might influence cardiac muscle cells, of which only one is implemented in this research. The remaining two mechanisms, specifically the mechanosensitive ion channels, need to be investigated;

2. metabolic modelling – the model developed in this research has only looked at the electrical and mechanical components of the cell. The model now needs to be coupled to a metabolic model, such as that presented in Ma & Zahalak (1991) which was developed coupled to the distribution-moment mechanics model (Zahalak & Ma 1990).

With a model of a single cardiac cell it is possible to investigate the effect of specific drugs on the cell. In order to be able to do this, the scope of the models implemented needs to be increased to include the signalling pathways between the different components of the cell. Work in this area has recently started but has yet to be investigated thoroughly with respect to a fully coupled model of a cardiac cell.

It is possible, using various numerical techniques, to extend a detailed cellular model of single cardiac cells to model the entire cardiac organ. When this is considered, additional factors outide the cell need to be taken into account. For example, how do adjacent cells physically interact during the contraction–relaxation cycle.

Work has already been performed to include biophysical ionic current models in a distributed finite element model of the heart (Sands 1998), and this now needs to be extended to include the coupled electromechanical cell model developed in this thesis.

Bibliography

Allen, D. G. & Kurihara, S. (1982), ’The effects of muscle length on intracellular calcium transients in mammalian cardiac muscle’, *J. Physiol.* **327**, 79–94.

Arai, A., Kodama, I. & Toyama, J. (1996), ’Roles of Cl^- channels and Ca^{2+} mobilization in stretch-induced increase of SA node pacemaker activity’, *Am. J. Physiol.* **270**.

Banijamali, H. S., Gao, W., MacIntosh, B. R. & ter Keurs, H. E. D. J. (1991), ’Force-interval relations of twithces and cold contractures in rat cardiac trabeculae. effect of ryanodine’, *Circ. Res.* **69**, 937–948.

Beeler, G. W. & Reuter, H. (1977), ’Reconstruction of the action potential of ventricular myocardial fibres’, *J. Physiol.* **268**, 177–210.

Bergel, D. A. & Hunter, P. J. (1979), The mechanics of the heart, *in* N. H. C. Hwang, D. R. Gross & D. J. Patel, eds, ’Quantitative Cardiovascular Studies, Clinical and Research Applications of Engineering Principles’, University Park Press, Baltimore, chapter 4, pp. 151–213.

Berlin, J. R., Bassani, W. M. & Bers, D. M. (1994), ’Intrinsic cytosolic calcium buffering properties of single rat cardiac myocytes’, *Biophys. J.* **67**, 1775–1787.

Berne, R. M. & Levy, M. N., eds (1993), *Physiology*, 3rd edn, Mosby, 11830 Westline Industrial Drive, St. Louis, Missouri 63146.

Brady, A. J. (1991), ’Length dependence of passive stiffness in single cardiac myocytes’, *Am. J. Physiol.* **260**, H1062–H1071.

Brady, A. J. & Farnsworth, S. P. (1986), ’Cardiac myocyte stiffness following extraction with detergent and high salt solutions’, *Am. J. Physiol.* **250**, H932–H943.

de Leon, M., Wang, Y., Jones, L., Perez-Reyes, E., Wei, X., Soong, T. W., Snutch, T. P. & Yue, D. T. (1995), ’Essential Ca^{2+}-binding motif for Ca^{2+}-sensitive inactivation of the L-type Ca^{2+} channels’, *Science* **270**, 1502–1506.

DiFrancesco, D. & Noble, D. (1985), 'A model of cardiac electrical activity incorporating ionic pumps and concentration changes', *Phil. Trans. R. Soc. Lond.* **B307**, 353–398.

Dupont, G., Pontes, J. & Goldbeter, A. (1996), 'Modelling spiral Ca^{2+} waves in single cardiac cells; role of spatial heterogeneity created by the nucleus', *Am. J. Physiol.* **271**, C1390–C1399.

Edman, K. A. P. (1975), 'Mechanical deactivation induced by active shortening in isolated muscle fibres of the frog', *J. Physiol.* **246**, 255–275.

Fabiato, A. (1983), 'Calcium-induced release of calcium from the cardiac sarcoplasmic reticulum', *Am. J. Physiol.* **245**, C1–C4.

Fabiato, A. & Fabiato, F. (1976), 'Dependence of calcium release, tension generation and restoring forces on sarcomere length in skinned cardiac cells', *Eur. J. Cardiol.* **4**, 13–27.

Fabiato, A. & Fabiato, F. (1978), 'Myofilament-generated tension oscillations during partial calcium activation and activation dependence of the sarcomere length-tension relation of skinned cardiac cells', *J. Gen. Physiol.* **72**, 667–699.

Gamble, J., Taylor, P. B. & Kenno, K. A. (1992), 'Myocardial stretch alters twitch characteristics and Ca^{2+} loading of sarcoplasmic reticulum in rat ventricular muscle', *Circ. Res.* **26**, 865–870.

Glass, L., Hunter, P. J. & McCulloch, A. D., eds (1991), *Theory of Heart: Biomechanics, Biophysics, and Nonlinear Dynamics of Cardiac Function*, Springer-Verlag, New York.

Gordon, A. M. & Ridgway, E. B. (1990), 'Stretch of active muscle during the declining phase of the calcium transient produces biphasic changes in calcium binding to the activating sites', *J. Gen. Physiol.* **96**, 1013–1035.

Granzier, H., Helmes, M. & Trombitas, K. (1996), 'Nonuniform elasticity of titan in cardiac myocytes: A study using immunoelectron microscopy and cellular mechanics', *Biophys. J.* **70**, 430–442.

Granzier, H., Kellermayer, M., Helmes, M. & Trombitas, K. (1997), 'Titan elasticity and mechanism of passive force development in rat cardiac myocytes probed by thin-filament excitation', *Biophys. J.* **73**, 2043–2053.

Granzier, H. M. L. & Irving, T. C. (1995), 'Passive tension in cardiac musle: Contribution of collagen, titan, microtubles, and intermediate filaments', *Biophys. J.* **68**, 1027–1044.

Hadley, R. W. & Lederer, W. J. (1991), ’Ca^{2+} and voltage inactivate Ca^{2+} channels in guinea-pig ventricular myocytes through independent mechanisms’, *J. Physiol. Lond.* **44**, 257–268.

Helmes, M., Trombitas, K. & Granzier, H. (1996), ’Titan develops restoring force in rat cardiac myocytes’, *Circ. Res.* **79**, 619–626.

Hilgemann, D. W. & Noble, D. (1987), ’Excitation-contraction coupling and extracellular calcium transients in rabbit atrium: Reconstruction of basic cellular mechanisms’, *Proc. R. Soc. Lond.* **230**, 163–205.

Hill, A. V. (1938), ’Heat of shortening and the dynamic constants of muscle’, *Proc. Roy. Soc. B* **126**, 136–195.

Holmes, K. C. (1995), ’The actomyosin interaction and its control by tropomyosin’, *Biophys. J.* **68**, S2–S7.

Hunter, P. J. (1995), Myocardial constitutive laws for continuum models of the heart, *in* S. Sideman & R. Beyar, eds, ’Molecular and Subcellular Cardiology’, Plenum Press, New York, pp. 303–318.

Hunter, P. J., McCulloch, A. D. & ter Keurs, H. E. D. J. (1998), ’Modelling the mechanical properties of cardiac muscle’, *Prog. Biophys. molec. Biol.* **00**, 1–44.

Hunter, P. J., Neilsen, P. M. F., LeGrice, I. J. & Smaill, B. H. (1992), An anatomical heart model with applications to myocardial activation and ventricular mechanics, *in* T. C. Pilkinton, B. Loftis, J. F. Thompson, S. L. Y. Woo, T. C. Palmer & T. F. Budinger, eds, ’High Performance Computing in Biomedical Research’, CRC Press Inc., chapter 1, pp. 3–26.

Hunter, P. J. & Smaill, B. H. (1989), ’The analysis of cardiac function: a continuum approach’, *Prog. Biophys. molec. Biol.* **52**, 101–164.

Huntsman, L. L., Rondinone, J. F. & Martyn, D. A. (1983), ’Force-length relations in cardiac muscle segments’, *Am. J. Physiol.* **244**, H701–H707.

Huxley, H. E. (1969), ’The mechanism of myocardial contraction’, *Science* **164**, 1356–1361.

Imredy, J. P. & Yue, D. T. (1994), ’Mechanism of Ca^{2+}-sensitive inactivation of L-type Ca^{2+} channels’, *Neuron* **12**, 1301–1318.

Jack, J. J. B., Noble, D. & Tsien, R. W. (1983), *Electric Current Flow in Excitable Media*, Oxford University Press, Oxford, UK.

Jafri, M. S., Rice, J. J. & Winslow, R. L. (1998), ’Cardiac Ca^{2+} dynamics: the roles of ryanodine receptor adaptation and sarcoplasmic reticulum load’, *Biophys. J.* **74**, 1149–1168.

Janssen, P. M. L. & Hunter, W. C. (1995), ’Force, not sarcomere length, correlates with prologation of isosarcometric contraction’, *Am. J. Physiol.* **269**, H676–H685.

Katz, A. M. (1992), *Physiology of the Heart*, 2^{nd} edn, Raven Press, Ltd., 1185 Avenue of the Americas, New York 10036.

Keizer, J. & Levine, L. (1996), ’Ryanodine receptor adaptation and Ca^{2+} induced Ca^{2+} release-dependent Ca^{2+} oscillations’, *Biophys. J.* **71**, 3477–3487.

Kohl, P. (1995), ’Mechano-electric feedback: Impact on heart rhytm’, *Futura* **10**, 240–252.

Kohl, P., Day, K. & Noble, D. (1998), ’Cellular mechanisms of cardiac mechano-electric feedback in a mathematical model’, *Can. J. Cardiol.* **14**(1), 111–119.

Lakatta, E. G. (1992), Length modulation of muscle performance. frank-starling law of the heart, *in* H. A. Fozzard, H. A. Haber, E. Jennings, R. B. Katz & A. M. Morgan, eds, ’The Heart and Cardiovascular System’, 2^{nd} edn, Raven Press, Ltd., 1185 Avenue of the Americas, New York 10036, chapter 49, pp. 1325–1351.

LeGrice, I. J., Smaill, B. H., Chai, L. Z., Edgar, S. G., Gavin, J. B. & Hunter, P. J. (1995), ’Laminar structure of the heart: ventricular myocyte arrangement and connective tissue architecture in the dog’, *Am. J. Physiol.* **269**, H571–H582.

Linke, W. A., Popov, V. I. & Pollack, G. H. (1994), ’Passive and active tension in single cardiac myofibrals’, *Biophys. J.* **67**, 782–792.

Luo, C. & Rudy, Y. (1991), ’A model of the ventricular cardiac action potential: Depolarisation, repolarisation, and their interaction’, *Circ. Res.* **68**, 1501–1526.

Luo, C. & Rudy, Y. (1994*a*), ’A dynamic model of the cardiac ventricular action potential: I. simulations of ionic currents and concentration changes’, *Circ. Res.* **74**(6), 1071–1096.

Luo, C. & Rudy, Y. (1994*b*), ’A dynamic model of the cardiac ventricular action potential: II. afterdepolarizations, triggered activity, and potentiation’, *Circ. Res.* **74**(6), 1097–1113.

Ma, S. P. & Zahalak, G. I. (1991), ’A distribution-moment model of energetics in skeletal muscle’, *ASME J. Biomech. Eng.* **24**, 21–35.

Matsuda, N., Hagiwara, N., Shoda, M., Kasanuki, H. & Hosoda, S. (1996), 'Enhancement of the L-type Ca^{2+} current by mechanical stimulation in single rabbit cardiac myocytes', *Circ. Res.* **78**(4).

McAllister, R. E., Noble, D. & Tsien, R. W. (1975), 'Reconstruction of the electrical activity of cardiac purkinje fibres', *J. Physiol.* **251**, 1–59.

Mullins, L. J. (1977), 'A mechanism for Na/Ca transport', *J. Gen. Physiol.* **70**, 681–695.

Mullins, L. J. (1981), *Ion transport in the heart*, Raven Press, Ltd., 1185 Avenue of the Americas, New York 10036.

Noble, D. & Noble, S. J. (1984), 'A model of the sino-atrial node electrical activity based on a modification of the DiFrancesco-Noble (1984) equations', *Proc. R. Soc. Lond.* **222**, 295–304.

Opie, L. H. (1984), *The Heart*, Grune and Stratton, Inc, 24/28 Oval Road, London NW1 7DX.

Reuter, H. (1974), 'Exchange of calcium ions in the mammalian myocardium', *Circ. Res.* **34**, 599–605.

Sands, G. B. (1998), Mathematical Model of Ventricular Activation in an Anatomically Accurate Deforming Heart, PhD thesis, University of Auckland, Auckland, New Zealand.

Schouten, V. J. A. & ter Keurs, H. E. D. J. (1986), 'The force-frequency relationship in rat myocardium. the influence of muscle dimensions', *Pflueg. Arch.* **407**, 14–17.

Schouten, V. J. A., van Deen, J. K., de Tombe, P. & Verveen, A. A. (1987), 'Force-interval relationship in heart muscle of mammals: a calcium compartment model', *Biophys. J.* **51**, 13–36.

Shampine, L. F. & Gordon, M. K. (1975), *Computer solution of ordinary differential equations*, W H Freeman and Company, San Francisco.

Shiner, J. S. & Solaro, R. J. (1984), 'The Hill coefficient for the Ca^{2+} activation of striated muscle contraction', *Biophys. J.* **46**, 541–543.

Shirokov, R., Levis, R., Shirokov, N. & Rios, E. (1993), 'Ca^{2+}-dependent inactivation of cardiac L-type Ca^{2+} channels does not affect their voltage sensor', *J. Gen. Physiol.* **102**, 1005–1030.

Smaill, B. H. & Hunter, P. J. (1991), Structure and function of of the diastolic heart: Material properties of passive mechanics, *in* L. Glass, P. J. Hunter & A. D. McCulloch, eds, 'Theory of Heart: Biomechanics, Biophysics, and Nonlinear Dynamics of Cardiac Function', Springer-Verlag, New York, pp. 1–29.

Solaro, R. J. (1993), Modulation of activation of cardiac myofilaments by beta-adrenergic agonists, *in* J. A. Lee & D. G. Allen, eds, 'Modulation of cardiac calcium sensitivity', OUP, Oxford, pp. 160–177.

Tang, Y. & Othmer, H. G. (1994), 'A model of calcium dynamics in cardiac myocytes based on kinetics of ryanodine-sensitive calcium channels', *Biophys. J.* **67**, 2223–2235.

ter Keurs, H. E. D. J., Rijnsburger, W. H., van Heuningen, R. & Nagelsmit, M. J. (1980), 'Tension development and sarcomere length in rat cardiac trabeculae. evidence of length-dependent activation', *Circ. Res.* **46**, 703–714.

Torrent-Guasp, F. (1996), 'The ventricular myocardial band'.
*http://www.medynet.com/hipertension.sec/BMV/index_i.htm

Wagner, J. & Keizer, J. (1994), 'Effects of rapid buffers on Ca^{2+} diffusion and Ca^{2+} oscillations', *Biophys. J.* **67**, 447–456.

Winegrad, S. (1980), The importance of passive elements in the contraction of the heart, *in* J. Bann, A. C. Arntzenius & E. L. Yellin, eds, 'Cardiac Dynamics', Martinus Nijhoff, The Hague, pp. 11–12.

Zahalak, G. I. & Ma, S. P. (1990), 'Muscle activation and contraction: Constitutive relations based directly on cross-bridge kinetics', *ASME J. Biomech. Eng.* **112**, 52–62.

Zeng, J., Laurita, K. R., Rosenbaum, D. S. & Rudy, Y. (1995), 'Two components of the delayed rectifier K^{+} current in ventricular myocytes of the guinea pig type: Theoretical formulation and their role in repolarization', *Circ. Res.* **77**(1), 140–152.

Appendix A

Model Parameters and Variables

This appendix contains all the model parameters and variables for the different models implemented in this research. A brief description of each parameter and variable is given along with its standard value and units.

A.1 DiFrancesco–Noble

Table A.1 shows the standard parameter values used in this research, and Table A.2 shows the initial conditions of the model variables, for the DFN model. Some parameters, marked *, are used by the OxSoft HEART implementation (Section 6.2.1) and are not mentioned in the description of the DFN model given in Section 3.1.

Parameter	Definition	Value
	Calcium background current – $I_{Ca,b}$	
$g_{Ca,b}$	Calcium background conductance	0.02 μS
	Calcium channel (L-type) – $I_{Ca(L)}$	
$vsurfca^*$	Fixed surface potential on Ca^{2+} channel	50 mV
$P_{Ca,L}$	Ca^{2+} permeability of fast Ca^{2+} channel	15
τ_{f2}	Time constant for recovery from Ca^{2+}-induced inactivation	0.1 s
$P^*_{Ca,T}$	Permeability of $I_{Ca(T)}$ channels	0
$CAMODE^*$	Choice of $I_{Ca(L)}$ equations	1
$CANMODE^*$	Selectivity for fast Ca^{2+} channel	0
	Extracellular calcium	
$CAOMODE^*$	Computation of [Ca^{2+}]$_o$	0
	Sodium - calcium exchange – I_{NaCa}	
k_{NaCa}	Scaling factor for Na$^+$–Ca^{2+} exchange	0.02
$\overline{I_{NaCa}}$	Limiting (maximum) value of I_{NaCa}	1000 nA
n_{NaCa}	Na$^+$–Ca^{2+} exchange ratio (Na$^+$:Ca^{2+})	3
d_{NaCa}	Constant in denominator of full equation for I_{NaCa}	0.001
γ	Position of the energy peak	0.5
$scale^*$	General scaling factor	1
$NMODE^*$	Choice of function for I_{NaCa}	1

Table A.1 – continued on next page

Table A.1 – continued from previous page

Calcium pump – $I_{p(Ca)}$		
$kslpump^*$	Scaling constant for sarcolemmal Ca^{2+} pump	1
$kmslpump^*$	Binding constant for sarcolemmal Ca^{2+} pump	1
Mitochondria		
$MMODE^*$	Mitochondrial Ca^{2+}	0
Membrane parameters		
C_m	Membrane capacitance	$0.0756\ \mu\mathrm{F}$
V_e	Volume of extracellular space	$0.1\ \mathrm{mm}^3$
R_s^*	Series resistance (external circuit)	$0\ \Omega$
Calcium release from the SR – I_{rel}		
V_{NSR}	Absolute volume of the release store	$0.02\ \mathrm{mm}^3$
$srleak^*$	Ca^{2+} leak from the release store	0
τ_{rel}	Release time constant	0.05 s
r	Power for Ca^{2+}-activated release	2
$K_{m,Ca}$	Constant for activation of Ca^{2+} release	0.001 mM
Calcium uptake pump – I_{up}		
V_{JSR}	Absolute volume of Ca^{2+} uptake store	$0.05\ \mathrm{mm}^3$
$\overline{[\mathrm{Ca}^{2+}]_{JSR}}^*$	Maximum value of Ca^{2+} in uptake store	5 mM
$kcyca^*$	Ca^{2+} binding constant (SR pump on cytosol side)	1
$ksrca^*$	Ca^{2+} binding constant (SR pump on SR side)	1
$kxcs^*$	Translocation constant of free SR pump sites	1
$SRMODE^*$	SR Ca^{2+}-sequestration	1
Intracellular calcium		
$calim^*$	Minimum value of $[\mathrm{Ca}^{2+}]_i$	10^{-5} mM
Troponin		
$ktrocon^*$	Rate constant for Ca^{2+} binding to troponin	10^5
$ktrocoff^*$	Rate constant for Ca^{2+} dissociation from troponin	200
$ktromon^*$	Rate constant for Mg^{2+} binding to troponin	10
$ktromoff^*$	Rate constant for Mg^{2+} dissociation from troponin	33.3
$ktocmon^*$	Rate constant for Ca^{2+} binding to Mg^{2+}-troponin	10^4
$ktrocmoff^*$	Rate constant for Ca^{2+} dissociation from Mg^{2+}-troponin	0.33
Calmodulin		
$[\mathrm{CMDN}]_{tot}^*$	Concentration of calmodulin	0.00767 mM
$kcalon^*$	Rate constant for Ca^{2+} binding to calmodulin	10^5
$kcaloff^*$	Rate constant for dissociation from calmodulin	50
$BMODE^*$	Ca^{2+} buffering	0
Transient outward channel – I_{to}		
$K_{m,to}$	Constant for K^+ activation of I_{to}	10 mM
gto^*	Scaling factor for I_{to}	1
$shiftto^*$	Parameter for shifting voltage-dependence of I_{to}	0
$TOMODE^*$	Choice of I_{to} equation	1
Potassium rectifier – I_{K1}		
$K_{m,K1}$	Constant for K^+ activation of I_{K1}	210 mM
$\overline{g}_{K1}$	Maximum conductance for I_{K1}	$920\ \mu\mathrm{S}$
$shiftk1^*$	Parameter for shifting the voltage-dependence of I_{K1}	0
$KMODE^*$	Choice of I_K equation	0
Potassium delayed rectifier – I_K		
$\overline{I_K}$	Maximum outward current for I_K	180 nA
Intracellular magnesium		
$[\mathrm{Mg}^{2+}]_i$	Internal Mg^{2+} concentration	0.02 mM
Extracellular sodium		
$[\mathrm{Na}^+]_o$	External Na^+ concentration	140 mM

Table A.1 – continued on next page

Table A.1 – continued from previous page

	Extracellular potassium	
$[\mathrm{K}^+]_b$	Bulk external K^+	4 mM
	Sodium - potassium exchange – I_{NaK}	
$K_{m,K}$	Constant for K^+ activation of Na^+-K^+ pump	1 mM
$K_{m,Na}$	Constant for Na^+ activation of Na^+-K^+ pump	40 mM
$\underline{P_{NaK}}$	Permeability of I_{NaK} channels	0.12
$\overline{I}_{NaK}$	Maximum value of I_{NaK}	125 nA
n_{NaK}	Na^+–K^+ pump ratio (Na^+:K^+)	1.5
	Sodium background current – $I_{Na,b}$	
g_B	Background conductance (used when $g_{Na,b} = g_{K,b}$)	0 μS
$g_{Na,b}$	Conductance for Na^+ component of I_b	0.18 μS
$g_{K,b}$	Conductance for K^+ component of I_b	0 μS
	Fast sodium channel – I_{Na}	
$\overline{g}_{Na}$	Maximum fast sodium conductance	750 μS
$NAMODE^*$	Choice of I_{Na} equations	1
	Hyperpolarising-activated Na^+-K^+ **current –** I_f	
$K_{m,f}$	Constant for K^+ activation of I_f	45 mM
$\overline{g}_{f,Na}$	Maximum conductance for $I_{f,Na}$	3 μS
$\overline{g}_{f,K}$	Maximum conductance for $I_{f,K}$	3 μS
$YMODE^*$	Kinetics of I_f	0
	Other parameters	
$kcachoff^*$	Fraction of channels with bound Ca^{2+}	0.001
$gnak^*$	Ca^{2+}-activated shunt conductance	1 μS
$pca2^*$	Permeability of ICa2 channels	0
$pcak^*$	K^+ permeability of ICa (L??) channels	0.01
$iachm^*$	Maximum value of IACh	0 nA
$iscal^*$	Scaling factor for tabulation of currents	1
$pulsesize^*$	Value of voltage repetitive pulses	0 mV
$ipulsesize^*$	Value of current repetitive pulses	0 nA
on^*	Initial time of onset of pulses	10^4 s
off^*	Initial time of switchoff of pulses	10^4 s
rep^*	Repetition cycle time for pulses	10^4 s
I_{stim}	Stimulus current (additional to pulse and Ipulse)	-250 nA
re^*	Electrode resistance (external circuit)	10^4 Ω
amp^*	Clamp amplification factor (external circuit)	0
dx^*	Distance interval (preparation geometry)	5
$ninterval^*$	Number of distance intervals (preparation geometry)	0
$preplength^*$	Length of cylinder (preparation geometry)	2 mm
$AMODE^*$	$[\mathrm{Ca}^{2+}]_i$ activation	4
$RMODE^*$	Voltage dependence of repriming	0
	Single cell parameters	
$nape^*$	Sodium concentration in perfusion electrode	1 mM
$cape^*$	Calcium concentration in perfusion electrode	1 mM
kpe^*	Potassium concentration in perfusion electrode	1 mM
$tnap^*$	Time constant for Na^+ perfusion	1 s
$tcap^*$	Time constant for Ca^{2+} perfusion	1 s
tkp^*	Time constant for K^+ perfusion	1 s
	Diffussion space parameters	
pf^*	Rate constant for diffusion	0.7
$tort^*$	Tortuosity factor	1.41
	Control modes	
$MODE^*$	Operating mode	1

Table A.1 – continued on next page

Table A.1 – continued from previous page

$PMODE^*$	Current/voltage mode	0
$PREP^*$	Preparation type	1
$SPACE^*$	Diffusion space type	4

TABLE A.1: Model parameters for the DiFrancesco–Noble model.

Variable	Definition	Initial value
V_m	Membrane potential	$-75\,\mathrm{mV}$
$[\mathrm{Na}^+]_i$	Intracellular sodium concentration	$8\,\mathrm{mM}$
$[\mathrm{K}^+]_c$	Cleft potassium concentration (three compartment model only)	$0\,\mathrm{mM}$
$[\mathrm{Ca}^{2+}]_i$	Intracellular calcium concentration	$5 \times 10^{-5}\,\mathrm{mM}$
y	Gating variable for I_f	0.2
X	Gating variable for I_K	0.01
d	$I_{Ca(L)}$ activation gating variable	0.005
f	$I_{Ca(L)}$ inactivation gating variable	1
h	I_{Na} inactivation gating variable	0.8
m	I_{Na} activation gating variable	0.01
$[\mathrm{K}^+]_i$	Intracellular potassium concentration	$140\,\mathrm{mM}$
$[\mathrm{Ca}^{2+}]_{NSR}$	Calcium concentration in uptake store	$2\,\mathrm{mM}$
$[\mathrm{Ca}^{2+}]_{JSR}$	Calcium concentration in release store	$1\,\mathrm{mM}$
p	Repriming variable (calcium translocation within the SR)	1
f_2	Slow calcium inactivation gating variable	0
d_3^*	Activation of $I_{Ca(T)}$	0
f_3^*	Inactivation of $I_{Ca(T)}$	0
r	Inactivation variable for I_{to}	0
q	Activation variable for I_{to}	0
$[\mathrm{CMDNCa}]$	Concentration of calcium bound to calmodulin	$0\,\mathrm{mM}$
$[\mathrm{TRPNCa}]$	Concentration of calcium bound to troponin	$0.049\,\mathrm{mM}$
$[\mathrm{TRPNMg}]$	Concentration of magnesium bound to troponin	$0.0429\,\mathrm{mM}$
$[\mathrm{MgTRPNCa}]$	Concentration of calcium bound to Mg^{2+}-troponin	$0\,\mathrm{mM}$
$[\mathrm{Ca}^{2+}]_o$	Extracellular calcium concentration	$2\,\mathrm{mM}$
$[\mathrm{Ca}^{2+}]_{mito}$	Mitochondrial calcium concentration	$0\,\mathrm{mM}$
$F1^*$	Precursor fraction	0
$F2^*$	Activator fraction	0
$F3^*$	Product fraction	0
*	Light chain conformation	0
*	Cross-bridge reactions	0
$[\mathrm{Ca}^{2+}]_{tot}^*$	Total cytosolic calcium concentration	$0\,\mathrm{mM}$

TABLE A.2: Initial conditions for the DiFrancesco–Noble model.

A.2 Luo–Rudy (LR-II)

Tables A.3 and A.4 give the standard set of parameter and inital variable values used with the non-coupled LR model.

Parameter	Definition	Value
I_{stim}	Stimulus current	$-100\ \mu\text{A}\cdot\text{cm}^{-2}$
	Calcium background current – $I_{Ca,b}$	
$\overline{g}_{Ca,b}$	Maximum conductance for $I_{Ca,b}$	$30.16\times10^{-4}\ \mu\text{S}\cdot\text{cm}^{-2}$
	L-type calcium channel – $I_{Ca(L)}$	
$K_{m,Ca}$	Half saturation concentration of the $I_{Ca(L)}$ channel	0.0006 mM
P_{Ca}	Permeability of membrane to calcium ions	$5.4\times10^{-4}\ \text{cm}\cdot\text{s}^{-1}$
	Extracellular calcium	
γ_{Cao}	Activity coefficient of extracellular calcium	0.341
	Sodium - calcium exchange – I_{NaCa}	
k_{NaCa}	Scaling factor of sodium - calcium exchanger current	$2000\ \mu\text{A}\cdot\text{cm}^{-2}$
$K_{m,Na}$	Half saturation concentration of sodium channel	87.5 mM
$K_{m,Ca}$	Half saturation concentration of calcium channel	1.38 mM
η	Position of energy barrier controlling voltage dependence of I_{NaCa}	0.35
k_{sat}	Saturation factor of I_{NaCa} at very negative potentials	0.1
	Sarcolemmal calcium pump – $I_{p(Ca)}$	
$K_{m,pCa}$	Half saturation concentration of calcium channel	5×10^{-4} mM
$\overline{I_{p(Ca)}}$	Maximum current through channel $I_{p(Ca)}$	$1.15\ \mu\text{A}\cdot\text{cm}^{-2}$
	Nonspecific calcium channel – $I_{ns(Ca)}$	
$K_{m,nsCa}$	Half saturation concentration of calcium channel	0.0012 mM
P_{nsCa}	Permeability of membrane to calcium ions	$1.75\times10^{-7}\ \text{cm}\cdot\text{s}^{-1}$
	Membrane parameters	
C_m	Membrane capacitance	$1\ \mu\text{F}\cdot\text{cm}^{-2}$
A_{cap}	Capacitive membrane area $1.53\times10^{-4}\ \text{mm}^2$	
T	Temperature	37 °C
V_{myo}	Volume of myoplasm	$2.584\times10^{-5}\ \mu\text{L}$
	Calcium release from SR – I_{rel}	
$\overline{[\text{CSQN}]}$	Maximum concentration of calsequestrin	10 mM
$K_{m,CSQN}$	Half saturation concentration of calsequestrin	0.8 mM
$K_{m,rel}$	Half saturation concentration of release channel	8×10^{-4} mM
τ_{on}	Time constant of activating calcium release from JSR	2 ms
τ_{off}	Time constant of inactivating calcium release from JSR	2 ms
$\Delta[\text{Ca}^{2+}]_{i,th}$	Threshold for external triggering of calcium release from JSR	1.8×10^{-4} mM
$\overline{G_{rel}}$	Maximum rate constant of calcium release from JSR	$60\ \text{ms}^{-1}$
V_{JSR}	Volume of JSR	$1.82\times10^{-7}\ \mu\text{L}$
	Calcium translocation – I_{tr}	
τ_{tr}	Time constant of calcium transfer from NSR to JSR	180 ms
	Calcium uptake pump – I_{up}	
$K_{m,up}$	Half saturation concentration of calcium channel	9.2×10^{-4} mM
$\overline{[\text{Ca}^{2+}]_{NSR}}$	Maximum calcium ion concentration in NSR	15 mM
I_{up}	Maximum calcium uptake from myoplasm to NSR (flux)	$0.005\ \text{mM}\cdot\text{ms}^{-1}$
V_{NSR}	Volume of NSR	$2.098\times10^{-6}\ \mu\text{L}$
	Intracellular calcium	
γ_{Cai}	Activity coefficient of intracellular calcium	1
	Troponin	
$\overline{[\text{TRPN}]}$	Maximum concentration of troponin-C	0.07 mM
$K_{m,TRPN}$	Half saturation concentration of troponin buffering	0.0005 mM
	Calmodulin	
$\overline{[\text{CMDN}]}$	Maximum concentration of calmodulin	0.05 mM
$K_{m,CMDN}$	Half saturation concentration of calmodulin	0.00238 mM
	Potassium plateau current – I_{Kp}	

Table A.3 – continued on next page

Table A.3 – continued from previous page

$\overline{g}_{Kp}$	Maximum conductance of the I_{Kp} channel	$0.0183\ \mu\mathrm{S}\cdot\mu\mathrm{F}^{-1}$
	Potassium rectifier – I_{K1}	
P_K	Permeability of membrane to potassium	$1.93\times10^{-7}\ \mathrm{cm}\cdot\mathrm{s}^{-1}$
	Intracellular sodium	
γ_{Nai}	Activity coefficient of intracellular sodium	0.75
	Intracellular potassium	
γ_{Ki}	Activity coefficient of intracellular potassium	0.75
	Extracellular sodium	
$[\mathrm{Na}^+]_o$	External sodium concentration	$140\ \mathrm{mM}$
γ_{Nao}	Activity coefficient of extracellular sodium	0.75
	Extracellular potassium	
$[\mathrm{K}^+]_o$	External potassium concentration	$5.4\ \mathrm{mM}$
γ_{Ko}	Activity coefficient of extracellular potassium	0.75
	Sodium - potassium exchange – I_{NaK}	
$\underline{P_{NaK}}$	Permeability ratio of sodium to potassium	0.01833
$\overline{I_{NaK}}$	Maximum current through Na^+-K^+ channel	$1.5\ \mu\mathrm{A}\cdot\mathrm{cm}^{-2}$
$K_{m,Nai}$	Half concentration of sodium channel	$10\ \mathrm{mM}$
$K_{m,Ko}$	Half concentration of potassium channel	$1.5\ \mathrm{mM}$
	Sodium backgrond current – $I_{Na,b}$	
$\overline{g}_{Na,b}$	Maximum conductance of channel $I_{Na,b}$	$0.00141\ \mathrm{mS}\cdot\mu\mathrm{F}^{-1}$
	Fast sodium channel – I_{Na}	
$\overline{g}_{Na}$	Maximum conductance of channel I_{Na}	$16\ \mathrm{mS}\cdot\mu\mathrm{F}^{-1}$
P_{Na}	Permeability of membrane to sodium ions	$6.75\times10^{-7}\ \mathrm{cm}\cdot\mathrm{s}^{-1}$

TABLE A.3: Model parameters for the Luo–Rudy model.

Variable	Definition	Initial value
V_m	Membrane potential	$1.0\ \mu\mathrm{F}\cdot\mathrm{cm}^{-2}$
$[\mathrm{Na}^+]_i$	Intracellular sodium ion concentration	$10\ \mathrm{mM}$
$[\mathrm{Ca}^{2+}]_i$	Intracellular calcium ion concentration	$1.2\times10^{-4}\ \mathrm{mM}$
x	Gating variable for I_K	0
d	Calcium activation gating variable	0
f	Calcium inactivation gating variable	1
h	Sodium inactivation gating variable	1
m	Sodium activation gating variable	0
j	Sodium slow inactivation gating variable	1
$[\mathrm{K}^+]_i$	Intracellular potassium ion concentration	$145\ \mathrm{mM}$
$[\mathrm{Ca}^{2+}]_{NSR}$	Calcium ion concentration with SR uptake store	$1.8\ \mathrm{mM}$
$[\mathrm{Ca}^{2+}]_{JSR}$	Calcium ion concentration with SR release store	$1.8\ \mathrm{mM}$
$[\mathrm{TRPNCa}]$	Concentratino of calcium ions bound to troponin	$1.2\times10^{-4}\ \mathrm{mM}$
$[\mathrm{Ca}^{2+}]_o$	Extracellular calcium ion concentration	$1.8\ \mathrm{mM}$

TABLE A.4: Initial conditions for the Luo–Rudy model.

A.3 Jafri–Rice–Winslow

The following two tables (Tables A.5 and A.6) contain the set of parameters and variables defined by the JRW model. The standard value for each parameter and intial value is given, with a brief description of the parameter/variable.

Parameter	Definition	Value
I_{stim}	Stimulus current	$-100\,\mu\text{A}\cdot\text{cm}^{-2}$
	Calcium background current – $I_{Ca,b}$	
$\overline{g}_{Ca,b}$	Maximium background Ca^{2+} current conductance	$0.006032\,\text{mS}\cdot\mu\text{F}^{-1}$
	L-type calcium channel – $I_{Ca(L)}$	
f	Transition rate into open state	$0.3\,\text{ms}^{-1}$
g	Transition rate out of open state	$2.0\,\text{ms}^{-1}$
f'	Transition rate into open state for mode Ca	$0.0\,\text{ms}^{-1}$
g'	Transition rate out of open state for mode Ca	$0.0\,\text{ms}^{-1}$
a	Mode transition parameter	2.0
b	Mode transition parameter	2.0
w	Mode transition parameter	$0.01\,\text{ms}^{-1}$
$\overline{P}_{Ca}$	L-type Ca^{2+} channel permeability to Ca^{2+}	$33.75\times10^{-4}\ \text{cm}\cdot\text{s}^{-1}$
$\overline{P}_{K}$	L-type Ca^{2+} channel permeability to K^{+}	$1.0\times10^{-7}\ \text{cm}\cdot\text{s}^{-1}$
$I_{Ca(L),Ca_{half}}$	$I_{Ca(L)}$ level that reduces $\overline{P}_K$ by half	$-0.458\,\mu\text{A}\cdot\text{cm}^{-2}$
	Sodium calcium exchange current – I_{NaCa}	
k_{NaCa}	Scaling factor for Na^{+}-Ca^{2+} exchange	$5000\,\mu\text{A}\cdot\text{cm}^{-2}$
$K_{m,Na}$	Na^{+} half saturation constant for Na^{+}-Ca^{2+} exchange	$87.5\,\text{mM}$
$K_{m,Ca}$	Ca^{2+} half saturation constant for Na^{+}-Ca^{2+} exchange	$1.38\,\text{mM}$
k_{sat}	Na^{+}-Ca^{2+} exchange saturation at very negative potentials	0.1
η	Controls voltage dependence of Na^{+}-Ca^{2+} exchange	0.35
	Calcium pump – $I_{p(Ca)}$	
$\overline{I_{p(Ca)}}$	Maximum sarcolemmal Ca^{2+} pump current	$1.15\,\mu\text{A}\cdot\text{cm}^{-2}$
$K_{m,p(Ca)}$	Ca^{2+} half saturation constant for sarcolemmal Ca^{2+} pump	$0.5\,\mu\text{M}$
	Nonspecific calcium current – $I_{ns(Ca)}$	
$P_{ns(Ca)}$	Nonspecific current channel permeability	$0.0\ \text{cm}\cdot\text{s}^{-1}$
$K_{m,ns(Ca)}$	Ca^{2+} half saturation constant for nonspecific current	$1.2\,\mu\text{M}$
	Membrane parameters	
F	Faraday's constant	$96.5\ \text{coul}\cdot\text{mmol}^{-1}$
T	Absolute temperature	310 K
R	Ideal gas constant	$8.314\ \text{J}\cdot\text{mol}^{-1}\cdot\text{K}^{-1}$
C_m	Capacitive membrane area	$1.534\times10^{-4}\ \text{cm}^2$
V_{myo}	Myoplasmic volume	$25.84\times10^{-6}\ \mu\text{L}$
V_{SS}	Subspace volume	$1.485\times10^{-9}\ \mu\text{L}$
	Calcium release from the SR – I_{rel}	
v_1	Maximum RyR channel Ca^{2+} permeability	$1.8\,\text{ms}^{-1}$
k_a^+	RyR P_{C_1}–P_{O_1} rate constant	$0.01215\,\mu\text{M}^{-4}\cdot\text{ms}^{-1}$
k_a^-	RyR P_{O_1}–P_{C_1} rate constant	$0.1425\,\text{ms}^{-1}$
k_b^+	RyR P_{O_1}–P_{O_2} rate constant	$0.00405\,\mu\text{M}^{-3}\cdot\text{ms}^{-1}$
k_b^-	RyR P_{O_2}–P_{O_1} rate constant	$1.930\,\text{ms}^{-1}$
k_c^+	RyR P_{O_1}–P_{C_2} rate constant	$0.018\,\text{ms}^{-1}$
k_c^-	RyR P_{C_2}–P_{O_1} rate constant	$0.0008\,\text{ms}^{-1}$
n	RyR Ca^{2+} cooperativity parameter P_{C_1}–P_{O_1}	4
m	RyR Ca^{2+} cooperativity parameter P_{O_1}–P_{O_2}	3
$[\text{CSQN}]_{tot}$	Total NSR calsequestrin concentration	$15.0\,\text{mM}$
$K_{m,CSQN}$	Ca^{2+} half saturation constant for calsequestrin	
V_{JSR}	JSR volume	$0.12\times10^{-6}\ \mu\text{L}$
τ_{xfer}	Time constant for transfer from subspace to myoplasm	$3.125\,\text{ms}$
	Calcium translocation – I_{tr}	

Table A.5 – continued on next page

Table A.5 – continued from previous page

τ_{tr}	Time constant for transfer from NSR to JSR	34.48 ms
	Calcium uptake pump – I_{up}	
v_2	Ca^{2+} leak rate constant from the NSR	5.80×10^{-5} ms^{-1}
v_3	SR Ca^{2+}-ATPase maximum pump rate	$1.8\ \mu M \cdot ms^{-1}$
$K_{m,up}$	Half-saturation constant for SR Ca^{2+}-ATPase pump	$0.5\ \mu M$
V_{NSR}	NSR volume	$2.098 \times 10^{-6}\ \mu L$
	Troponin	
$[LTRPN]_{tot}$	Total myoplasmic Tn low-affinity site concentration	$70.0\ \mu M$
$[HTRPN]_{tot}$	Total myoplasmic Tn high-affinity site concentration	$140.0\ \mu M$
k^{+}_{htrpn}	Ca^{2+} on rate constant for Tn high-affinity sites	$2.0 \times 10^{7}\ M^{-1} \cdot s^{-1}$
k^{-}_{htrpn}	Ca^{2+} off rate constant for Tn high-affinity sites	$0.066\ s^{-1}$
k^{+}_{ltrpn}	Ca^{2+} on rate constant for Tn low-affinity sites	$4.0 \times 10^{7}\ M^{-1} \cdot s^{-1}$
k^{-}_{ltrpn}	Ca^{2+} off rate constant for Tn low-affinity sites	$40.0\ s^{-1}$
	Calmodulin	
$[CMDN]_{tot}$	Total myoplasmic calmodulin concentration	$50.0\ \mu M$
$K_{m,CMDN}$	Ca^{2+} half saturation constant for calmodulin	$2.38\ \mu M$
	Potassium plateau current – I_{Kp}	
$\overline{g}_{Kp}$	Maxium plateau K^{+} channel conductance	$0.00828\ mS \cdot \mu F^{-1}$
	Potassium delayed rectifier – I_K	
$P_{Na,K}$	Na^{+} permeability of K^{+} channels	0.01833
	Extracellular sodium	
$[Na^{+}]_o$	External Na^{+} concentration	140.0 mM
	Extracellular potassium	
$[K^{+}]_o$	External K^{+} concentration	5.4 mM
	Sodium potassium exchange current – I_{NaK}	
$\overline{I_{NaK}}$	Maximum Na^{+}-K^{+} pump current	$1.3\ \mu A \cdot cm^{-2}$
$K_{m,Nai}$	Na^{+} half saturation constant for Na^{+}-K^{+} pump	10.0 mM
$K_{m,Ko}$	K^{+} half saturation constant for Na^{+}-K^{+} pump	1.5 mM
	Sodium background current – $I_{Na,b}$	
$\overline{g}_{Na,b}$	Maximum background Na^{+} current conductance	$0.00141\ mS \cdot \mu F^{-1}$
	Fast sodium channel – I_{Na}	
$\overline{g}_{Na}$	Maximum Na^{+} channel conductance	$12.8\ mS \cdot \mu F^{-1}$

TABLE A.5: Model parameters for the Jafri–Rice–Winslow model.

Variable	Definition	Initial value
t	Time	0.0 ms
V_m	Membrane potential	−86.1638 mV
$[Na^{+}]_i$	Intracellular Na^{+} concentration	10.2042 mM
$[Ca^{2+}]_i$	Intracellular Ca^{2+} concentration	9.94893×10^{-5} nM
x	Gating variable for I_K	9.28836×10^{-4}
y	$I_{Ca(L)}$ inactivation gate (called f in CELL)	0.998983
h	I_{Na} inactivation gate	0.988354
m	I_{Na} activation gate	3.28302×10^{-2}
j	I_{Na} slow inactivation gate	0.992540
$[K^{+}]_i$	Intracellular K^{+} concentration	143.727 mM
$[Ca^{2+}]_{NSR}$	Ca^{2+} concentration in uptake store (NSR)	1.24891 mM
$[Ca^{2+}]_{JSR}$	Ca^{2+} concentration in release store (JSR)	1.17504 mM
$[Ca^{2+}]_o$	Extracellular Ca^{2+} concentration	1.8 mM
$[Ca^{2+}]_{SS}$	Ca^{2+} concentration within the subspace	1.36058×10^{-4} mM
P_{C_1}	Fraction of RyR channels in the P_{C_1} state	0.762527

Table A.6 – continued on next page

Table A.6 – continued from previous page

P_{O_1}	Fraction of RyR channels in the P_{O_1} state	1.19168×10^{-3}
P_{O_2}	Fraction of RyR channels in the P_{O_2} state	6.30613×10^{-9}
P_{C_2}	Fraction of RyR channels in the P_{C_2} state	0.236283
C_0	L-type Ca^{2+} channel closed state mode normal	0.997208
C_1	L-type Ca^{2+} channel closed state mode normal	6.38897×10^{-5}
C_2	L-type Ca^{2+} channel closed state mode normal	1.535×10^{-9}
C_3	L-type Ca^{2+} channel closed state mode normal	1.63909×10^{-14}
C_4	L-type Ca^{2+} channel closed state mode normal	6.56337×10^{-20}
O	L-type Ca^{2+} channel conducting state mode normal	9.84546×10^{-21}
C_{Ca0}	L-type Ca^{2+} channel closed state mode Ca	2.72826×10^{-3}
C_{Ca1}	L-type Ca^{2+} channel closed state mode Ca	6.99215×10^{-7}
C_{Ca2}	L-type Ca^{2+} channel closed state mode Ca	6.71989×10^{-11}
C_{Ca3}	L-type Ca^{2+} channel closed state mode Ca	2.87031×10^{-15}
C_{Ca4}	L-type Ca^{2+} channel closed state mode Ca	4.59752×10^{-20}
O_{Ca}	L-type Ca^{2+} channel conducting state mode Ca	0.0
$[\mathrm{LTRPNCa}]$	Concentration of Ca^{2+} bound to low-affinity Tn binding sites	$6.349973\ \mu\mathrm{M}$
$[\mathrm{HTRPNCa}]$	Concentration of Ca^{2+} bound to high-affinity Tn binding sites	$135.9813\ \mu\mathrm{M}$

TABLE A.6: Initial conditions for the Jafri–Rice–Winslow model.

A.4 Hunter–McCulloch–ter Keurs

Table A.7 gives a brief description of the HMT model parameters with their respective values. The standard set of initial conditions is given in Table A.8, with a description of each of the model variables.

Variable	Definition	Initial value
	Calcium release from the SR – I_{rel}	
$[Ca^{2+}]_{max}$	Ca^{2+} twitch maximum	$1.0\ \mu\mathrm{M}$
τ_{Ca}	Ca^{2+} twitch time constant	60.0 ms
	Troponin (Tn)	
ρ_0	Ca^{2+} binding rate constant	$0.1\ \mathrm{ms}^{-1} \cdot \mu\mathrm{M}^{-1}$
ρ_1	Ca^{2+} dislocation rate constant	$0.163\ \mathrm{ms}^{-1}$
$[Ca^{2+}]_{bmax}$	Maximum initially bound Ca^{2+}	$2.0\ \mu\mathrm{M}$
γ		2.6
	Tropomyosin (Tm)	
α_0	Tm rate constant	$0.002\ \mathrm{ms}^{-1}$
n_{ref}	Hill parameter	6.9
pC_{50ref}	Hill parameter	6.2
	Steady state mechanics	
T_{ref}	Reference tension	$125.0\ \mathrm{kPa}$
β_0	Isometric length dependence	1.45
β_1	Hill n length dependence	1.95
β_2	Hill pC_{50} length dependence	0.31
	Cross-bridges	
a	Fading memory curvature	0.5

Table A.7 – continued on next page

Table A.7 – continued from previous page

α_1	Rate constant associated with the first order slow tension recovery	$0.033\,\mathrm{ms}^{-1}$
α_2	Rate constant associated with the second order fast tension recovery	$2.850\,\mathrm{ms}^{-1}$
α_3	Rate constant associated with the second order fast tension recovery	$2.850\,\mathrm{ms}^{-1}$
A_1	Weighting coefficient associated with the first order slow tension recovery	50.0
A_2	Weighting coefficient associated with the second order fast tension recovery	175.0
A_3	Weighting coefficient associated with the second order fast tension recovery	175.0
	Passive mechanics	
a_1	Limiting strain when cell is in tension	0.22
b_1	Curvature of the uniaxial stress-strian curve when the cell is in tension	1.0
k_1	relative contribution of the e_{11} strain energy term	$0.2\,\mathrm{kPa}$
a_2	Limiting strain when cell is in compression	0.41
b_2	Curvature of the uniaxial stress-strian curve when the cell is in compression	6.8
k_2	relative contribution of the e_{22} strain energy term	$0.06\,\mathrm{kPa}$
a_3	Limiting strain	1.037
b_3	Curvature of the uniaxial stress-strian curve	0.398
k_3	relative contribution of the e_{33} strain energy term	$0.31\,\mathrm{kPa}$

TABLE A.7: Model parameters for the Hunter–McCulloch–ter Keurs model.

Variable	Definition	Initial value
t	Time	$0.0\,\mathrm{ms}$
λ	Extension ratio[1]	
T	Tension	$0.0\,\mathrm{kPa}$

TABLE A.8: Initial conditions for the Hunter–McCulloch–ter Keurs model.

A.5 Coupled JRW–HMT Model

Presented in Table A.9 is the full set of model parameters and their values for the coupled JRW–HMT model developed in Chapter 5. The variables for the coupled JRW–HMT model are given in Table A.10 with their initial values. The values which differ from their standard values given in Tables (A.5)–(A.8) are marked $^?$. An explanation for these differences can be found in Section 5.2.

Parameter	Definition	Value
I_{stim}	Stimulus current	$-100\,\mu\mathrm{A}\cdot\mathrm{cm}^{-2}$

Table A.9 – continued on next page

---

[1] The extension ratio is set via the CELL interface, defining the value of λ at each point in time.

Table A.9 – continued from previous page

	Calcium background current – $I_{Ca,b}$	
$\overline{g}_{Ca,b}$	Maximium background Ca^{2+} current conductance	$0.006032\,\mathrm{mS}\cdot\mu\mathrm{F}^{-1}$
	L-type calcium channel – $I_{Ca(L)}$	
f	Transition rate into open state	$0.3\ \mathrm{ms}^{-1}$
g	Transition rate out of open state	$2.0\ \mathrm{ms}^{-1}$
f'	Transition rate into open state for mode Ca	$0.0\ \mathrm{ms}^{-1}$
g'	Transition rate out of open state for mode Ca	$0.0\ \mathrm{ms}^{-1}$
a	Mode transition parameter	2.0
b	Mode transition parameter	2.0
w	Mode transition parameter	$0.01\ \mathrm{ms}^{-1}$
$\overline{P}_{Ca}$	L-type Ca^{2+} channel permeability to Ca^{2+}	$33.75\times10^{-4}\ \mathrm{cm}\cdot\mathrm{s}^{-1}$
$\overline{P}_{K}$	L-type Ca^{2+} channel permeability to K^{+}	$1.0\times10^{-7}\ \mathrm{cm}\cdot\mathrm{s}^{-1}$
$I_{Ca(L),Ca_{half}}$	$I_{Ca(L)}$ level that reduces $\overline{P}_K$ by half	$-0.458\,\mu\mathrm{A}\cdot\mathrm{cm}^{-2}$
	Sodium calcium exchange current – I_{NaCa}	
k_{NaCa}	Scaling factor for Na^{+}-Ca^{2+} exchange	$5000\,\mu\mathrm{A}\cdot\mathrm{cm}^{-2}$
$K_{m,Na}$	Na^{+} half saturation constant for Na^{+}-Ca^{2+} exchange	$87.5\ \mathrm{mM}$
$K_{m,Ca}$	Ca^{2+} half saturation constant for Na^{+}-Ca^{2+} exchange	$1.38\ \mathrm{mM}$
k_{sat}	Na^{+}-Ca^{2+} exchange saturation at very negative potentials	0.1
η	Controls voltage dependence of Na^{+}-Ca^{2+} exchange	0.35
	Calcium pump – $I_{p(Ca)}$	
$\overline{I_{p(Ca)}}$	Maximum sarcolemmal Ca^{2+} pump current	$1.15\,\mu\mathrm{A}\cdot\mathrm{cm}^{-2}$
$K_{m,p(Ca)}$	Ca^{2+} half saturation constant for sarcolemmal Ca^{2+} pump	$0.5\,\mu\mathrm{M}$
	Nonspecific calcium current – $I_{ns(Ca)}$	
$P_{ns(Ca)}$	Nonspecific current channel permeability	$0.0\ \mathrm{cm}\cdot\mathrm{s}^{-1}$
$K_{m,ns(Ca)}$	Ca^{2+} half saturation constant for nonspecific current	$1.2\,\mu\mathrm{M}$
	Membrane parameters	
F	Faraday's constant	$96.5\ \mathrm{coul}\cdot\mathrm{mmol}^{-1}$
T	Absolute temperature	$310\ \mathrm{K}$
R	Ideal gas constant	$8.314\ \mathrm{J}\cdot\mathrm{mol}^{-1}\cdot\mathrm{K}^{-1}$
C_m	Capacitive membrane area	$1.534\times10^{-4}\ \mathrm{cm}^2$
V_{myo}	Myoplasmic volume	$25.84\times10^{-6}\,\mu\mathrm{L}$
V_{SS}	Subspace volume	$1.485\times10^{-9}\,\mu\mathrm{L}$
	Calcium release from the SR – I_{rel}	
v_1	Maximum RyR channel Ca^{2+} permeability	$1.8\ \mathrm{ms}^{-1}$
k_a^+	RyR P_{C_1}–P_{O_1} rate constant	$0.01215\,\mu\mathrm{M}^{-4}\cdot\mathrm{ms}^{-1}$
k_a^-	RyR P_{O_1}–P_{C_1} rate constant	$0.1425\ \mathrm{ms}^{-1}$
k_b^+	RyR P_{O_1}–P_{O_2} rate constant	$0.00405\,\mu\mathrm{M}^{-3}\cdot\mathrm{ms}^{-1}$
k_b^-	RyR P_{O_2}–P_{O_1} rate constant	$1.930\ \mathrm{ms}^{-1}$
k_c^+	RyR P_{O_1}–P_{C_2} rate constant	$0.018\ \mathrm{ms}^{-1}$
k_c^-	RyR P_{C_2}–P_{O_1} rate constant	$0.0008\ \mathrm{ms}^{-1}$
n	RyR Ca^{2+} cooperativity parameter P_{C_1}–P_{O_1}	4
m	RyR Ca^{2+} cooperativity parameter P_{O_1}–P_{O_2}	3
$[\mathrm{CSQN}]_{tot}$	Total NSR calsequestrin concentration	$15.0\ \mathrm{mM}$
$K_{m,CSQN}$	Ca^{2+} half saturation constant for calsequestrin	
V_{JSR}	JSR volume	$0.12\times10^{-6}\,\mu\mathrm{L}$
τ_{xfer}	Time constant for transfer from subspace to myoplasm	$3.125\ \mathrm{ms}$
	Calcium translocation – I_{tr}	
τ_{tr}	Time constant for transfer from NSR to JSR	$34.48\ \mathrm{ms}$
	Calcium uptake pump – I_{up}	
v_2	Ca^{2+} leak rate constant from the NSR	$5.80\times10^{-5}\ \mathrm{ms}^{-1}$

Table A.9 – continued on next page

Table A.9 – continued from previous page

v_3	SR Ca^{2+}-ATPase maximum pump rate	$1.8\,\mu\mathrm{M}\cdot\mathrm{ms}^{-1}$
$K_{m,up}$	Half-saturation constant for SR Ca^{2+}-ATPase pump	$0.5\,\mu\mathrm{M}$
V_{NSR}	NSR volume	$2.098\times10^{-6}\,\mu\mathrm{L}$
	Troponin	
$[\mathrm{LTRPN}]_{tot}$	Total myoplasmic Tn low-affinity site concentration	$70.0\,\mu\mathrm{M}$
$[\mathrm{HTRPN}]_{tot}$	Total myoplasmic Tn high-affinity site concentration	$140.0\,\mu\mathrm{M}$
k^{+}_{htrpn}	Ca^{2+} on rate constant for Tn high-affinity sites	$2.0\times10^{7}\ \mathrm{M}^{-1}\cdot\mathrm{s}^{-1}$
k^{-}_{htrpn}	Ca^{2+} off rate constant for Tn high-affinity sites	$0.066\,\mathrm{s}^{-1}$
k^{+}_{ltrpn}	Ca^{2+} on rate constant for Tn low-affinity sites	$4.0\times10^{7}\ \mathrm{M}^{-1}\cdot\mathrm{s}^{-1}$
k^{-}_{ltrpn}	Ca^{2+} off rate constant for Tn low-affinity sites	$40.0\,\mathrm{s}^{-1}$
ρ_0	Ca^{2+} binding rate constant	$0.1\,\mathrm{ms}^{-1}\cdot\mu\mathrm{M}^{-1}$
ρ_1	Ca^{2+} dislocation rate constant	$0.163\,\mathrm{ms}^{-1}$
$[\mathrm{Ca}^{2+}]_{bmax}$	Maximum initially bound Ca^{2+}	$2.0\,\mu\mathrm{M}$
γ		2.6
	Tropomyosin (Tm)	
α_0	Tm rate constant	$0.002\,\mathrm{ms}^{-1}$
n_{ref}	Hill parameter	4.25
pC_{50ref}	Hill parameter	5.33
	Steady state mechanics	
T_{ref}	Reference tension	$125.0\,\mathrm{kPa}$
β_0	Isometric length dependence	1.45
β_1	Hill n length dependence	1.95
β_2	Hill pC_{50} length dependence	0.31
	Calmodulin	
$[\mathrm{CMDN}]_{tot}$	Total myoplasmic calmodulin concentration	$50.0\,\mu\mathrm{M}$
$K_{m,CMDN}$	Ca^{2+} half saturation constant for calmodulin	$2.38\,\mu\mathrm{M}$
	Cross-bridges	
a	Fading memory curvature	0.5
α_1	Rate constant associated with the first order slow tension recovery	$0.033\,\mathrm{ms}^{-1}$
α_2	Rate constant associated with the second order fast tension recovery	$2.850\,\mathrm{ms}^{-1}$
α_3	Rate constant associated with the second order fast tension recovery	$2.850\,\mathrm{ms}^{-1}$
A_1	Weighting coefficient associated with the first order slow tension recovery	50.0
A_2	Weighting coefficient associated with the second order fast tension recovery	175.0
A_3	Weighting coefficient associated with the second order fast tension recovery	175.0
	Potassium plateau current – I_{Kp}	
$\overline{g}_{Kp}$	Maxium plateau K^{+} channel conductance	$0.00828\,\mathrm{mS}\cdot\mu\mathrm{F}^{-1}$
	Potassium delayed rectifier – I_K	
$P_{Na,K}$	Na^{+} permeability of K^{+} channels	0.01833
	Extracellular sodium	
$[\mathrm{Na}^{+}]_o$	External Na^{+} concentration	$140.0\,\mathrm{mM}$
	Extracellular potassium	
$[\mathrm{K}^{+}]_o$	External K^{+} concentration	$5.4\,\mathrm{mM}$
	Sodium potassium exchange current – I_{NaK}	
$\overline{I_{NaK}}$	Maximum Na^{+}-K^{+} pump current	$1.3\,\mu\mathrm{A}\cdot\mathrm{cm}^{-2}$
$K_{m,Nai}$	Na^{+} half saturation constant for Na^{+}-K^{+} pump	$10.0\,\mathrm{mM}$
$K_{m,Ko}$	K^{+} half saturation constant for Na^{+}-K^{+} pump	$1.5\,\mathrm{mM}$

Table A.9 – continued on next page

Table A.9 – continued from previous page

	Sodium background current – $I_{Na,b}$	
$\overline{g}_{Na,b}$	Maximum background Na^+ current conductance	$0.00141\,\mathrm{mS}\cdot\mu\mathrm{F}^{-1}$
	Fast sodium channel – I_{Na}	
$\overline{g}_{Na}$	Maximum Na^+ channel conductance	$12.8\,\mathrm{mS}\cdot\mu\mathrm{F}^{-1}$
	Passive mechanics	
a_1	Limiting strain when cell is in tension	0.22
b_1	Curvature of the uniaxial stress-strian curve when the cell is in tension	1.0
k_1	relative contribution of the e_{11} strain energy term	0.2 kPa
a_2	Limiting strain when cell is in compression	0.41
b_2	Curvature of the uniaxial stress-strian curve when the cell is in compression	6.8
k_2	relative contribution of the e_{22} strain energy term	0.06 kPa
a_3	Limiting strain	1.037
b_3	Curvature of the uniaxial stress-strian curve	0.398
k_3	relative contribution of the e_{33} strain energy term	0.31 kPa

TABLE A.9: Model parameters for the coupled JRW–HMT model.

Variable	Definition	Initial value
t	Time	0.0 ms
V_m	Membrane potential	$-86.1638\,\mathrm{mV}$
$[\mathrm{Na}^+]_i$	Intracellular Na^+ concentration	10.2042 mM
$[\mathrm{Ca}^{2+}]_i$	Intracellular Ca^{2+} concentration	9.94893×10^{-5} nM
x	Gating variable for I_K	9.28836×10^{-4}
y	$I_{Ca(L)}$ inactivation gate (called f in CELL)	0.998983
h	I_{Na} inactivation gate	0.988354
m	I_{Na} activation gate	3.28302×10^{-2}
j	I_{Na} slow inactivation gate	0.992540
$[\mathrm{K}^+]_i$	Intracellular K^+ concentration	143.727 mM
$[\mathrm{Ca}^{2+}]_{NSR}$	Ca^{2+} concentration in uptake store (NSR)	1.24891 mM
$[\mathrm{Ca}^{2+}]_{JSR}$	Ca^{2+} concentration in release store (JSR)	1.17504 mM
$[\mathrm{Ca}^{2+}]_o$	Extracellular Ca^{2+} concentration	1.8 mM
$[\mathrm{Ca}^{2+}]_{SS}$	Ca^{2+} concentration within the subspace	1.36058×10^{-4} mM
P_{C_1}	Fraction of RyR channels in the P_{C_1} state	0.762527
P_{O_1}	Fraction of RyR channels in the P_{O_1} state	1.19168×10^{-3}
P_{O_2}	Fraction of RyR channels in the P_{O_2} state	6.30613×10^{-9}
P_{C_2}	Fraction of RyR channels in the P_{C_2} state	0.236283
C_0	L-type Ca^{2+} channel closed state mode normal	0.997208
C_1	L-type Ca^{2+} channel closed state mode normal	6.38897×10^{-5}
C_2	L-type Ca^{2+} channel closed state mode normal	1.535×10^{-9}
C_3	L-type Ca^{2+} channel closed state mode normal	1.63909×10^{-14}
C_4	L-type Ca^{2+} channel closed state mode normal	6.56337×10^{-20}
O	L-type Ca^{2+} channel conducting state mode normal	9.84546×10^{-21}
C_{Ca0}	L-type Ca^{2+} channel closed state mode Ca	2.72826×10^{-3}
C_{Ca1}	L-type Ca^{2+} channel closed state mode Ca	6.99215×10^{-7}
C_{Ca2}	L-type Ca^{2+} channel closed state mode Ca	6.71989×10^{-11}
C_{Ca3}	L-type Ca^{2+} channel closed state mode Ca	2.87031×10^{-15}
C_{Ca4}	L-type Ca^{2+} channel closed state mode Ca	4.59752×10^{-20}
O_{Ca}	L-type Ca^{2+} channel conducting state mode Ca	0.0

Table A.10 – continued on next page

Table A.10 – continued from previous page

$[\mathrm{LTRPNCa}]$	Concentration of Ca^{2+} bound to low-affinity Tn binding sites	$6.349973\ \mu\mathrm{M}$
$[\mathrm{HTRPNCa}]$	Concentration of Ca^{2+} bound to high-affinity Tn binding sites	$135.9813\ \mu\mathrm{M}$
λ	Extension ratio (see Footnote (1), page 158)	
T	Tension	$0.0\ \mathrm{kPa}$

TABLE A.10: Initial conditions for the coupled JRW–HMT model.

Appendix B

Model Implementation

The following listing gives the actual code developed to implement the models used in this thesis. The coupled model developed is included in the listings for each of the individual models.

B.1 DiFrancesco–Noble

SUBROUTINE DN(T,Y,F)

```
C#### Subroutine: DN
C###  Description:
C###    Called by the ODE integrator.

      IMPLICIT NONE
      INCLUDE 'cmiss$reference:b12.cmn'
      INCLUDE 'cmiss$reference:deoxs00.cmn'
      INCLUDE 'cmiss$reference:oxs002.cmn'
      INCLUDE 'cmiss$reference:oxs003.cmn'
!     Parameter List
      REAL*8 F(*),T,Y(*)

C *** Call RATES except when instantaneous IV plots are
C *** being computed
      IF(.NOT.((PMODE.EQ.1).AND.PLOTT)) THEN
        CALL DFN_RATES(Y,F)
      ENDIF
C *** In all cases compute currents and set voltage clamp
C *** if required
      CALL DFN_CURRENTS(Y,F)
C *** Compute changes in ion conc.s except when IV plots are
C *** being computed. Also compute when T=TSTART to obtain
C *** values for imNa and imCa for subroutines NAISS and CAISS.
      IF(.NOT.(PLOTT.AND.T.NE.TSTART)) THEN
        CALL DFN_CONCENTRATIONS(Y,F)
      ENDIF
      F1=F(1)

      RETURN
      END
```

SUBROUTINE DFN_RATES(Y,F)

```
C#### Subroutine: DFN_RATES
C###  Description:
C###    Computes the rate coefficients for the gating variables for
C###    HEART.
C###    This version (2.0) includes Hilgemann formulation of Ca current
C###    inactivation (series V and Ca instead of parallel formulation of
C###    the DiFrancesco-Noble model).
C###    Update 1.4 incorporated separate T & L channels for the "fast"
C###    calcium current.

      IMPLICIT NONE
      INCLUDE 'cmiss$reference:deoxs00.cmn'
      INCLUDE 'cmiss$reference:oxs001.cmn'
      INCLUDE 'cmiss$reference:oxs003.cmn'
      INCLUDE 'cmiss$reference:oxs004.cmn'
!     Parameter List
      REAL*8 F(*),Y(*) !,T
!     Local Variables
      REAL*8 FSS,Z3

      IF(Y(1).NE.ESAV) THEN
        CALL DFN_RATES_SUB(ALPHA,BETA,SHIFT,Y(1),FSS)
C *** DPN 19/03/1998 - adjust beta(15) with [Ca]i
        BETA(15) = BETA(15)*Y(4)
      ENDIF    ! end of computation of gate rate coefficients
C *** Check for quasi-instantaneous & steady state ivplots.
C *** For slow clamps set gates to steady state values.
C *** In mode 2 use steady state ina and isi negative to -85
C *** (note: this speeds computation.  if you wish to compute
C *** inward tail currents negative to -85 remove third condition)
      IF(SLOW.OR.PLOTT) THEN
        IF((.NOT.PLOTT).OR.(PMODE.GT.2)) THEN
          Y(5) = ALPHA(5)/(ALPHA(5)+BETA(5))
          F(5) = 0.0d0
          Y(6) = ALPHA(6)/(ALPHA(6)+BETA(6))
          F(6) = 0.0d0
        ENDIF
        Y(7) = ALPHA(7)/(ALPHA(7)+BETA(7))
        F(7) = 0.0d0
C ***   In CAMODE 7 use steady state value FSS
        IF(CAMODE.NE.7) THEN
          Y(8) = ALPHA(8)/(ALPHA(8)+BETA(8))
        ELSE
          Y(8) = FSS
        ENDIF
        F(8) = 0.0d0
        Y(9)  = ALPHA(9)/(ALPHA(9)+BETA(9))
        F(9)  = 0.0d0
        Y(10) = ALPHA(10)/(ALPHA(10)+BETA(10))
        F(10) = 0.0d0
        IF( (CAMODE.EQ.2).OR.(CAMODE.EQ.4).OR.(CAMODE.EQ.5)
     '  .OR.(CAMODE.EQ.6)) THEN
          Y(15) = ALPHA(15)/(ALPHA(15)+BETA(15))
        ELSE
          Y(15) = 1.0d0
        ENDIF
        F(15) = 0.0d0
        IF(PCA3.NE.0) THEN
          Y(16) = ALPHA(16)/(ALPHA(16)+BETA(16))
          Y(17) = ALPHA(17)/(ALPHA(17)+BETA(17))
        ELSE
          Y(16) = 0.0d0
          Y(17) = 0.0d0
        ENDIF
        F(16) = 0.0d0
        F(17) = 0.0d0                  ! correction  2.0
        IF(PCA2.NE.0) THEN
          Y(32) = ALPHA(32)/(ALPHA(32)+BETA(32))
          Y(33) = ALPHA(33)/(ALPHA(33)+BETA(33))
        ELSE
```

```
          Y(32) = 0.0d0
          Y(33) = 0.0d0
        ENDIF
        F(32) = 0.0d0
        F(33) = 0.0d0                  ! correction  2.0
        IF(TOMODE.NE.0) THEN
          Y(18) = ALPHA(18)/(ALPHA(18)+BETA(18))
          IF(TOMODE.EQ.2) THEN
            Y(19) = ALPHA(19)/(ALPHA(19)+BETA(19))
          ELSE
            Y(19) = 1.0d0
          ENDIF
        ELSE
          Y(18) = 1.0d0
          Y(19) = 1.0d0
        ENDIF
        F(18) = 0.0d0
        F(19) = 0.0d0
      ELSE
C ***   When not in slow mode, compute gate rates etc
C ***   compute dy/dt, dx/dt
        F(5) = SPEED(5)*(ALPHA(5)-Y(5)*(ALPHA(5)+BETA(5)))
        F(6) = SPEED(6)*(ALPHA(6)-Y(6)*(ALPHA(6)+BETA(6)))
C ***   compute dr/dt and dq/dt
        IF((TOMODE.NE.0)) THEN
          F(18) = SPEED(18)*(ALPHA(18)-Y(18)*(ALPHA(18)+BETA(18)))
          IF(TOMODE.EQ.2) THEN
            F(19) = SPEED(19)*(ALPHA(19)-Y(19)*(ALPHA(19)+BETA(19)))
          ELSE
            F(19) = 0.0d0
            Y(19) = 1.0d0
          ENDIF
        ELSE
          F(18) = 0.0d0
          F(19) = 0.0d0
          Y(18) = 1.0d0
          Y(19) = 1.0d0
        ENDIF
C ***   compute dd/dt, df/dt, & dh/dt
        F(7) = SPEED(7)*(ALPHA(7)-Y(7)*(ALPHA(7)+BETA(7)))
        IF(CAMODE.LE.6) THEN
C ***     When CAMODE.LT.7 use DiFrancesco-Noble formulation
          F(8) = SPEED(8)*(ALPHA(8)-Y(8)*(ALPHA(8)+BETA(8)))
        ELSE IF(CAMODE.EQ.7) THEN
C ***     When CAMODE=7 use Randy’s formulation
          F(8) = ALPHA(8)*(FSS-Y(8))
        ELSE IF(CAMODE.EQ.8) THEN
C ***     When CAMODE=8 use Hilgemann formulation
          Z1 = (1.0d0-Y(8))*(1.0d0-CACHOFF) ! -Ca/not V-inactivated
          Z3 = (1.0d0-Y(8))*CACHOFF         ! +Ca/not V-inactivated
          F(8) = SPEED(8)*(120.0d0*Z3+Z1)*BETA(8)-Y(8)*ALPHA(8)
        ENDIF
        IF( (CAMODE.EQ.2).OR.(CAMODE.EQ.4).OR.(CAMODE.EQ.5)
     '  .OR.(CAMODE.EQ.6)) THEN
          F(15) = SPEED(15)*(ALPHA(15)-Y(15)*(ALPHA(15)+BETA(15)))
        ELSE
          F(15) = 0.0d0
        ENDIF
C ***   compute dd3/dt and df3/dt
        IF(PCA3.NE.0) THEN
          F(16) = SPEED(16)*(ALPHA(16)-Y(16)*(ALPHA(16)+BETA(16)))
          F(17) = SPEED(17)*(ALPHA(17)-Y(17)*(ALPHA(17)+BETA(17)))
        ELSE
          F(16) = 0.0d0
          F(17) = 0.0d0
        ENDIF
C ***   compute d and f changes for T channel
        IF(PCA2.NE.0) THEN
          F(32) = SPEED(32)*(ALPHA(32)-Y(32)*(ALPHA(32)+BETA(32)))
          F(33) = SPEED(33)*(ALPHA(33)-Y(33)*(ALPHA(33)+BETA(33)))
        ELSE
          F(32) = 0.0d0
          F(33) = 0.0d0
        ENDIF
C ***   test whether ina at steady state
        IF(GNASS) THEN
          Y(9) = ALPHA(9)/(ALPHA(9)+BETA(9))
          F(9) = 0.0d0
        ELSE
          F(9) = SPEED(9)*(ALPHA(9)-Y(9)*(ALPHA(9)+BETA(9)))
        ENDIF
C ***   compute dm/dt when fast is true, else use steady state value
        IF(FAST) THEN
          F(10) = SPEED(10)*(ALPHA(10)-Y(10)*(ALPHA(10)+BETA(10)))
        ELSE
          Y(10) = ALPHA(10)/(ALPHA(10)+BETA(10))
          F(10) = 0.0d0
        ENDIF
      ENDIF
      RETURN
      END
```

SUBROUTINE DFN_RATES_SUB(ALPHA,BETA,SHIFT,POT,FSS)

```
C#### Subroutine: DFN_RATES_SUB
C###  Description:
C###    <html><pre>
C###    Computes the rate coefficients for the gating variables for
C###    HEART.
C###    This version (2.0) includes Hilgemann formulation of Ca current
C###    inactivation (series V and Ca instead of parallel formulation of
C###    the DiFrancesco-Noble model).
C###    Update 1.4 incorporated separate T & L channels for the "fast"
C###    calcium current.
C###    ALPHA(5) = y gate (I(f))
C###      "   6  = x gate (I(K))
C###      "   7  = d gate (Ca activation)
C###      "   8  = f gate (Ca inactivation)
C###      "   9  = h gate (Na inactivation gate)
C###      "  10  = m gate (Na activation gate)
C###      "  14  = Ca store repriming
C###      "  15  = slow Ca inactivation
C###      "  16  = D3 (activation of I(Ca,3) =I(Ca(L)) ??)
C###      "  17  = F3 (inactivation of I(Ca,3))
C###      "  18  = I(to) inactivation
C###      "  19  = I(to) activation
C###      "  32  = activation of T channel Ca current
C###      "  33  = inactivation of T channel Ca current
C###    </pre></html>

      IMPLICIT NONE
      INCLUDE ’cmiss$reference:b12.cmn’
      INCLUDE ’cmiss$reference:deoxs00.cmn’
      INCLUDE ’cmiss$reference:oxs003.cmn’
!     Parameter List
      REAL*8 ALPHA(33),BETA(33),SHIFT(33),SPEED(33),POT,FSS
!     Local Variables
      REAL*8 E0

C *** y rate equations as in MNT model with alpha/beta interchanged
      E0 = POT+52.0d0-SHIFT(5)
      ALPHA(5) = 0.05d0*DEXP(-0.067d0*E0)
      IF(DABS(E0).LT.1.d-5) THEN
        BETA(5) = 2.5d0
      ELSE
        BETA(5) = E0/(1.0d0-DEXP(-0.2d0*E0))
      ENDIF
      IF(KMODE.EQ.0) THEN
C *** x rate equations as in MNT model when kmode = 0
        E0 = POT+50.0d0-SHIFT(6)
        ALPHA(6) = 0.5d0*DEXP(0.0826d0*E0)/(1.0d0+DEXP(0.057d0*E0))
        E0 = POT+20.0d0-SHIFT(6)
        BETA(6) = 1.3d0*DEXP(-0.06d0*E0)/(1.0d0+DEXP(-0.04d0*E0))
      ELSE IF(KMODE.EQ.1) THEN
C *** x rates  based  on DiFrancesco,  Noma  & Trautwein  and Oxford
C *** sinus  results  when  kmode = 1
        E0 = POT+22.0d0-SHIFT(6)
        IF(DABS(E0).LT.1.d-4) THEN
          ALPHA(6) = 2.5d0
          BETA(6)  = 2.5d0
        ELSE
          ALPHA(6) = 0.5d0*E0/(1.0d0-DEXP(-E0/5.0d0))
          BETA(6)  = 0.357d0*E0/(DEXP(E0/7.0d0)-1.0d0)
        ENDIF
      ELSE IF(KMODE.EQ.2) THEN
C *** x rates slower in diastolic range if kmode = 2
        E0 = POT+22.0d0-SHIFT(6)
        IF(DABS(E0).LT.1.d-4) THEN
          ALPHA(6) = 2.5d0
          BETA(6)  = 2.5d0
        ELSE
          ALPHA(6) = 0.5d0*E0/(1.0d0-DEXP(-E0/5.0d0))
          BETA(6)  = 0.178d0*E0/(DEXP(E0/15.0d0)-1.0d0)
        ENDIF
      ELSE IF(KMODE.EQ.3) THEN
C *** Galveston rate functions used when kmode = 3
        E0 = POT+26.488d0-SHIFT(6)
        IF(DABS(E0).LT.1.d-4) THEN
          ALPHA(6) = 0.1072d0
        ELSE
          ALPHA(6) = 0.01344d0*E0/(1.0d0-DEXP(-0.124d0*E0))
        ENDIF
        BETA(6) = 0.2063d0*DEXP(-0.039268d0*E0)
      ENDIF
C *** Compute ca rates
      IF(CAMODE.EQ.1.OR.CAMODE.EQ.2.OR.CAMODE.EQ.5.OR.CAMODE.EQ.8)
     '  THEN
C *** If camode = 1, 2, 5 or 8 use ’Oxford’ sinus d & f
C *** CAMODE 8 is the Hilgemann formulation
        E0 = POT+24.0d0-SHIFT(7)
        IF(DABS(E0).LT.1.d-4) THEN
          ALPHA(7) = 120.0d0
        ELSE
          ALPHA(7) = 30.0d0*E0/(1.0d0-DEXP(-E0/4.0d0))
        ENDIF
        IF(DABS(E0).LT.1.d-4) THEN
          BETA(7) = 120.0d0
        ELSE
          BETA(7) = 12.0d0*E0/(DEXP(E0/10.0d0)-1.0d0)
        ENDIF
      ELSE IF(CAMODE.EQ.3.OR.CAMODE.EQ.4.OR.CAMODE.EQ.6) THEN
C *** if camode = 3, 4 or 6 use Galveston d equations
        E0 = POT+12.07d0-SHIFT(7)
        IF(DABS(E0).LT.1.d-4) THEN
          ALPHA(7) = 10.7d0
        ELSE
          ALPHA(7) = 18.1d0*E0/(1.0d0-DEXP(-0.169d0*E0))
        ENDIF
        BETA(7) = 40.18d0*DEXP(-0.0459d0*E0)
      ELSE IF(CAMODE.EQ.7) THEN
C *** if CAMODE=7 use Calgary d equations
        E0 = POT+9.1d0-SHIFT(7)
        ALPHA(7) = 10.0d0*E0/(1.0d0-DEXP(-E0/8.23d0))
        BETA(7)  = ALPHA(7)*DEXP(-E0/8.23d0)
      ENDIF
      IF(CAMODE.LE.6) THEN
C *** In all camodes except 7 & 8 use ’oxford’ f equations
        E0 = POT+34-SHIFT(8)
        IF(DABS(E0).LT.1.d-4) THEN
          ALPHA(8) = 25.0d0
        ELSE
          ALPHA(8) = 6.25d0*E0/(DEXP(E0/4.0d0)-1.0d0)
        ENDIF
        BETA(8) = 50.0d0/(1.0d0+DEXP(-E0/4.0d0))
      ELSE IF(CAMODE.EQ.7) THEN
C *** In CAMODE=7 use Randy’s f formulation
        E0 = 0.03368d0*(POT+10.0d0)
        E0 = E0*E0
        ALPHA(8) = 19.6978d0*DEXP(-E0)+19.78848d0
        FSS = (1.0d0-0.01d0)/(1.0d0+DEXP(-((-28.05d0-POT)/8.58d0)))
```

```
        FSS = FSS+0.01d0+1.0d0/(1.0d0+DEXP((50.0d0-POT)/20.0d0))
        BETA(8) = 0.0d0
      ELSE IF(CAMODE.EQ.8) THEN
C *** In CAMODE=8 use Hilgemann formulation
        E0 = POT+34.0d0-SHIFT(8)
        IF(DABS(E0).LT.1.d-4) THEN
          ALPHA(8) = 25.0d0
        ELSE
          ALPHA(8) = 6.25d0*E0/(DEXP(E0/4.0d0)-1.0d0)
        ENDIF
        BETA(8) = 12.0d0/(1.0d0+DEXP(-(E0/4.0d0)))
C *** Note: rest of Hilgemann form left until computation of F(8)
      ENDIF
      IF((CAMODE.EQ.2).OR.(CAMODE.EQ.4)) THEN
C *** In camode 2 or 4 compute slow ca inactivation
        E0 = POT+34.0d0-SHIFT(15)
        IF(DABS(E0).LT.1.d-4) THEN
          ALPHA(15) = 2.5d0
        ELSE
          ALPHA(15) = 0.625d0*E0/(DEXP(E0/4.0d0)-1.0d0)
        ENDIF
        BETA(15) = 5.0d0/(1.0d0+DEXP(-E0/4.0d0))
      ELSE IF((CAMODE.EQ.5).OR.(CAMODE.EQ.6)) THEN
C **  In camode 5 & 6  inactivation is ca induced using equation:
C **      df2/dt = alpha(15)(1 - f2)   -   beta(15)*cai*f2
C **  The equations use the relations:
C **      ALPHA(15) = 1/TAUF2
C **  Where TAUF2 is the limiting recovery time constant when (Ca)i->0
C **      BETA(15) = ALPHA(15)/KMINACT
C **  where KMINACT is (Ca)i for half inactivation in steady state.
C **
C **  For convenience in programming the actual BETA(15) in the program
C **  is (Ca)i*BETA(15). This enables the same differential equation to
C **  be used later in the program regardless of the value of CAMODE
        BETA(15) = ALPHA(15)/KMINACT
      ENDIF
C *** ca store repriming equations based on those for f for voltage dep.
      E0 = POT+34.0d0-SHIFT(14)
      IF(DABS(E0).LT.1.d-4) THEN
        ALPHA(14) = 2.5d0
      ELSE
        ALPHA(14) = 0.625d0*E0/(DEXP(E0/4.0d0)-1.0d0)
      ENDIF
      BETA(14) = 5.0d0/(1.0d0+DEXP(-E0/4.0d0))
C *** NB  HILGEMANN ITO STILL TO BE ADDED !!!!!!!!!!!!!!!!!!!!!!
C *** Ito inactivation based on Dario’s modification of Fozzard &
C *** Hiraoka (J.Physiol, 1973)
      IF(TOMODE.NE. 0) THEN
        E0 = POT-SHIFT(18)
        ALPHA(18) = 0.033d0*DEXP(-E0/17.0d0)
        BETA(18) = 33.0d0/(1.0d0+DEXP(-(E0+10.0d0)/8.0d0))
        IF(TOMODE.EQ.2) THEN
C ***   Ito activation based on MNT model equations
          E0 = POT-SHIFT(19)
          IF(DABS(E0).LT.1.d-4) THEN
            ALPHA(19) = 80.0d0
          ELSE
            ALPHA(19) = 8.0d0*E0/(1.0d0-DEXP(-0.1d0*E0))
          ENDIF
          BETA(19) = 80.0d0/(0.1d0+DEXP(0.0888d0*E0))
        ENDIF
      ENDIF
C *** Slow ca current: GP cell model
      IF(PCA3.NE.0) THEN
        E0 = POT+55.0d0-SHIFT(16)
        IF(DABS(E0).LT.1.d-4) THEN
          ALPHA(16) = 5.0d0
        ELSE
          ALPHA(16) = 1.25d0*E0/(1.0d0-DEXP(-E0/4.0d0))
        ENDIF
        IF(DABS(E0).LT.1.d-4) THEN
          BETA(16) = 5.0d0
        ELSE
          BETA(16) = 0.5d0*E0/(DEXP(E0/10.0d0)-1.0d0)
        ENDIF
        E0 = POT+45.0d0-SHIFT(17)
        IF(DABS(E0).LT.1.d-4) THEN
          ALPHA(17) = 0.84d0
        ELSE
          ALPHA(17) = 0.21d0*E0/(DEXP(E0/4.0d0)-1.0d0)
        ENDIF
        BETA(17) = 1.7d0/(1.0d0+DEXP(-E0/4.0d0))
      ENDIF
      IF(PCA2.NE.0) THEN
C *** Low threshold T channel
C *** provisionally, this channel is given the same equations as for
C *** the L channel (ICA). You should use SHIFT32, SHIFT33, SPEED32 and
C *** SPEED33 to shift the activation and inactivation curves and to
C *** increase the rates. When more information is available, these
C *** equations will be updated
        E0 = POT+24.0d0-SHIFT(32)
        IF(DABS(E0).LT.1.d-4) THEN
          ALPHA(32) = 120.0d0
        ELSE
          ALPHA(32) = 30.0d0*E0/(1.0d0-DEXP(-E0/4.0d0))
        ENDIF
        IF(DABS(E0).LT.1.d-4) THEN
          BETA(32) = 120.0d0
        ELSE
          BETA(32) = 12.0d0*E0/(DEXP(E0/10.0d0)-1.0d0)
        ENDIF
        E0 = POT+34.0d0-SHIFT(33)
        IF(DABS(E0).LT.1.d-4) THEN
          ALPHA(33) = 25.0d0
        ELSE
          ALPHA(33) = 6.25d0*E0/(DEXP(E0/4.0d0)-1.0d0)
        ENDIF
        BETA(33) = 50.0d0/(1.0d0+DEXP(-E0/4.0d0))
      ENDIF
      IF(NAMODE.EQ.1) THEN
C *** For NAMODE=1  m & h equations based on Colatsky & Brown,
C     Lee & Powell
        E0 = POT+41.0d0-SHIFT(10)
        IF(DABS(E0).LT.1.d-5) THEN
          ALPHA(10) = 2000.0d0
        ELSE
          ALPHA(10) = 200.0d0*E0/(1.0d0-DEXP(-0.1d0*E0))
        ENDIF
        BETA(10) = 8000.0d0*DEXP(-0.056d0*(POT+66.0d0-SHIFT(10)))
        ALPHA(9) = 20.0d0*DEXP(-0.125d0*(POT+75.0d0-SHIFT(9)))
        BETA(9)  = 2000.0d0/(320.0d0*DEXP(-0.1d0*(POT+75.0d0-
     ’    SHIFT(9)))+1.0d0)
      ELSE IF(NAMODE.EQ.2) THEN
C ***   For NAMODE=2 use Calgary atrial rate equations
        E0 = POT-31.23d0-SHIFT(10)
        ALPHA(10) = 757.22d0*E0/(1.0d0-DEXP(-0.0617d0*E0))
        E0 = POT+52.853d0-SHIFT(10)
        BETA(10) = 2256.5d0*DEXP(-0.0418d0*E0)
        E0 = POT+85.45d0-SHIFT(9)
        ALPHA(9) = 51.1d0*DEXP(-0.1235d0*E0)
        E0 = POT+2.91d0-SHIFT(9)
        BETA(9) = 1270.7d0/(2.5d0+DEXP(-0.0764d0*E0))
      ENDIF

      RETURN
      END
```

SUBROUTINE DFN_CURRENTS(Y,F)

```
C#### Subroutine: DFN_CURRENTS
C###  Description:
C###    Computes ionic currents for HEART
C###    This version includes the options for Hilgemann’s formulation of
C###    ITO (version 2.0) Anticipates Hilgemann Ca inactivation.

      IMPLICIT NONE
      INCLUDE ’cmiss$reference:deoxs00.cmn’
      INCLUDE ’cmiss$reference:oxs001.cmn’
      INCLUDE ’cmiss$reference:oxs003.cmn’
      INCLUDE ’cmiss$reference:oxs004.cmn’
!     Parameter List
      REAL*8 F(*),Y(*) !,T
!     Common blocks
      REAL*8                    IIto,IICaCa,IICaK,IICaNa,IIK,IINa,
     ’  IIFK,IIFNA
      COMMON /DFN_MAX_CURRENTS/ IIto,IICaCa,IICaK,IICaNa,IIK,IINa,
     ’  IIFK,IIFNA
!     Local Variables
      INTEGER L
      REAL*8 E0,ECA,EK,EKC(0:11),EMH,ENA,ENACA,
     ’  IBKC(0:11),ICAKC(0:11),IFKC(0:11),IFNAC(0:11),
     ’  IK1C(0:11),IKC(0:11),IMKC(0:11),IPC(0:11),
     ’  ITOC(0:11),ITOT,
     ’  Z2,Z3,Z4,Z5

      IIK = 0.0d0
      IICaCa = 0.0d0
      IICaK = 0.0d0
      IICaNa = 0.0d0
      IIto = 0.0d0
      IINa = 0.0d0
      IIFK = 0.0d0
      IIFNA = 0.0d0

      IF(CAMODE.EQ.8) THEN
        CACHOFF = Y(4)/(KCACHOFF+Y(4))
        CACHON  = (1.0d0-Y(8))*(1.0d0-CACHOFF)
      ELSE
        CACHON  = Y(8)
      ENDIF
C *** Assume 12% K leak in m3h channel
      ENA = -RTONF*DLOG(Y(2)/NAO)
      IF(SPACE.GT.2) THEN
        Z1 = Y(3)
      ELSE
        Z1 = K
      ENDIF
      EMH = RTONF*DLOG((NAO+PNAK*Z1)/(Y(2)+PNAK*Y(11)))
      IINa = GNA*(Y(1)-EMH)
      INA = Y(9)*Y(10)*Y(10)*Y(10)*IINa ! h * m*m*m * INa(max)
C *** Background inward current. Note that the background channel may
C *** either have separate values for GBNA & GBK or one may assume
C**** equal Na & K conductance (set GB only) as in Colqhoun,Neher,
C**** Reuter & Stevens.
      IBNA = GBNA*(Y(1)-ENA)
C *** Calculate Na Ca exchange current.
C *** For details of formulation of equations for inaca see Mullins,L.
C *** 1977  J.gen.physiol. 70, 681-695
C *** 1981  Ion Transport in Heart. Raven press and
C *** Noble, D. (1986) In Cardiac Muscle: Regulation of Exitation
C *** and Contraction ( Ed R.D. Nathan), Academic Press.
C *** Note that the procedure will hold inaca constant if ivplot is not
C *** instantaneous to eliminate large transient inaca at very negative
C *** potentials
      IF(.NOT.(MODE.LT.7.AND.PLOTT.AND.PMODE.GT.1)) THEN
        IF(Y(4).LT.1.d-8) Y(4) = 1.d-8
        ECA = -0.5d0*RTONF*DLOG(Y(4)/CAO)
        IF(Y(2).LT.1.d-5) Y(2) = 1.d-5
        IF(INT(NNACA+.01d0).EQ.2) THEN
          INACA = 0.0d0
        ELSE
          ENACA = (NNACA*ENA-2.0d0*ECA)/(NNACA-2.0d0)
          Z1 = RTONF*2.0d0/(NNACA-2.0d0)
          IF(NMODE.EQ.0) THEN
C ***       When NMODE is 0 use simple sinh formulation for inaca
C ***       Strongly recommended not to use this mode
            INACA = KNACA*(DEXP((Y(1)-ENACA)/Z1)-DEXP(-(Y(1)-ENACA)
     ’        /Z1))/2.0d0
          ELSE IF(NMODE.EQ.1) THEN
```

```
C ***       When NMODE is 1 use Ca and Na activated inaca
            Z4 = 1.0d0
            Z5 = 1.0d0
            DO L = 1,INT(NNACA+.01d0)   !CMISS 21/3/89
              Z4 = Z4*NAO
              Z5 = Z5*Y(2)
            ENDDO
            Z2 = 1.0d0+DNACA*(Y(4)*Z4+CAO*Z5)
            Z3 = Z5*CAO*DEXP(2.0d0*YNACA*Y(1)/Z1)
            Z3 = Z3-Z4*Y(4)*DEXP(-2.0d0*(1.0d0-YNACA)*Y(1)/Z1)
            INACA = KNACA*Z3/Z2
          ENDIF
          IF(DABS(INACA).GT.INACAM) THEN
            IF(INACA.GT.0.0d0) THEN
              INACA =  INACAM
            ELSE
              INACA = -INACAM
            ENDIF
          ENDIF
          IF(KNACA.LT.0.0d0) INACA = 0.0d0
        ENDIF
      ENDIF
C *** Background inward calcium current
      IBCA = GBCA*(Y(1)-ECA)
      IF(SPACE.GT.2) THEN
C ***   Compute K dependent currents for 3 compartment model and for
C ***   non-restricted ecs
        IF(Y(3).LT.1.d-5) Y(3) = 1.d-5
        EK = RTONF*DLOG(Y(3)/Y(11))
C ***   IK1 rectifier described by blocking particle model with K activation.
C ***   K activation uses Michaelis Menten - cf Sakmann & Trube
        E0 = Y(1)-EK+10.0d0-SHIFTK1
        IK1 = GK1*(Y(3)/(KMK1+Y(3)))*(Y(1)-EK)/(1.0d0+DEXP(E0/
     ’    (0.5d0*RTONF)))
        IF(TOMODE.EQ.0.OR.TOMODE.EQ.1) THEN
C ***     When TOMODE.EQ.0,1 ito described by outward rectifier with
C ***     instantaneous voltage activation
          E0 = Y(1)+10.0d0-SHIFTTO
          IF(DABS(E0).LT.1.d-4) THEN
            ITO = 1.4d0*(0.2d0+(Y(3)/(KMTO+Y(3))))
          ELSE
            ITO = 0.28d0*(0.2d0+(Y(3)/(KMTO+Y(3))))*E0/(1.0d0-
     ’        DEXP(-0.2d0*E0))
          ENDIF
          ITO = GTO*ITO*(Y(11)*DEXP(0.02d0*Y(1))-Y(3)*DEXP(-0.02d0*
     ’      Y(1)))
C ***     DPN 1/4/98 - grab the max (steady-state??) current
          IIto = ITO
          IF(TOMODE.EQ.1) ITO = Y(18)*ITO
        ELSE IF(TOMODE.EQ.2) THEN
C ***     When TOMODE=2 use full equations
          IIto = 0.28d0*(0.2d0+(Y(3)/(KMTO+Y(3))))
          IIto = GTO*ITO*(Y(11)*DEXP(0.02d0*Y(1))-Y(3)*DEXP(-0.02d0*
     ’      Y(1)))
          ITO = Y(18)*Y(19)*IIto
        ELSE IF(TOMODE.EQ.3.OR.TOMODE.EQ.4) THEN
C ***     When TOMODE=3,4 use Hilgemann formulation
          E0 = Y(1)-SHIFTTO
          IF(TOMODE.EQ.4) THEN
            F(17) = ((1.0d0/(1.0d0+DEXP(-(Y(1)+35.0d0)/5.0d0)))-
     ’        Y(17))*ALPHA(17)
          ELSE
            F(17) = 0.0d0
            Y(17) = (1.0d0/(1.0d0+DEXP(-(Y(1)+35.0d0)/5.0d0)))
          ENDIF
C ???     DPN 1/4/98 - grab the max (steady-state??) current  ???
C          ITO = GTO*Y(17)*(Y(1)-EK)/(1.0d0+DEXP(E0/25.0d0))
           IIto = GTO*(Y(1)-EK)/(1.0d0+DEXP(E0/25.0d0))
           ITO = IIto * Y(17)
        ENDIF
C ***   IK uses rate theory inward rectifier, no -ve slope, no xover
        IIK = IKM*(Y(11)-Y(3)*DEXP(-Y(1)/RTONF))/140.0d0
        IK  = Y(6)*IIK ! x * IIK
        IF(KMODE.EQ.3) IK = Y(6)*IK
C ***   Version 1.3 uses Acetyl-choline activated channel with i(V)
C ***   relation based on IK fully-activated relation
        IACH = IACHM*(Y(11)-Y(3)*DEXP(-Y(1)/RTONF))/140.0d0
C ***   IF(based on DiFrancesco (1981,1982) - K activation with
C ***   linear K and Na components
        IIFK  = GFK *(Y(3)/(KMF+Y(3)))*(Y(1)-EK)
        IIFNA = GFNA*(Y(3)/(KMF+Y(3)))*(Y(1)-ENA)
        IFK  = Y(5)*IIFK
        IFNA = Y(5)*IIFNA
C ***   K component of ICA assumes 1% K permeability
        Z1 = PCAK*PCA*(Y(1)-VSURFCA)/(RTONF*(1.0d0-DEXP(-(Y(1)-VSURFCA)/
     ’    RTONF)))
        IICaK = Z1*(Y(11)*DEXP(VSURFCA/RTONF)
     ’    -Y(3)*DEXP(-(Y(1)-VSURFCA)/RTONF))
        ICAK = Y(7) * CACHON * IICaK !cachon = f, y(7) = d
        IF((CAMODE.EQ.2).OR.(CAMODE.EQ.4).OR.(CAMODE.EQ.5).OR.
     ’    (CAMODE.EQ.6)) ICAK = Y(15)*ICAK
C ***   NaK pump current activated by Nai and Kc
        IP = PUMP*(Y(2)/(KMNA+Y(2)))*Y(3)/(KM+Y(3))
C ***   K contribution to background channel
        IBK = GBK*(Y(1)-EK)
C ***   Compute total K flux as a current.
C ***   Note that version 2.0 includes ITO in this sum
        IMK = IK+IK1+IFK+ICAK+IBK+ITO-IP/(NNAK-1.0d0)
      ELSE IF(SPACE.LT.3) THEN
C ***   All K dependent currents computed as function of (K)c and of
C ***   radial distance for cylinder or sphere.
C ***   current functions otherwise same as in previous section
        DO L = 0,DEPTH
          IF(KCE(L).LT.1.d-4) KCE(L) = IDINT(1.d-4) !1.d-4
          EKC(L) = RTONF*DLOG(KCE(L)/Y(11))
          E0 = Y(1)-EKC(L)+10.0d0-SHIFTK1
          IK1C(L) = GK1*(KCE(L)/(KMK1+KCE(L)))*(Y(1)-EKC(L))
          IK1C(L) = IK1C(L)/(1.0d0+DEXP(E0/(0.5d0*RTONF)))
          E0 = Y(1)+10.0d0-SHIFTTO
          IF(DABS(E0).LT.0.001d0) THEN
            ITOC(L) = 5.0d0*(0.2d0+(KCE(L)/(KMTO+KCE(L))))
          ELSE
            ITOC(L) = (0.2d0+(KCE(L)/(KMTO+KCE(L))))*E0/(1.0d0
     ’        -DEXP(-0.2d0*E0))
          ENDIF
          ITOC(L)  = 0.28d0*GTO*ITOC(L)*(Y(11)*DEXP(0.02d0*Y(1))
     ’      -KCE(L)*DEXP(-0.02d0*Y(1)))
          IF(TOMODE.NE.0) ITOC(L) = Y(18)*ITOC(L)
          IKC(L)   = IKM*(Y(11)-KCE(L)*DEXP(-Y(1)/RTONF))/140.0d0
          IFKC(L)  = GFK*(KCE(L)/(KMF+KCE(L)))*(Y(1)-EKC(L))
          IFNAC(L) = GFNA*(KCE(L)/(KMF+KCE(L)))*(Y(1)-ENA)
          IPC(L) = PUMP*(Y(2)/(KMNA+Y(2)))*KCE(L)/(KM+KCE(L))
          Z1 = PCAK*PCA*(Y(1)-VSURFCA)/(RTONF*(1.0d0-DEXP(-(Y(1)-
     ’      VSURFCA)/RTONF)))
          ICAKC(L) = Z1*(Y(11)*DEXP(VSURFCA/RTONF)
     ’      -KCE(L)*DEXP(-(Y(1)-VSURFCA)/RTONF))
          IBKC(L) = GBK*(Y(1)-EKC(L))
          IF((CAMODE.EQ.2).OR.(CAMODE.EQ.4).OR.(CAMODE.EQ.5).OR.
     ’      (CAMODE.EQ.6)) THEN
            IF(KMODE.EQ.3) THEN
              IMKC(L) = Y(6)*Y(6)*IKC(L)+IK1C(L)+Y(5)*IFKC(L)+
     ’          Y(7)*Y(15)*ICAKC(L)+IBKC(L)-IPC(L)/(NNAK-1.0d0)
            ELSE
              IMKC(L) = Y(6)*IKC(L)+IK1C(L)+Y(5)*IFKC(L)+Y(7)*Y(15)*
     ’          ICAKC(L)+IBKC(L)-IPC(L)/(NNAK-1.0d0)
            ENDIF
          ELSE
            IF(KMODE.EQ.3) THEN
              IMKC(L) = Y(6)*Y(6)*IKC(L)+IK1C(L)+Y(5)*IFKC(L)+
     ’          Y(7)*ICAKC(L)+IBKC(L)-IPC(L)/(NNAK-1.0d0)
            ELSE
              IMKC(L) = Y(6)*IKC(L)+IK1C(L)+Y(5)*IFKC(L)+Y(7)*ICAKC(L)+
     ’          IBKC(L)-IPC(L)/(NNAK-1.0d0)
            ENDIF
          ENDIF
        ENDDO
        K   = 0.0d0
        IK1 = 0.0d0
        IK  = 0.0d0
        IFK = 0.0d0
        IIFK = IFK
        IBK = 0.0d0
        IFNA= 0.0d0
        IIFNA = IFNA
        IP  = 0.0d0
        IMK = 0.0d0
        ICAK= 0.0d0
        IICaK = ICAK
        ITO = 0.0d0
        IACH= 0.0d0
      ENDIF
C *** Total K dependent currents obtained by integrating radially
      IF(SPACE.EQ.1) THEN
C ***   Cylindrical case
        DO L = 1,DEPTH
          Z1 = (DBLE(L)-0.5d0)/DBLE(DEPTH*DEPTH)
          IK1 = IK1+(IK1C(L-1)+IK1C(L))*Z1
          ITO = ITO+(ITOC(L-1)+ITOC(L))*Z1
          IIK = IIK+(IKC(L-1)+IKC(L))*Z1
          IF(KMODE.EQ.3) THEN
            IK = IK + (Y(6)*Y(6)*IKC(L-1)+Y(6)*Y(6)*IKC(L))*Z1
          ELSE
            IK = IK + (Y(6)*IKC(L-1)+Y(6)*IKC(L))*Z1
          ENDIF
C ***     Version 1.3 --- Set IACH if needed
          IIFK = IIFK+(IFKC(L-1)+IFKC(L))*Z1
          IIFNA = IIFNA+(IFNAC(L-1)+IFNAC(L))*Z1
          IFK = IFK+(Y(5)*IFKC(L-1)+Y(5)*IFKC(L))*Z1
          IFNA = IFNA+(Y(5)*IFNAC(L-1)+Y(5)*IFNAC(L))*Z1
          IP = IP+(IPC(L-1)+IPC(L))*Z1
          IF((CAMODE.EQ.2).OR.(CAMODE.EQ.4).OR.(CAMODE.EQ.5).OR.
     ’      (CAMODE.EQ.6)) THEN
            ICAK = ICAK+(Y(7)*Y(15)*ICAKC(L-1)+Y(7)*Y(15)*ICAKC(L))*Z1
          ELSE
            ICAK = ICAK+(Y(7)*ICAKC(L-1)+Y(7)*ICAKC(L))*Z1
          ENDIF
          IICaK = IICaK + (ICAKC(L-1)+ICAKC(L))*Z1
          IBK = IBK+(IBKC(L-1)+IBKC(L))*Z1
          IMK = IMK+(IMKC(L-1)+IMKC(L))*Z1
          K = K+(KC(L-1)+KC(L))*Z1
        ENDDO
      ELSE IF(SPACE.EQ.2) THEN
C ***   Spherical case
        DO L = 1,DEPTH
          Z1 = DBLE(L*L*L-(L-1)*(L-1)*(L-1))/DBLE(DEPTH*DEPTH*DEPTH)
          IK1 = IK1+0.5d0*(IK1C(L-1)+IK1C(L))*Z1
          ITO = ITO+0.5d0*(ITOC(L-1)+ITOC(L))*Z1
          IIK = IIK+0.5d0*(IKC(L-1)+IKC(L))*Z1
          IF(KMODE.EQ.3) THEN
            IK = IK+0.5d0*(Y(6)*Y(6)*IKC(L-1)+Y(6)*Y(6)*IKC(L))*Z1
          ELSE
            IK = IK+0.5d0*(Y(6)*IKC(L-1)+Y(6)*IKC(L))*Z1
          ENDIF
C ***     Version 1.3  ------- Set IACH if needed
          IIFK = IFK+0.5d0*(IFKC(L-1)+IFKC(L))*Z1
          IIFNA = IFNA+0.5d0*(IFNAC(L-1)+IFNAC(L))*Z1
          IFK = IFK+0.5d0*(Y(5)*IFKC(L-1)+Y(5)*IFKC(L))*Z1
          IFNA = IFNA+0.5d0*(Y(5)*IFNAC(L-1)+Y(5)*IFNAC(L))*Z1
          IP = IP+0.5d0*(IPC(L-1)+IPC(L))*Z1
          IF((CAMODE.EQ.2).OR.(CAMODE.EQ.4).OR.(CAMODE.EQ.5).OR.
     ’      (CAMODE.EQ.6)) THEN
            ICAK = ICAK+0.5d0*(Y(7)*Y(15)*ICAKC(L-1)+
     ’        Y(7)*Y(15)*ICAKC(L))*Z1
          ELSE
            ICAK = ICAK+0.5d0*(Y(7)*ICAKC(L-1)+
     ’        Y(7)*ICAKC(L))*Z1
          ENDIF
          IICAK = IICAK+0.5d0*(ICAKC(L-1)+ICAKC(L))*Z1
          IBK = IBK+0.5d0*(IBKC(L-1)+IBKC(L))*Z1
          IMK = IMK+0.5d0*(IMKC(L-1)+IMKC(L))*Z1
          K = K+0.5d0*(KC(L-1)+KC(L))*Z1
        ENDDO
      ENDIF
C *** For details of formulation of components of ICA see
C *** Reuter & Scholz, J.Physiol,1977,264,17-47
C *** The formulation here uses the constant field
C *** current voltage relations from that paper but does not
C *** use their (incorrect) equation for the channel
C *** reversal potential. See Campbell, Giles, Hume & Noble,
C *** J.Physiol (1987). The reversal potential is computed in
C *** procedure CAREV.
! DPN 19/02/98 CAREV unused ???
C**
C *** The correspondence with patch clamp work is that ICA
C *** corresponds best to the L current, ICA2 corresponds to
C *** the T current and ICA3 corresponds to the ICas of
```

```
C *** Lee et al, Proc Roy Soc 1984
      Z1 = (Y(1)-VSURFCA)/(RTONF*(1.0d0-DEXP(-(Y(1)-VSURFCA)/
     '  (0.5d0*RTONF))))
      Z1 = Z1*(Y(4)*DEXP(VSURFCA/(0.5d0*RTONF))
     '  -CAO*DEXP(-(Y(1)-VSURFCA)/(0.5d0*RTONF)))
      IICaCa = 4.0d0*PCA*Z1
      ICACA = Y(7) * CACHON * IICaCa
      IF(PCA2.NE.0.0d0) THEN
        ICA2 = 4.0d0*PCA2*Y(32)*Y(33)*Z1
      ELSE
        ICA2 = 0.0d0
      ENDIF
      IF(PCA3.NE.0.0d0) THEN
        ICA3 = 4.0d0*PCA3*Y(16)*Y(17)*Z1
      ELSE
        ICA3 = 0.0d0
      ENDIF
      Z1 = PCAK*PCA*(Y(1)-VSURFCA)/(RTONF*(1.0d0-DEXP(-(Y(1)-VSURFCA)/
     '  RTONF)))
      IICaNa = Z1*(Y(2)*DEXP(VSURFCA/RTONF)
     '  -NAO*DEXP(-(Y(1)-VSURFCA)/RTONF))
      ICANA = Y(7) * CACHON * IICaNa
      IF((CAMODE.EQ.2).OR.(CAMODE.EQ.4).
     'OR.(CAMODE.EQ.5).OR.(CAMODE.EQ.6)) THEN
        ICANA = Y(15)*ICANA
        ICACA = Y(15)*ICACA
      ENDIF
      IF(CANMODE.EQ.0) THEN
        ICANA = 0.0d0
        IICaNa = 0.0d0
      ENDIF
      ICA = ICACA+ICANA+ICAK
C *** Compute activation of Ca sensitive currents (other than inaca)
C *** each current is computed according to equation
C *** i  =  i ( mi  +  (cai/(cai + cact))
C *** where mi is minimum value of current, expressed as a fraction
C *** of the value in amode 0 and cact is the calcium concentration
C *** for half-activation
      IF((AMODE.EQ.1).OR.(AMODE.EQ.9)) THEN
        IK1 = IK1*(MIK1+(Y(4)/(Y(4)+CACT(1))))
      ENDIF
      IF((AMODE.EQ.2).OR.(AMODE.EQ.9)) THEN
        IK = IK*(MIK+(Y(4)/(Y(4)+CACT(2))))
      ENDIF
      IF((AMODE.EQ.3).OR.(AMODE.EQ.9)) THEN
        IBK  = IBK *(MIB+(Y(4)/(Y(4)+CACT(3))))
        IBNA = IBNA*(MIB+(Y(4)/(Y(4)+CACT(3))))
      ENDIF
      IF((AMODE.EQ.4).OR.(AMODE.EQ.9)) THEN
        ITO = ITO*(MITO+(Y(4)/(Y(4)+CACT(4))))
      ENDIF
      IF((AMODE.EQ.5).OR.(AMODE.EQ.9)) THEN
        INAK = 0.5d0*(Y(4)/(Y(4)+CACT(3)))*(GNAK*(Y(1)-ENA)+GNAK*(Y(1)-
     '    EK))
      ENDIF
C *** Total current
C *** DPN 15/04/98 - adding switches to each current
      ITOT = ISWTCH(16)*INA+ISWTCH(5)*ICA+ISWTCH(6)*ICA2+ISWTCH(7)*ICA3
     '  +ISWTCH(13)*IK+ISWTCH(12)*IFNA+ISWTCH(11)*IFK+ISWTCH(19)*IP
     '  +ISWTCH(4)*IBNA+ISWTCH(3)*IBK+ISWTCH(2)*IBCA+ISWTCH(14)*IK1
     '  +ISWTCH(20)*ITO+IPULSE+STIM+ISWTCH(17)*INACA+ISWTCH(18)*INAK
      ITOT = ITOT+ISWTCH(1)*IACH                    !Version 1.3
C *** Set dV/dt = 0 to give voltage clamp (modes 2 - 8).
C *** In  mode  2 compute effect of series resistance and of
C *** external clamp circuit. In action potential mode set
C *** dV/dt = - total current/capacitance
      IF(CLAMP) THEN
        F(1) = 0.0d0
      ELSE
        F(1) = -CAP*ITOT
      ENDIF
      IF(MODE.EQ.2) THEN
        IF((RS.NE.0.0d0).AND.(AMP.EQ.0.0d0)) THEN
          F(1) = (EC-Y(1)-ITOT*RS)/(C*RS)
        ENDIF
        IF(AMP.NE.0.0d0) THEN
          F(1) = (-ITOT+(AMP*(EC-Y(1))/(RE+RS*(1.0d0+AMP))))/C
        ENDIF
      ENDIF

      RETURN
      END
```

SUBROUTINE DFN_CONCENTRATIONS(Y,F)

```
C#### Subroutine: DFN_CONCENTRATIONS
C###  Description:
C###    Computes ion concentrations for HEART

      IMPLICIT NONE
      INCLUDE ’cmiss$reference:deoxs00.cmn’
      INCLUDE ’cmiss$reference:oxs001.cmn’
      INCLUDE ’cmiss$reference:oxs003.cmn’
      INCLUDE ’cmiss$reference:oxs004.cmn’
      INCLUDE ’cmiss$reference:oxs005.cmn’
!     Parameter List
      REAL*8 F(*),Y(*)!,T
!     Local Variables
      INTEGER L,NNREL
      REAL*8 CAFMIT,ENA,
     ’  FCTROP,FCYT,FMTROP,FSR,
     ’  IMCA,
     ’  IMNA,IREL,ITRAN,IUP,
     ’  Z2,Z3,Z4,Z5!,DCNP,DCP,FCYTFREE,FSRFREE

C *** d(Na)i/dt = net sodium current/(F x internal volume)
C *** assume fraction of ibna carried by Na prop. to (Na)o
      IMNA = INA+(IBNA*NAO/140.0d0)+IFNA+ICANA+(IP*NNAK/(NNAK-1.0d0))
      IF(NNACA.GT.2.0d0) IMNA = IMNA+INACA*NNACA/(NNACA-2.0d0)
      F(2) = -IMNA/VIF
C *** Add Na change due to perfusion
      IF(SPACE.EQ.5) F(2) = F(2)+(NAPE-Y(2))/TNAP
C *** For 3 compartment case set d(K)c/dt = iK/VF - K diffusion
      IF(SPACE.EQ.3) THEN
        F(3) = IMK/VF-PF*(Y(3)-KB)
      ELSE
        F(3) = 0.0d0
      ENDIF
C *** When ecs is not restricted, set [K]c = K[b]
      IF((SPACE.EQ.4).OR.(SPACE.EQ.5)) Y(3) = KB
C *** Compute mitochondrial calcium
      IF(MMODE.EQ.1) THEN
        Z1 = (KCMUP/Y(4))**NCMUP
        Z1 = ALPHA(25)/(1.0d0+Z1)
        Z2 = (KNMREL/Y(2))**NNMREL
        Z3 = 1.0d0/(1.0d0+KCMREL/Y(25))
        Z2 = BETA(25)*Z3/(1.0d0+Z2)
        Z4 = 0.0639d0*Z3*BETA(25)
        Z1 = Z1-Z2-Z4
        F(25) = Z1/VMIT
        CAFMIT = Z1/VI
      ELSE
        F(25) = 0.0d0
      ENDIF
C *** Compute calcium stores
      IF(.NOT.CASS) THEN
        IF(BMODE.EQ.0) THEN           ! D-N formulation
          DO L = 20,23
            F(L) = 0.0d0
          ENDDO
        ELSE IF(BMODE.EQ.1) THEN      ! Calgary formulation
          F(20) = ALPHA(20)*Y(4)*(1.0d0-Y(20))-BETA(20)*Y(20)
          F(21) = ALPHA(21)*Y(4)*(1.0d0-Y(21))-BETA(21)*Y(21)
          F(22) = ALPHA(22)*MG*(1.0d0-Y(22)-Y(23))-BETA(22)*Y(22)
          F(23) = ALPHA(23)*Y(4)*(1.0d0-Y(22)-Y(23))-BETA(23)*Y(23)
        ELSE IF(BMODE.EQ.2) THEN      ! Hilgemann formulation
          IF(BUFFAST) THEN
            F(31)= 0.0d0
            Y(31)= Y(4) + Y(20) + Y(21)
            F(21)=(CTROP-Y(21))*ALPHA(21)*Y(4)-Y(21)*BETA(21)
            F(20)=(MTROP-Y(20))*ALPHA(20)*Y(4)-Y(20)*BETA(20)
          ELSE
C ***       Calculate steady state buffers using the Hilgemann formulation.
            CONTINUE=.TRUE.
            DO WHILE(CONTINUE)
              Z2 = Y(21)
              Z3 = Y(20)
              Y(21) = (CTROP*(Y(20)-Y(31)))/
     ’          (Y(21)-Y(31)-CTROP+Y(20)-BETA(21)/ALPHA(21))
              Y(20) = (MTROP*(Y(21)-Y(31)))/
     ’          (Y(20)-Y(31)-MTROP+Y(21)-BETA(20)/ALPHA(20))
              IF((DABS((Z2-Y(21))/Y(21))+DABS((Z3-Y(20))
     ’          /Y(20))).LT.0.001d0) CONTINUE=.FALSE.
            ENDDO
            Y(4)  = Y(31)-Y(20)-Y(21)
            F(4)  = 0.0d0
            F(21) = 0.0d0
            F(20) = 0.0d0
          ENDIF
          CACHOFF = Y(4)/(KCACHOFF+Y(4))
          FCTROP  = Y(21)/CTROP
          FMTROP  = Y(20)/MTROP
          F(22)   = 0.0d0
          F(23)   = 0.0d0
        ENDIF
        IF(SRMODE.EQ.0) THEN          ! SR calcium release and trans-
fer zero
          DO L = 12,14
            F(L) = 0.0d0
            Y(L) = 0.0d0
          ENDDO
          DO L = 26,28
            F(L) = 0.0d0
            Y(L) = 0.0d0
          ENDDO
          IUP   = 0.0d0
          IREL  = 0.0d0
          ITRAN = 0.0d0
        ELSE IF(SRMODE.EQ.1) THEN     ! DiFrancesco-Noble SR model
          IUP   = ALPHA(12)*Y(4) *(CA12M-Y(12))
          ITRAN = ALPHA(13)*Y(14)*(Y(12)-Y(13))
C ***     When rmode is zero repriming is voltage dependent
          IF(RMODE.EQ.0) THEN
            F(14) = SPEED(14)*(ALPHA(14)*(1.0d0-Y(14))-BETA(14)*Y(14))
          ELSE
            Y(14) = 1.0d0
            F(14) = 0.0d0
          ENDIF
          Z4 = 1.0d0
          Z5 = 1.0d0
          NNREL=INT(NREL+0.1d0) !CMISS addition 21/3/89
          DO L = 1,NNREL
            Z5 = Z5*Y(4)
            Z4 = Z4*KMCA
          ENDDO
          IREL  = BETA(13)*Y(13)*Z5/(Z5+Z4)
          F(12) = (IUP -ITRAN)/(2.0d0*V12F)
          F(13) = (ITRAN-IREL)/(2.0d0*V13F)
          DO L = 26,30
            F(L) = 0.0d0
            Y(L) = 0.0d0
          ENDDO
        ELSE IF(SRMODE.EQ.2) THEN       ! Hilgemann formulation
          Z3 = DEXP(0.08d0*(Y(1)-40.0d0))    ! Voltage dependence of release
          Z1 = Y(4)/(Y(4)+0.0005d0)
          Z1 = Z1*Z1                    ! Regulatory Ca binding site
          Z4 = BETA(26)*Z1+ALPHA(26)*Z3 ! Activation rate
          Z2 = BETA(27)*Z1+ALPHA(27)    ! Inactivation rate
          Y(26) = 1.0d0-Y(28)-Y(27)
```

```
          F(26) = Y(28)*BETA(28)-Y(26)*Z4    ! Precursor fraction
          F(27) = Y(26)*Z4-Y(27)*Z2          ! Activator fraction
          F(28) = Y(27)*Z2-Y(28)*BETA(28)    ! Product   fraction
          BETA(13) = Y(27)/(Y(27)+0.25d0)
          BETA(13) = BETA(13)*BETA(13)       ! Open rel channel fraction
          ITRAN = ALPHA(13)*(Y(12)-Y(13))    ! Change in uptake store
C ***     SR PUMP EQUATIONS
C ***     NOTE that all concentration changes to and from the cytosol
C ***     are calculated as concentration changes with respect to the
C ***     cytosol, and related by fractional volumes to the changes of
C ***     other states
          Z1 = KCYCA*KXCS/KSRCA                 ! K1 in paper
          Z2 = Y(4)+Y(12)*Z1+KCYCA*KXCS+KCYCA   ! K2 in paper
          FCYT = Y(4)/Z2                        ! Fr uptake Ca sites
          FSR  = Y(12)*Z1/Z2                    ! Fr back SR sites
          IUP = FCYT*ALPHA(12)-FSR*BETA(12)     ! SR Ca uptake
          F(12) = IUP*VI/SRVOL-ITRAN            ! Uptake store
          IREL  = (BETA(13)*KMCA+SRleak)*Y(13)  ! Conc change of rel st
          F(13) = ITRAN*V12/V13-IREL            ! Release store
C ***     Note: W(8)=10 =0.2/0.02=fsrrel/fsrup -See Hilgemann PCIN1.PAS
        ENDIF
        IMCA = ICACA+IBCA+ICA2+ICA3-2.0d0*INACA/(NNACA-2.0d0)
        IF(SRMODE.LT.2) THEN     ! Pre-Hilgemann formulations
          IF(CABUFF) THEN
            F(4) = 0.0d0
          ELSE
            F(4) = (-IMCA+IREL-IUP)/(2.0d0*VIF)
            IF(BMODE.GT.0) THEN
C ***         When BMODE = 1 use Calgary buffer equations to subtract
C ***         calcium taken up by buffers and to adjust calcium space
              Z1 = NCALMOD*CALMOD*F(20)+NCTROP*CTROP*F(21)
              Z1 = Z1+NMTROP*MTROP*F(23)
              F(4) = F(4)/(CAVOL*BUFVOL)
              F(4) = F(4)-Z1
            ENDIF
          ENDIF
        ELSE                     ! Hilgemann formulation
          IF(SLPUMPMODE) THEN
            IMCA = IMCA+(Y(4)/(Y(4)+KMSLPUMP))*KSLPUMP
          ENDIF
          IF(BUFFAST) THEN
            F(4) = -IMCA/(2.0d0*VIF)-IUP+IREL*SRVOL*V13/(VI*V12)-F(21)-
     '        F(20)
          ELSE
            F(31)= -IMCA/(2.0d0*VIF)-IUP+IREL*SRVOL*V13/(VI*V12)
          ENDIF
          IF(CONTRACTMODE) THEN
            F(29) = (1.0d0-Y(29))*FMTROP*FCTROP*FCTROP*ALPHA(29)
     '        -Y(29)*BETA(29)
            F(30) = (1.0d0-Y(30))*Y(29)*ALPHA(30)-Y(30)*BETA(30)
          ELSE
            F(29) = 0.0d0
            F(30) = 0.0d0
          ENDIF
        ENDIF
        IF(MMODE.EQ.1) F(4) = F(4)-CAFMIT
      ELSE IF(CASS) THEN
C ***   If (Ca)i at steady state do not compute f(4)
        IF(NMODE.EQ.0) THEN
C ***     sinh function for INACA
C ***     NOTE: strongly recommended not to use this mode for INACA
          Z1 = (ICACA+IBCA+ICA2+ICA3)*(NNACA-2.0d0)/(2.0d0*KNACA)
          Z2 = (2.0d0*RTONF/(NNACA-2.0d0))*DLOG(Z1+SQRT((Z1*Z1)+1.0d0))
          ENA = -RTONF*DLOG(Y(2)/NAO) !?? is this correct PJH? 15Jan91
          Z1 = 0.5d0*(NNACA-2.0d0)*(-Y(1)+(NNACA*ENA/(NNACA-2.0d0))
     '      +Z2)/(0.5d0*RTONF)
          Y(4) = CAO*DEXP(-Z1)
        ELSE IF(NMODE.EQ.1) THEN
C ***     Full function for INACA
          Z1 = Y(1)*(NNACA-2.0d0)/(2.0d0*RTONF)
          Z2 = (ICACA+IBCA+ICA2+ICA3)*(NNACA-2.0d0)/(2.0d0*KNACA)
          Z4 = 1.0d0
          Z5 = 1.0d0
          DO L = 1,INT(NNACA+.01d0)  !CMISS 21/3/89
            Z4 = Z4*Y(2)
            Z5 = Z5*NAO
          ENDDO
          Z3 = Z4*CAO*DEXP(2.0d0*YNACA*Z1)
          Z3 = Z3-Z2*(1.0d0+DNACA*CAO*Z4)
          Y(4) = Z3/(Z5*(Z2*DNACA+DEXP(-2.0d0*(1.0d0-YNACA)*Z1)))
        ENDIF
        IF(Y(4).LT.CALIM) Y(4) = 0.99d0*CALIM
        F(4) = 0.0d0
C ***   Compute steady state calcium stores
        Z5 = 1.0d0
        Z4 = 1.0d0
        NNREL=INT(NREL+0.1d0) !CMISS addition 21/3/89
        DO L = 1,NNREL
          Z5 = Z5*Y(4)
          Z4 = Z4*KMCA
        ENDDO
        Z1 = (Z5+Z4)/Z5
        IF(RMODE.EQ.0) THEN
          Y(14) = ALPHA(14)/(ALPHA(14)+BETA(14))
        ELSE
          Y(14) = 1.0d0
        ENDIF
        Z2 = Y(4)*CA12M*(1.0d0+ALPHA(13)*Y(14)*Z1/BETA(13))
        Z3 = ALPHA(13)*Y(14)/ALPHA(12)
        Z4 = Z3+Y(4)*(1.0d0+ALPHA(13)*Y(14)*Z1/BETA(13))
        Y(12) = Z2/Z4
        Y(13) = Y(4)*ALPHA(12)*Z1*(CA12M-Y(12))/BETA(13)
        IF(DEBUG) WRITE(*,*) 'STEADY STATE LOOP'
        F(12) = 0.0d0
        F(13) = 0.0d0
        F(14) = 0.0d0
      ENDIF
C *** Compute extracellular calcium change
      IF(CAOMODE.EQ.1) THEN                       !1.2
        F(24) = 0.5d0*IMCA/VF-DIFFCA*(Y(24)-CAB)
        CAO   = Y(24)
      ELSE
        F(24) = 0.0d0                              !1.2
      ENDIF
C *** Compute change in intracellular potassium
      F(11) = -IMK/VIF
C *** Compute Ca & K changes due to perfusion
      IF(SPACE.EQ.5) THEN
        F(4)  = F(4) +(CAPE-Y(4))/TCAP
        F(11) = F(11)+(KPE-Y(11))/TKP
      ENDIF

      RETURN
      END
```

B.2 Luo–Rudy

SUBROUTINE LR(t,Y,Func)

```
C#### Subroutine: LR
C###  Description:
C###    Computes RHS of Luo-Rudy equations.
C###    Voltage is in mV & time in ms.

      IMPLICIT NONE
      INCLUDE 'cmiss$reference:deoxs00.cmn'
      INCLUDE 'cmiss$reference:lr001.cmn'
!     Parameter List
      REAL*8 t,Y(*),Func(*)
!     Common blocks
      REAL*8        I_Na,I_Ca,I_K,F_NSR,F_JSR
      COMMON /isum/ I_Na,I_Ca,I_K,F_NSR,F_JSR
      REAL*8        TRPN,CMDN,CSQN
      COMMON /buff/ TRPN,CMDN,CSQN
      REAL*8        I(19),ICa !DPN 3/10/97 - extending I()
      COMMON /curr/ I,ICa
!     Local Variables
      REAL*8 VRatio_MJ, VRatio_MN, flux
      REAL*8 ALFA(7),BETA(7),I_stim,m,h,j,d,f,X !,Cm,V
      REAL*8 Iv_temp

! Assign names to variables
      m = Y(8)     !Y( 2)
      h = Y(7)     !Y( 3)
      j = Y(9)     !Y( 4)
      d = Y(5)     !Y( 5)
      f = Y(6)     !Y( 6)
      X = Y(4)     !Y( 7)

      VRatio_MJ = VolJSR/VolMyo
      VRatio_MN = VolNSR/VolMyo

! Setting the stimulus current
      IF ((t.GE.TPS).AND.(t.LE.TPS+TP)) THEN
        I_stim=Istim
      ELSE
        I_stim=0.d0
      ENDIF

! Compute rate constants
      CALL L_R_RATES(Y,ALFA,BETA)

! Compute ionic currents
      CALL LR_CURRENTS(t,Y,ALFA,BETA)
      flux = I(13)*VRatio_MJ+(-I(14)+I(15))*VRatio_MN

! Compute o.d.e. RHS
C *** DPN 15/04/98 - adding switch to each current in the total
      Iv_temp = ISWTCH(14)*I(4)+ISWTCH(21)*I(5)+ISWTCH(18)*I(7)
     '  +ISWTCH(26)*I(9)+ISWTCH(2)*I(10)+ISWTCH(4)*I(11)
      Iv_temp = ISWTCH(24)*Iv_temp ! turns all time indep. currents off
      Func( 1) =  -(I_stim+ISWTCH(16)*I(1)+ISWTCH(5)*I(2)
     '  +ISWTCH(13)*I(3)+ISWTCH(17)*I(6)+ISWTCH(22)*I(8)
     '  +Iv_temp)/Cm
      Func( 8) =  ALFA(1)*(1.d0-m) - BETA(1)*m
      Func( 7) =  ALFA(2)*(1.d0-h) - BETA(2)*h
      Func( 9) =  ALFA(3)*(1.d0-j) - BETA(3)*j
      Func( 5) =  ALFA(4)*(1.d0-d) - BETA(4)*d
      Func( 6) =  ALFA(5)*(1.d0-f) - BETA(5)*f
      Func( 4) =  ALFA(6)*(1.d0-X) - BETA(6)*X
      FUNC( 2) =  -(I_Na*ACap)/(VolMyo*Farad)
      FUNC( 3) =  -(I_Ca*ACap)/(VolMyo*2.d0*Farad)+flux
      FUNC(10) =  -(I_K*ACap) /(VolMyo*Farad)
      FUNC(12) =  -F_JSR
      FUNC(11) =  -F_NSR
      FUNC(13) =  -((ICa+I(9)+I(10))*1.d-3)/2.d0
      FUNC(14) = 0.0d0 ![Ca]o constant

      RETURN
      END
```

SUBROUTINE L_R_RATES(Y,ALFA,BETA)

```
C#### Subroutine: L_R_RATES
C###  Description:
C###    <html><pre>
C###    Computes the rate coefficients for the gating variables.
C###    ALFA (1) = m
C###      "   2  = h
C###      "   3  = j
C###      "   4  = d
C###      "   5  = f
C###      "   6  = X
C###      "   7  = K1
C###    BETA (1) = m
C###      "   2  = h
C###      "   3  = j
C###      "   4  = d
C###      "   5  = f
C###      "   6  = X
C###      "   7  = K1
C###    </pre></html>

      IMPLICIT NONE
      INCLUDE 'cmiss$reference:deoxs00.cmn'
      INCLUDE 'cmiss$reference:lr001.cmn'
!     Parameter List
      REAL*8 ALFA(*),BETA(*),Y(*)
!     Common blocks
      REAL*8        CaNSR,CaJSR,Ko !,Nai,Ki,Cai,Nao,Cao
      COMMON /conc/ CaNSR,CaJSR,Ko !,Nai,Ki,Cai,Nao,Cao
!     Local Variables
      REAL*8 d0,f0,Tau_d,Tau_f
      REAL*8 V,EK1 !,RTONF,TEMP,Ko,Ki

      V = Y(1)
! Standard ionic concentrations
      Ki   = Y(10)                    ![K]i
! Compute the K1 reversal potential (mV)
      EK1 = RTONF*dlog(Ko/Ki)         !K1 reversal potential (mV)
! Fast Na channel gates m,h,j
```

```
      ALFA(1) = 0.32d0*(V+47.13d0)/(1.d0-dexp(-0.1d0*(V+47.13d0)))   !m
      BETA(1) = 0.08d0*dexp(-V/11.d0)                                  !m
      IF(V.GE.-40.d0) THEN
        ALFA(2) = 0.d0                                                 !h
        BETA(2) = 1.d0/(0.13d0*(1.d0+dexp((V+10.66d0)/(-11.1d0))))     !h
        ALFA(3) = 0.d0                                                 !j
        BETA(3) = 0.3d0*dexp(-2.535d-7*V)/(1.d0+dexp(-0.1d0*(V+32.d0)))!j
      ELSE IF(V.LT.-40.d0) THEN
        ALFA(2) = 0.135d0*dexp((80.d0+V)/(-6.8d0))                     !h
        BETA(2) = 3.56d0*dexp(0.079d0*V)+(3.1d5*dexp(0.35d0*V))        !h
        ALFA(3) = (-1.2714d5*dexp(0.2444d0*V)-3.474d-5*
     '            dexp(-0.04391d0*V))*(V+37.78d0)/(1.d0+dexp(0.311d0*
     '            (V+79.23d0)))                                        !j
        BETA(3) = 0.1212d0*dexp(-0.01052d0*V)/(1.d0+dexp(-0.1378d0
     '            *(V+40.14d0)))                                       !j
      ENDIF
! L-type Ca channel gates d,f
      d0    = 1.d0/(1.d0+dexp(-(V+10.d0)/6.24d0))
      Tau_d = d0*(1.d0-dexp(-(V+10.d0)/6.24d0))/(0.035d0*(V+10.d0))
      f0    = (1.d0/(1.d0+dexp((V+35.06d0)/8.6d0)))+(0.6d0/
     '         (1.d0+dexp((50.d0-V)/20.d0)))
      Tau_f = 1.d0/(0.0197d0*dexp(-((0.0337d0*(V+10.d0))**2))+0.02d0)
      ALFA(4) = d0/Tau_d              !d
      BETA(4) = (1.d0-d0)/Tau_d       !d
      ALFA(5) = f0/Tau_f              !f
      BETA(5) = (1.d0-f0)/Tau_f       !f
! Time-dep. K channel gate X
      ALFA(6) = 7.19d-5*(V+30.d0)/(1.d0-dexp(-0.148d0*(V+30.d0)))     ! X
      BETA(6) = 1.31d-4*(V+30.d0)/(-1.d0+dexp(0.0687d0*(V+30.d0)))    ! X
! Time-indep. K channel gate K1
      ALFA(7) = 1.02d0/(1.d0+dexp(0.2385d0*(V-EK1-59.215d0)))
      BETA(7) = (0.49124d0*dexp(0.08032d0*(V-EK1+5.476d0))
     '          +dexp(0.06175d0*(V-EK1-594.31d0)))
     '          /(1.d0+dexp(-0.5143d0*(V-EK1+4.753d0)))

      RETURN
      END
```

SUBROUTINE LR_CURRENTS(t,Y,ALFA,BETA)

```
C#### Subroutine: LR_CURRENTS
C###  Description:
C###    Computes ionic currents for Luo-Rudy model

C**** Potentials, gating variables, internal concentrations
C**** Y( 1) = V                                              Y( 1)
C**** Y( 2) = m   (Na V- & t- dep. activation gate)          Y( 8)
C**** Y( 3) = h   (Na fast V- & t- dep. inactivation gate)   Y( 7)
C**** Y( 4) = j   (Na slow V- & t- dep. inactivation gate)   Y( 9)
C**** Y( 5) = d   (Ca V- & t- dep. activation gate)          Y( 5)
C**** Y( 6) = f   (Ca V- & t- dep. inactivation gate)        Y( 6)
C****         fCa (Ca Ca-dep. inactivation gate)
C**** Y( 7) = X   (K  V- & t- dep. activation gate)          Y( 4)
C****         Xi  (K  V-dep. inactivation gate)
C**** Y( 8) = internal Na concentration                      Y( 2)
C**** Y( 9) = internal Ca concentration                      Y( 3)
C**** Y(10) = internal K concentration                       Y(10)
C**** Y(11) = CaJSR concentration                            Y(12)
C**** Y(12) = CaNSR concentration                            Y(11)
C**** Y(13) = internal Ca concentration at T tubules due to L-type channels
C****                                                        Y(13)
C**** Y(14) = extracellular [Ca] (constant???)
C**** Currents (uA/uF)
C**** I( 1) = INa
C**** I( 2) = ICa_t
C**** I( 3) = IK
C**** I( 4) = IK1
C**** I( 5) = IKp
C**** I( 6) = INaCa
C**** I( 7) = INaK
C**** I( 8) = InsCa
C**** I( 9) = IpCa
C**** I(10) = ICab
C**** I(11) = INab
C**** I(12) = Iv
C**** I(13) = Irel (flux)
C**** I(14) = Iup (flux)
C**** I(15) = Ileak (flux)
C**** I(16) = Itr (flux)
C**** I(17) = ICa
C**** I(18) = ICaK
C**** I(19) = ICaNa
C**** total current for each ions
C**** I_Na  = sum of currents containing Na ions
C**** I_Ca  = sum of currents containing Ca ions
C**** I_K   = sum of currents containing K ions
C**** F_JSR = sum of fluxes moving into JSR
C**** F_NSR = sum of fluxes moving into NSR

      IMPLICIT NONE
      INCLUDE 'cmiss$reference:deoxs00.cmn'
      INCLUDE 'cmiss$reference:oxs005.cmn'
      INCLUDE 'cmiss$reference:lr001.cmn'
!     Parameter List
      REAL*8 t,Y(*),ALFA(*),BETA(*)
!     Common blocks
      REAL*8        I_Na,I_Ca,I_K,F_NSR,F_JSR
      COMMON /isum/ I_Na,I_Ca,I_K,F_NSR,F_JSR
      REAL*8        I(19),ICa !DPN 3/10/97 - extending I()
      COMMON /curr/ I,ICa
      REAL*8        TRPN,CMDN,CSQN
      COMMON /buff/ TRPN,CMDN,CSQN
      REAL*8        CaNSR,CaJSR,Ko !,Nai,Ki,Cai,Nao,Cao
      COMMON /conc/ CaNSR,CaJSR,Ko !,Nai,Ki,Cai,Nao,Cao
      REAL*8        Cai_on,Cai2
      COMMON /Cai_/ Cai_on,Cai2
```

```
      REAL*8                  IICa,IICaK,IICaNa,IINa,IIK,IIK1,fca
      COMMON /LR_MAX_CURRENTS/ IICa,IICaK,IICaNa,IINa,IIK,IIK1,fca
!     Local Variables
      REAL*8 V,m,h,j,d,f,X
!     Variables for fast Na current
      REAL*8 ENa
!     Variables for L-type Ca channel
      REAL*8 ICaK,ICaNa
!     Variables for time dependent K current
      REAL*8 EK,GGK,Xi!,PNaK
!     Variables for time independent K current
      REAL*8 EK1,GGK1,K10
!     Variables for Plateau K current
      REAL*8 EKp,Kp
!     Variables for NaK pump
      REAL*8 fNaK,sigma
!     Variables for nonspecific Ca activated current
      REAL*8 EnsCa,Vns,InsNa,IInsNa,InsK,IInsK
!     Variables for Ca background current
      REAL*8 ECaN!, GGCab
!     Variables for Na background current
      REAL*8 ENaN!, GGNab
!     Variables for Ca buffers in the myoplasm
      REAL*8 Cabuffer,CaJSRbuffer
!     Variables for Ca fluxes in SR
      REAL*8 Grel,GGrel
!     Variables for Ca induced Ca release of JSR
      REAL*8 t_CICR
!     Variables for Ca uptake and leakage of NSR
      REAL*8 Kleak
      REAL*8 VRatio_JN

! Initialising the volume parameters
      VRatio_JN = VolNSR/VolJSR       !volume ratio between JSR and NSR
! Initialising the thermodynamic parameters
      V     = Y(1)                    !membrane potential (mV)
! Standard ionic concentrations in mmol/L
      Nai   = Y(2)   !Y(8)       ![Na]i
      Cai   = Y(3)   !Y(9)       ![Ca]i
      Ki    = Y(10)      ![K]i
! Ca buffers in the myoplasm
      TRPN     = TRPNTRPN*(Cai/(Cai+KmTRPN))
      CMDN     = CMDNCMDN*(Cai/(Cai+KmCMDN))
! Ca fluxes in the sarcoplasmic reticulum
      CaJSR = Y(12)  !Y(11)                   !mmol/L
      CaNSR = Y(11)  !Y(12)                   !mmol/L
! Ca buffer in JSR and CSQN
      CSQN      = CSQNCSQN*(CaJSR/(CaJSR+KmCSQN))
! Ca flux in the SR after taking CSQN buffering into account
      CaJSRbuffer = CaJSR-CSQN
      IF(t.GE.TPS)THEN
        IF(CaJSRbuffer.GT.1.d-3)THEN
          CaJSR = CaJSRbuffer
        ELSE
          CaJSR = 1.d-3
        ENDIF
      ENDIF
! Ionic currents in the sarcolemma
! Fast Na current INa
      m = Y(8)  !Y(2)
      h = Y(7)  !Y(3)
      j = Y(9)  !Y(4)
      ENa  = RTONF*dlog(Nao/Nai)      !Na reversal potential (mV)
      IINa = GGNa * (V-ENa)
      I(1) = m*m*m * h * j * IINa
! L-type Ca current ICa_t
```

```
      d = Y(5)
      f = Y(6)
      KmCa = KmCa_L !0.6d-3                  !mmol/L
      fCa  = 1.d0/(1.d0+(Cai/KmCa)**2)!Ca-dep. inact.n gate of L-type Ca
      IICa = PCa*4.d0*(V/RTONF)*Farad*(gCai*Cai*dexp(2.d0*V/RTONF)
     '       -gCao*Cao)/(dexp(2.d0*V/RTONF)-1.d0)
      IICaNa = PNa*(V/RTONF)*Farad*(gNai*Nai*dexp(V/RTONF)-gNao*Nao)
     '                           /(dexp(V/RTONF)-1.d0)
      IICaK  = PK*(V/RTONF)*Farad*(gKi*Ki*dexp(V/RTONF)-gKo*Ko)
     '                           /(dexp(V/RTONF)-1.d0)
      ICa   = d*f*fCa*IICa
      ICaK  = d*f*fCa*IICaK
      ICaNa = d*f*fCa*IICaNa
      I(17) = ICa
      I(18) = ICaK
      I(19) = ICaNa
      I(2)   = ICa + ICaK + ICaNa
! Time-dep. K current IK
      X    = Y(4)  !Y(7)                     !V- & t- dep. K-activation gate
      Xi   = 1.d0/(1.d0+dexp((V-56.26d0)/32.1d0))
     '                                !V-dep. K-inactivation gate
      GGK  = 0.282d0*dsqrt(Ko/5.4d0)  !millisiemens/uF
      EK   = RTONF*dlog((Ko+PNaK*Nao)/(Ki+PNaK*Nai))
                                      !K reversal potential
      IIK = GGK*(V-EK)
      I(3) = IIK * Xi * X * X
! Time-indep. K current IK1
      GGK1 = 0.75d0*dsqrt(Ko/5.4d0)   !millisiemens/uF
      EK1  = RTONF*dlog(Ko/Ki)        !K1 reversal potential
      K10  = ALFA(7)/(ALFA(7)+BETA(7))
      IIK1 = GGK1 * (V - EK1)
      I(4) = IIK1 * K10
! Plateau K current IKp
      EKp  = EK1                      !Kp reversal potential
      Kp   = 1.d0/(1.d0+dexp((7.488d0-V)/5.98d0))
      I(5) = GGKp*Kp*(V-EKp)
! Na-Ca exchanger current INaCa
      KmCa  = KmCa_NaCa !1.38d0    !half sat.n conc of Ca channel (mmol/L)
      I(6)  = kNaCa*(dexp(eta*V/RTONF)*Nai**3*Cao
     '             -dexp((eta-1.d0)*V/RTONF)*Nao**3*Cai)
     '             /((KmNa**3+Nao**3)*(KmCa+Cao)
     '             *(1.d0+ksat*dexp((eta-1.d0)*V/RTONF)))
! Na-K pump INaK
      sigma = (1.d0/7.d0)*(dexp(Nao/67.3d0)-1.d0)
     '                                ![Na]o-dependence factor of fNak
      fNaK  = 1.d0/(1.d0+0.1245d0*dexp(-0.1d0*V/RTONF)
     '        +0.0365d0*sigma*dexp(-V/RTONF))
      I(7)  = IINaK*fNaK*Ko/((Ko+KmKo)*(1.d0+dsqrt((KmNai/Nai)**2)))
! Non-specific Ca-activated current InsCa
      EnsCa  = RTONF*dlog((Ko+Nao)/(Ki+Nai))
      Vns    = V-EnsCa
      IInsK  = PnsCa*(Vns/RTONF)*Farad*(gNai*Nai*dexp(Vns/RTONF)
```

```
     '                          -gNao*Nao)/(dexp(Vns/RTONF)-1.d0)
      InsK   = IInsK /(1.d0+(KmnsCa/Cai)**3)
      IInsNa = PnsCa*(Vns/RTONF)*Farad*(gKi*Ki*dexp(Vns/RTONF)
     '                          -gKo*Ko)/(dexp(Vns/RTONF)-1.d0)
      InsNa  = IInsNa/(1.d0+(KmnsCa/Cai)**3)
      I(8)   = InsK + InsNa
! Sarcolemmal Ca pump IpCa
      I(9)   = IIpCa*(Cai/(KmpCa+Cai))
! Ca background current ICab
      ECaN   = 0.5d0*RTONF*dlog(Cao/Cai) !Nernst potential of Ca
      I(10)  = GGCab*(V-ECaN)
! Na background current INab
      ENaN   = ENa                    !Nernst potential of Na
      I(11)  = GGNab*(V-ENaN)
! Total time independent current
      I(12)  = I(4) + I(5) + I(7) + I(9) + I(10) + I(11)
! Compute Cai change at 2 ms after onset of stimulus
      IF((t.GE.TPS).AND.(t.LT.TABT+TPS))THEN
        Cai_on = Y(13)
        IF(DEBUG) write (*,*) 'Cai_on = ', Cai_on
      ENDIF
      IF((t.GE.2.d0+TPS).AND.(t.LT.2.d0+TABT+TPS))THEN
        Cai2 = Y(13)-Cai_on
        IF(DEBUG) write (*,*) 'Cai2 = ', Cai2
      ENDIF
! Ca induced Ca release of JSR
      IF(Cai2.GT.Caith) THEN
        GGrel = GGrel_
      ELSE
        GGrel = 0.d0
      ENDIF
      !time of Ca-induced Ca-release
      t_CICR  = t-(TPS+2.0d0)
      Grel  = GGrel*((Cai2-Caith)/(Kmrel+Cai2-Caith))
     '       *(1.d0-dexp(-t_CICR/Tau_on))*dexp(-t_CICR/Tau_off)
      I(13) = Grel*(CaJSR-Cai)
! Ca uptake and leakage of NSR Iup and Ileak
      Kleak      = IIup/CaNSRCaNSR        !ms-1
      I(15)      = Kleak*CaNSR            !mmol/L/ms
      I(14)      = IIup*(Cai/(Cai+Kmup))  !mmol/L/ms
! Translocation of Ca ions from NSR to JSR Itr
      I(16)  = (CaNSR-CaJSR)/Tau_tr       !mmol/L/ms
! Computes current carrying the five ions
      I_Na  = I(1)+ICaNa+3.0d0*I(6)+3.0d0*I(7)+InsNa+I(11)
      I_Ca  = ICa-I(6)+I(9)+I(10)
      I_K   = ICaK+I(3)+I(4)+I(5)-2.0d0*I(7)+InsK
      F_NSR = -I(14)+I(15)+I(16)
      F_JSR = I(13)-I(16)*VRatio_JN

      RETURN
      END
```

B.3 Jafri–Rice–Winslow

SUBROUTINE JRW(t,y,F)

```
C#### Subroutine: JRW
C###  Description:
C###    compute Jafri-Rice-Winslow eqns

      IMPLICIT NONE

      INCLUDE 'cmiss$reference:cell00.cmn'
      INCLUDE 'cmiss$reference:deoxs00.cmn'
 ! Passed variables
      REAL*8 t,y(*),F(*)
      REAL*8 ENa,EK,EK1,EKp,ECaN,ENaN
      COMMON /JRW_EP/ ENa,EK,EK1,EKp,ECaN,ENaN
      REAL*8 JRW_INa,JRW_ICa,JRW_IK,JRW_IK1,JRW_IKp,JRW_INaCa,JRW_INaK,
     '  JRW_InsCa,JRW_IpCa,JRW_ICaK,JRW_ICab,JRW_INab,
     '  JRW_InsNa,JRW_InsK,Jrel,Jleak,Jup,Jtr,Jxfer,Jtrpn
      COMMON /JRW_I/ JRW_INa,JRW_ICa,JRW_IK,JRW_IK1,JRW_IKp,JRW_INaCa,
     '  JRW_INaK,JRW_InsCa,JRW_IpCa,JRW_ICaK,JRW_ICab,JRW_INab,
     '  JRW_InsNa,JRW_InsK,Jrel,Jleak,Jup,Jtr,Jxfer,Jtrpn
      REAL*8 alfa_m,beta_m,alfa_h,alfa_j,beta_h,beta_j,
     '  alfa_x,beta_x,alfa_K1,beta_K1,alfa_Ca,beta_Ca
      COMMON /JRW_RATE/ alfa_m,beta_m,alfa_h,alfa_j,beta_h,beta_j,
     '  alfa_x,beta_x,alfa_K1,beta_K1,alfa_Ca,beta_Ca
      REAL*8           RTF
      COMMON /JRW_RTF/ RTF
      !troponin kinetics for coupled problems
      REAL*8      Rho0,Rho1,Cb_max
      COMMON /Tn/ Rho0,Rho1,Cb_max
      REAL*8         Tref,beta0,beta1,beta2,gamma,Ca_scale
      COMMON /SS_To/ Tref,beta0,beta1,beta2,gamma,Ca_scale
      REAL*8 Save_T,Save_To
      COMMON /COUPLING_TENSION/ Save_T,Save_to
      !local variables
      REAL*8 V,mNa,hNa,jNa,xK,CaSubSpace,CaJSR,CaNSR,HTRPNCa,
     '  LTRPNCa,PO1,PO2,PC1,PC2,yL,C0,C1,C2,C3,C4,O,Cca0,Cca1,Cca2,
     '  Cca3,Cca4,Oca,Bi,BSS,BJSR,
     '  y_inf,tau_y,alfa_Ca_dash,beta_Ca_dash,gama_Ca,JRW_STIMSIZE,TTo
      REAL*8 ALPHA(6),BETA(6)

 ! State variables
      V       = y( 1) !membrane potential
      mNa     = y( 7) !Na channel m gate
      hNa     = y( 6) !Na channel h gate
      jNa     = y( 8) !Na channel j gate
      xK      = y( 4) !K  channel x gate
      Nai     = y( 2) !intracellular [Na]
      Ki      = y( 9) !intracellular [K]
      Cai     = y( 3) !intracellular [Ca]
      CaSubSpace = y(13) !subspace [Ca]
```

```
      CaJSR   = y(11) !junctional SR [Ca]
      CaNSR   = y(10) !network SR [Ca]
      HTRPNCa = y(31) !Tn binding: fraction of Ca bound to low  affin-
ity site
      LTRPNCa = y(30) !Tn binding: fraction of Ca bound to high affin-
ity site
      PO1     = y(15) !RyR channel, open state 1
      PO2     = y(16) !RyR channel, open state 2
      PC1     = y(14) !RyR channel, closed state 1
      PC2     = y(17) !RyR channel, closed state 2
      yL      = y( 5) !L-type Ca channel: voltage inactivation gate
      C0      = y(18) !L-type Ca channel: mode normal,  closed state 0
      C1      = y(19) !L-type Ca channel: mode normal,  closed state 1
      C2      = y(20) !L-type Ca channel: mode normal,  closed state 2
      C3      = y(21) !L-type Ca channel: mode normal,  closed state 3
      C4      = y(22) !L-type Ca channel: mode normal,  closed state 4
      O       = y(23) !L-type Ca channel: mode normal,  open state
      Cca0    = y(24) !L-type Ca channel: mode calcium, closed state 0
      Cca1    = y(25) !L-type Ca channel: mode calcium, closed state 1
      Cca2    = y(26) !L-type Ca channel: mode calcium, closed state 2
      Cca3    = y(27) !L-type Ca channel: mode calcium, closed state 3
      Cca4    = y(28) !L-type Ca channel: mode calcium, closed state 4
      Oca     = y(29) !L-type Ca channel: mode calcium, open state
      Cao     = y(12) !extracellular Ca
 ! Buffer scale factors
      Bi   = 1.d0/(1.d0+JRW_CMDN_tot*JRW_km_CMDN/(JRW_km_CMDN+Cai  )**2)
      BSS  = 1.d0/(1.d0+JRW_CMDN_tot*JRW_km_CMDN/
     '  (JRW_km_CMDN+CaSubSpace )**2)
      BJSR = 1.d0/(1.d0+JRW_CSQN_tot*JRW_km_CSQN/(JRW_km_CSQN+CaJSR)**2)
 ! Fluxes
      Jrel  = JRW_v1*(PO1+PO2)*(CaJSR-CaSubSpace) !RyR channel flux
      Jleak = JRW_v2*(CaNSR-Cai) !leak flux from NSR to myoplasm
      Jup   = JRW_v3*Cai**2/(JRW_km_up**2+Cai**2) !SR Ca-ATPase pump flux
      Jtr   = (CaNSR-CaJSR)/JRW_tau_tr !transfer flux from NSR to JSR
      Jxfer = (CaSubSpace-Cai)/JRW_tau_xfer !transfer flux from SS to myoplasm
C *** If solving coupled problem, need to include tension dependence
C *** release.
      IF (MECHANICS_MODEL.EQ.2.AND.TENSION_DEPENDENT_RELEASE) THEN
        ! use HMT parameters for low-affinity troponin
        IF (DABS(Save_To).LT.1.0d-10) THEN
          TTo = 0.0d0
        ELSE
          TTo = Save_T/(gamma*Save_To)
        ENDIF
        F(30)  =  JRW_kp_ltrpn*Cai*(JRW_LTRPN_tot-LTRPNCa) !eqn 47
     '    -JRW_km_ltrpn*(1.0d0-TTo)*LTRPNCa
      ELSE
        F(30)  =  JRW_kp_ltrpn*Cai*(JRW_LTRPN_tot-LTRPNCa) !eqn 47
```

```
     '    -JRW_km_ltrpn*LTRPNCa
      ENDIF
      Jtrpn = JRW_kp_htrpn*Cai*(JRW_HTRPN_tot-HTRPNCa)
     '     - JRW_km_htrpn*HTRPNCa
     '  + F(30)
 ! Equilibrium potentials
      ENa  = RTF*DLOG(JRW_Nao/Nai) !Na channel
      EK   = RTF*DLOG((JRW_Ko+JRW_PNaK*JRW_Nao)/(Ki+JRW_PNaK*Nai)) !K  channel
      EK1  = RTF*DLOG(JRW_Ko/Ki) !K1 channel
      EKp  = EK1 !Kp channel
      ECaN = 0.5d0*RTF*DLOG(Cao/Cai) !Ca background
      ENaN = ENa !Na background

      CALL JRW_RATES(V,EK1,ALPHA,BETA)

      alfa_m = ALPHA(1)
      alfa_h = ALPHA(2)
      alfa_j = ALPHA(3)
      alfa_x = ALPHA(4)
      alfa_k1 = ALPHA(5)
      alfa_Ca = ALPHA(6)
      beta_m = BETA(1)
      beta_h = BETA(2)
      beta_j = BETA(3)
      beta_x = BETA(4)
      beta_k1 = BETA(5)
      beta_Ca = BETA(6)

      CALL JRW_CURRENTS(y) !ionic currents

C *** Set the stimulus size.
      CALL JRW_CHANGE(t,JRW_STIMSIZE)

 ![ 1] dV/dt
      F( 1)  = -(JRW_STIMSIZE + ISWTCH(16)*JRW_INa
     '  +ISWTCH(5)*ISWTCH(8)*JRW_ICa
     '  +ISWTCH(13)*JRW_IK+ISWTCH(14)*JRW_IK1+ISWTCH(21)*JRW_IKp
     '  +ISWTCH(17)*JRW_INaCa+ISWTCH(18)*JRW_INaK
     '  +ISWTCH(22)*JRW_InsCa+ISWTCH(23)*JRW_IpCa
     '  +ISWTCH(5)*ISWTCH(9)*JRW_ICAK+ISWTCH(2)*JRW_ICab
     '  +ISWTCH(4)*JRW_INab) !eqn 39
 ![ 2] dm/dt
      F( 7)  = alfa_m*(1.d0-mNa)-beta_m*mNa !eqn 40
 ![ 3] dh/dt
      F( 6)  = alfa_h*(1.d0-hNa)-beta_h*hNa !eqn 41
 ![ 4] dj/dt
      F( 8)  = alfa_j*(1.d0-jNa)-beta_j*jNa !eqn 42
 ![ 5] dx/dt
      F( 4)  = alfa_x*(1.d0-xK)-beta_x*xK !eqn 43
 ![ 6] dNai/dt
      F( 2)  = -(JRW_INa+JRW_INab+JRW_InsNa+3.d0*JRW_INaCa+
     '  3.d0*JRW_INaK)*JRW_Acap/(JRW_V_myo*JRW_Faraday) !eqn 44
 ![ 7] dKi/dt
      F( 9)  = -(JRW_IK+JRW_IK1+JRW_IKp+JRW_InsK+JRW_ICaK-
     '  2.d0*JRW_INaK)*JRW_Acap/(JRW_V_myo*JRW_Faraday) !eqn 45
 ![ 8] dCai/dt
      F( 3)  = Bi*(Jleak+Jxfer-Jup-Jtrpn-(JRW_ICab-2.d0*JRW_INaCa+
     '  JRW_IpCa)*JRW_Acap/(2.d0*JRW_V_myo*JRW_Faraday)) ! eqn 13
 ![ 9] dCaSS/dt
      F(13)  = BSS*(Jrel*JRW_V_JSR/JRW_V_SS-Jxfer*JRW_V_myo/JRW_V_SS
     '  -JRW_ICa*JRW_Acap/(2.d0*JRW_V_SS*JRW_Faraday)) !eqn 14
 ![10] dCaJSR/dt
      F(11)  = BJSR*(Jtr-Jrel) !eqn 15
 ![11] dCaNSR/dt
      F(10)  = (Jup-Jleak)*JRW_V_myo/JRW_V_NSR !eqn 16
     '  -Jtr*JRW_V_JSR/JRW_V_NSR
 ![12] dHTRPNCa/dt
      F(31)  =  JRW_kp_htrpn*Cai*(JRW_HTRPN_tot-HTRPNCa) !eqn 46
     '  -JRW_km_htrpn*HTRPNCa
 ![13] dLTRPNCa/dt
C *** DPN 23/07/98 - move the calculation of dLTRPNCa/dt up to where
C ***                Jtrpn is evaluated.

 ![14] dPC1/dt
      F(14)  = -JRW_kap*CaSubSpace**JRW_n*PC1+JRW_kam*PO1 !eqn 89
 ![15] dPO1/dt
      F(15)  = JRW_kap*CaSubSpace**JRW_n*PC1-JRW_kam*PO1 !eqn 90
     '  -JRW_kbp*CaSubSpace**JRW_m*PO1+JRW_kbm*PO2
     '  -JRW_kcp*PO1+JRW_kcm*PC2
 ![16] dPO2/dt
      F(16)  =  JRW_kbp*CaSubSpace**JRW_m*PO1-JRW_kbm*PO2 !eqn 91
 ![17] dPC2/dt
      F(17)  =  JRW_kcp*PO1-JRW_kcm*PC2 !eqn 92
 ![18] dy/dt
      y_inf  =  1.0d0/(1.d0+DEXP((V+55.d0)/7.5d0))
     '  + 0.1d0/(1.d0+DEXP((-V+21.d0)/6.d0))
      tau_y  =  20.d0+600.d0/(1.d0+DEXP((V+30.d0)/9.5d0))
      F( 5)  =  (y_inf-yL)/tau_y !eqn 34
 ![19] dC0/dt
      alfa_Ca_dash = alfa_Ca*JRW_a
      beta_Ca_dash = beta_Ca/JRW_b
      gama_Ca      = 0.1875d0*CaSubSpace
      F(18)  = beta_Ca*C1+JRW_w*Cca0-(4.d0*alfa_Ca+gama_Ca)*C0 !eqn 22
 ![20] dC1/dt
      F(19)  = 4.d0*alfa_Ca*C0+2.d0*beta_Ca*C2+JRW_w/JRW_b *Cca1
     '  -(     beta_Ca+3.d0*alfa_Ca+gama_Ca*JRW_a   )*C1 !eqn 23
 ![21] dC2/dt
      F(20)  = 3.d0*alfa_Ca*C1+3.d0*beta_Ca*C3+JRW_w/JRW_b**2*Cca2
     '  -(2.d0*beta_Ca+2.d0*alfa_Ca+gama_Ca*JRW_a**2)*C2 !eqn 24
 ![22] dC3/dt
      F(21)  = 2.d0*alfa_Ca*C2+4.d0*beta_Ca*C4+JRW_w/JRW_b**3*Cca3
     '  -(3.d0*beta_Ca+     alfa_Ca+gama_Ca*JRW_a**3)*C3 !eqn 25
 ![23] dC4/dt
      F(22)  =      alfa_Ca*C3+        JRW_g*O+JRW_w/JRW_b**4*Cca4
     '  -(4.d0*beta_Ca  + JRW_f  +  gama_Ca*JRW_a**4)*C4 !eqn 26
 ![24] dO/dt
      F(23)  = JRW_f*C4-JRW_g*O !eqn 27
 ![25] dCca0/dt
      F(24)  =      beta_Ca_dash*Cca1+gama_Ca*C0 !eqn 28
     '  -(4.d0*alfa_Ca_dash+JRW_w)*Cca0
 ![26] dCca1/dt
      F(25)  = 4.d0*alfa_Ca_dash*Cca0+2.d0*beta_Ca_dash*Cca2 !eqn 29
     '  +gama_Ca*JRW_a*C1
     '  -(     beta_Ca_dash     +3.d0*alfa_Ca_dash
     '  +JRW_w/JRW_b   )*Cca1
 ![27] dCca2/dt
      F(26)  = 3.d0*alfa_Ca_dash*Cca1+3.d0*beta_Ca_dash*Cca3 !eqn 30
     '  +gama_Ca*JRW_a**2*C2
     '  -(2.d0*beta_Ca_dash     +2.d0*alfa_Ca_dash
     '  +JRW_w/JRW_b**2)*Cca2
 ![28] dCca3/dt
      F(27)  = 2.d0*alfa_Ca_dash*Cca2+4.d0*beta_Ca_dash*Cca4 !eqn 31
     '  +gama_Ca*JRW_a**3*C3
     '  -(3.d0*beta_Ca_dash     +     alfa_Ca_dash
     '  +JRW_w/JRW_b**3)*Cca3
 ![29] dCca4/dt
      F(28)  =      alfa_Ca_dash*Cca3+JRW_g_dash*Oca !eqn 32
     '  +gama_Ca*JRW_a**4*C4
     '  -(4.d0*beta_Ca_dash     +JRW_f_dash
     '  +JRW_w/JRW_b**4)*Cca4
 ![30] dOca/dt
      F(29)  =        JRW_f_dash*Cca4-JRW_g_dash*Oca !eqn 33
 ![31] dCao/dt
      F(12)  = 0.0d0 !extra Ca constant.

      RETURN
      END
```

SUBROUTINE JRW_RATES(V,EK1,ALPHA,BETA)

```
C#### Subroutine: JRW_RATES
C###  Description:
C###    <html><pre>
C###    Calculates the rate coefficients for the JRW model.
C###    (1) = m }
C###    (2) = h } fast sodium gates
C###    (3) = j }
C###    (4) = X - K channel
C###    (5) = K1 - time independent K channel
C###    (6) = Ca - L-type calcium channel (d&f gates combined??)
C###    </pre></html>

      IMPLICIT NONE
      ! Passed Parameters
      REAL*8 V,EK1,ALPHA(6),BETA(6)

      ! Na channel gating rate constants
      ALPHA(1)  =  0.32d0*(V+47.13d0)/(1.d0-DEXP(-0.1d0*(V+47.13d0)))
      BETA(1)  = 0.08d0*DEXP(-V/11.d0)
      IF(V.GE.-40.d0) THEN
        ALPHA(2) = 0.d0
        ALPHA(3) = 0.d0
        BETA(2) = 1.d0/(0.13d0*(1.d0+DEXP(-(V+10.66d0)/11.1d0)))
        BETA(3) = 0.3d0*DEXP(-2.535d-7*V)
     '    /(1.d0+DEXP(-0.1d0*(V+32.d0)))
      ELSE
        ALPHA(2) = 0.135d0*DEXP(-(80.d0+V)/6.8d0)
        ALPHA(3) = (-1.27140d5*DEXP(0.2444d0*V)
     '    -3.474d-5*DEXP(-0.04391d0*V))
     '    *(V+37.78d0)/(1.d0+DEXP(0.311d0*(V+79.23d0)))
        BETA(2) = 3.56d0*DEXP(0.079d0*V)+3.1d5*DEXP(0.35d0*V)
        BETA(3) = 0.1212d0*DEXP(-0.01052d0*V)
     '    /(1.d0+DEXP(-0.1378d0*(V+40.14d0)))
      ENDIF !V
 ! K channel gating rate constants
      ALPHA(4)  = 7.19d-5*(V+30.d0)/( 1.d0-DEXP(-0.148d0*(V+30.d0)))
      BETA(4)  = 1.31d-4*(V+30.d0)/(-1.d0+DEXP(0.0687d0*(V+30.d0)))
 ! K1 channel gating rate constants
      ALPHA(5) = 1.02d0/(1.d0+DEXP(0.2385d0*(V-EK1-59.215d0)))
      BETA(5) = (0.4912d0*DEXP(0.08032d0*(V-EK1+5.476d0))
     '  +DEXP(0.06175d0*(V-EK1-594.31d0)))
     '  /(1.d0+DEXP(-0.5143d0*(V-EK1+4.753d0)))
 ! Ca channel gating rate constants
      ALPHA(6) = 0.4d0*DEXP((V+12.d0)/10.d0)
      BETA(6) = 0.05d0*DEXP(-(V+12.d0)/13.d0)

      RETURN
      END
```

SUBROUTINE JRW_CURRENTS(y)

```
C#### Subroutine: JRW_CURRENTS
C###  Description:
C###    Evaluate currents for JRW model.

      IMPLICIT NONE
      INCLUDE 'cmiss$reference:cell00.cmn'

! Passed variables
      REAL*8 y(*)
!Common blocks
      REAL*8 alfa_m,beta_m,alfa_h,alfa_j,beta_h,beta_j,
```

```
     '  alfa_x,beta_x,alfa_K1,beta_K1,alfa_Ca,beta_Ca
      COMMON /JRW_RATE/ alfa_m,beta_m,alfa_h,alfa_j,beta_h,beta_j,
     '  alfa_x,beta_x,alfa_K1,beta_K1,alfa_Ca,beta_Ca
      REAL*8 ENa,EK,EK1,EKp,ECaN,ENaN
      COMMON /JRW_EP/ ENa,EK,EK1,EKp,ECaN,ENaN
      REAL*8 JRW_INa,JRW_ICa,JRW_IK,JRW_IK1,JRW_IKp,JRW_INaCa,JRW_INaK,
     '  JRW_InsCa,JRW_IpCa,JRW_ICaK,JRW_ICab,JRW_INab,
     '  JRW_InsNa,JRW_InsK,Jrel,Jleak,Jup,Jtr,Jxfer,Jtrpn
      COMMON /JRW_I/ JRW_INa,JRW_ICa,JRW_IK,JRW_IK1,JRW_IKp,JRW_INaCa,
     '  JRW_INaK,JRW_InsCa,JRW_IpCa,JRW_ICaK,JRW_ICab,JRW_INab,
     '  JRW_InsNa,JRW_InsK,Jrel,Jleak,Jup,Jtr,Jxfer,Jtrpn
      REAL*8           RTF
      COMMON /JRW_RTF/ RTF
      !local variables
      REAL*8 V,mNa,hNa,jNa,xK,Nai,Ki,Cai,Cao,yL,O,Oca,VRTF,GK,Xi,GK1,
     '  K1inf,Kp,sigma,fNaK,InsNa_max,InsK_max,TVRTF,ICa_max,PK_dash

      V       = y( 1) !membrane potential
      mNa     = y( 7) !Na channel m gate
      hNa     = y( 6) !Na channel h gate
      jNa     = y( 8) !Na channel j gate
      xK      = y( 4) !K  channel x gate
      Nai     = y( 2) !intracellular [Na]
      Ki      = y( 9) !intracellular [K]
      Cai     = y( 3) !intracellular [Ca]
      yL      = y( 5) !L-type Ca channel: voltage inactivation gate
      O       = y(23) !L-type Ca channel: mode normal,  open state
      Oca     = y(29) !L-type Ca channel: mode calcium, open state
      Cao     = y(12) !extracellular Ca

      VRTF = V / RTF                        ! VF/RT (dimensionless)
 ! Na channel current
      JRW_INa   = JRW_GNa_max*mNa*mNa*mNa*hNa*jNa*(V-ENa) !eqn 48
 ! K channel current
      GK    = 0.1128d0*DSQRT(JRW_Ko/5.4d0) !eqn 62
      Xi    = 1.d0/(1.d0+DEXP((V-56.26d0)/32.1d0)) !eqn 63
      JRW_IK    = GK*Xi*xK*xK*(V-EK) !eqn 60
 ! K1 channel current
      GK1   = 0.75d0*DSQRT(JRW_Ko/5.4d0) !eqn 68
      K1inf = alfa_K1/(alfa_K1+beta_K1) !eqn 69
      JRW_IK1   = GK1*K1inf*(V-EK1) !eqn 66
 ! Kp channel current
      Kp    = 1.d0/(1.d0+DEXP((7.488d0-V)/5.98d0)) !eqn 74
      JRW_IKp   = JRW_GKp_max*Kp*(V-EKp) !eqn 72
 ! NaCa exchanger current
      JRW_INaCa = JRW_kNaCa*(DEXP(JRW_eta*VRTF)*Nai*Nai*Nai*Cao !eqn 75
     '  -DEXP((JRW_eta-1.d0)*VRTF)*JRW_Nao*JRW_Nao*JRW_Nao*Cai)
     '  /((JRW_km_Na**3+JRW_Nao**3)*(JRW_km_Ca+Cao)
     '  *(1.d0+JRW_ksat*DEXP((JRW_eta-1.d0)*VRTF)))
 ! NaK pump current
      sigma = (DEXP(JRW_Nao/67.3d0)-1.d0)/7.d0 !eqn 78
      fNaK  = 1.d0/(1.d0+0.1245d0*DEXP(-0.1d0*VRTF) !eqn 77
     '  +0.0365d0*sigma*DEXP(-VRTF))
      JRW_INaK  = JRW_INaK_max*fNaK*JRW_Ko/(JRW_Ko+JRW_km_Ko) !eqn 76
     '  /(1.d0+(JRW_km_Nai/Nai)**1.5d0)
 ! Nonspecific Ca-activated channel current
      InsNa_max = JRW_P_ns*VRTF*JRW_Faraday !eqn 81
     '  *0.75d0*(Nai*DEXP(VRTF)-JRW_Nao)/(DEXP(VRTF)-1.d0)
      JRW_InsNa     = InsNa_max/(1.d0+(JRW_km_ns/Cai)**3) !eqn 80
      InsK_max  = JRW_P_ns*VRTF*JRW_Faraday !eqn 83
     '  *0.75d0*(Ki*DEXP(VRTF)-JRW_Ko)/(DEXP(VRTF)-1.d0)
      JRW_InsK      = InsK_max/(1.d0+(JRW_km_ns/Cai)**3) !eqn 82
      JRW_InsCa     = JRW_InsNa+JRW_InsK !eqn 79
 ! Sarcolemmal Ca pump current
      JRW_IpCa      = JRW_ICap_max*Cai/(JRW_km_Cap+Cai) !eqn 84
 ! Ca background current
      JRW_ICab      = JRW_GCab_max*(V-ECaN) !eqn 85
 ! Na background current
      JRW_INab      = JRW_GNab_max*(V-ENaN) !eqn 87
 ! L-type Ca currents
      TVRTF     = 2.d0*VRTF
      JRW_ICa   = JRW_PCa*yL*(O+OCa)*4.d0*VRTF*JRW_Faraday !eqn 37
     '  *(1.d-3*DEXP(TVRTF)-0.341d0*Cao)/(DEXP(TVRTF)-1.d0)
      ICa_max   = JRW_PCa*4.0d0*VRTF*JRW_Faraday*(0.001d0*DEXP(TVRTF)-
     '  0.341d0*Cao)/(DEXP(TVRTF)-1.0d0)
      PK_dash   = JRW_PK/(1.d0+ICa_max/JRW_ICa_half) !eqn 1
      JRW_ICaK      = PK_dash*yL*(O+OCa)*VRTF*JRW_Faraday !eqn 38
     '  *(Ki*DEXP(VRTF)-JRW_Ko)/(DEXP(VRTF)-1.d0)

      RETURN
      END
```

SUBROUTINE JRW_CHANGE(t,JRW_STIMSIZE)

```
C#### Subroutine: JRW_CHANGE
C###  Description:
C###    Sets the stimulus size depending on the time

      IMPLICIT NONE

      INCLUDE 'cmiss$reference:cell00.cmn'
      INCLUDE 'cmiss$reference:deoxs00.cmn'
      !Passed variables
      REAL*8 t,JRW_STIMSIZE

      REAL*8 PERIOD,stimulation_time

C *** Set the stimulus curent
      IF (t.GE.TPS.AND.t.LE.TPS+TP) THEN
        JRW_STIMSIZE = JRW_Istim
      ELSE
        JRW_STIMSIZE = 0.0d0
      ENDIF
C *** Evaluate the new stimulus time
      IF(STIM_FREQ.GT.0.0d0) THEN
        IF (t.GT.TPS+TP) THEN
          PERIOD = 1.0d0 / (STIM_FREQ*1.0d-3) !freq in Hz (1/s -> 1/ms)
          TPS = TPS + PERIOD
        ENDIF
      ENDIF

      RETURN
      END
```

B.4 Hunter–McCulloch–ter Keurs

SUBROUTINE FM_SOLVE(TBEG,TNEXT,count,T,TFINAL,EXTENSION_RATIO_VALUES)

```
C#### Subroutine: FM_SOLVE
C###  Description:
C###    Solves the HMT model for a given test, between
C###    TBEG and TNEXT

      IMPLICIT NONE
      INCLUDE 'cmiss$reference:oxs005.cmn'
!     Parameter list
      INTEGER count
      REAL*4 EXTENSION_RATIO_VALUES(*)
      REAL*8 TBEG,TNEXT,T,TFINAL
!     Common Blocks
      REAL*8      PI
      COMMON /PI/ PI
      INTEGER    IDOP,Model,Integration,Muscle_type,Test_type,Icouple
      COMMON /I/ IDOP,Model,Integration,Muscle_type,Test_type,Icouple
      !To params
      REAL*8         Tref,beta0,beta1,beta2,gamma,Ca_scale
      COMMON /SS_To/ Tref,beta0,beta1,beta2,gamma,Ca_scale
      !Ca kinetics
      REAL*8      Ca_max,Ca_tau
      COMMON /Ca/ Ca_max,Ca_tau
      !Tn kinetics
      REAL*8      Rho0,Rho1,Cb_max
      COMMON /Tn/ Rho0,Rho1,Cb_max
      !Tm kinetics
      REAL*8      ALFA0,AA0,Tm_n_0,Tm_p50_0
      COMMON /Tm/ ALFA0,AA0,Tm_n_0,Tm_p50_0
      !Xb kinetics
      REAL*8      a,ALFA(3),AA(3)
      COMMON /XB/ a,ALFA,AA
      !Passive muscle
      REAL*8        a11,b11,k11
      COMMON /Tp_1/ a11,b11,k11
      REAL*8        a22,b22,k22
      COMMON /Tp_2/ a22,b22,k22
      REAL*8        a33,b33,k33
      COMMON /Tp_3/ a33,b33,k33
      REAL*8        L
      COMMON /PROP/ L
      !Test protocols
      REAL*8        Pulse_interval
      COMMON /STIM/ Pulse_interval
      REAL*8        Step_time,Step_magnitude,Step_duration,
     '              Max_step_magnitude,
     '              Osc_time,Osc_magnitude,Osc_period,Osc_freq,
     '              step_times(20),step_durations(20),
     '              step_magnitudes(20)
      INTEGER       current_step,number_of_steps
      COMMON /TEST/ Step_time,Step_magnitude,Step_duration,
     '              Max_step_magnitude,
     '              Osc_time,Osc_magnitude,Osc_period,Osc_freq,
     '              step_times,step_durations,
     '              step_magnitudes,number_of_steps,current_step
      REAL*8      tt
      COMMON /TT/ tt
      REAL*8          MECH_TIMESCALE,MECH_TSTART,MECH_TEND,MECH_DT,
     '                MECH_TABT,MECH_TPS,TP_mem
      COMMON /MECH_T/ MECH_TIMESCALE,MECH_TSTART,MECH_TEND,MECH_DT,
     '                MECH_TABT,MECH_TPS,TP_mem
      REAL*8         Load
      COMMON /Load_/ Load
      REAL*8        mech_pCa,Ca_m,z,Cb,PHI(3),To_initial
      COMMON /VARS/ mech_pCa,Ca_m,z,Cb,PHI,To_initial
      REAL*8             Ca_from_membrane,Ca_new_from_membrane,
     '  LTRPNCa_from_JRW
      COMMON /STORED_CA/ Ca_from_membrane,Ca_new_from_membrane,
     '  LTRPNCa_from_JRW
      REAL*8 Save_T,Save_To
      COMMON /COUPLING_TENSION/ Save_T,Save_to
```

```
      INTEGER                    current_time_step,previous_time_step
      COMMON /TIME_VARIABLE_INFO/ current_time_step,previous_time_step
!     Local Variables
      REAL*8 dL,FM_INTEGRAND2,Fm,FN_TM,To,FN_TO,Q,FN_Q,Ca,FN_CA,Ca_new,
     '  Fn,FN_TN,Cb_new,z_new,Lprev,z0,G,FN_G,dGdL,dPHI

C *** if not solving a coupled system, loop through the tabulation
C *** interval
C *** else, solve only once, i.e., the time step is the tabulation
C *** interval
      IF (Test_type.LT.20) THEN

      DO tt = TBEG,TNEXT,MECH_DT
        count=count+1
        IF(count.EQ.5) count=0
        IF (Test_type.EQ.8.OR.Test_type.EQ.9
     '    .OR.Test_type.EQ.-99) THEN !length steps, or
                                     !non-coupled time variable
C ***     DPN 30 April 98 - time variable info
          previous_time_step = current_time_step
          current_time_step = current_time_step + 1
          dL = 0.5d0*(FM_INTEGRAND2(tt-MECH_DT,EXTENSION_RATIO_VALUES,
     '      MECH_DT)+
     '      FM_INTEGRAND2(tt,EXTENSION_RATIO_VALUES,MECH_DT))*
     '      MECH_DT
          L  = L+dL !new length
          Fm = FN_TM(Cb,z,L) !tropomyosin kinetics
          z  = z + MECH_DT*Fm !prediction step for z
          To = FN_TO(L,z) !isometric tension
          Q  = FN_Q(PHI,MECH_DT,EXTENSION_RATIO_VALUES)!Xbridge kinetics
          T  = To*(1.d0+a*Q)/(1.d0-Q) !tension
        ELSE IF(Test_type.EQ.5) THEN !isometric test
          Ca     = 0.01d0 + FN_CA(tt   ,Ca_m)
          Ca_new = 0.01d0 + FN_CA(tt+MECH_DT,Ca_m)
          mech_pCa=6.d0-DLOG10(Ca) !Ca is in uM
          Fn = FN_TN(Ca,Cb,T,T) !troponin kinetics
          Fm = FN_TM(Cb,z,L) !tropomyosin kinetics
          Cb_new = Cb + MECH_DT*Fn !prediction step for Cb
          z_new  =  z + MECH_DT*Fm !prediction step for z
          Cb = Cb + 0.5d0*MECH_DT*(Fn+FN_TN(Ca_new,Cb_new,T,T)) !new Cb
          z  =  z + 0.5d0*MECH_DT*(Fm+FN_TM(Cb_new,z_new,L)) !new z
          T = FN_TO(L,z)
        ELSE IF(Test_type.EQ.14) THEN
          Lprev=L
          z0= z
          G = 1.d6 !just large initial value
          DO WHILE(DABS(G).GT.1.d-6) !Newton iterations
            G    =  FN_G(tt,MECH_DT,L      ,Lprev,Cb,z0,PHI,T,To,Load)
            dGdL = (FN_G(tt,MECH_DT,L+1.d-4,Lprev,Cb,z0,PHI,T,To,Load)
     '        -G)/1.d-4
            L    =  L - G/dGdL !new length
          ENDDO
          z=z0
          dPHI=(L-Lprev)/(ALFA(1)*MECH_DT)
     '      *DEXP(ALFA(1)*tt)*(1.d0-DEXP(-ALFA(1)*MECH_DT))
          PHI(1)=PHI(1)+dPHI
        ENDIF !Test_type
      ENDDO !tt
      TFINAL = tt

      ELSE !solving coupled system, solve once.

        count=count+1
        IF(count.EQ.5) count=0
C ***   use the [Ca]i from the membrane model
C ***   DPN 02/02/98 - add Ca_scale
        Ca     = Ca_from_membrane * Ca_scale
        Ca_new = Ca_new_from_membrane * Ca_scale
        mech_pCa=6.d0-DLOG10(Ca) !Ca is in uM
        tt = TBEG
        IF (Test_type.EQ.20) THEN !isometric test
C *** DPN 12/06/98 - use LTRPNCa if using JRW membrane model
          IF (LTRPNCa_from_JRW.LT.0.0d0) THEN
            Fn = FN_TN(Ca,Cb,T,T) !troponin kinetics
            Fm = FN_TM(Cb,z,L) !tropomyosin kinetics
            Cb_new = Cb + MECH_TABT*Fn !prediction step for Cb
            z_new  =  z + MECH_TABT*Fm !prediction step for z
            Cb = Cb + 0.5d0*MECH_TABT*(Fn+FN_TN(Ca_new,Cb_new,T,T)) !newCb
            z  =  z + 0.5d0*MECH_TABT*(Fm+FN_TM(Cb_new,z_new,L)) !new z
          ELSE
            Fm = FN_TM(Cb,z,L) !tropomyosin kinetics
            Cb = LTRPNCa_from_JRW
            z_new  =  z + MECH_TABT*Fm
            z  =  z + 0.5d0*MECH_TABT*(Fm+FN_TM(Cb,z_new,L)) !new z
          ENDIF !
          T = FN_TO(L,z)
          Save_T = T
          Save_To = T
        ELSE IF (Test_type.EQ.21) THEN !non-isometric test
C *** DPN 12/01/98 - adding non-isometric test (step change in length)
          Fn = FN_TN(Ca,Cb,T,To) !troponin kinetics
          dL = 0.5d0*(
     '      FM_INTEGRAND2(TBEG-MECH_TABT,EXTENSION_RATIO_VALUES,
     '      MECH_TABT)+
     '      FM_INTEGRAND2(TBEG,EXTENSION_RATIO_VALUES,MECH_TABT))
     '      *MECH_TABT
          Fm = FN_TM(Cb,z,L) !tropomyosin kinetics
          L  = L+dL !new length
C *** DPN 12/06/98 - use LTRPNCa if using JRW membrane model
          IF (LTRPNCa_from_JRW.LT.0.0d0) THEN
            Cb_new = Cb + MECH_TABT*Fn !prediction step for Cb
            z_new  =  z + MECH_TABT*Fm !prediction step for z
            Cb = Cb + 0.5d0*MECH_TABT*(Fn+FN_TN(Ca_new,Cb_new,T,To))!new Cb
            z  =  z + 0.5d0*MECH_TABT*(Fm+FN_TM(Cb_new,z_new,L)) !new z
          ELSE
            z_new  =  z + MECH_TABT*Fm !prediction step for z
            Cb = LTRPNCa_from_JRW
            z  =  z + 0.5d0*MECH_TABT*(Fm+FN_TM(Cb,z_new,L)) !new z
          ENDIF
          To = FN_TO(L,z) !isometric tension
          Q  = FN_Q(PHI,MECH_TABT,EXTENSION_RATIO_VALUES)!Xbridge kinetics
          T  = To*(1.d0+a*Q)/(1.d0-Q) !tension
          Save_T = T
          Save_To = To
        ELSE IF (Test_type.EQ.99) THEN !coupled, time variable used
C ***     DPN 30 April 98 - time variable info
          previous_time_step = current_time_step
          current_time_step = current_time_step + 1
          Fn = FN_TN(Ca,Cb,Save_T,Save_To) !troponin kinetics
C ***     DPN 30 April 98 - use the values from the time variable
          dL = 0.5d0*(FM_INTEGRAND2(TBEG-MECH_TABT,
     '      EXTENSION_RATIO_VALUES,MECH_TABT)+
     '      FM_INTEGRAND2(TBEG,EXTENSION_RATIO_VALUES,MECH_TABT))
     '      *MECH_TABT
          Fm = FN_TM(Cb,z,L) !tropomyosin kinetics
          L  = L+dL !new length
C *** DPN 12/06/98 - use LTRPNCa if using JRW membrane model
          IF (LTRPNCa_from_JRW.LT.0.0d0) THEN
            Cb_new = Cb + MECH_TABT*Fn !prediction step for Cb
            z_new  =  z + MECH_TABT*Fm !prediction step for z
            Cb = Cb + 0.5d0*MECH_TABT*(Fn+FN_TN(Ca_new,Cb_new,T,To))!new Cb
            z  =  z + 0.5d0*MECH_TABT*(Fm+FN_TM(Cb_new,z_new,L)) !new z
          ELSE
            z_new  =  z + MECH_TABT*Fm !prediction step for z
            Cb = LTRPNCa_from_JRW
            z  =  z + 0.5d0*MECH_TABT*(Fm+FN_TM(Cb,z_new,L)) !new z
          ENDIF
          To = FN_TO(L,z) !isometric tension
          Q  = FN_Q(PHI,MECH_TABT,EXTENSION_RATIO_VALUES)!Xbridge kinetics
          T  = To*(1.d0+a*Q)/(1.d0-Q) !tension
          Save_T = T
          Save_To = To
        ENDIF
        TFINAL = TBEG + MECH_TABT
      ENDIF !coupled/non-coupled system

      RETURN
      END
```

HMT functions

```
      REAL*8 FUNCTION FN_TM(Cb1,z1,L)

C#### Function: FN_TM
C###  Type: REAL*8
C###  Description:
C###    Tropomyosin kinetics for fading memory model (dz/dt)

      IMPLICIT NONE
      INCLUDE 'cmiss$reference:cell00.cmn'
!     Parameter List
      REAL*8 Cb1,z1,L
!     Common Blocks
      REAL*8         Tref,beta0,beta1,beta2,gamma,Ca_scale
      COMMON /SS_To/ Tref,beta0,beta1,beta2,gamma,Ca_scale
      REAL*8         ALFA0,AA0,Tm_n_0,Tm_p50_0
      COMMON /Tm/    ALFA0,AA0,Tm_n_0,Tm_p50_0
      REAL*8      Rho0,Rho1,Cb_max
      COMMON /Tn/ Rho0,Rho1,Cb_max
!     Local Variables
      REAL*8 C50,Tm_n,Tm_p50,Cb_norm

      Tm_n   =Tm_n_0  *(1.d0+beta1*(L-1.d0)) !length dependence for n
      Tm_p50 =Tm_p50_0*(1.d0+beta2*(L-1.d0)) !length dependence for p50
      C50=10**(6.d0-Tm_p50) !uM
C DPN 05/08/98 - scale dz/dt by normalised [Ca]b
      Cb_norm = Cb1/Cb_max
      FN_TM=alfa0*(((Cb1/C50)*Cb_norm)**Tm_n *(1.d0-z1) - z1)

      RETURN
      END

      REAL*8 FUNCTION FN_TO(L,z)

C#### Function: FnTo
C###  Type: REAL*8
C###  Description:
C###    Tension-length-pCa relation for fading memory model

      IMPLICIT NONE
!     Parameter List
      REAL*8 L,z !,Cb
!     Common Blocks
      REAL*8         Tref,beta0,beta1,beta2,gamma,Ca_scale
      COMMON /SS_To/ Tref,beta0,beta1,beta2,gamma,Ca_scale

      FN_TO=Tref*(1.d0+beta0*(L-1.d0))*z

      RETURN
      END

      REAL*8 FUNCTION FN_ZSS(Cb,C50,n)

C#### Function: FN_ZSS
C###  Type: REAL*8
C###  Description:
C###    Steady state z for fading memory model

      IMPLICIT NONE
!     Parameter List
      REAL*8 Cb,C50,n

      FN_ZSS= (Cb/C50)**n/(1.d0+(Cb/C50)**n)

      RETURN
      END

      REAL*8 FUNCTION FN_TO_SS(L,Cb)

C#### Function: FN_TO_SS
C###  Type: REAL*8
```

```
C###  Description:
C###    Steady state tension-length-pCa relation for fading memory model

      IMPLICIT NONE
!     Parameter List
      REAL*8 L,Cb !,z
!     Common Blocks
      REAL*8         Tref,beta0,beta1,beta2,gamma,Ca_scale
      COMMON /SS_To/ Tref,beta0,beta1,beta2,gamma,Ca_scale
      REAL*8         alfa0,AA0,Tm_n_0,Tm_p50_0
      COMMON /Tm/    alfa0,AA0,Tm_n_0,Tm_p50_0
!     Local Variables
      REAL*8 C50,n,p50
      REAL*8 FN_ZSS

      n   = Tm_n_0  *(1.d0+beta1*(L-1.d0)) !length dependence for n
      p50 = Tm_p50_0*(1.d0+beta2*(L-1.d0)) !length dependence for p50
      C50 = 10**(6.d0-p50) !uM

      FN_TO_SS=Tref*(1.d0+beta0*(L-1.d0))*FN_ZSS(Cb,C50,n)

      RETURN
      END

      REAL*8 FUNCTION FN_Q(PHI,dt,EXTENSION_RATIO_VALUES)

C#### Function: FN_Q
C###  Type: REAL*8
C###  Description:
C###    Returns updated Q & PHI for current timestep dt, from fading
C###    memory model.

      IMPLICIT NONE
      INCLUDE ’cmiss$reference:oxs005.cmn’
!     Parameter List
      REAL*4 EXTENSION_RATIO_VALUES(*)
      REAL*8 PHI(3),dt
!     Common Blocks
      INTEGER     IDOP,Model,Integration,Muscle_type,Test_type,Icouple
      COMMON /I/  IDOP,Model,Integration,Muscle_type,Test_type,Icouple
      REAL*8      a,ALFA(3),AA(3)
      COMMON /XB/ a,ALFA,AA
      REAL*8          MECH_TIMESCALE,MECH_TSTART,MECH_TEND,MECH_DT,
     ’                MECH_TABT,MECH_TPS,TP_mem
      COMMON /MECH_T/ MECH_TIMESCALE,MECH_TSTART,MECH_TEND,MECH_DT,
     ’                MECH_TABT,MECH_TPS,TP_mem
      INTEGER                     current_time_step,previous_time_step
      COMMON /TIME_VARIABLE_INFO/ current_time_step,previous_time_step
!     Local Variables
      REAL*8 dPHI !,Q,RELERR
      REAL*8 FM_INTEGRAND1

      ! 1st Fading Memory term
      dPHI=0.5d0*(FM_INTEGRAND1(1,0.d0,EXTENSION_RATIO_VALUES)+
     ’  FM_INTEGRAND1(1,dt,EXTENSION_RATIO_VALUES))*dt
      PHI(1)=DEXP(-ALFA(1)*dt)*PHI(1)+dPHI
      ! 2nd Fading Memory term
      dPHI=0.5d0*(FM_INTEGRAND1(2,0.d0,EXTENSION_RATIO_VALUES)+
     ’    FM_INTEGRAND1(2,dt,EXTENSION_RATIO_VALUES))*dt
      PHI(2)=EXP(-ALFA(2)*dt)*PHI(2)+dPHI
      ! 3rd Fading Memory term
      dPHI=0.5d0*(FM_INTEGRAND1(3,0.d0,EXTENSION_RATIO_VALUES)+
     ’    FM_INTEGRAND1(3,dt,EXTENSION_RATIO_VALUES))*dt
      PHI(3)=EXP(-ALFA(3)*dt)*PHI(3)+dPHI

      FN_Q = AA(1)*PHI(1)+AA(2)*PHI(2)+AA(3)*PHI(3)

      RETURN
      END

      REAL*8 FUNCTION FM_INTEGRAND1(FMterm,tau,EXTENSION_RATIO_VALUES)

C#### Function: FM_INTEGRAND1
C###  Type: REAL*8
C###  Description:
C###    Evaluate integrand for one component of fading memory
C###    hereditary integral. FMterm is 1, 2 or 3 for each rate
C###    constant term.

      IMPLICIT NONE
      INCLUDE ’cmiss$reference:oxs005.cmn’
!     Parameter List
      INTEGER FMterm
      REAL*4  EXTENSION_RATIO_VALUES(*)
      REAL*8  tau
!     Common Blocks
      INTEGER    IDOP,Model,Integration,Muscle_type,Test_type,Icouple
      COMMON /I/ IDOP,Model,Integration,Muscle_type,Test_type,Icouple
      REAL*8      a,ALFA(3),AA(3)
      COMMON /XB/ a,ALFA,AA
      REAL*8        Pulse_interval
      COMMON /STIM/ Pulse_interval
      REAL*8        Step_time,Step_magnitude,Step_duration,
     ’              Max_step_magnitude,
     ’              Osc_time,Osc_magnitude,Osc_period,Osc_freq,
     ’              step_times(20),step_durations(20),
     ’              step_magnitudes(20)
      INTEGER       current_step,number_of_steps
      COMMON /TEST/ Step_time,Step_magnitude,Step_duration,
     ’              Max_step_magnitude,
     ’              Osc_time,Osc_magnitude,Osc_period,Osc_freq,
     ’              step_times,step_durations,
     ’              step_magnitudes,number_of_steps,current_step
      REAL*8      tt
      COMMON /TT/ tt
      REAL*8          MECH_TIMESCALE,MECH_TSTART,MECH_TEND,MECH_DT,
     ’                MECH_TABT,MECH_TPS,TP_mem
      COMMON /MECH_T/ MECH_TIMESCALE,MECH_TSTART,MECH_TEND,MECH_DT,
     ’                MECH_TABT,MECH_TPS,TP_mem
      INTEGER                     current_time_step,previous_time_step
      COMMON /TIME_VARIABLE_INFO/ current_time_step,previous_time_step
!     Local Variables
      REAL*8 u

      !Set scaled myofilament shortening velocity
      IF(Test_type.EQ.7) THEN       !Isometric twitch
        u = 0.d0
      ELSE IF(Test_type.EQ.8.OR.Test_type.EQ.21) THEN !step change
                                                      !in length
        IF(tt-tau.GE.Step_time.AND.tt-tau.LT.Step_time+
     ’    Step_duration) THEN
          u = Step_magnitude/Step_duration
        ELSE
          u = 0.d0
        ENDIF
      ELSE IF(Test_type.EQ.9) THEN !multiple length steps
        IF(tt-tau.GE.step_times(current_step).AND.
     ’    tt-tau.LT.step_times(current_step)+
     ’    step_durations(current_step)) THEN
          u = step_magnitudes(current_step)/step_durations(current_step)
          current_step = current_step + 1
        ELSE
          u = 0.d0
        ENDIF
      ELSE IF(Test_type.EQ.10) THEN !Stiffness
        IF(tt-tau.GE.Osc_time) THEN
          u =Osc_magnitude*Osc_freq*DSIN(Osc_freq*(tt-tau-Osc_time))
        ELSE
          u = 0.d0
        ENDIF
      ELSE IF(Test_type.EQ.14) THEN !Isotonic shortening
        u = Step_magnitude/Step_duration
      ELSE IF(ABS(Test_type).EQ.99) THEN !time variable used
        IF(previous_time_step.EQ.0) THEN
          u = 0.0d0
        ELSE
          u = DBLE(EXTENSION_RATIO_VALUES(current_time_step) -
     ’      EXTENSION_RATIO_VALUES(previous_time_step)) / MECH_TABT
        ENDIF
      ELSE
        u = 0.d0
      ENDIF

      FM_INTEGRAND1=DEXP(-ALFA(FMterm)*tau)*u

      RETURN
      END

      REAL*8 FUNCTION FM_INTEGRAND2(tau,EXTENSION_RATIO_VALUES,STEP)

C#### Function: FM_INTEGRAND2
C###  Type: REAL*8
C###  Description:
C###    Evaluate integrand for integral of velocity.

      IMPLICIT NONE
      INCLUDE ’cmiss$reference:oxs005.cmn’
!     Parameter List
      REAL*4 EXTENSION_RATIO_VALUES(*)
      REAL*8 tau,STEP
!     Common Blocks
      INTEGER    IDOP,Model,Integration,Muscle_type,Test_type,Icouple
      COMMON /I/ IDOP,Model,Integration,Muscle_type,Test_type,Icouple
      REAL*8        Step_time,Step_magnitude,Step_duration,
     ’              Max_step_magnitude,
     ’              Osc_time,Osc_magnitude,Osc_period,Osc_freq,
     ’              step_times(20),step_durations(20),
     ’              step_magnitudes(20)
      INTEGER       current_step,number_of_steps
      COMMON /TEST/ Step_time,Step_magnitude,Step_duration,
     ’              Max_step_magnitude,
     ’              Osc_time,Osc_magnitude,Osc_period,Osc_freq,
     ’              step_times,step_durations,
     ’              step_magnitudes,number_of_steps,current_step
      REAL*8          MECH_TIMESCALE,MECH_TSTART,MECH_TEND,MECH_DT,
     ’                MECH_TABT,MECH_TPS,TP_mem
      COMMON /MECH_T/ MECH_TIMESCALE,MECH_TSTART,MECH_TEND,MECH_DT,
     ’                MECH_TABT,MECH_TPS,TP_mem
      INTEGER                     current_time_step,previous_time_step
      COMMON /TIME_VARIABLE_INFO/ current_time_step,previous_time_step

!     Local Variables
      REAL*8 u

      ! Set scaled myofilament shortening velocity
      IF(Test_type.EQ.7) THEN      !Isometric
        u = 0.d0
      ELSE IF(Test_type.EQ.8.OR.Test_type.EQ.21) THEN !step change
                                                      !in length
        IF(tau.GE.Step_time.AND.tau.LT.Step_time+Step_duration) THEN
          u = Step_magnitude/Step_duration
        ELSE
          u = 0.d0
        ENDIF
      ELSE IF(Test_type.EQ.9) THEN !multiple length steps
        IF(tau.GE.step_times(current_step).AND.
     ’    tau.LT.step_times(current_step)+
     ’    step_durations(current_step)) THEN
          u = step_magnitudes(current_step)/step_durations(current_step)
          current_step = current_step + 1
        ELSE
          u = 0.d0
        ENDIF
      ELSE IF(Test_type.EQ.10) THEN !Stiffness
        IF(tau.GE.Osc_time) THEN
          u = Osc_magnitude*Osc_freq*DSIN(Osc_freq*(tau-Osc_time))
        ELSE
          u = 0.d0
        ENDIF
      ELSE IF(Test_type.EQ.14) THEN !Isotonic shortening
        u = Step_magnitude/Step_duration
      ELSE IF(ABS(Test_type).EQ.99) THEN !coupled, time variable used
        IF(previous_time_step.EQ.0) THEN
          u = 0.0d0
        ELSE
          u = DBLE(EXTENSION_RATIO_VALUES(current_time_step) -
     ’      EXTENSION_RATIO_VALUES(previous_time_step)) / STEP
        ENDIF
      ELSE
        u = 0.d0
      ENDIF
      FM_INTEGRAND2 = u

      RETURN
      END
```

```
      REAL*8 FUNCTION TP1(L)

C#### Function: TP1
C###  Type: REAL*8
C###  Description:
C###    Passive tension-length relation for fibre axis

      IMPLICIT NONE
!     Parameter List
      REAL*8 L
!     Common Blocks
      REAL*8        a11,b11,k11
      COMMON /Tp_1/ a11,b11,k11
!     Local Variables
      REAL*8 e

      e=0.5d0*(L*L-1.d0)
      TP1= k11*e*(2.d0+b11*e/(a11-e))/(a11-e)**b11

      RETURN
      END

      REAL*8 FUNCTION TP2(L)

C#### Function: TP2
C###  Type: REAL*8
C###  Description:
C###    Passive tension-length relation for sheet axis

      IMPLICIT NONE
!     Parameter List
      REAL*8 L
!     Common Blocks
      REAL*8        a22,b22,k22
      COMMON /Tp_2/ a22,b22,k22
!     Local Variables
      REAL*8 e

      e=0.5d0*(L*L-1.d0)
      TP2= k22*e*(2.d0+b22*e/(a22-e))/(a22-e)**b22

      RETURN
      END

      REAL*8 FUNCTION TP3(L)

C#### Function: TP3
C###  Type: REAL*8
C###  Description:
C###    Passive tension-length relation for sheet normal

      IMPLICIT NONE
!     Parameter List
      REAL*8 L
!     Common Blocks
      REAL*8        a33,b33,k33
      COMMON /Tp_3/ a33,b33,k33
!     Local Variables
      REAL*8 e

      e=0.5d0*(L*L-1.d0)
      TP3= k33*e*(2.d0+b33*e/(a33-e))/(a33-e)**b33

      RETURN
      END

      REAL*8 FUNCTION FN_G(tt,dt,L,Lprev,Cb,z0,PHI,T,To,Load)

C#### Function: FN_G
C###  Type: REAL*8
C###  Description:
C###    G=T-Load, where T is calc.d from L

      IMPLICIT NONE
      INCLUDE 'cmiss$reference:oxs005.cmn'
!     Parameter List
      REAL*8 tt,dt,L,Lprev,Cb,z0,PHI(3),T,To,Load
!     Common Blocks
      INTEGER     IDOP,Model,Integration,Muscle_type,Test_type,Icouple
      COMMON /I/  IDOP,Model,Integration,Muscle_type,Test_type,Icouple
      REAL*8      a,ALFA(3),AA(3)
      COMMON /XB/ a,ALFA,AA
!     Local Variables
      REAL*8 FN_TM,Q,FN_TO,z,dPHI

      z  = z0 + dt*FN_TM(Cb,z0,L)                 !tropomyosin kinetics
      dPHI=(L-Lprev)/(ALFA(1)*dt)
     '     *DEXP(ALFA(1)*tt)*(1.d0-DEXP(-ALFA(1)*dt))
      Q  = AA(1)*DEXP(-ALFA(1)*tt)*(PHI(1)+dPHI)      !Xbridge kinetics
      To = FN_TO(L,z)                                 !isometric tension
      T  = To*(1.d0+a*Q)/(1.d0-Q)                     !tension

      FN_G = T-Load

      RETURN
      END
```